Development and characterisation of a biomimetic liver on chip featuring 3D hepatic coculture with an endothelial barrier

Taha Messelmani

Par **Taha MESSELMANI**

Development and characterisation of a biomimetic liver on chip featuring 3D hepatic coculture with an endothelial barrier

Thèse présentée
pour l'obtention du grade
de Docteur de l'UTC

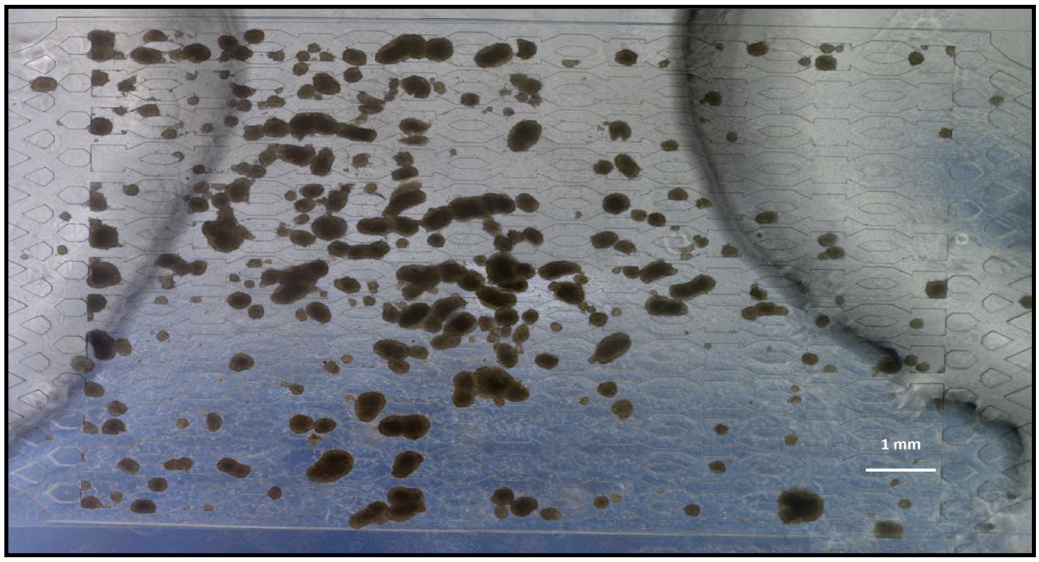

Soutenue le 13 avril 2023
Spécialité : Biomécanique et Bio-ingénierie : Unité de Recherche en Biomécanique et Bio-ingénierie (UMR-7338)
D2736

Thèse présentée pour l'obtention du grade de Docteur
de **L'Université de Technologie de Compiègne**
Ecole doctorale n° 71 : Sciences pour l'ingénieur
Spécialité : Biomécanique et Bio-ingénierie
BMBI CNRS UMR 7338

Soutenue le 13 avril 2023

Development and characterisation of a biomimetic liver on chip featuring 3D hepatic coculture with an endothelial barrier

Taha Messelmani

Membres du jury :

Pr. LE GAC Séverine, University of Twente – Enschede, Netherlands	Rapporteur
Pr. HAUTEFEUILLE Mathieu, Institut de Biologie Paris-Seine – Paris, France	Rapporteur
Dr. CORLU Anne, DR CNRS UMR INSERM 1241 - Rennes, France	Examinateur
Dr. KLIEBER Sylvie, SANOFI - Vitry-sur-seine, France	Examinateur
Pr. GUENIN Erwann, TIMR UTC-ESCOM – UTC, Compiègne, France	Président du jury
Dr. LECLERC Eric, DR CNRS IRL 2820 – LIMMS, Tokyo, Japan	Directeur de thèse
Dr. JELLALI Rachid, IR CNRS UMR 7338 – UTC, Compiègne, France	Directeur de thèse
Dr. LE GOFF Anne, MC CNRS UMR 7338 – UTC, Compiègne, France	Encadrante
Dr. LEGALLAIS Cécile, DR CNRS UMR 7338 – UTC, Compiègne, France	Membre invité
Dr. MAUBON Nathalie, CEO/CSO - HCS Pharma, Lille, France	Membre invité

Abstract

During drugs development programs, animal models are commonly used for the assessment of the metabolism and toxicity of drug candidates. Several legal frameworks are being settled to promote the replacement, the reduction, and the refinement of these experiments. The liver is a central organ involved in the detoxification of exogenous molecules. Accordingly, the development of models mimicking the functions of the liver remain a challenging objective. Conventionally, liver cells are cultured *in vitro* in 2D Petri dishes but this conformation leads to a rapid loss of their functions. In recent years, the association between tissue engineering and organ-on-chip technology led to the development of more accurate alternative models that mimic the liver functions. The aim of this thesis is to develop a biomimetic liver-on-chip platform by coupling a hepatocyte biochip and an endothelial-like barrier. The goal is to mimic the passage of molecules through the liver sinusoid endothelial barrier and then their metabolism with the hepatocytes.

In the first part, we used organ-on-chip technology and ECM-based hydroscaffold to organise the cells in 3D structures. The potential of our model was compared with static Petri dishes and the spheroids formed were characterised structurally and functionally. In the second part, we characterized the formation of an endothelial barrier and identified specific markers indicating the conservation of the phenotype of endothelial cells. We established the coculture conditions and analysed the potential of coupling the endothelial barrier with the hepatocyte-on-chip to metabolize the APAP as a candidate molecule. Finally, we analysed the metabolomic signature of each condition, crosstalk between the cells, and identified the metabolic signature of APAP injury and described the reactions happening at metabolic level. In the last part, we proposed tracks of improvement by using primary hepatocytes or by integrating the endothelial barrier and the hepatocytes in the same bi-compartmentalized biochip.

Table of contents

List of figures

List of tables

General introduction

The screening of newly discovered molecules must undergo a long process of preclinical trials to ensure their efficacity, safety and innocuity. During these trials, animal testing has been used by pharmaceutical companies as the reference method to identify the potential effect of these molecules. Nonetheless, these experiments require a significant economic investment and raises ethical problems. To set up a framework to supervise these experiments, European directives require the integration of the 3R guidelines (replace, reduce, refine) and welfare standards for the treatment of animals in the different steps of drug discovery process. In order to follow these directives, several research projects are trying to develop relevant *in vitro* models that will come in place or in addition to animal models. The liver, a central organ, involved in the metabolism of exogenous molecules, is the subject of different alternative models aiming for the recreation of its functions.

Conventionally, liver models consist of a static monolayered culture of hepatocytes on which hepatotoxicity and metabolic assays are implemented. However, the loss of metabolic functionalities and the hepatocyte dedifferentiation create a disparity between these models and the *in vivo* situation. In addition, by only using hepatocytes, these models do not capture the complexity of the liver micro architecture and only partially mimick liver functions. *In vivo*, drug molecules are distributed through the blood circulation system until arrival to the liver. Once in the liver, a bidirectional mass transfer occurs through the liver sinusoid endothelial cells, between the mixture of arterial and venous blood and the hepatocytes. Hence, advanced *in vitro* models need to be developed to better predict the liver behaviour. Accordingly, the association between 3D organization of the cells and organ-on-chip technology is emerging as a relevant tool for the recreation of physiological relevant *in vitro* responses.

It is in this context that the ANR project Mimliveronchip (ANR-19-CE19-0020) was launched to develop a fully integrated platform for cell culture and the high-throughput assay for drug screening. This PhD thesis is funded by the ANR project and aims at developing an advanced liver-on-chip model for drug toxicity screening applications. The model consists of an LSEC barrier coupled with hepatocytes cultured into an advanced biochip integrating a hyaluronic acid based hydroscaffold. The achievement of this project required several steps which will be presented in the following chapters.

Firstly, we presented the state of art for the usage of liver-on-chip devices for the risk assessment of drugs and pollutants (**chapter 1**). In this first chapter, we contextualized the thesis project by describing the liver physiology, the need of relevant models to mimic its

behaviour and the different tools needed for the development of liver on chip models. Then we described different applications that were developed using the liver-on-chip and multi organ-on-chip models for the risk assessment of chemicals.

Then, in order to develop our advanced liver-on-chip model, we used the HepG2/Ca cell line for the proof of concept of the 3D organization of the hepatocytes into spheroids using a HA-based hydroscaffold integrated in our biochip. Results obtained in the microfluidic device were compared with the same hydroscaffold integrated into conventional Petri dishes (**chapter 3**). The biochip was connected in our parallelization platform Integrated Dynamic Cell Cultures in Microsystems (IDCCM) and the structures and functions of the *in situ* formed spheroids was analysed.

In order to integrate an endothelial barrier into our model, we used the SK-HEP-1 cell line and the parallelization device Integrated Insert in a Dynamic Microfluidic Platform (IIDMP) developed in our laboratory. The device allowed us to cultivate hepatocytes in our advanced biochip and couple it with an endothelial barrier consisting of a confluent monolayer of SK-HEP-1 cells cultivated on culture insert (**chapter 4**). The parameters of coculture were set up, and the different parameters were analysed to study the cell-to-cell communication between the two compartments. Then as a concrete application we used APAP as a candidate molecule to demonstrate the potential of our model to mimic the hepatic first passage.

In order to deepen our understanding in our developed model, we used a metabolomic on chip approach to analyse each type of cultures and conditions (**chapter 5**). The metabolomic profiles of the different conditions were analysed and associated with the different metabolic pathways involved. Then, mechanistic hypothesis was proposed to the response of our model to APAP injury.

Finally, we presented preliminary results of the *in situ* 3D organization of primary human hepatocytes into spheroids in our advanced liver-on-chip model (**chapter 6**). The spheroid functions and organization were analysed, and the model was tested with two candidate molecules: phenacetin and omeprazole. Then we proposed a new design for a bi-compartmentalized biochip including a thin permeable membrane (**chapter 6**). Preliminary characterization was achieved to demonstrate its potential as a replacement for the usage of the IIDMP.

In summary, the core of this thesis is to investigate the importance of integrating endothelial barrier for the recreation of a more relevant liver-on-chip models for drug screening applications. We successfully combined microfluidic systems, 3D spheroid organization and multi-cellular culture to biomimetically reproduce the xenobiotics first pass.

Chapter 1: General context

In this chapter, we discuss the development of liver organ-on-chip technology and its use in toxicity studies. First, we introduce the physiology of the liver and summarize the traditional experimental models for toxicity studies. We then present liver OoC technology, including the general concept, materials used, cell sources, and different approaches. We review the prominent liver OoC and multi-OoC integrating the liver for drug and chemical toxicity studies. Finally, we conclude with the future challenges and directions for developing or improving liver OoC models. The first sections of this chapter are literally extracted from our critical review: “Liver organ-on-chip models for toxicity studies and risk assessment”[1].

Additional sections 1.8.1 and 1.8.2 further present the role of the liver sinusoidal endothelial cells in the liver physiology, review existing different liver-on-chip models integrating an LSEC or an LSEC-like barrier and introduce the objectives of the thesis.

[1] **Messelmani T**, Morisseau L, Sakai Y, Legallais C, Le Goff A, Leclerc E, Jellali R. Liver organ-on-chip models for toxicity studies and risk assessment, **Lab on a Chip,** 2022, 22, 2423-2450, **Review DOI:10.1039/D2LC00307D**

1.1. Xenobiotics, pollutants and toxicity

From the early to mid-1990s, a traditional method was established for the search of new organic molecules with biological activity. This method consisted of identifying an untreated disease or a clinical case, and then generating hypotheses of inhibition or activation of proteins, involved in a metabolic pathway, to induce a therapeutic effect. Nowadays, the fully automated systems are being used for high-throughput screening of tens of thousands to hundreds of thousands of molecules per day on a purified target protein (Hughes et al., 2011). In general, from the identification of a potentially active molecule until its commercialization, there is a minimum of 11.5 years and on average more than 1 billion dollars of investment (Wouters et al., 2020).

In addition to the economic impact these drug discovery programs cause; the considered molecules pass through a long process of trials in order to ensure their therapeutical effect and their safety. The first preclinical phase consists of 6 major steps: an optimization of the manufacturing and the formulation of the drug substance called scale-up, the design of dosage, development and validation of analytical and bioanalytical methods, metabolism and pharmacokinetics, toxicology and safety and finally documentation of good manufacturing practices (GMP) of the medicinal product (Steinmetz et al., 2009). In several of these steps, rodent and non-rodent mammalian models are used to define the pharmacokinetic profile and general safety, as well as to identify toxicity profiles. For these models, a group of animals, usually dogs and rats, is selected and made up of a few animals of the same sex in order to establish the dose intervals to be administered. Once the interval has been identified, the group size is multiplied by 3 for gender and for dose to obtain statistically comparable data (McGonigle et al., 2010). The preclinical phase is followed by the clinical first phase which is devoted to the study of the pharmacology of the molecule on humans. Evaluations of pharmacokinetic parameters and tolerances on healthy volunteers by varying the number of doses and their intensity. Followed by the phase II of clinical development, which consists of exploring the therapeutic effect of the drug, including between 100 to 250 patients and deepening the studies of safety and pharmacological effect. And finally, the last phase which aims to confirm the therapeutic effect and consists in carrying out the safety and efficacy tests on a large population of patients and in parallel the preparation of the marketing authorization file (MA) for validation by the competent authorities (Schultz et al., 2019).

In addition to the toxicity risks encountered when taking drugs, the human body is exposed daily to a mixture of numerous chemicals. These chemicals mixtures constitute a major challenge for the risk assessment (Valdiviezo et al., 2022). Indeed, the safety evaluation is

based on the assessments of individual substances. However, in nature, humans are exposed to a full mixture of chemicals through numerous pathways creating combined effects that could be greater than those of individual components. To better evaluate the toxicity of these molecules, different research programs were launched in Europe such as the EU research consortia SOLUTIONS, EuroMix, HBM4EU, EDC-MixRisk and EUToxRisk and the powering research through innovative methods for mixtures in epidemiology (PRIME) program at the United States (Luo et al., 2022). The approach used in these programs to evaluate the chemical mixture's toxicity is to search for individual known toxicological signatures for known chemicals such as pesticides, heavy metals and persistent organic pollutants (POPs) in the chemical mixtures. However, the lack of toxicity data for the other emerging chemicals limits this approach for the study of environmental toxicant mixtures (Hammel et al., 2020). To better understand the mechanism of action of these newly discovered pollutants, data needs to be generated using conventional animal testing.

To deal with the expansion of the number of newly discovered potential drugs and pollutants and to better supervise the experiments involved in the drug discovery process, several legal texts have looked into the subject to create a legislative framework that regulates these uses. In the European Union, the regulations in force since June 1, 2007 are the REACH law. To this is added the 3R rule adopted in France under decree no. 2013-118 which sets up guidelines to reduce, refine and replace the use of animal testing (Aske et al., 2017).
The liver, the centre of metabolism of exogenous molecules to which humans are exposed, is the subject of various research projects. These models aim to replace the use of animals testing.

1.2. Physiology of the liver

The liver is subdivided into 2 parts, a left and a right lobe. It is connected to the portal vein and the hepatic artery, which ensure respectively 75% and 25% of the blood supply, and the hepatic veins, which provide drainage. In addition, the bile ducts ensure the evacuation of exocrine secretions toward the intestine. The liver is constituted of approximatively 1 million lobules which are its constitutional units. These lobules, most of the time, are hexagonal in shape, at each corner of the hexagon is a portal triad which consists of a hepatic artery, a portal vein and a bile duct. The central vein on the other hand crosses the centre of the lobular structure (Figure 1.1, Si-Tayeb et al., 2010). The hepatic acinus is considered the functional unit of the liver and defined by the surface between two neighbouring central veins and two neighbouring portal triads (overlapping between two lobules, Figure 1.1, Gu and Manautou 2012; Usta et al., 2015). The liver is composed of at least 15 different types of

cells. Hepatocytes (parenchymal cells) represent approximately 60% of the total cells and 80% of the total volume of the liver, and are responsible for its metabolic activity. The non-parenchymal cells (NPC) represent 40% of the total liver cells and are comprised of sinusoidal endothelial cells (LSECs, ~16%), Kupffer cells (15%), hepatic stellate cells (HSCs, 5%) and biliary epithelial cells (Malarkey et al., 2005). The LSEC are specialized endothelial cells forming the primary barrier between the blood and hepatocytes, and play the role of filter for fluids and particles passing through the blood and the space of Disse. They are characterized by their high potential for endocytosis and the presence of fenestrae, which is a unique characteristic among other Endothelial cells. The local immune cells of the liver are the Kupffer cells, which are derived from monocytes and characterized by a high phagocytic potential. They produce cytokines that induce the inflammatory reaction and ensure the crosstalk between the other cells. Hepatic stellate cells store vitamins and lipids, and produce the extracellular matrix (Malarkey et al., 2005). The liver's ECM is composed of 5 to 10% of collagen in addition to glycoproteins, laminin, vitronectin, fibronectin and proteoglycans (Bykov et al. 2004).

The liver is considered as a unique organ due to its irrigation by both arterial (hepatic artery, ~25%) and venous (portal circulation, ~ 75%) blood through the liver sinusoid (Figure 1.1). This irrigation creates a temporal and zonal distribution of oxygen, nutrient and hormone concentrations in the various zones of the liver lobules (Bale and Borenstein 2018; Beckwitt et al., 2018). The variation of these components, especially the oxygen tension, regulates the liver zonation and functionality. Indeed, the segregation of the liver into different zones creates different hepatocytes functions depending on their location in the different zones of the lobule. The zones can be divided following the oxygen and glucose gradient resulting in a high albumin and urea synthesis for the hepatocytes exposed to relatively rich oxygen and glucose at the periphery of the lobules and an increased glycolysis for the internal cells (Deng et al., 2019; Kietzmann 2017; Lee et al., 2021, Figure 1.1). The hepatotoxicity of exogenous molecules is also directly affected by the zonation phenomena. The zones with a rich oxygen tension correspond to the region where the CYP activity and the cells are less damaged and vice versa which leads to differences in hepatotoxicity. Such heterogeneity and specificity are considered as a survival strategy for each cell to perform simultaneously, independently and using the resources efficiently (Kietzmann 2017; Lee et al., 2021; Malarkey et al., 2005).

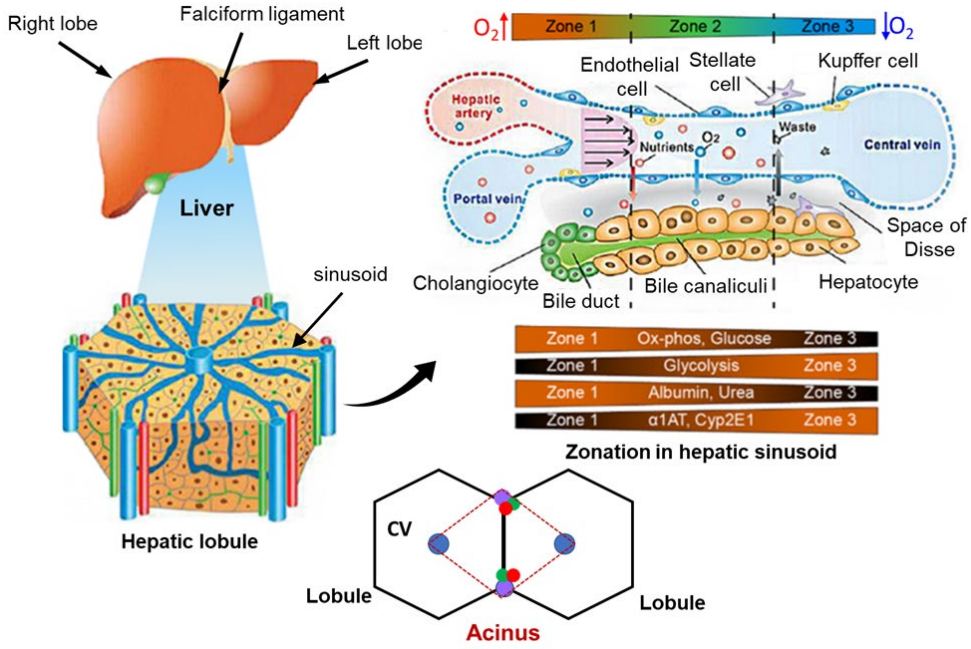

Figure 1.1. *Liver anatomy and schematic representation of hepatic acinus and zonation in hepatic sinusoid (reproduced with permission from Deng et al., 2019 and Ma et al., 2018).*

1.2.1. Liver metabolic activity

More than 500 vital functions have been identified and associated with the liver. It plays an important role in glucose homeostasis by transforming excess circulating glucose into glycogen (glycogenesis), or by degrading stored glycogen into glucose (glycolysis). In the absence of glycogen, the liver synthesizes glucose from lactate, glycerol, or amino acids (gluconeogenesis, Gebhardt et al. 1992). The liver is involved in the digestive system by secreting bile, a fluid produced by hepatocytes, secreted into bile ducts through bile canaliculi, and excreted into the duodenum. Bile emulsifies non-soluble compounds such as lipids, cholesterol and vitamins, and facilitates their absorption and digestion (Dosch et al., 2019). In addition to bile, the liver synthesizes many proteins and amino acids and plays a key role in lipid metabolism. Liver hepatocytes are the only cell type producing albumin, which is a carrier protein for hydrophobic substances such as hormones, vitamins, and enzymes. Albumin helps maintain the volume balance between blood plasma and interstitial fluid (Yuwen et al., 2017).

Another major role played by the liver is the storage and metabolism of fat-soluble vitamins. Vitamins are essential constituents that play an important role in catalyzing metabolic reactions to produce energy (Semba et al. 2012). They are provided mainly by external contributions such as food as only a few are synthesized by the body, but they remain in insufficient quantity to allow its metabolic reactions to function properly. Most vitamins are

not presented as a single specific molecule, but rather as a group of related compounds that provide the essential molecular ingredient. Many of these vitamins are concentrated, metabolized in active molecules, and stored in the liver, especially the fat-soluble vitamins (Almazroo et al., 2017). They reach the liver through the intestines via absorption as chylomicrons or very low-density lipoproteins (VLDL). Of these vitamins, vitamin A is stored in stellate cells and can be oxidized to retinoic acid and then to retina for phototransduction. It can also be conjugated into glucuronide to be secreted in the bile. Vitamin D3 for its part, and regardless of its source, must undergo 25-hydroxylation by the CYP-450 system in the liver followed by hydroxylation in the kidneys for it to be functional (Almazroo et al., 2017).

1.2.3. Metabolism of xenobiotics

In addition to the numerous metabolic activities, the liver ensures the metabolism of xenobiotics. Xenobiotics are natural or synthetic substances which occur in the living organism, but which are foreign to it. They can come from drug use, auto-intoxication, or the chemical industry *via* environmental, food and water pollution. Such molecules can cause acute or subacute, chronic, or repeated toxicity, depending on the dose. Deactivating and eliminating xenobiotics usually takes place in the liver. By carrying out biotransformation, the liver's hepatocytes transform the xenobiotics, from being mainly lipophilic, to mainly hydrophilic, thus facilitating their elimination (Gu and J. E. Manautou et al. 2012). This is done by a succession of enzymatic reactions (oxidation, reduction, hydrolysis, etc.) via the enzymatic complex of cytochromes P450. Their metabolisms go through two reactions, Phase I and Phase II. Although most drug metabolism reactions in the liver aim to break xenobiotics down, for some drugs during the first hepatic passage, the pharmacologically inactive molecule may become active to overcome problems related to bioavailability and adsorption. The drug is introduced into the body in an inactive form and is activated by the liver, which we generally refer to as a prodrug (Omiecinski et al., 2011).

Phase I metabolic reactions are characterized by enzymes from the cytochrome P450 superfamily (CYP450). These enzymes were discovered in the late 1980s and encompass more than 115 genes and pseudogenes. They are labelled with CYP1A1 up to CYP51P3 and are distributed in different proportions. By analyzing the total protein quantity of CYP450, we find mainly CYP3A4 at 22.1%, CYP2E1 at 15.3% and CYP2C9 at 14.6% (Almazroo et al., 2017). CYP450 enzymes can be classified according to their substrates (xenobiotics, fatty acids, vitamins, eicosanoids, sterols, etc.). The main role of these enzymes is to modify the foreign substances (mainly lipophilic products) to facilitate their excretion by the liver and kidneys. They catalyse a series of reactions, mainly oxidation, by adding one or more oxygen atoms to the foreign substance. However, they can also catalyse

other reactions, such as sulfoxidation, aromatic hydroxylation, aliphatic hydroxylation, N-dealkylation, O-dealkylation and desamination (Sandson et al. 2015). The xenobiotics metabolized in phase I are conjugated enzymatically, in phase II, with a hydrophilic compound by a transferase enzyme such as glucuronyltransferase, sulfotransferase and glutathione S-transferase. These reactions aim to transform the molecules into soluble substances to facilitate their elimination through the bile and urine (Lewis and Kleiner et al. 2012), although the phase I and II metabolic reactions mainly contribute to the elimination of the most pharmacologically-active compound. They can also bioactivate prodrugs into their active metabolite. These reactions promote the appearance of new substances (metabolized or bioactivated), and their accumulation in the liver causes a disruption in intracellular homeostasis, inducing toxicity or an idiosyncratic cascade leading to apoptosis or necrosis (Lewis and Kleiner 2012).

1.3. Current experimental liver models for toxicity studies

Considering the role of the liver in the metabolism of exogenous molecules, plus its exposure to a variety of potentially toxic compounds, it is important to use experimental models to anticipate hepatotoxicity. A successful model should sustain liver-specific function and accurately predict human *in vivo* responses to exogenous toxicants (Soldatow et al., 2013). To perform toxicological studies and pharmacological tests, several experimental models are used in laboratories. They can be classified as *in vivo* (animal experimentation), *ex vivo*, and *in vitro* tests.

1.3.1. Animal experimentation

Animal models are of undeniable value in medical research, and murine models have been playing an essential role in studies on both xenobiotic toxicity and liver pathologies. Rodent models (mice, rats, and guinea pigs) are used in the first line to study hepatotoxic damage. The mechanisms of toxicity appear to be the same in rodents and humans for certain drugs, like *acetaminophen* (APAP). Mice remain the preferred model for *APAP* overdose studies due to the similarity in the toxic doses in both species (McGill and Jaeschke 2019). Nonetheless, species-specific differences in characteristics between rodents and humans have become apparent as research progresses. Thus, to bridge this gap, chimeric mice with livers repopulated by human hepatocytes have been developed. The livers of these chimeric mice express human drug-metabolizing enzymes, making it possible to better predict human disposition of drugs with a human-specific metabolism (Bateman et al., 2014; Foster et al., 2014).

Current regulatory guidelines usually require safety and tolerability data from two species: a rodent and a non-rodent, before administering potential new medicines to humans in the first clinical trials (Prior et al., 2018; Son et al., 2020). Dogs are the default non-rodent used in toxicology studies with multiple scientific advantages, including similarity in the organs and physiology, adequate background data and availability (Son et al., 2020). Rabbits are mostly used to evaluate reproductive and developmental toxicity as they are phylogenetically close to humans (Barrow 2016). Moreover, they are relevant models for safety and pharmacology studies as their cardiovascular system has structural similarities with that of humans (Schmitt et al., 2015). Recently, minipigs have increasingly replaced dogs and rabbits in toxicology studies (particularly in the EU) due to ethical and scientific advantages. Minipigs effectively exhibit relevant similarity to humans: skin, cardiovascular system, gastrointestinal tract anatomy, and breeding habits (Schmitt et al., 2015; Son et al., 2020).

Significant interspecies differences in metabolism exist that confound the direct extrapolation of data from laboratory animal species into man in the development of pharmaceuticals (Martignoni et al., 2006; Son et al., 2020). Non-Human Primates (NHPs), composed of monkeys and apes, are phylogenetically closer to humans than other species but involve high study costs associated with ethical issues (Nakamura et al., 2021). Although animal models have significantly contributed to medical research, drug screening, and toxicity studies, they present two major disadvantages: significant interspecies differences with humans, and ethical considerations.

1.3.2. Human *ex vivo* models

Many commonly used *ex vivo* hepatotoxicity assays rely on liver slices, and whole perfused livers. Liver slices consist of maintaining the viability of all the cell types of the liver, as well as the multicellular histoarchitecture of the hepatic environment (Vickers and Fisher 2018). Human precision-cut liver slices (PCLS) are usually obtained from partial hepatectomies, surgical waste to be discarded, explanted tissue, or non-transplantable tissue. Cell viability can be maintained for up to 5 days in standard cultures (van Delft et al., 2014) and recent reports suggest that this may be extended to 15 to 21 days under precise conditions (Kartasheva-Ebertz et al., 2021).

Preserving the complex cellular interactions, the original 3D architecture, and the lobular structure of the liver in human PCLS provide the essential requirement for a good model, increasing the investigation of xenobiotic toxicity and our understanding of the pathophysiology of different liver diseases. Despite many similarities, it is important to notice altered gene expression between liver slices and the liver. During PCLS culture, inflammatory genes are upregulated and, in contrast, genes involved in xenobiotics and lipid

metabolism are significantly downregulated. This contrast in gene expression between *ex vivo* and *in vivo* conditions is mostly explained by the activation of several adaptation and stress responses to the new environmental condition of PCLS (van Delft et al., 2014). Another disadvantage of using PCLS in toxicology is the laborious preparation and culture procedure that may differ from operator to operator. Moreover, the short lifespan of PCLS can be an obstacle to studying the chronic effects of drug and chemical exposure. In addition, poor penetration of compounds into the inner cell layers of slices and inter-assay variability due to different preservation of cells in different slices have been reported (Guillouzo, 1998; Li, 2011). On the other hand, it is important to specify that PCLS are mostly prepared from rat livers and are used in comparison and extrapolation to the human situation.

1.3.3. 2D *in vitro* models

Today, due to the aim of replacing animal experiments whenever possible (3R), most liver hepatotoxicity studies rely on *in vitro* experimental models (Díaz et al., 2020). In the last 60 years, hepatocyte *in vitro* assays have focused on evaluating ADMET (Absorption, Distribution, Metabolism, Excretion and Toxicology) of new drugs using 2D cell cultures (de Angelis et al., 2019; Jaroch et al., 2018). Thus, there are several *in vitro* liver models that differ depending on their culture conditions and conformations, cell types used and other additional culture parameters (Godoy et al., 2013).

Primary hepatocyte suspensions are an easy method for performing high-throughput toxicity studies (Elaut et al., 2006). Some studies demonstrated that hepatocyte suspension provides a more accurate estimate of internal clearance rates and retains a higher level of functionality when compared to conventional monolayer culture (Griffin and Sul 2004; Jouin et al., 2006; Shaw et al., 1988). However, isolation protocols and the lack of cell-matrix/cell-cell contact leads to a loss of cell polarity, integrity, and dedifferentiation. Thus, hepatocytes in suspension have a short life-span (often a few hours) which is insufficient for developing and studying toxicity (Soldatow et al., 2013).

Static monolayer culture is the conventional 2D cellular model (Andria et al., 2010; Soldatow et al., 2013). Animal or human hepatocytes are grown in plastic Petri dishes and are exposed to changes in nutrient concentrations and catabolite accumulation over time. Periodically refreshing culture medium is necessary to remove accumulated catabolites and renew nutrients. Under standard culture conditions, hepatocytes can preserve cell-cell interactions and liver specific function, making possible a wide range of applications: short-term hepatotoxicity, cytochrome P450 induction and inhibition, drug interactions, pharmacokinetics, and pharmaco-dynamics. Furthermore, this 2D cellular model system is

easier to manipulate in the laboratory, is low cost, and is much more widely accepted ethically than the use of animal models (Duval et al., 2017; Milner et al., 2020). Although 2D cell culture models basically have some advantages, they are limited in their applications. Current mainstream 2D models fail either to capture the complexities of multicellularity or to maintain cell phenotypic characteristics for long cultivation. On the other hand, when using animal cells similar to *in vivo* animal experiments, it is difficult to obtain an accurate *in vitro-in vivo* extrapolation in humans using *in vitro* models based on animal cells (Kyffin et al., 2018).

Sandwich-cultured hepatocytes (SCH) are a powerful *in vitro* tool that can be used to study hepatobiliary drug transport, species differences in drug transport, transport protein regulation, drug-drug interactions, and hepatotoxicity (Andria et al., 2010). This model is composed of primary hepatocytes cultured between two layers of extracellular matrix, traditionally collagen type I or Matrigel®. Maintaining hepatocytes in a sandwich-cultured configuration increases and maintains albumin secretion, cell morphology and polarized architecture, cell viability, basal and induced enzyme activities, and mimics *in vivo* biliary excretion rates (Duval et al., 2017; Kyffin et al., 2018; Milner et al., 2020; Soldatow et al., 2013). For these reasons, sandwich-cultured hepatocytes are a pertinent *in vitro* model for investigating drug-drug interactions, clearance predictions and the mechanisms underlying hepatotoxicity, such as cholestasis (Dunn et al., 1989; Keemink et al., 2015; Liu et al., 1999; Mingoia et al., 2007). Despite the great potential attributed to this culture technique, expression of the genes responsible for the detoxification function of the liver decreases over time due to cell dedifferentiation. However, gene expression of phase II enzymes remains at a relatively high level in comparison with monolayer hepatocyte culture (de Bruyn et al., 2013; Kimoto et al., 2011; Norikazu et al., 2018; Soldatow et al., 2013). Another limitation of the sandwich-cultured hepatocytes model is the batch-to-batch variation in extracellular matrix substrates. Therefore, several approaches to overcome the limitations of the *in vitro* liver models have been proposed, including adjusting components of the culture medium and extracellular matrix, changing the cell culture format from monolayer to 3D organization, adding flow to the culture system, and culturing hepatocytes with non-parenchymal cells.

1.3.4. 3D *in vitro* models

In recent decades, there has been much evidence indicating that 3D cell culture more accurately reflects *in vivo* physiology by mimicking the architecture and cell-cell contacts found in intact tissue (Chatterjee et al., 2014). Thus, more and more research has focused on developing and optimizing various liver 3D culture strategies as superior tools for a multitude of applications in drug development (Mathijs et al., 2009).

One strategy for 3D hepatic tissues is to cultivate cells within scaffolds. These scaffolds are composed of natural or synthetic materials such as alginate, Matrigel®, loofa sponge or poly(lactic-co-glycolic) acid (PLGA), and allowed to mimic *in vivo* conditions thanks to their macroporous (>100µm) structure and native representation of ECM, as well as their capacity to transport nutrients and waste during cell cultivation (Hosseini et al., 2019; Pampaloni et al., 2009, 2007; Schaefer et al., 2012). Furthermore, the specific functions of hepatocytes, such as albumin synthesis, urea secretion, and CYP activity, are sustained (Chen et al., 2003; Makadia and Siegel 2011). Despite the advantages of scaffold-based culture, problems with controlling pore size and porosity, large batch-to-batch variations upon isolation from biological tissues and poor biomechanical strength have been observed (Han et al., 2019; Schaefer et al., 2012).

Hepatic spheroids were constructed with the assumption that cellular aggregates better mimic liver tissue characteristics. These spheroids can be generated from primary hepatocytes, cell lines or stem cell-derived hepatocyte-like cells by using different methods, such as hanging drop or culture plastic dishes with a non-adhesive surface. Establishing 3D cell-cell contacts and the secretion of ECM proteins within hepatic spheroids ensures the maintenance of differentiated liver functions such as albumin production and metabolic activity (Godoy et al., 2013; Skardal et al., 2012). Moreover, liver spheroids have been shown to be viable, functional, and stable in extended cultures of up to 4 to 5 weeks, unlike conventional hepatocyte 2D cultures (dedifferentiation after 2-3 days, Kazemnejad 2009). Nevertheless, hepatic spheroids have limited applications because of the presence of a hypoxic/necrotic core within the spheroid due to low oxygen diffusion or accumulated bile acids (Bell et al., 2016; Lauschke et al., 2016). Hepatic spheroids can also be encapsulated inside semi-permeable beads composed of biomaterials, such as alginate, and packed into a column to be perfused (Hendriks et al., 2016; Štampar et al., 2020). These systems preserve cell viability and functionality, as well as protecting cells from shear stress. Disadvantages include poor stability of the hepatocyte suspension, mass transfer problems, degradation of the microcapsules over time, and difficulties for cell retrieval (Lauschke et al., 2016; Makadia and S. J. Siegel 2011).

Progress in 3D bioprinting technology has led to the development of 3D liver bioprinting technology. This culture system consists in the fabrication of complex 3D biomimetic architectures using precise layer-by-layer deposits of biological materials with spatial control thanks to a computer (Selden et al., 2013). The three major bioprinting techniques are inkjet, laser-assisted, and extrusion bioprinting. Biological materials, called bio-inks, are composed of synthetic or natural hydrogel pre-polymer solution with encapsulated cells (Guo et al., 2003). More recently, decellularized extracellular matrices have been used as bio-ink

allowing the retention of a composition and relevant cues for cells (Pati and Cho 2017). Cells within 3D liver printing are in close proximity to each other, and rapidly form tight junctions and deposit their own ECM, yielding solid microtissues that resemble native liver in cellular density. This cell organization led to an increase in liver-specific gene expression, metabolic product secretion and CYP450 induction (Matai et al., 2020; Schaefer et al., 2012). Furthermore, 3D liver printing has advantages in terms of precise control, repeatability, scalability, and individual design. Nevertheless, printing techniques may reduce cell viability or induce other unknown consequences (Guo et al., 2003).

1.4. Liver organ-on-chip

As described above, several approaches have been developed in recent years to build an appropriate physiological micro-environment for liver tissue maintenance, and to improve the metabolic function of hepatocytes *in vitro*, including 3D cultures on scaffolds/hydrogels, spheroids, organoids and co-culture models (Polidoro et al., 2021; Ruoß et al., 2020). These approaches improve liver tissue organization, cell-cell and cell-ECM interactions, cell polarization, and maintenance of the liver functions (Polidoro et al., 2021). Nevertheless, despite their considerable advantages over traditional 2D culture models in Petri dishes, static 3D cultures still lack several key features essential for reproducing a physiologically relevant environment for liver cells. This is due to the absence of flow which is a key feature for the reproduction of mechanical cues (shear stress), zonation and multiple cell/organ co-cultures (Bovard et al., 2017; Moradi et al., 2020). The integration of dynamic culture presents several advantages regarding to the cell's metabolism via the constant renewal of the culture medium by supplying nutrients and the evacuating the cumulative toxins. In addition, the multi-organ coupling associated with biological barriers allows a better understanding of the ADMET profile of newly discovered molecules (Redaelli and Long 2022). In the last decade, organ-on-chip (OoC) technology has emerged as a promising alternative for overcoming these limitations by reproducing a more physiological microenvironment that reproduces the key biological features of cells and organs *in vivo* (Bovard et al., 2017; Moradi et al., 2020). Thus, OoC technology appears to be a powerful tool for replacing the traditional paradigms based on animal experiments and 2D/3D *in vitro* static cell culture methods (Ingber 2020). Figure 1.2. illustrate and compare liver OoC technology with the different experimental liver model for toxicity studies.

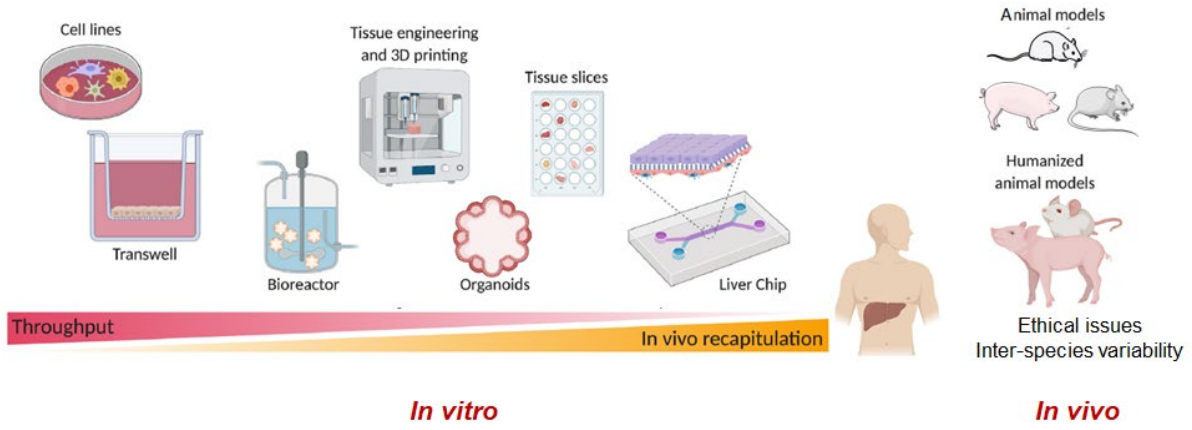

Figure 1. 2. *Current liver experimental models for toxicity studies. The schematic representation of in vitro models highlights the throughput and physiological relevance of each model (reproduced with permission from Moradi et al., 2020).*

1.4.1. OoC technology

OoC technology refers to a class of microfluidic devices that make possible the culture of cells or tissues in a dynamic environment engineered to reproduce the physiological architecture and function, and the associated *in vivo* microenvironment (Bhatia and Ingber 2014). These devices that mimic the functions of organs *in vitro* are also called microphysiological systems (MPS, Piergiovanni et al., 2021). An OoC consists of three principal elements: i) a microfluidic device, most commonly based on glass or polymeric material, with microchannels for medium perfusion and microchambers for cell culture; ii) living cells or tissues; iii) microfluidic flow (generated by a pump or pressure controller) through the device's inlet/outlet providing culture medium for the cells/tissues (van Berlo et al., 2021). The cell culture in microfluidic biochips allows precise control of the cell micro-environment and can faithfully emulate multiple characteristics of native cells/organs: 3D architectures, cell-cell and cell-ECM interactions, continuous nutrient exchange and waste removing, zonation, physiological shear stress, and chemical gradients (Akarapipad et al., 2021; Bhatia and Ingber 2014; Moradi et al., 2020). Using microfluidic devices can also efficiently reproduce physiological multiorgan interactions, where the multiple organ models cultured in separate biochips or multi-OoC platform are connected together through microfluidic tubing or microchannels (Essaouiba et al., 2020. Malik et al., 2021; Picollet-D'hahan et al., 2021). Moreover, microfluidic technology offers the advantages of incorporating biosensors and bio-actuators to control the cultures, provide rapid analysis, and apply electrical or mechanical stimuli (Akarapipad et al., 2021; Malik et al., 2021; van Berlo et al., 2021).

Selecting appropriate materials for the microfluidic device is one of the fundamental steps in OoC development. As the devices are used for biological applications and cultures of living cells, there are several parameters to consider regarding the choice of the material: biocompatibility, optical transparency for microscopic imaging, robust and tunable mechanical properties, ease of sterilization, chemical inertness and gas permeability (Campbell et al., 2020; Kurth et al., 2020; Malik et al., 2021). The cost and ease of fabrication are also important factors when considering large-scale production and OoC standardization (Campbell et al., 2020; Kurth et al., 2020). Due to its distinctive properties, including biocompatibility, good transparency, and permeability to oxygen, polydimethylsiloxane (PDMS) remains the most frequently used materiel for OoC devices (Ahadian et al., 2018; Campbell et al., 2020; Picollet-D'hahan et al., 2021). In addition, PDMS is inexpensive, easily processable with soft lithography for prototyping, and its elasticity makes it possible to replicate complex 3D microstructures with regular and precise patterns (Ahadian et al., 2018; Suzuki et al., 2017). Nevertheless, PDMS also has several limitations, particularly strong absorption of hydrophobic molecules and incompatibility with mass production (Campbell et al., 2020; Toepke and Beebe 2006). To overcome the drawbacks associated with PDMS-based OoC, glass can be used due to its outstanding properties, especially low drug absorptivity, transparency, and biocompatibility. However, glass remains costly and not gas permeable (Campbell et al., 2020; Ding et al., 2020). In the last decade, several alternative materials have been used for OoC applications. These alternatives include mainly elastomers and thermoplastic polymers: thermoset polyester (TPE), polyurethane (PU), styrene-(ethylene/butylene)-styrene (SEBS) copolymer, tetrafluoroethylene-propylene (FEPM), perfluoropolyether (PFPE), poly (methyl methacrylate) (PMMA), cyclic olefin copolymer (COC), polycarbonate (PC), polystyrene (PS), poly (vinyl chloride) (PVC), polysulfone, poly (lactic acid) and polytetrafluoroethylene (PTFE) (Campbell et al., 2020; Ding et al., 2020; Gencturk et al., 2017; Jellali et al., 2016a; Ren et al., 2013; Sollier et al., 2011). Of the polymeric materials, thermoplastics are excellent candidates for large-scale production and commercialization as they are low-cost and can be processed by injection molding (Ren et al., 2013). Combining two or more materials is another promising approach for developing hybrid devices drawing benefits from different substrates while avoiding their limitations. In recent years, several hybrid microfluidic devices combining PDMS with PC, glass and COC or fluorinated ethylene propylene (FEP) with COC have been reported in the literature (Chang et al., 2014; Kulsharova et al., 2021; Tan et al., 2019; Tonin et al., 2016). Recently, progress in 3D bioprinting has offered the opportunity to introduce new materials, such as hydrogels (naturel or synthetic): collagen, alginate, gelatine, hyaluronic acid, polyethylene glycol (PEG),

polylactic acid (PLA), polylactic-co-glycolic acid (PLGA) and polycaprolactone (PCL) (Bhattacharjee et al., 2016; Campbell et al., 2020; Yi et al., 2017).

Microfluidic devices can be manufactured using various microfabrication methods, including photolithography, soft lithography, laser and chemical etching, micromilling, hot embossing, injection moulding and 3D printing (Kurth et al., 2020; Puryear et al., 2020). The choice of manufacturing process depends on the material. As PDMS is the preferred OoC substrate, soft lithography or replica moulding remains the most common microfabrication technique for OoC (Puryear et al., 2020). Soft lithography implies the casting of a mixture of liquid PDMS and a curing agent on a mould previously manufactured by lithography or etching. After curing by heating, the micro-structured PDMS layer is peeled from the mould and sealed to a glass cover or another PDMS layer using plasma treatment to form the microfluidic device (Bhatia and Ingber 2014; Tsao 2016). Hot embossing and injection moulding, two processes suitable for industrial production, are the methods of choice to process thermoplastics (Ren et al., 2013; Tsao 2016). In both processes, materials are heated above their glass-transition temperature (Tg) (under high pressure). The reshapable materials are then brought into contact with the mould and the patterned device is obtained after cooling (Tsao 2016; Waldbaur et al., 2011). The bonding of such thermoplastic devices can be achieved using thermal fusion, solvents, surface modification and adhesives (Tsao 2016). Of the new technologies, 3D printing has emerged in recent years as a promising tool for microfluidic biochip manufacturing. 3D bioprinting, or additive manufacturing, is a process of creating layer-by-layer a 3D object through the selective application of materials (Bhattacharjee et al., 2016; Waldbaur et al., 2011). There are three main 3D printing techniques suitable for microfluidic biochip manufacturing: stereolithography (SL), fused deposition modelling (FDM) and photopolymer jetting (multi-jet modelling, MJM) (Bhattacharjee et al., 2016; Puryear et al., 2020; Weisgrab et al., 2019). The use of 3D printing offers several advantages, including the rapid and cost-effective production of devices with highly complex architectures and shapes, and the possibility of easily integrating various elements into the microfluidic device, such as sensors, connectors and valves (Ho et al., 2015; Weisgrab et al., 2019; Zhou 2017). The major limitations of 3D printing technologies remain their lack of biocompatibility, the insufficient patterning resolution and the non-transparency of the materials, which excludes microscopic imaging (necessary in microfluidic applications) (Bhattacharjee et al., 2016; Picollet-D'hahan et al., 2021).

1.4.2. Cell sources for liver OoC

In addition to the microfluidic biochip design and material, the choice of cell types and sources is crucial for building correct and physiologically relevant *in vitro* liver models and

particularly OoC models. Hepatocytes represent approximately 60% of the total liver cells and are responsible for most hepatic functions. Thus, hepatocytes are the major/unique cell type in a liver OoC. The potential hepatocyte sources for liver OoC can be divided into three main groups: primary cells (animal and human), immortalized cells, and induced pluripotent stem cells (iPSCs) (Beckwitt et al., 2018; Moradi et al., 2020). The advantages and limitations of the different types of hepatocytes are presented in Figure 1.3. To construct liver OoC models that adequately reflect the complexity and functionalities of the liver, hepatocytes can be cultured with non-parenchymal cells (NPCs): liver sinusoidal endothelial cells (LSECs), Kupffer cells (KCs), hepatic stellate cells (HSCs) and cholangiocytes.

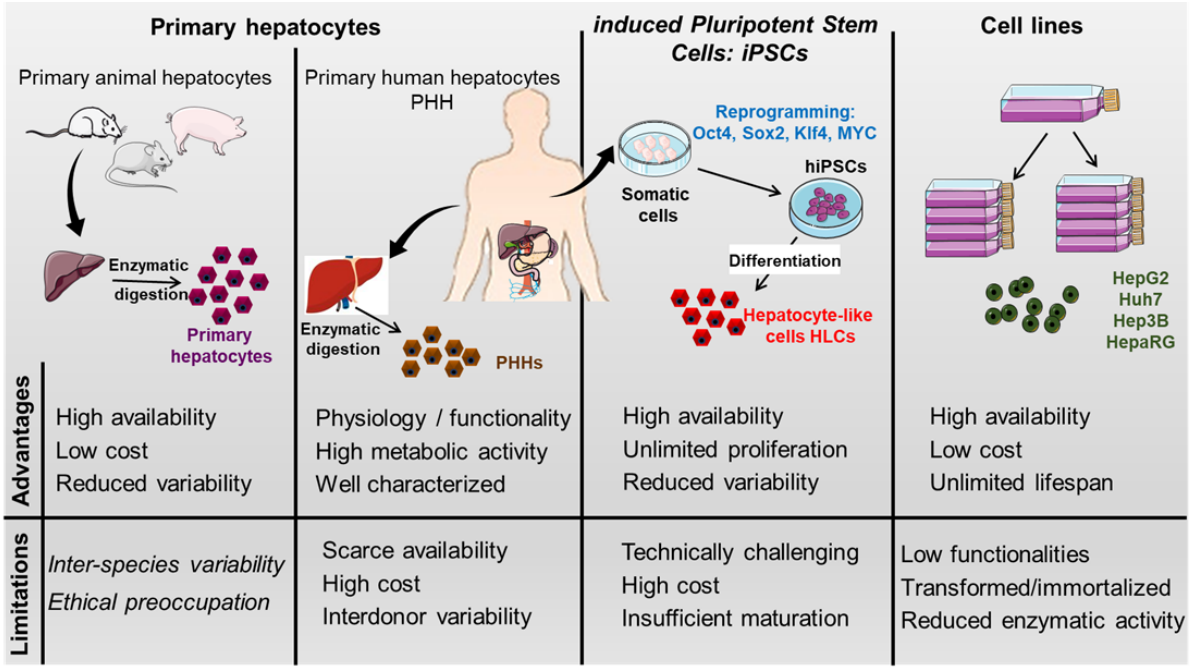

Figure 1.3. *A summary of advantages and limitations of the potential cell sources of hepatocytes for in vitro liver OoC models.*

1.4.2.1. Primary hepatocytes

Primary human hepatocytes (PHH) obtained from liver biopsies or non-transplantable livers are still considered to be the gold standard for developing human-relevant *in vitro* liver models. Due to their origin, they accurately reflect the physiology and functionality of the liver and represent an invaluable model for *in vitro* drug metabolism and toxicity studies (Beckwitt et al., 2018; Donato and Tolosa 2019; Zeilinger et al., 2016). Moreover, the development of cryopreservation protocols has facilitated access to PHHs and their use for *in vitro* models (Khetani et al., 2015; Zeilinger et al., 2016). PHHs lose their phenotypes and functionalities after two/three days when cultured in a 2D static environment (LeCluyse et al. 2005). Nowadays, progress in tissue engineering and microfabrication (3D spheroids and

hydroscaffold culture, and OoC) makes it possible to maintain functional PHH cultures for several weeks (Bell et al., 2016; Hegde et al., 2014; Jellali et al., 2016b; Moradi et al., 2020; Zeilinger et al., 2016). However, despite the progress in hepatocyte extraction, cryopreservation and culture, the use of PHHs remains limited by several factors, including the inability to proliferate, high costs, limited availability, and batch-to-batch variability.

Primary hepatocytes from animals can be also used for *in vitro* liver models. These hepatocytes, especially from rats and mice, are widely used because of their attractivity. They represent an abundant source of fresh primary cells and exhibit good stability and hepatic functionality in culture (Beckwitt et al., 2018). However, there are considerable limitations for the use of animal hepatocytes: functional differences between animal and human hepatocytes (differential cytochrome activity), inter-species variability and ethical concerns (Beckwitt et al., 2018; Khetani et al., 2015; Olson et al., 2000). In recent years, the use of Upcyte hepatocytes for drug metabolism and toxicity studies has been reported in several works (Burkard et al., 2012; Ramachandran et al., 2015; Tolosa et al., 2016). Upcyte hepatocytes are PHHs genetically modified to acquire proliferative capacity without being immortalized and retaining the phenotype of primary cells (Burkard et al., 2012). Nevertheless, although these cells present several interesting properties, there is a considerable lack of information regarding their phenotypic stability and performance (compared to other cell sources, Lauschke et al., 2016).

1.4.2.2. Hepatic cell lines

The alternative choices to PHHs are immortalized hepatic cell lines, such as HepaRG, Fa2N-4, HepG2/C3a, Hep3B, Huh7 (Donato et al., 2013). Cell lines are derived from tumour tissue (hepatocellular carcinoma) or generated by immortalization of primary hepatocytes (Donato et al., 2013). These cells are widely used in drug metabolism and toxicology studies due to their many advantages, including the unlimited propagation potential, ease of use, good availability, stable phenotype, lack of inter-donor variability, and low costs (Gomez-Lechon et al., 2008; Zeilinger et al., 2016). However, they present limited performances and functionalities regarding metabolic activity and sensitivity to hepatotoxins and are only suitable for the early stages of drug or chemical evaluations (Beckwitt et al., 2018; Deng al, 2019; Kuna et al., 2018). Among immortalized cells, the human hepatocellular carcinoma-derived HepG2/C3a line is one of the most commonly used for *in vitro* liver models (Gómez-Lechón et al., 2014). Although HepG2/C3a exhibit several hepatic characteristics (albumin secretion, metabolism of several xenobiotics), they lack relevance for drug screening and toxicity studies because of their low and variable levels of CYP450 enzymatic activity and poor expression of transporters (Gómez-Lechón et al., 2014; Khetani et al., 2015; Moradi et

al., 2020). HepaRG cells, human bipotent progenitor cells, are an interesting alternative to PHHs for preclinical drug metabolism and hepatotoxicity assessments. Altogether, HepaRG present similar features to those of PHHs, including high expression of phase I and II drug metabolizing enzymes, secretion of liver plasma proteins and of hepatobiliary transporters (Fernandez-Checa et al., 2021; Zeilinger et al., 2016). The major drawbacks of these cells are the use of DMSO for differentiation, and the long culture process.

1.4.2.3. Human induced pluripotent stem cells (hiPSCs)

In recent decades, human hepatocyte-like cells (HLCs) derived from stem cells (adult stem cells and pluripotent stem cells PSCs) have emerged as an attractive cell source for *in vitro* liver models, with the potential for large-scale production. Stem cells are capable of self-renewing and differentiating into mature cells of a particular tissue type, allowing the generation of all cell types from the human body (Coll et al., 2018; Zeilinger et al., 2016). Of these stem cells, PSCs, i.e. embryonic stem cells (ESCs) and induced pluripotent stem cells (iPSCs), are the most commonly studied for differentiation in HLCs (Boeri et al., 2019). The use of human embryonic stem cells (hESCs) raises ethical problems and is strictly regulated, or even prohibited in many countries (Volarevic et al., 2018). iPSCs can be obtained from somatic cells following the reprogramming technology developed by Yamanaka's team (Takahashi et al., 2007). Contrary to ESCs, hiPSCs raise fewer ethical problems and can be easily established from abundant cell sources such as skin fibroblasts, blood cells, and renal epithelial cells in urine samples (Karagiannis et al., 2019). Currently, it is assumed that hiPSCs can be differentiated using several protocols and generate HLCs reproducing many hepatic features, including morphology, albumin and urea secretion, glycogen storage, and drug metabolism (Beckwitt et al., 2018; Si-Tayebet al., 2010; Takayama al., 2012; Zeilinger et al., 2016). In addition to availability, the advantages of hiPSCs include minor batch variability and good sensitivity (comparable to PHHs) for detecting drugs causing hepatotoxicity (Gómez-Lechón et al., 2014; Ware et al., 2015). Therefore, hiPSCs could provide a limitless supply of hepatocytes for drug/chemical hepatotoxicity assessments. However, there are still some limitations to the widespread use of hiPSCs: incomplete maturation of hepatocytes, epigenetic memory, and high cost and experimentation time (Beckwitt et al., 2018).

1.4.2.4. Non-parenchymal cells (NPCs)

As for PHHs, there are three main sources of NPCs for liver OoC development: primary cells, hepatic cell lines, and hiPSCs (Beckwitt et al., 2018; Gough et al., 2020). Human primary LSECs, KCs and HSCs can be isolated, separately or simultaneously, from the liver

using the same protocol as hepatocytes (enzymatic digestion, Zeilinger et al., 2016). Although primary NPCs are the best choice for reproducing the *in vivo* microenvironment, their use is limited due to scarce availability, low yield and the presence of impurities during the isolation process, high costs and rapid loss of functions in *in vitro* culture (such as loss of fenestration for LSECs and non-specific activation for HSCs and KCs, Beckwitt et al., 2018; Khazali et al., 2017; Xu et al., 2005). As an alternative to primary NPCs, several immortalized cell lines have been developed and used in co-culture with hepatocytes: TMNK-1, TRP3 and SKHEP-1 for LSECs; hTERT-HSC, GREF-X, LI90, TWNT-1, LX-1 and LX-2 for HSCs; THP-1 and U-937 for KCs, and MMNK and HepaRG for cholangiocytes (Beckwitt et al., 2018; Gough et al., 2020; Khazali et al., 2017; Maepa and Ndlovu 2020; Xu et al., 2005). However, immortalized NPCs lack the main features of primary cells and do not emulate *in vivo* physiology (Beckwitt et al., 2018; Gough et al., 2020). In recent years, several protocols have been proposed for iPSC differentiation into LSECs (Danoy et l., 2021; Koui t al.,2017), HSCs (Coll et al., 2018; Koui t al.,2017; Vallverdú et al., 2021), KCs (Tasnim et a., 2019) and cholangiocytes (de Assuncao et al., 2015; Sampaziotis et al., 2015). Nevertheless, contrary to the abundance of studies related to HLC generation, only a few protocols have aimed to differentiate iPSCs into NPCs. Moreover, the cells obtained are only partially mature and the protocols used still need to be improved by optimizing culture medium (small molecules and growth factors concentrations), supports of culture (3D, ECM and dynamic microfluidic cultures) and coculture of different liver cell types (Tricot et al., 2022).

1.4.3. Different liver OoC approaches

1.4.3.1. 2D monolayer culture

The most common approach when developing microfluidic systems for the monolayer culture of cells is based on lithography patterned substrates. It has been proven that culturing hepatocytes on these substrates enhances the hepatic functionalities by precisely and reproducibly controlling the distribution of the different cell types and providing biochemical cues for both parenchymal and non-parenchymal cells (Kidambi et al., 2007). The pioneers of the liver-on-chip models were Allen & Bhatia, who developed a polysulfone-based perfusable flat-plate bioreactor and used it to co-culture primary rat hepatocytes with fibroblasts from the cell line J2-3T3 (Allen and Bhatia, 2003; Allen et al., 2005). Comparing their developed model with conventional static 6-well plates, they demonstrated that the oxygen gradients produced by the flow circulation recreated regional compartmentalization, which mimics the liver zonation which cannot be observed in static plates.

Depending on the applications and the cell's preferences, different substrates and coatings can be used to enhance adhesion and proliferation. Jellali et al. proved that, depending on the substrates (PFPE or PDMS) and the coatings (fibronectin or collagen), the behaviour of the cells differed (Jellali et al., 2016a). Schoenenberger et al. reported similar findings, demonstrating that cell (Madin-Darby canine kidney cell line, MDCK) adherence to fibronectin-coated surfaces was less effective than other proteins, such as collagen IV, collagen I, laminin and vitronectin (Schoenenberger et al., 1994). To investigate the potential of liver biochips compared to conventional Petri dishes, Jellali et al. developed a microfluidic bioreactor for human hepatocyte culture (Jellali et al., 2016b). The biochip was composed of microchambers connected by microchannels, allowing the circulation of culture medium inside the network, and was coated with collagen for hepatocyte adhesion. The hepatocytes retained their activity while showing increased expression of major cytochrome P450 genes and higher urea and albumin production in comparison with Petri dishes. In addition, when exposed to midazolam and phenacetin, the hepatocytes maintained their metabolic activity. This was confirmed by measuring CY3A4 and CYP1A2 activity which was 5000 and 100 times higher, respectively, in biochips than in Petri dishes. The authors successfully maintained the culture of functional hepatocytes in biochips for 13 days (Jellali et al., 2016b).

In the natural liver, hepatocytes are shielded by a layer of sinusoidal endothelial cells, which protects them from the direct shear of blood flow and influences mass transport consistency (Ng et al., 2006). Xia et al. developed a laminar-flow perfusion bioreactor for immediate-overlay sandwich culture of hepatocytes. The bioreactor consists of an acrylic body and top sealed with an O-ring (Figure 1.4A). First, the hepatocytes are extracted and seeded on a collagen-coated membrane and overlaid with collagen-coated inserts. Then, the system is secured with the O-rings. The sandwich cassette is then deposed in the cellular compartment of the bioreactor. The culture chamber is connected by two channels linked to a peristaltic pump for flow circulation. They successfully maintained liver specific functions for two weeks, with hepatocytes exhibiting restored polarity and biliary excretion. In addition, the cells produced sensitive and consistent drug toxicity responses (Xia et al., 2009).

1.4.3.2. Matrix-free liver spheroids/organoids-on-chip

The previously described two-dimensional (2D) monolayer culture does not reflect *in vivo* physiology where the tissues are in 3D with different topographical organization that affects cell responses (Lee et al., 2014). Different approaches have been used to construct such a 3D communication network, like hanging drop, spinner flask, cells cultured on non-adherent surfaces, and micromoulding (Ma et al., 2018). The principle of these methods consists of reassembling the cells by applying an external force or by conditioning the cells to self-

assemble. The cells re-created in suspension pass through an aggregation step, followed by a compaction phenomenon to form compact 3D structures (spheroids or organoids). Weng et al. worked on developing a scaffold-free liver-on-chip mimicking the liver lobule (Weng et al., 2017). This was achieved by cultivating primary hepatocytes and hepatic stellate cells (HSCs) on a micropatterned PDMS biochip. To obtain the 3D structure, the cells were deposited on the multi-layered collagen coated PDMS to form the 3D biological template. The system was enclosed with a hydrophilic flow diverter making possible vertical cell anchorage and connected to a peristaltic pump circulating the culture medium. The system was designed in a hexagonal form with six inlets and one central outlet mimicking the flow arriving from the portal vein and evacuated from the central vein. Following the flow diversion, the F-actin polarized to the peripheral cortex of the cells and developed a 3D intracellular skeletal network which formed a hierarchical tissue. Building the hepatic hierarchical organization mimicking *in vivo* conditions demonstrated the potential of the model in recreating hepatic zonation, which is a key feature for predicting hepatotoxicity.

Another approach is commonly used to form scaffold-free spheroids by cultivating cells in concave microwells. Ma et al. developed a concave microwell based on PDMS-membrane-PDMS sandwich multilayer chips for hepatocyte culture (Figure 1.4B, Ma et al., 2018). The system integrated the possibility of forming scaffold-free spheroids using a V-shape structure and the mimicking of hepatic sinusoidal endothelial cells. The cells are seeded in PDMS V-shaped microwells for spheroid formation, then a perfusion system is mounted using a transwell-based microporous membrane on top of which the culture medium circulates. This model demonstrated high cell viability and maintenance of hepatic polarity, liver-specific functions and improved metabolic activity compared to conventional perfusion methods.

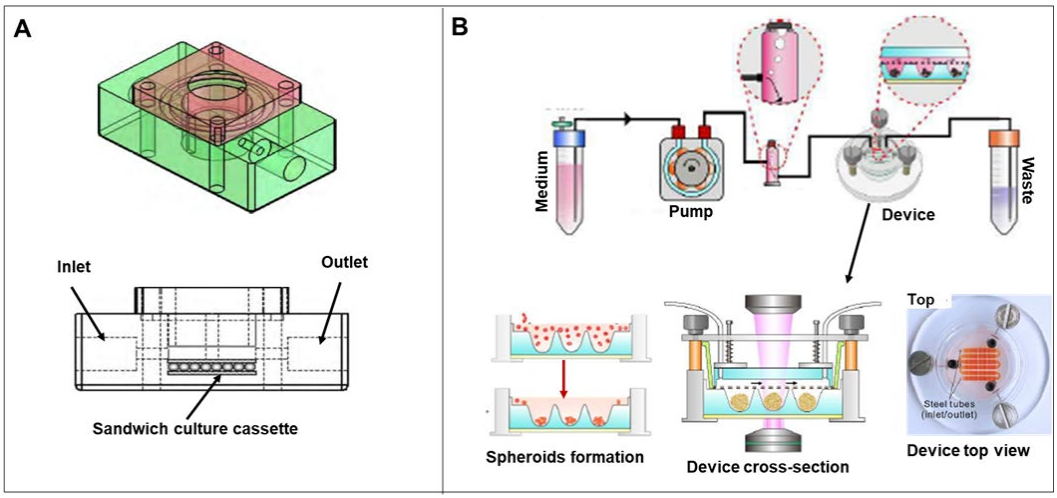

Figure 1.4. *Examples of liver OoC platforms with different approaches. (A) laminar-flow perfusion bioreactor for sandwich culture of monolayer of rat hepatocytes (reproduced with permission from Xia et al., 2009); (B) biomimetic liver-on-a-chip platform with V-shape microwells (3D-LOC) allowing HepG2/C3a spheroids formation and long-term culture (reproduced with permission from Ma et al.,2018)*

1.4.3.3. Scaffold/hydrogel-based 3D liver OoC

One of the main focuses of liver research and development is the 3D organization of cells to obtain relevant liver phenotypes and functionalities. In addition to the cell self-assembly methods cited above, 3D organization of cells can be obtained using a hydrogel/scaffold matrix (alginate, hyaluronic acid, gelatine, collagen, Matrigel) integrated within the biochip (Deng et al., 2019). Using hydrogel and scaffold reproduces ECM behaviour and offers the possibility of tuning the cells' microenvironment by modifying the composition of the matrix and/or the mechanical properties (Cui et al., 2017; Fang and Eglen, 2017). Toh et al. developed a 3D hepatocyte chip (3D HepaTox Chip) based on a multiplex microfluidic channel allowing the 3D culture and maintenance of hepatocyte functions (Toh et al., 2009). The biochip consists of a central culture compartment where cell suspension of hepatocytes is loaded using a single inlet. The cells were cultured in a methylated collagen and negatively-charged HEMA-MMA-MAA terpolymer, which is a matrix favouring the 3D organization of hepatocytes. The central chamber is flanked by 2 side perfusion compartments with elliptical micropillars through which the culture medium and drug solution pass by diffusion to the hepatocytes, generating a gradient of concentration. The hepatocytes cultured in the biochip showed cell-cell and cell-ECM interactions, maintained their metabolic functions, and made it possible to assess the hepatotoxicity of 5 model drugs (acetaminophen, diclofenac, quinidine, rifampicin and ketoconazole).

Considering that the elastic properties of the liver depend on its physiological state, Boulais et al. integrated an alginate-based cryogel with controlled stiffness into a hepatic biochip (Boulais et al., 2021). They successfully managed to obtain a fine-tuned Young's modulus between that of relatively soft, healthy tissue (~4 kPa) and that of a cirrhotic tissue associated with greater stiffness (~ 15 kPa). The hydrogel made it possible to create a 3D microenvironment which, associated with the perfusable culture system, represents a promising tool for reliable *in vitro* model for drug toxicity and efficacy studies (Boulais et al., 2021).

Hydrogels containing cells can even be shaped to form larger structures. For instance, Massa et al. encapsulated the HepG2/C3a cell line in a gelatine methacryloyl (GelMA) hydrogel and constructed a central vessel using a sacrificial agarose fibre (Figure 1.5A, Massa et al., 2017). The central vessel was used as a hollow capillary where endothelial cells were seeded and cultured to form a perfusable monolayer. Through this monolayer, nutrients, oxygen media and drugs could diffuse to reach the 3D organized hepatocytes. This vascularized liver tissue model was subsequently used for continuous perfusing flow and the authors assessed the metabolic activity and viability of the cells after being treated

with APAP. They found that incorporating vascular components led to an increase in viability of the hepatocytes compared to those that were directly exposed. This can be explained by the delay in the drugs' diffusion due to their passage through the barrier or their metabolization, which may lower their concentration. Massa et al. thus reproduced *in vivo* vascularization which created a more realistic drug response *in vitro* (Massa et al., 2017).

1.4.3.4. 3D liver OoC using bioprinting

Recently, 3D bioprinting has been used to manufacture organ-on-chip models. Bioprinting is based on using a bio-ink (composed of cells, matrix, and nutrients) which is precisely deposited on a scaffold layer-by-layer to generate a tissue. Thanks to its ability to print multiple materials and cell types simultaneously, with good spatial resolution, and obtain the desired 3D cellular arrangement, bioprinting can facilitate the creation of a biomimetic environment with the biochip. Thus, the combination of bioprinting and organ-on-chip makes it possible to create complex and biomimetic *in vitro* models for simulation, mechanistic and pharmacological modulation (Yu and Choudhury, 2019).

Organ-on-a-chip models often consist of 3D complex structures composed of microchannels, allowing them to replicate the architecture of native tissue and organs. However, it is hard to control the property and microstructure of soft scaffolds. Bioprinting bypasses this drawback by allowing fine-tuning of the mechanical properties, porosity, micro-structure, and polymerization mechanisms of the hydrogel scaffolds (Lee and D. W. Cho, 2016).

In the last decade, several 3D-printed liver-on-chip models have been developed. Snyder et al. studied the effectiveness of a radioprotective pro-drug by integrating cell printing into a microfluidic device (Snyder al., 2011). The printed biochip was composed of a PDMS substrate and a glass cover. Hepatocytes (HepG2) and epithelial cells (M10) were individually embedded in a Matrigel solution then printed within the PDMS substrate into separate chambers and the whole system was then dynamically perfused with a syringe pump. The authors highlighted that their printed microfluidic device was able to maintain the metabolism activities of both cell types (Snyder al., 2011).

Recently, another liver-on-a-chip platform has been developed by Bhise et al., with hepatic spheroids (HepG2/C3a cells) fabricated via direct bioprinting in a microfluidic bioreactor device (Figure 1.5B, Bhise et al., 2016). This model consists of liver tissue printed directly into a microfluidic device which is then assembled around the bioprinted tissue, and serves as a bioreactor to maintain long-term viability (30-day culture period). During the 30 days of culture, the HepG2/C3a spheroids remained functional (albumin, alpha-1 Antitrypsin and transferrin secretions) and exhibited major hepatocyte markers (cytokeratin 18, MRP2 bile canalicular protein and tight junction protein ZO-1). Further, this device bypasses a major

drawback of microfluidics by being easily disassembled and reassembled, thus allowing access to the cells over the course of the experiment (Bhise et al., 2016; Knowlton and Tasoglu 2016)[1,2].

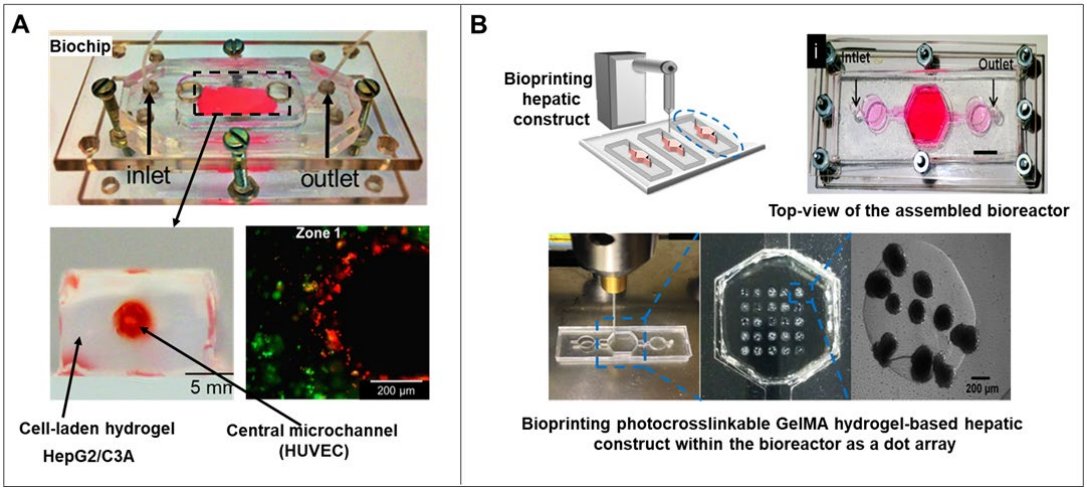

Figure 1.5. *Examples of liver OoC platforms with different approaches. (A) 3D vascularized liver OoC model created with HepG2/C3a cells encapsulated in a gelatin methacryloyl hydrogel and HUVECs cells into a central microchannel (reproduced with permission from Massa et al. 2017): (B) microfluidic liver-on-a-chip model with direct bioprinting approach for the formation of 3D hepatic cell line (HepG2/C3a) spheroids (reproduced with permission from Bhise et al., 2016).*

1.4.4. Contribution of OoC technology to the improvement of *in vitro* liver models

The zonation of the hepatocytes in the liver sinusoid is a key feature of the liver characterized by a gradient of activities and functions along the lobule. This gradient remains rarely if ever reproduced in conventional in vitro static cultures (Lee et al., 2021). In contrast, microfluidic systems offer the ability to achieve a stable gradient mimicking liver zonation, especially for oxygen which play a key role in metabolic zonation (Kietzmann 2017). The dynamic flow allows the delivery of oxygen throughout culture medium perfusion and the diffusion (under laminar flow) creates the oxygen gradient (Lee et al., 2021). To improve and accurately control oxygen supply and diffusion in a microfluidic device, two main approaches are used: engineering and chemical approaches (Palacio-Castañeda et al., 2022). In engineering approach, the oxygen diffusion is controlled by combining oxygen-permeable (PDMS) and -impermeable (e.g., glass, PMMA, PS and PC) materials to build the microfluidic device (Funamoto et al., 2012; Palacio-Castañeda et al., 2022; Sleeboom et al., 2018). The chemical approach involves adding oxygen or oxygen scavenging/generating chemicals to the perfused fluid (Lee-Montiel et al., 2017; Palacio-Castañeda et al., 2022). OoC technology allows also the control of chemicals and hormones gradients to generate metabolic zonation (Lee et al., 2021; McCarty et al., 2016). Other advantages of the dynamic flow in OoC include the ability to provide controlled shear stress emulating the *in vivo*

mechanical stimulus applied by blood flow on cells and the regulation of drugs/metabolites concentrations, which facilitated drug screening (Lee et al., 2021).

The liver is composed of several cell types that interact with each other to maintain physiological functions. Therefore, coculture approaches are recommended to build relevant liver models. Unlike conventional culture methods, the advances in microfabrication techniques make the OoC technology suitable for co- or multi-culture of several cell types, while maintaining cell-cell interactions via the fluid perfusion (Lee et al., 2019). Among the relevant models, several groups have developed liver OoC devices integrating porous membrane hosting LSECs and mimicking endothelial barrier (Du et al., 2017; Hegde et al., 2014. Prodanov et al., 2016). These devices consist of two compartments separated by the porous membrane. The hepatocytes are generally hosted in the bottom chamber, whereas LSECs are cultivated in the perfused top chamber (upon the membrane) and allow the diffusion of nutrients and chemicals to hepatocytes.

In drug development and chemical risk assessment, the reproduction of ADMET (absorption, distribution, metabolism, excretion and toxicity) process is crucial to validate the safety and/or efficacy of the target molecule (Cheng et al., 2012). This process (ADMET) cannot be recreated with the conventional *in vitro* screening tools such as Petri dish and multi-well plate. Thanks to the fluidic flow, OoC technology allows the recreation of multiorgan interactions. In such multi-OoC platform, the different organs are cultured in separate biochips/compartment and connected together through microfluidic tubing or microchannels (Picollet-D'hahan et al., 2021). As the centre of chemicals/drug metabolism, the liver is present in the majority of multi-OoC reported in the literature (Lee et al., 2021; Picollet-D'hahan et al., 2021; van Berlo et al., 2021).

1.5. Liver OoC for toxicity studies

Several research works have been carried out on establishing liver-on-chip models to predict chemical toxicity. The main challenge encountered when developing these models is to recreate the *in vivo* microenvironment of the cells. Knowing that hepatocytes rapidly dedifferentiate when cultured *in vitro*, optimizations have been proposed to maintain their differentiation state and the maintenance of their functions, especially the metabolization of drugs/xenobiotics in an *in vivo*-like situation. Several parameters should be taken in consideration when developing a microfluidic system for hepatocyte culture (Brandon et al., 2003). The microfluidic system should be adapted for 3D cultures due to the advantages it confers in the promotion of cell-cell and cell-matrix interactions. In addition, the system should be suitable for the co-culture of different cell types, such as fibroblasts and endothelial cells which enhance hepatocyte functions (Sivaraman et al., 2005). A non-

exhaustive list of measurements has been assessed by Baudy et al., to build a relevant liver *in vitro* model (Baudy et al., 2020). The aim is to set up fundamental target thresholds to ensure that adequate quantities of metabolites are generated during drug testing. The first stage of the model validation process consists of characterizing performances by measuring albumin, urea and gene expression of the key metabolizing phase I/II enzymes and transporters over 14 days. Once the model passes this step it undergoes the second stage, which consists of assessing the predominant metabolizing enzymes and transporter functions, morphology, cytokine stability and the integrity of hepatobiliary networks. The result of these evaluations then either supports or rejects proceeding to the third stage where different compounds are tested to evaluate the sensitivity of the model for detecting major mechanistic categories of human hepatotoxicity (Baudy et al., 2020).

1.5.1. Drug toxicity studies

1.5.1.1. Drug-induced liver Injury (DILI)

DILI is a common cause of liver injury and accounts for approximately 50% of cases of acute liver failure (Donato and Tolosa, 2019). It occurs with an incidence ranging from 1 in 10 000 to 1 in 100 000 people, and it is the most common cause for drugs being withdrawn from the market and restricted for use (Kuna et al., 2018). The severity to DILI depends on the duration of exposure and the histological location of the injury. Depending on these factors, DILI can be considered acute or chronic, and manifests as hepatitis, cholestasis, or a mixed injury. The most important event in hepatitis is necrosis of the hepatocyte.

The first event occurring in DILI consists of inhibition of the mitochondrial respiratory chain. This inhibition causes an accumulation of the reactive oxygen species (ROS) and decreases adenosine triphosphate (ATP). In addition, the damage caused by toxic drugs inhibits the oxidation of fatty acids, which may cause steatosis or steatohepatitis (Fromenty and Pessayre, 1995). The association between these 3 events induces intracellular damage and leads to hepatocyte apoptosis. As apoptosis requires ATP, which is depleted because of the mitochondrial dysfunction, hepatocyte death follows a necrotic pathway, leading to hepatic inflammation (Leist et al., 1997).

The severity of DILI cases depends on the pathologies the liver is predisposed to and its sensitivity to the drugs that are metabolized. For example, hepatitis B, C, and non-alcoholic fatty liver disease (NAFLD) have been associated with increased susceptibility to the inflammatory reactions to the medication (Lee et al., 2005; Seeff et al., 1986). In addition, genetic factors predisposing patients to DILI have been identified as affecting polymorphisms on the cytochrome P450 enzymes which slow down either the metabolism of

toxic drugs or increase the generation of bioactive metabolites. Every class of medication can cause acute DILI that can be resolved by withdrawing the offending agent (Zafrani et al., 1979).

The failure to detect DILI during the drug development process can be attributed to the poor predictability of the screening methods (*in vitro*, *in vivo*, *ex vivo* and *in silico*) used in the preclinical phase (Donato and Tolosa, 2019). Current models are unreliable for detecting DILI due to the complex interactions involved in the genesis of DILI itself. In addition, these interactions imply genetic, non-genetic, and environmental factors that most of these models fail to recreate. The liver organ-on-chip models are emerging as an alternative solution for predicting hepatotoxicity thanks to the flexibility they confer (possibility of recreating a controlled cellular microenvironment) and the possibility of studying acute and chronic exposure to toxicants while maintaining cellular functionalities (Kuna et al., 2018).

1.5.1.2. Liver organ-on-chip model for drug toxicity

The pharmaceutical development of drugs is considered very costly ($2.6 billion per marketed drug) and inefficient (94% of drugs fail clinical trials, Knowlton and Tasoglu 2016). The most common cause of drug withdrawal during the clinical phase is drug-induced toxicity, caused by the low predictability of human liver toxicity. The battery of tests used for the marketing of potentially bioactive molecules requires the use of animal models for drug toxicity assays. As an alternative, researchers are starting to promote the potential of organ-on-chip-based platforms, essentially liver-on-chip due to the correlation between drug toxicity and hepatotoxicity, as an *in vitro* model for drug toxicity studies (Knowlton and Tasoglu 2016). In past decades, a variety of liver OoCs have emerged for different applications, including toxicity studies, studying metabolism, and disease modelling. Below, we review the applications of liver OoC in drug toxicity studies. We have also summarized in Table 1.1 the main liver OoC models reported for drug toxicity studies.

Snouber et al. investigated the toxicity of flutamide, an anticancer prodrug, and its toxic metabolite hydroxyflutamide on the HepG2/C3a cell line cultured in a PDMS biochip coated with fibronectin (Snouber et al., 2013). The metabolic activity of HepG2/C3a has been analysed by full metabolomic profiling. They observed a hepatotoxic reaction for the exposed group, illustrated by disrupted glucose homeostasis and mitochondrial dysfunctions compared to the non-exposed control group. In addition, the production of the toxic metabolite (hydroxyflutamide) led to specific mechanistic toxic signatures correlated with hepatotoxicity. Using the model designed, Snouber et al., proposed a list of biomarkers describing glutathione depletion, caused by both molecules' hepatotoxicity, which is followed by the death of the HepG2/C3a cells. Using the same liver biochip, Prot et al. investigated

acetaminophen (APAP) toxicity on HepG2/C3a cells using a proteomic and transcriptomic approach (Prot et al., 2011). They observed an induced NRF2 pathway and enhanced drug-related metabolism pathways. In addition, exposure to APAP provoked inhibited cell growth and a metabolic signature of APAP toxicity correlated with *in vivo* situations, such as modulated calcium homeostasis, lipid metabolism, and reorganization of the cytoskeleton. On the other hand, omics profiling revealed disturbances in DNA replication and the cell cycle in both the biochip and Petri dishes when exposed to APAP. Their research demonstrated the potential of microfluidic biochips as a tool for investigating drug toxicity studies.

To improve prediction of human hepatotoxicity, it is important to take into consideration *in vivo*-like hepatocyte organization and cell-matrix interactions. As described in Section 1.3.4, different approaches have been used to promote the 3D organization of the cells inside microfluidic systems. Zuchowska et al. investigated the effect of 5-fluorouracil (5-FU, an anticancer drug) on HepG2 spheroids formed in a microfluidic system integrating U-shaped designs (Figure 1.6A, Zuchowska et al., 2017). The intention to work with spheroids comes from their similarity to an early, vascular stage of tumours, which makes them an appropriate model for evaluating the cytotoxic properties of compounds. To obtain the HepG2 spheroid, the cells were seeded in a PDMS-based biochip composed of concave chambers and channels and, depending on the number of cells seeded, different spheroid diameters were obtained. They then correlated between the cross-sectional spheroid areas, which indicated the death or proliferation rate of the cells, and the cytotoxic effect of 5-FU. They observed a decrease in the cross-sectional area when the cells were treated with different concentrations of 5-FU. In addition, by evaluating the effect of the drug for 10 days, starting on the 8th day of exposure, the HepG2 spheroids acquired drug resistance for 5-fluorouracil. This phenomenon can only be noticed in the microfluidic systems, demonstrating the potential of the model designed by Zuchowska et al. for predicting drug resistance. Another application of the HepG2 spheroid-on-chip model for drug toxicity is the work by Knowlton et al., (Knowlton and S. Tasoglu, 2016) and Bhise et al., (Bhise et al., 2016) who developed a liver tissue model using a bioprinting approach for hepatic spheroids encapsulated in a hydrogel scaffold. The HepG2/C3a spheroids were assembled using a microwell technique then suspended in a gelatine methacryloyl (GelMA) hydrogel scaffold. Then, using a bioprinter, the spheroids were directly injected into the microfluidic device, forming liver tissue. By exposing these spheroids to an acute, toxic dose of APAP, they observed a significant decrease in both metabolic activity and cell density. The results obtained from this acute toxic exposure were correlated with similar animal and *in vitro* exposure models, confirming the potential for applying the model developed in drug toxicity analyses.

Hepatocyte cell lines have limited metabolic activity, which is a crucial feature when developing hepatic models for drug toxicity assessment. To overcome this limitation, Yu et al. used rat hepatocyte spheroids to evaluate the chronic drug response to diclofenac and acetaminophen in a liver-on-chip bioreactor (Figure 1.6B, Yu et al., 2017). The pre-formed hepatocyte spheroids were introduced into the biochip and compared with a collagen sandwich culture as the standard. By measuring the metabolism of phenacetin, bupropion, and midazolam, and the production of their metabolites: acetaminophen, OH-bupropion and OH-midazolam respectively, they observed enhanced hepatic functions that were correlated with the activity of CYP1A2, CYP2B1/2 and CYP3A2. In addition, the model was used to test the acute and chronic toxicity of diclofenac and APAP, and was found to be more sensitive in testing the chronic drug response. The toxic effect was only observed after 14 days of exposure and viability was significantly reduced compared to the collagen sandwich control.

One of the main challenges when developing a biomimetic liver model is ensuring its accuracy in predicting the toxicity of candidate drugs. Using rodent and non-rodent toxicity models may produce discordant results or fail to predict toxicity in humans. In the same context, Jang et al. designed a liver-chip containing species-specific rat, dog, and human primary hepatocytes co-cultured with liver sinusoidal endothelial cells, with and without Kupffer and hepatic stellate cells (Jang et al., 2019). The biochip was composed of 2 channels separated by a porous membrane. The upper channel hosted rat, dog, and human hepatocytes within an ECM-coated sandwich, and the lower channel contained species-specific liver endothelial cells, with or without Kupffer cells and/or stellate cells. By testing the toxicity of bosentan, a drug known to provoke DILI in humans but not in rats or dogs, they observed a hepatotoxic effect in the human liver-chip corresponding to the toxic plasmatic concentration which correlated the liver-chip response with the clinical response. In addition, the toxic concentration affected albumin secretion in humans and dogs, but not rats, which correlated with *in vivo* findings. Using the multispecies liver-chip detected the hepatotoxicity of bosentan more accurately than conventional sandwich monoculture plates. In addition to bosentan, after integrating species-specific nonparenchymal cells (NPC), hepatic stellate and Kupffer cells into the vascular channel, they tested the hepatotoxic effect of acetaminophen. They observed depletion of glutathione (GSH) and adenosine 5'-triphosphate (ATP) preceded by a decline in hepatocyte morphology and function. These results were confirmed by the decrease in albumin synthesis and the increase in oxidative stress-related markers.

Massa et al. successfully incorporated an engineered endothelial cell layer using human umbilical vein endothelial cells (HUVEC) in a 3D liver construct created with HepG2/C3a cells encapsulated in gelatine methacryloyl (GelMA) hydrogel (Figure 1.5A, Massa et al.,

2017). By continuously perfusing the vessel construct with APAP mixed with HUVEC culture media, they observed a decrease in HUVEC metabolic activity, viability, and damage disturbing confluency and the endothelial monolayer. In addition, when integrating the HepG2/C3a liver tissue, the APAP treatment resulted in cell death near the channel and higher viability in the vicinity of the channel. These results were correlated with those obtained when working with *ex vivo* models.

The integration of the HUVEC layer makes the model suitable for drug testing and promote the role of integrating vascularisation for their role in delaying the diffusion of drugs. Indeed, the HUVEC layer formed a barrier mimicking the *in vivo* drug administration process. in addition to their potential metabolic role for some drugs.

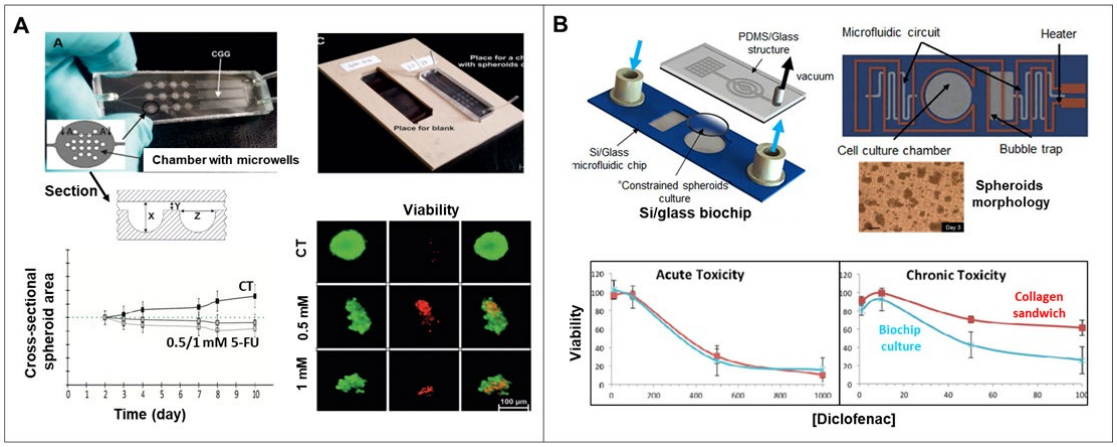

Figure 1.6. *Liver-on-a-chip models for drug toxicity assessment. (A) liver OoC microfluidic system integrating U-shaped designs for HepG2/C3a 3D spheroids formation and culture. The device enables long-term toxicity study of anticancer drug 5-fluorouracil with with simple and quick analysis (reproduced with permission from Zuchowska et al., 2017); (B) perfusion-incubator-liver-chip (PIC) for 3D culture of rat hepatocytes. The PIC integrates heater and CO2 system supply, and used for study of acute and chronic toxicity of APAP and diclofenac (reproduced with permission from Yu et al., 2017).*

1.5.2. Liver OoC for environmental and other toxicant studies

An environmental toxicant is any molecule produced by humans or introduced into the environment by human action. Toxicants represent a threat to human health, especially after long-term exposure (Mostafalou and Abdollahi, 2017). They can attain the human body through the skin, inhalation or ingestion, and be translocated to other organs by diffusion or transportation via the blood and lymph. Environmental toxicants can be classified into four major groups: natural toxins, heavy metals, endocrine-disrupting chemicals (EDCs), and nanomaterials (Akarapipad et al., 2021; Maqbool et al., 2016). Human exposure to environmental toxicants is mainly chronic through daily exposure to low doses (residues) of complex cocktails of toxicants present in the food supply, soil, water, atmosphere and

agricultural products (Jellali et al., 2018a). In risk assessment, most commonly, animal models or *in vitro* 2D cell cultures in Petri dishes are used. However, animal models lose their relevance when extrapolating the results to humans, and static cultures using conventional Petri dishes are poorly predictive and not suitable for long-term cultures (chronic studies). Due to their inherent advantages, such as a relevant physiological microenvironment and maintenance of long-term functionality, liver OoC systems offer a powerful approach for risk assessment of environmental toxicants. However, although liver OoC technology has been widely used for drug toxicity screening, only a few works have reported their use in environmental toxicology assays (Akarapipad et al., 2021) (summarized in Table 1.1).

Endocrine-disrupting chemicals (EDCs) are exogenous chemicals, such as pesticides and herbicides, that mimic, block, or interfere with endogenous hormones and other signalling chemicals in the endocrine system (Diamanti-Kandarakis et al., 2009). The widespread application of pesticides in the farming sector has contributed to the pollution of drinking water sources, vegetables, cattle food, milk, and fish. Dichlorodiphenyl- trichloroethane (DDT) and permethrin (PMT) are among the most prevalent pesticides in the environment and have been implicated in the development of different chronic diseases. DDT and PMT have been associated with dysregulation of liver lipids and glucose metabolism, and non-alcoholic fatty liver disease (NAFLD) (Mérida-Ortega et al., 2019; Rodríguez-Alcalá et al., 2015). Jellali et *a*l. used a rat liver organ-on-chip model coupled to multi-omics to investigate the liver damage induced by DDT, PMT and their combination (Figure 1.7A). The transcriptome and metabolome analysis highlighted a dose-dependent effect for all conditions, with a profile close to the control condition for low doses of pesticides. Furthermore, transcriptome modulation reflected liver inflammation, steatosis, necrosis, *PPAR* signalling and fatty acid metabolism (Jellali et al., 2018a; 2018b; 2021). Rotenone is a widely used organic pesticide known to induce oxidative stress and the mitochondrial dysfunction involved in the pathogenesis of Parkinson's disease (Katila et al., 2021; Radad et al., 2019). Bavli et al. developed a liver-on-chip model capable of maintaining 3D aggregates of HepG2/C3a cells for 28 days while monitoring oxygen uptake, glucose uptake, and lactate production rates over the same period. They noticed damage to respiratory cells directly after exposure to rotenone, in addition to an increase in cellular death and a drop in glucose uptake after 6h. Thus, their platform was able to monitor metabolic changes indicating mitochondrial and metabolic dysfunction after exposure to pesticides (Bavli et al., 2016).

Nanomaterials are very small materials that are 10000 times smaller than the thickness of a human hair. This small size gives them physical and chemical properties different from those

of “traditional” materials. Despite the widespread use of these nanomaterials in cell/tissue engineering and pharmacological/medical device development, knowledge of the toxicity and potential health risks associated with using nanomaterials remains extremely limited. Superparamagnetic iron oxide nanoparticles (SPION) are currently the only clinically approved metal oxide nanoparticles and the most used superparamagnetic nanoparticles (Singh et al., 2010; Vangijzegem et al., 2019). A microfluidic 3D liver-on-chip with three material layers, which contains primary rat hepatocytes, has been fabricated and tested using different concentrations (50, 100 and 200 µg/ml) of SPION for 3-day (short-term) and 1-week (long-term) cultures. Compared to static culture, the liver-on-chip with flow provided comparable viability and significantly higher liver-specific functions, up to 1-week. Moreover, the dynamic culture made it possible to mimic real cumulative exposure to SPION by minimizing possible agglomeration of the molecule, which caused more harmful effects in liver-specific functions (albumin and urea secretion) and viability, in a dose- and time-dependent manner (Figure 1.7B, Li et al., 2019). Recently, another study explored the hepatotoxicity of copper sulphide nanoparticles (CuSNPs) using hepatocyte spheroids in a multi-concave agarose chip. Exposure to CuSNPs caused a decrease in spheroid viability and hepatocyte-specific functions, such as albumin/urea production, glycogen deposits, and hepatobiliary transport. Moreover, alteration to mitochondrial membrane potential and increased production of reactive oxygen species demonstrated hepatocyte damage (Jiang et al., 2021).

Some molecules, although not toxic to humans in moderate quantities, can become so when overexposed. For instance, ethanol, which is the main component of alcoholic beverages and also present in many pharmaceuticals and cosmetic products, has become a target for toxicologists. Alcohol is the main cause of liver diseases as it is metabolized in the liver. Thus, developing *in vitro* models mimicking *in vivo* liver physiology is essential for understanding the mechanisms of alcoholic liver disease (ALD) and implementing treatment method. For this purpose, spheroids composed of rat primary hepatocytes and hepatic stellate cells (HSCs) were cultured in a fluidic chip to investigate the role of HSCs in livers with ALD, and an interstitial level of flow was applied to the chip to provide *in vivo* mimicking fluid activity (Lee et al., 2016). Hepatic function assessment showed lower albumin secretion and enzyme activity in the ethanol-treated group than in the control. Outcomes also demonstrated that HSCs were activated and contributed to the ALD process.

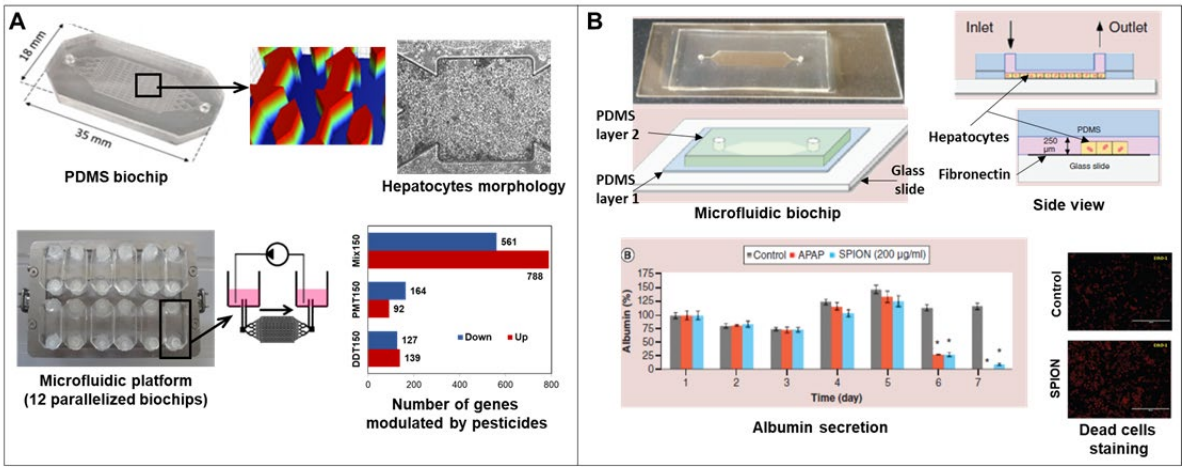

Figure 1.7. *Liver-on-a-chip models for chemical toxicity assessment. (A) PDMS biochip and platform for 12 biochip parallelization coupled to omics analysis for pesticides (permethrin and DDT) toxicity assessment on rat hepatocytes (reproduced with permission from-term toxicity of superparamagnetic iron oxide nanoparticles (SPION, reproduced with permission from Li et al., 2019)*

Table 1.1. *Overview of main liver OoC models used for drug and chemical toxicity studies*

	Cell model	Cell organizations/configuration	Drugs / Toxicans	Assays	Outcomes	Ref
Drug toxicity	Primary Rat hepatocytes Fibroblasts: J2-3T3 cell line	2D planar culture	Acetaminophen	Viability, O_2 distribution, CYP3B and CYP3A production	Recreation of the liver zonation Model adapted for the investigation of the spatial and temporal dynamics of hepatotoxicity	Allen et al., 2005
	HepG2 cell line	3D spheroids (bioprinted in GelMa)	Acetaminophen	Viability, bile canalicular development, albumin, A1AT expression, transferrin, ceruloplasmin	Maintenance of the hepatic functions for 30 days of culture Hepatotoxicity observed in the developed model correlated with the *in vivo* results	Bhise et al., 2016
	HepG2 cell line	3D spheroids (U-shape wells)	5-fluorouracil	Cross-sectional spheroids area, viability	Model for long-term 3D spheroids culture Simple and quick analysis Correlation between the spheroids size and the development of a resistance to anti-cancer drug	Zuchowska et al., 2017
	HepG2 cell line	2D (patterned biochip)	Flutamide Hydroxyflutamide	Proliferation, viability metabolic profiling	Demonstration of the potential of metabolomic-on-chip	Choucha-Snouber et al., 2013

					approach for predictive toxicology Correlation between the flutamide exposure and the mitochondrial disruption Extraction of the toxic metabolic signature of flutamide	
	HepG2 cell line	2D (patterned biochip)	Acetaminophen (APAP)	Proliferation, albumin, APAP metabolism, proteomic and transcriptomic analysis	Enhanced drug metabolism pathways compared to Petri dishes Extraction of the toxic metabolic signature of APAP Toxic metabolic signature similar to *in vivo* condition	Prot et al., 2011
	Primary human hepatocytes & dog & rat Co-cultured with LSEC, Kupffer and stellate cells	3D in Matrigel	Bosentan Acetaminophen	Viability, total glutathione, total ATP, albimin secretion, cytokines, gene expression CYP450 enzyme activity, AST, ALT and GDH	Creation of species-specific liver-chip models for drug toxicity assays Highlight of the potential of the model for the relevant detection of species-specific toxicity	Jang et al., 2019

	Primary rat hepatocytes	3D spheroids (agregated using PET-PAA-AHG and glass-PEG-AHG wells)	Diclofenac Acetaminophen	Viability, urea and albumin secretion, CYP1A2, CYP2B1/2 and CYP3A2 expression	Successfully maintained spheroids functions for 2-3 weeks Model supported repeated chronic and sub-acute drug tests The model integrated a heater, a temperature controller and active debubbler on chip	Yu et al., 2017
	HepG2 cell line Co-cultured with HUVEC	3D spheroids in GelMa	Acetaminophen	Viability, cellular metabolic activity	Integration of vascularization into the liver model for toxicity study Recreation of the endothelial barrier which delayed the passage of drugs Development of a model that recreate a more relevant *in vivo* drug response	Massa et al., 2017
	HepG2 cell line Endothelial cells: HUVEC Stellate cells: LX-2 Monocytes: U937 cell line	2D using materixgel	Acetaminophen	Viability, albumin and urea secretion, cytochrome P450 enzyme activities	Integration of the four hepatic cells layer in the liver-chip Maintenance of cell viability above 70% at day 15 Construction of a	Deng et al., 2020

					dose-and time-dependant APAP-induced disease model	
	Primary human hepatocytes and iPS differenciated into iHeps Fibroblasts: 3T3-J2 murine fibroblasts	3D encapsulated in PEG-DA hydrogel	Omeprazol Rifampin	Albumin production, Viability, CYP450 expression	Maintenance of a stable hepatic function for hepatocytes encapsulated in hydrogel droplets Perfusion successfully maintained the albumin secretion for 28 days The use of IPS cells promote the potential of using the model for patient-specific drug screening	Schepers et al., 2016
	HepaRG cell line Co-cultured with HUVEC	3D spheroids using wells inside the biochip	Methotrexate Cis-Diamineplatinum (II) dichloride Acetaminophen Cyclosporin Mitomycin C	Viability, expression of the phase I metabolic enzyme CYP450, albumin and urea secretion	The integration of endotheliocytes with hepatocytes improved hepatic functions Albumin, urea, CYP450 and polarity are better expressed in the liver-on-chip model than those in static condition Demonstration of the	bo Zheng et al., 2022

					toxicity of clinical drugs and heavy metal ions with higher sensitivity than traditional static 3D or 2D culture	
Environmental toxicity	Primary rat hepatocytes	2D (patterned biochip)	Dichlorodiphenyl-trichloroethane (DDT) Permethrin (PMT)	Viability, albumin and urea secretion, glucose consumption, ROS quantification, omics analysis	Used omics-on-chip approach to study the toxicity of pesticide The combination of different low doses of pesticides induce oxidative stress and cell death Pesticides at high doses provoke hepatotoxicity, perturbation of lipid metabolism and steatose	Jellali et al., 2018a; 2018b; 2021
	HepG2 cell line	3D spheroids using wells inside the biochip	Rotenone (R8875)	Viability, real-Time oxygen Measurement, bile canaliculi activity, mitochondrial activity, glucose consumption, lactate production, ATP/ADP ratio	Cells maintained for 28 days of culture Model capable of monitor real-time changes of metabolic pathways The metabolic shifts demonstrated the toxicity Of Retenone at concentrations considered safe	Bavli et al., 2016

					previously	
	Primary rat hepatocytes	2D (fibronectin coated biochip)	Superparamagnetic iron oxide nanoparticles (SPION)	Viability, albumin and urea synthesis	Maintenance of hepatocytes functions for up to 1 week The biochip is more sensible to the deleterious effect of SPION than static condition Results consistent with the responses of perfused hepatocytes to xenobiotics compared with static models	Li et al., 2019
	Primary human hepatocytes	3D spheroids (concave agarose chip)	Copper sulfide nanoparticles (CuSNP)	Viability, albumin and urea secretion, glycogen deposition, mitochondrial membrane potential, ROS	Successfully obtained spheroid in the agarose chip Hepatotoxic effect of CuSNP observed in the biochip Association of the mechanism with the hepatotoxicity	Jiang et al., 2021
	Primary human hepatocytes human primary	2D using extracellular matrix sandwich	Ethanol	Viability, albumin secretion,	The Liver chip detected the early critical events of	Nawroth et al., 2021

	LSECs Kupffer cells			cholesterol production, glycogen storage, cytokine, metabolomic analysis	ALD Modelling of the circulating endotoxins Modelling of the injury recover after abstinence from alcohol	
	primary rat hepatocytes Hepatic stellate cells	3D spheroids (concave microwells)	Ethanol	Viability, albumin and urea secretion	Viability of spheroids is sensible to the ethanol flow rate Development of a fibrosis structure in the exposed model to ethanol Model suitable to study reversible and irreversible alcohol liver disease	Lee et al., 2016

ALT: alanine aminotransferase, AST: aspartate aminotransferase, GDH: glutamate dehydrogenase ATP: adenosine triphosphate, ADP: adenosine diphosphate, A1AT: alpha-1-Antitrypsin, ROS: reactive oxygen species, GelMa :gGelatin methacryloyl, PET-PAA-AHG: Polyethylene terephthalate - polyacrylic acid - 1-O-(6′-aminohexyl)-D-galactopyranoside, PEG-AHG: poly(ethylene glycol) - 1-O-(6′-aminohexyl)-D-galactopyranoside

1.6. Multi-organ-on-chip model integrating liver for chemical-induced toxicity

The liver is interconnected to other organs or tissues by means of complex biological mechanisms that cause a complex global response upon exposure to xenobiotics. Traditional cell culture models mainly target a single organ or tissue and do not reproduce this level of complexity. Microphysiological system technology, which relies heavily on microfabrication and microfluidics, is ideal for mimicking such interactions in a reductionist way, by connecting and integrating multiple organs in a unique system. These multi-organ systems, termed as multi-organ-on-chip (multi-OoC), have emerged as potential tools for studying the toxicity of both drugs and environmental pollutants (Bhatia and Ingber 2014). Table 1.2 summarizes various multi-organ-on-chip systems integrating the liver and used for toxicity studies.

Drug-induced hepatotoxicity and nephrotoxicity are two major risks for human health. Theobald et al. designed a microsystem device composed of two interconnected chambers, for hepatic (HepG2) and kidney (Hek293) cells, making it possible to study both organs after exposure to toxins and drug (aflatoxin B1 (AFB1), benzo-alpha-pyrene (BαP) and rifampicin). AFB1 and BαP are known to induce primary toxicity in the liver leading to the production of epoxide, which is responsible for toxicity in other tissues and organs. The authors highlighted that xenobiotic metabolism-associated biomarkers of hepatic cells including albumin, urea, and CYPs were more stably and highly expressed under fluidic conditions. They also demonstrated the ability of this liver-kidney-on-chip device to support liver-kidney communication and reproduce the bioactivation, metabolism and clearance of both toxins and drugs (Theobaldet al., 2018).

The first pass metabolism illustrating the passage of chemicals/drugs through the intestines to the liver is important in determining the effects of xenobiotics and understanding their mechanism of action (Lee et al., 2021). Marin et al. developed a two-organ-chip platform to culture the intestines and liver for studying the absorption and metabolism of APAP (Marin et al., 2019). The intestinal barrier was produced by Caco-2 and HT-29 cells on a culture insert and the liver spheroids were produced with HepaRG and HHSTeC cells using the hanging drop technique and cultivated in the hepatic compartment. To mimic APAP absorption through the intestinal barrier, Marin et al. used two concentrations of APAP corresponding to oral and intravenous administration in the apical side and measured its passage through the barrier. *In vivo*, APAP is largely absorbed through the intestines but its toxic metabolites are only generated in the liver. The same phenomenon was observed with the model by Marin et al. when measuring the production of N-acetyl-p-benzo-quinone, a hepatotoxic metabolite of APAP. In addition, they obtained a similar absorption curve and metabolism phases to the

classic bioavailability curve obtained *in vivo* for most drugs. Intestine-liver microsystems can also be used for environmental toxicity assessment. Esch et al. simulated the oral uptake of a 50 nm carboxylated polystyrene nanoparticle with a gastrointestinal tract-liver-other tissue microsystem (Esch et al., 2014). They determined that ingestion of carboxylated polystyrene nanoparticles, even in low concentrations, cross the GI tract epithelium and affect liver tissue. They noticed an increase in aspartate aminotransferase (AST) levels in the culture medium despite the absence of a significant decrease in cell viability, suggesting transient and sublethal cell injury.

MOC may also improve the toxicological assessment of aerosols that have been implicated in the development of chronic obstructive pulmonary disease, asthma, or lung cancer. For this reason, Bovard et al. designed an acute and chronic toxicity study on a lung/liver biochip. The microsystem was composed of an air-liquid interface (ALI), where normal human bronchial epithelial (NHBE) cells were cultured, and a liver compartment with HepaRG™ spheroids. The capacity of liver cells to metabolize and regulate toxicity was assessed using AFB1. Outcomes showed that after 48 hours of exposure, AFB1 toxicity on NHBE ALI tissues decreased in co-culture conditions, proving that the HepaRG™-mediated detoxification protected/decreased from AFB1-mediated cytotoxicity (Bovard e al., 2018). In this same approach, Schimek et al. designed a HUMIMIC Chip3plus which included a large medium reservoir, an air-permeable membrane above the lung culture compartment to ensure optimal air circulation, and a liver compartment composed of HepaRG and primary human hepatic stellate cell (HHSteCs) spheroids (Figure 1.8A, Schimek et al., 2020). Thanks to the AFB1 treatment, they demonstrated crosstalk in the lung-liver coculture. After 24h of exposure, they observed a slight decrease in cell functionality and viability in the co-culture system in comparison to monoculture bronchial MucilAir. These results suggest a protective role for the liver spheroids which decreased AFB1 toxicity by metabolizing it. Moreover, a decrease in albumin production was observed, indicating hepatocyte alteration. This study thus reproduces and corroborates the findings reported by Bovard et al. (Bovard e al., 2018). Naphthalene, a pesticide used as an insecticide and repellent, has also been studied. Viravaidya et al. described the application of a two-cell system, four-chamber µCCA (Cell Culture Analogue) device composed of lung, liver, fat and other tissue for an *in vitro* ADMET study of naphthalene (Viravaidya et al., 2004). The study highlighted that naphthalene is metabolized by the liver into reactive metabolites which then circulate to the lung, causing glutathione depletion leading to oxidative stress and lung cell death (Esch et al., 2011; Viravaidya et al., 2004). These studies illustrate the potential of organ-on-chip models for pesticide toxicological studies and provide new tools for chemical risk assessment. Therefore, the lung/liver-on-a-chip platform presented here offers new

opportunities for studying the toxicity of inhaled aerosols, such as toxins or pesticides, and/or new drug candidates targeting the lungs.

Although drug toxicity mainly causes acute liver failure, it can also induce alterations in the brain as secondary effects. Studies have been conducted to determine drug-metabolized response in the brain. Materne et al. developed an MOC capable of maintaining in culture 3D spheroids of neurospheres derived from undifferentiated NT2 cells and liver cells (HepaRG and primary human hepatic stellate cells, Materne et al., 2015). They observed that exposure to the neurotoxic 2,5-hexanedione induced higher apoptosis rates within neurospheres and liver tissues in monoculture, when compared with the neurosphere-liver co-culture. Therefore, these outcomes suggest that single-tissue organ-on-chips are less predictive and accurate than multi-organ-on-chips. The liver-brain chip may also be useful for assessing the metabolism of drug candidates for certain neuropathologies. Li et al. designed a multi-interface liver-brain chip composed of three microchannels separated by a porous membrane and collagen to assess hepatic metabolism-dependent cytotoxicity of anti-brain-tumour drugs (Li et al., 2021). HepG2 and U87 cells were cultured in separate channels to mimic the liver and glioblastoma, while brain microvascular endothelial cells (BMECS) and cerebral astrocytes were co-cultured on collagen to mimic the blood-brain-barrier (BBB). They evaluated the physiological process of three common anti-tumour drugs: paclitaxel (PTX), capecitabine (CAP) and temozolomide (TMZ). Their results highlighted that the liver compartment enhanced the cytotoxicity of CAP on U87 cells but had no significant effect on TMZ. On the other hand, the BBB decreased the cytotoxicity of PTX, while no significant effects were observed on TMZ and CAP. These results demonstrated the importance of liver metabolism and the blood–brain barrier for evaluating anti-brain-tumour drugs and the potential of liver-brain-chips for evaluating anti-brain-tumour drugs in a more accurate manner (Li et al., 2021).

One of the most important targets of the toxic metabolites produced by the liver is the heart. To understand the dynamic interactions between these two organs, liver-heart models have been developed to predict off-target cardiac toxicity on liver metabolism. Soltantabar et al. 2021 developed a heart-liver-chip using HepG2 cells and H9c2 rat cardiomyocytes to test the toxicity effect of doxorubicin (Figure 1.8B, Soltantabar et al., 2021). The cardiotoxic effect of doxorubicin is due to its primary metabolite, doxorubicinol. The PDMS biochip was composed of 2 culture chambers interconnected by fluidic channels. After drug treatment, they observed the appearance of the cardiotoxic metabolite, doxorubicinol, and its toxic effect was confirmed by quantifying the viability of the cardiac cells within the model. They observed a significant difference in the apoptotic cells in the device compared to static culture. The model by Soltantabar et al. promotes the potential of multi-organ-on-chip

models for evaluating the toxicity of both the parent drug and its metabolites and the effect on both organs (Soltantabar et al., 2021).

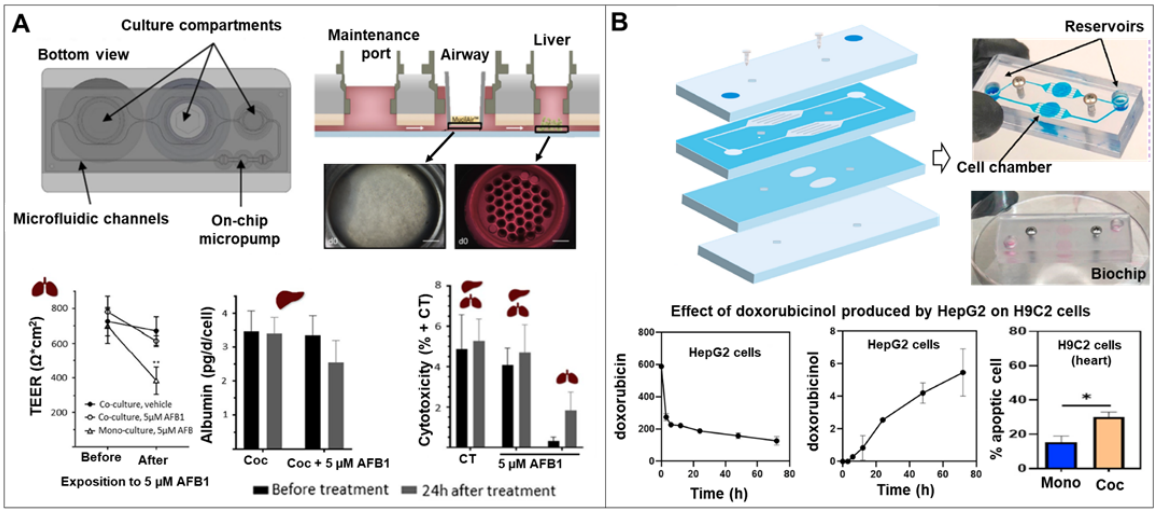

Figure 1.8. *Multi-organ platforms integrating liver OoC for toxicity studies. (A) liver-lung OoC platform to investigate organ crosstalk and assess the toxicity of inhaled substances, example of aflatoxin B1 (reproduced with permission from Schimek et al., 2020); (B) liver-heart-on-chip device to study the cardiotoxicity induced by doxorubicin and its metabolite (Doxorubicinol) produced by liver compartment (HepG2/C3a cell line, reproduced with permission from Soltantabar et al., 2021).*

Table 1.2. *Examples of multiorgan-on-chip platforms integrating liver used for drug and chemical toxicity studies.*

Culture model	Cell organizations/configuration	Drugs / Toxicans	Assays	Outcomes	Ref
Liver: HepG2 cell line Kidney: Hek293 cell line	2D monolayer (collagen coating)	Aflatoxin B1 (AFB1) Benzo-alpha-pyrene (BαP) Rifampicin	Viability, cytotoxicity, albumin and urea secretion, CYPs expression	Efficient toxins and drugs metabolization Multi-faceted physiological phenomena modelling	Theobald et al., 2018
Liver: HepaRG and Human primary hepatic stellate cells (HHSTeC) Intestine: Caco-2 and HT-29 cell lines	Intestine barrier using permeable membrane Liver spheroids using Hanging Drop Plates	Acetaminophen	Viability, Na-K-ATPase, MDR1, GSTA2, CYP3A4 and UGT1A1 expression, APAP uptake, albumin secretion	Maintenance of co-cultured spheroids Formation of a functional intestine barrier cell Low cytotoxicity on the intestine barrier cell even after 24h of treatment	Marin Et al., 2019
Liver: HepG2 cell line Intestine: Caco-2/HT29-MTX cell lines	Intestine barrier using permeable membrane 2D liver monolayer on poly-D-lysine and fibronectin coated surface	Carboxylated polystyrene nanoparticles	Viability, enzyme activity of ALT, AST, GDH and GGT, pH variation	Model demonstrated that nanoparticles traversed the intestinal barrier and reached the liver compartment The interaction between the two organs increased the toxic effect of nanoparticles Model suitable for assessing toxicities of environmental toxicants	Esch et al., 2014

Liver: HepaRG cell line Lung: NHBE cell line	Human 3D bronchial epithelial barrier Liver spheroids using ultra-low adhesion well plate	Aflatoxin B1 (AFB1)	Permeability, albumin and lactate production, glucose consumption, ATP, CYP1A1/1B1 expression of phase 1 metabolism associated genes	Maintenance of cell functions and viability during 28 days Suitable for testing drug efficacy and safety	Bovard et al., 2018
Liver: HepaRG cell line and HHSteC Lung: bronchial MucilAir culture	Spheroids using ultra-low-attachment microplate MUCILAIR™ for the branchial barrier	Aflatoxin B1 (AFB1)	Viability, barrier permeability albumin production, ATP content, tdT-mediated dUTP-digoxigenin nick-end labelling (TUNEL)/Ki67 staining, LDH release, ATP	Culture for 14 days with maintenance of cells functionalities and viability Organs interactions demonstrated using the toxicity of aflatoxin B1 Model suitable to evaluate the toxicity of inhaled substances	Schimek et al., 2020
Liver: HepG2 (human) and H4IIE (rat) cell lines Lung: L2 lung type II epithelial cells	2D monolayer: cells cultivated on matrigel	Naphthalene	CYP450 1A activity, MTS assay, naphthalene metabolites toxicity, intracellular GSH, hydrogen peroxide (H2O2) production	Mode suitable to study the ADME of naphthalene Naphthalene reactive metabolites are produced by the liver but the lung is more sensitive for their effect	Viravaidya et al., 2004
Liver: HepaRG cell line and HHSteC Neural system: NTera-2/cl.D1 (NT2) cell line	hanging drop for liver spheroids Spinner vessel for neurospheres	2,5-hexanedione	Viability, glucose consumption, lactate and LDH production, gene expression	Maintenance of cell functions and viability during 14 days Correlation between drug toxicity and tissue-tissue communication	Materne et al., 2015
Liver: HepG2 cell line BBB barrier: primary BMECS and cerebral astrocytes Brain: U87 cell line	2D monolayer: cells cultivated on collagen coating	Paclitaxel (PTX) Capecitabine (CAP) Temozolomide (TMZ)	Barrier permeability, viability, drug metabolites detection by mass spectrometry, TEER measurement	Design of an efficient multi interfaces device Evaluation of anti-brain tumor drugs Correlation between drug response and properties	Li et al., 2021

Liver: HepG2 cell line Heart: H9c2 cell line	3D using PepGel™ PGmatrix-Spheroid	Doxorubicin (DOX)	Viability, urea production DOX metabolism	Device allowing to evaluate both parent drug and its metabolites Toxicity of metabolites produced by liver on heart cells	Soltantabar et al., 2021
Heart: iPSc derived cardiomyocytes Liver: Cryopreserved human primary hepatocytes (PHH)	2D using fibronectin (iPSc) and collagen (PHH) coating	Diclofenac sodium Ketoconazole Hydrocortisone Acetaminophen	Viability, albumin and LDH production, CYP expression Cardiac function	Model suitable for acute and chronic drug exposure associated with transdermal drug delivery	Pires De Mello et al., 2020
Liver: HepG2 and HepaRG cell line Kidney: MDCK cell line	2D using a fibronectin coating	Ifosfamide chloroacetaldehyde	Proliferation, cell cycle repartition, CYP expression	Organs interactions observed through the toxicity of the ifosfamide and its nephrotoxic metabolite produced by the liver The nephrotoxicity of ifosfamide is only observed when associated with its metabolite the chloroacetaldehyde The chloroacetaldehyde decrease viability and causes perturbations of the intracellular calcium release	Choucha-Snouber et al., 2013

1.7. Conclusion and future challenges

Over the past few decades, liver OoC technology has undergone significant progress and has now become a promising *in vitro* test system for different applications, especially in drug toxicity screening and environmental risk assessment. The significant advancements in tissue engineering, biomaterials, design and microfabrication, stem cell technologies and knowledge of the liver microenvironment make it possible to build liver OoC with highly complex and specific cellular architectures. Thanks to the use of bioprinting, organoid technology and hydrogels/hydroscaffolds, it is possible to construct vasculature and 3D architecture, as well as to model mechanical properties, cell-cell and cell-ECM interactions. The evolution in perfusion systems makes possible precise control of media flow reproducing flow, mechanical stimuli and dilutions of metabolites and paracrine signals similar to those in physiological situations. Currently, liver OoC benefits from the iPSC technology that provides a readily-available human cell source and makes it possible to develop multicellular liver OoC (hepatocytes + NPCs) using cells from the same donor (same genetic background). Such developments, coupled with easy imaging and the possibility of incorporating biosensors and connecting OoC to analytical tools, make liver OoC technology a powerful tool for both replacing the traditional “black box” of animal-based and conventional 2D *in vitro*-based paradigms, and promoting the implementation of the '3Rs' (replacement, reduction, and refinement of animal models).

Although it is recognized today that the liver OoC models will replace many animal experiments, many obstacles still need to be addressed in the future. PDMS is the most widely used material for constructing liver OoC. PDMS absorbs hydrophobic molecules and is not suitable for tests using drugs/chemicals. With the progress made in microfabrication techniques, a variety of devices with new materials have been proposed. However, detailed comparisons of these devices with PDMS-based biochips, including biological performances/functions, long-term cultures, interactions with cells and molecules, and utility as pharmacokinetic models are needed to validate their use in toxicology studies and drug screening. Cell sourcing is one of the keys to the development of relevant liver OoC models. Human iPSC-derived hepatocytes provide great cell sources for liver OoC. Nevertheless, the protocols for hiPSC differentiation lead to immature and heterogeneous hepatocytes. Furthermore, only very few protocols are available for iPSC differentiation into NPCs, which are essential for construction of relevant multicellular liver OoC. The protocols for iPSC differentiation into hepatocytes and NPCs need to be further explored to obtain highly mature hepatic cells. The other major challenges for OoC technology are standardization and compatibility with standard laboratory equipment. To address these issues, several

initiatives and consortia involving the OoC community, pharmaceutical companies, academic researchers, and standards development organisations (SDOs) have emerged in recent years. These actions have been reinforced by recognition of the potential for OoC technology and increasing financial support from the European Union (EU), the United States, and the Japanese government for project relate to OoC.

1.8. Objectives and approach of the thesis

Most of the liver-on-chip models presented above are based on the culture of hepatocytes in microstructured designs in order enhance their metabolic activity and extend their lifespan. This approach does not fully take in consideration the complex physiology of the liver. Indeed, in addition to the hepatocytes, the liver is composed of 40% of NPCs which play important roles in the liver functions and homeostasis.

1.8.1. Non-parenchymal cells: LSEC barrier and support functions

Liver sinusoids are blood vessels with a diameter of 5 to 10 µm which delimit the interface between the circulating blood cells on one side and the hepatocytes on the other side. The sinusoid is composed of LSECs (15-20%) and Kupffer cells (15%) from the luminal side and hepatic stellate cells (5%) in the space of Disse side. Kupffer cells are derived from monocytes and characterized by a high phagocytic potential. They produce cytokines that induce the inflammatory reaction and ensure the crosstalk between the other resident cells. Hepatic stellate cells also known as fat-storing cells are a major storage site for vitamins and lipids (Lefkowitch et al., 2016). In addition, they produce the liver extracellular matrix which is composed of 5 to 10% of collagen in addition to glycoproteins, laminin, vitronectin, fibronectin and proteoglycans (Bykov et al., 2004). Finally, the LSEC contribute to different physiological processes such as the adjustment of the homeostasis balance, intervene in pathological processes, inflammation, angiogenesis and in vascular tone by vasodilation or vasoconstriction to regulate venous hepatic pressure (Poisson et al., 2017). LSECs have a discontinuous architecture: their membranes are not connected at the level of cell junctions but rather at the level of a region called fenestration. The endocytic power of LSEC is considered the highest among all endothelial cells. These fenestrations, a unique feature of LSECs, associated with the absence of a basal membrane, constitute the permeable and selective barrier of the liver. The size and number of fenestrations depend on the region and the physiological condition of the liver, it varies between 50 and 150 nm and between a hundred to several thousand per cell. There are more fenestrations in the centrilobular region than in the periportal region of the hepatic lobule (Szafranska et al., 2021).

In a healthy liver, LSECs are in contact on the one hand with arterial blood rich in O_2 and on the other hand with blood derived from the intestine and pancreas, rich in bile acid, nutrients, insulin, glucagon and hormones. On the abluminal side, they interact with stellate cells and hepatocytes, which defines their nature as a bidirectional exchange region. Molecules such as metabolites, plasma proteins, drugs and lipoproteins cross LSECs to the Disse space and subsequently to hepatocytes for their metabolisms. As for larger molecules, capable of deforming through the pores of the membranes, they can go through the phenomenon of selective permeability (Poisson et al., 2017). During embryogenesis, LSECs gradually lose continuous endothelial cell markers such as CD31 also known as platelet endothelial adhesion molecule (PCAM-1) and CD34 to acquire adult sinusoidal cell markers such as CD4, CD32 and intracellular adhesion molecule 1 (ICAM-1). In adults, the markers expressed in LSECs are heterogeneous, depending on the markers observed, the origin of LSECs may differ between stemming from a common progenitor of endothelial and blood cells called "hemangioblast" and stemming from the endocardium of the sinus. This difference in embryological origins could explain the heterogeneity of the markers expressed (Gage et al., 2020).

Under normal physiological conditions, the liver has a tolerance towards circulating antigens since it receives all kinds of molecules from the intestine and the general blood circulation, making a classic immune response devastating. Knowing that LSECs play a major role in the reception of a large panoply of circulating molecules from the blood, its role has been reported in the generation of immune tolerance. Indeed, LSECs may be classified as non-myelogenic antigen-presenting cells and may express MHC type II which presents exogenous antigens. Or, by a cross-presentation phenomenon, the LSECs present exogenous Ag via MHC type I to a CD8+ helper T cell, which leads to a kind of immune tolerance (Berg et al., 2006). otherwise, the inflammation is initiated after the presentation of the antigens by the LSEC to the local immune system of the liver also called Kupffer cells (Shetty et al., 2018).

1.8.2. Integration of LSEC barrier in liver OoC

The integration of endothelial cells into organs-on-chip and especially liver-on-chip models remain a challenging objective for the recreation of physiological relevant in vitro systems. LSECs, lining the blood vessels, are presented as the last barrier separating the hepatocytes from the blood flow circulation. In addition, cultivating primary rat LSEC and hepatocytes in collagen gel sandwich showed a higher albumin production, an increase of native CYP activity compared to mono cultivated hepatocytes (Bale et al., 2014).

In this context, (Nakao et al., 2011) tried to recreate an endothelial-like barrier. The microsystem is divided into 2 independent circuits, cell culture area and culture medium circulation circuit, separated by endothelial-like barrier consisting of 2 µm pillars. Despite the LSEC acellular approach used in this barrier model, the hepatocytes cultivated under perfusion without shear stress aligned into a hepatic cord and more *in vivo* bile canaliculi network were developed, in comparison with the random alignments observed when hepatocytes are cultivated in well plates. This alignement has been demonstrated to promote the formation of bile canaliculi along the cord-like structure. The model developed by Nakao et al. 2011 highlights the importance of integrating an endothelial-like barrier for the recreation of a more *in vivo*-like model.

In order to study cell-cell interactions and the role of the secretion factors produced by the LSEC and the NPC, Du et al., 2017 and Nawroth et al., 2021 used Emulate, inc Liver chip. The chip is bi-compartmented and the two culture chambers are separated by thin permeable membrane. (Du et al., 2017) studied the interaction between primary murine hepatic cells cultivated in the lower chamber, the hepatic stellate cells cultivated in the basolateral surface of the porous membrane and the Kupffer cells and the LSEC both cultivated in the upper chamber. They concluded that the shear stress and the integration of NPC enhanced the albumin and HGF secretion and increased the neutrophil recruitment recreating. The liver model developed by Du et al., 2017 has the potential for the understanding of the paracrine communications and the molecular mechanisms among the distinct hepatic cells. On the other hand, (Nawroth et al., 2021) used the same microfluidic system to model alcohol-associated liver disease. To do so, they injected primary human hepatocytes embed into an ECM scaffold in the upper chamber and human primary LSEC and Kupffer cells in the lower chamber. The liver-chip developed by Nawroth et al. 2021 recapitulated the established markers to ethanol exposure such as an increase of oxidative stress and a remodelling of the bile canalicular network compared to untreated condition.
Despite the difficulties in maintaining NPC functionalities over extended period of time, their integration especially the LSEC barrier in liver-chip models remain an important objective for the understanding of the liver physiology and disease processes (Nawroth et al., 2021).

1.8.3. Objectives of the thesis

Following the approaches exposed above, we propose in this thesis project to develop an advanced liver-on-chip model integrating a liver sinusoidal endothelial cell barrier for drug screening applications. The model is intended to mimic the two major events encountered by xenobiotics in the liver. Firstly, their passage through the endothelial barrier then their metabolism by the hepatocytes. The goal with this project is to propose a relevant and

reliable model that can be used to predict the toxicity of molecules during the preclinical phase.

The theoretical design of the proposed model is presented in figure 1.9. To achieve this project each compartment should be characterized individually. Then, optimizations should be considered to ensure the coculture of the different cell populations while maintaining their respective phenotypes. To do so :

- Firstly, the hepatocytes-on-chip compartment should be characterized and the 3D in situ organization of the hepatocyte spheroids should be ensured.
- Then, the permeability of LSEC barrier should be assessed and the coculture parameters of the two cell populations should be setup
- Finally, the communications between the two cell populations should be studied in order to better understand the model kinetics and promote the use of our developed model.

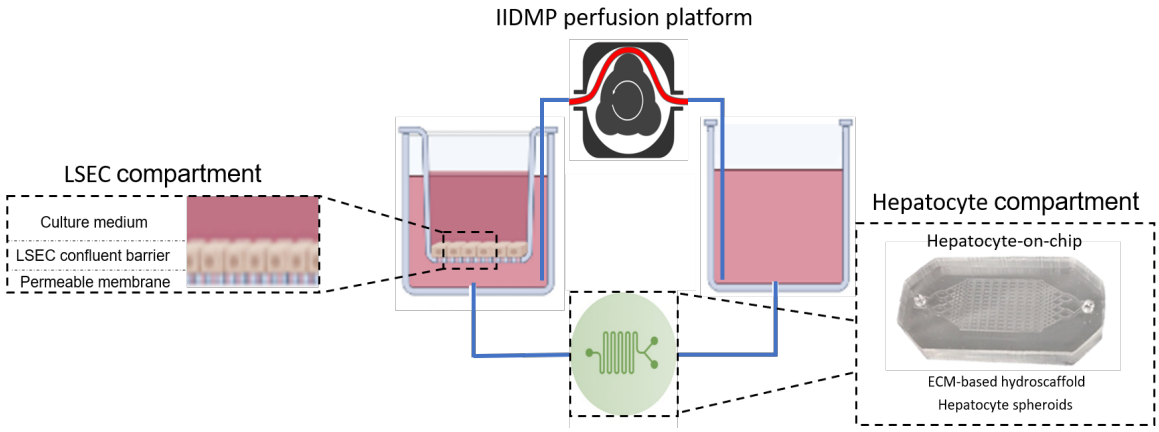

Figure 1. 9. *Illustration of the liver-on-chip model integrating an LSEC barrier.*

The project is divided into different chapters corresponding to the different steps leading to the development of our model:

- **Development of a liver-on-chip integrating a hydroscaffold mimicking the liver's extracellular matrix**

In this chapter, we integrated an ECM-based hydroscaffold into our liver-chip. The HepG2/C3a cell line was then used to proof the concept of the hepatocytes *in situ* organization in a 3D conformation. Then, we followed-up the spheroids formation and compared their structure and functions with static hydroscaffold integrated Petri dishes.

- **Coculture model of a liver sinusoidal endothelial cell barrier and hepatocyte spheroids-on-chip in an advanced fluidic platform**

The SK-HEP-1 cell line is used as an LSEC model and cultivated on a culture insert. The cells form a confluent monolayer which is used as the LSEC barrier. The barrier is then characterized using different tracer molecules and the permeability is assessed. A candidate molecule, the acetaminophen, is then used to proof the biotransformation capability of our model.

- **Investigation of the metabolomic crosstalks between liver sinusoidal endothelial cells and hepatocytes exposed to paracetamol using organ-on-chip technology**

In this chapter, we use a gas chromatography mass spectrometry to investigate the response of our model to acetaminophen injury. The metabolomic profiles of each type of cultures and conditions are analyzed and acetaminophen-induced toxicity signature identified.

Although we setup culture parameters for the co-culture of the HepG2/C3a and SK-HEP-1 cell lines, and proved its metabolic potential, the gold standard in pharmaceutical industries is the use of primary human hepatocytes. In the last chapter, we present preliminary results of using primary human hepatocytes in our ECM-based hydroscaffold. Due to lack of time in the analysis we present few preliminary characterizations for their organization and functions.

1.9. References

Ahadian S, Civitarese R, Bannerman D, Mohammadi MH, Lu R, Wang E, Davenport-Huyer L, Lai B, Zhang B, Zhao Y, Mandla S, Korolj A, Radisic M. Organ-on-a-chip platforms: A convergence of advanced materials, cells, and microscale technologies. *Adv. Healthcare Mater.,* 2018, 7, 1700506. DOI: 10.1002/adhm.201700506.

Akarapipad P, Kaarj K, Liang Y, Yoon JY. Environmental toxicology assays using organ-on-chip. *Annu. Rev. Anal. Chem*., 2021, 14, 155-183. DOI: 10.1146/annurev-anchem-091620-091335.

Allen JW, Bhatia SN. Formation of steady-state oxygen gradients *in vitro*: application to liver zonation. *Biotechnol. Bioeng*., 2003, 82, 253-262. DOI: 10.1002/bit.10569.

Allen JW, Khetani SR, Bhatia SN. *In vitro* zonation and toxicity in a hepatocyte bioreactor. *Toxicol. Sci*., 2005, 84, 110-119. DOI: 10.1093/toxsci/kfi052.

Almazroo OA, Miah MK, Venkataramanan R. Drug metabolism in the liver. *Clin. Liver Dis.,* 2017, 21, 1–20.

Andria B, Bracco A, Cirino G, Chamuleau RAFM. Liver cell culture devices. *Cell Med.,* 2010, 1, 55-70. DOI: 10.3727/215517910X519274.

Aske K C, Waugh C A. Expanding the 3R principles: More rigour and transparency in research using animals. *EMBO Reports*, 2017, *18*(9), 1490. DOI: 10.15252/EMBR.201744428

Bale SS, Borenstein JT. Microfluidic cell culture platforms to capture hepatic physiology and complex cellular interactions. *Drug Metab. Dispos.,* 2018, 46, 1638-1646.

Bale S S, Golberg I, Jindal R, McCarty W J, Luitje M, Hegde M, Bhushan A, Usta O B, Yarmush M L. Long-Term Coculture Strategies for Primary Hepatocytes and Liver Sinusoidal Endothelial Cells. 2014, *21*(4), 413–422. DOI: 10.1089/TEN.TEC.2014.0152

Barrow P. Revision of the ICH guideline on detection of toxicity to reproduction for medicinal products: SWOT analysis. *Reprod. Toxicol.,* 2016, 64, 57-63. DOI: 10.1016/j.reprotox.2016.03.048

Bateman TJ, Reddy VGB, Kakuni M, Morikawa Y, Kumar S. Application of chimeric mice with humanized liver for study of human-specific drug metabolism. *Drug Metab. Dispos.,* 2014, 42, 1055-1065.

Baudy AR, Otieno MA, Hewitt P, Gan J, Roth A, Keller D, Sura R, van Vleet TR, Proctor WR. Liver microphysiological systems development guidelines for safety risk assessment in the pharmaceutical industry. *Lab Chip*, 2020, 20, 215-225. DOI: 10.1039/c9lc00768g.

Bavli D, Prill S, Ezra E, Levy G, Cohen M, Vinken M, Vanfleteren J, Jaeger M, Nahmias Y. Real-time monitoring of metabolic function in liver-on-chip microdevices tracks the

dynamics of mitochondrial dysfunction. *Proc. Natl. Acad. Sci. U. S. A.,* 2016, 113, E2231-E2240. DOI: 10.1073/pnas.1522556113.

Beckwitt CH, Clark AM, Wheeler S, Taylor DL, Stolz DB, Griffith L, Wells A. Liver 'organ on a chip'. *Exp. Cell Res*., 2018, 363, 15-25.

Berg M, Wingender G, Djandji D, Hegenbarth S, Momburg F, Hämmerling G, Limmer A, Knolle P. Cross-presentation of antigens from apoptotic tumor cells by liver sinusoidal endothelial cells leads to tumor-specific CD8+ T cell tolerance. *European Journal of Immunology*, 2006, *36*(11), 2960–2970. DOI: 10.1002/EJI.200636033

Bell CC, Hendriks DFG, Moro SML, Ellis E, Walsh J, Renblom A, Fredriksson Puigvert L, Dankers ACA, Jacobs F, Snoeys J, Sison-Young RL, Jenkins RE, Nordling A, Mkrtchian S, Park BK, Kitteringham NR, Goldring CEP, Lauschke VM, Ingelman-Sundberg M. Characterization of primary human hepatocyte spheroids as a model system for drug-induced liver injury, liver function and disease. *Sci. Rep.,* 2016, 6, 25187. DOI: 10.1038/srep25187.

Bhatia SN, Ingber DE. Microfluidic organs-on-chips. *Nat. Biotechnol.,* 2014, 32, 760-772. DOI: 10.1038/nbt.2989.

Bhattacharjee N, Urrios A, Kang S, Folch A. The upcoming 3D-printing revolution in microfluidics. *Lab Chip*, 2016, 16, 1720-1742. DOI: 10.1039/c6lc00163g.

Bhise NS, Manoharan V, Massa S, Tamayol A, Ghaderi M, Miscuglio M, Lang Q, Zhang YS, Shin SR, Calzone G, Annabi N, Shupe TD, Bishop CE, Atala A, Dokmeci MR, Khademhosseini A. A liver-on-a-chip platform with bioprinted hepatic spheroids. *Biofabrication,* 2016, 8, 014101. DOI: 10.1088/1758-5090/8/1/014101.

Boeri L, Izzo L, Sardelli L, Tunesi M, Albani D, Giordano C. Advanced organ-on-a-chip devices to investigate liver multi-organ communication: Focus on gut, microbiota and brain. Bioengineering, 2019, 6, 91. DOI: 10.3390/bioengineering6040091.

Boulais L, Jellali R, Pereira U, Leclerc E, Bencherif SA, Legallais C. Cryogel-integrated biochip for liver tissue engineering. *ACS Appl. Bio Mater*., 2021, 4, 5617-5626. DOI: 10.1021/acsabm.1c00425.

Bovard D, Iskandar A, Luettich K, Hoeng J, Peitsch MC. Organs-on-a-chip: A new paradigm for toxicological assessment and preclinical drug development. *Toxicol. Res. Appl.,* 2017, 1, 239784731772635. DOI: 10.1177/2397847317726351.

Bovard D, Sandoz A, Luettich K, Frentzel S, Iskandar A, Marescotti D, Trivedi K, Guedj E, Dutertre Q, Peitsch MC, Hoeng J. A lung/liver-on-a-chip platform for acute and chronic toxicity studies. *Lab Chip,* 2018, 18, 3814-3829. DOI: 10.1039/c8lc01029c.

Brandon EFA, Raap CD, Meijerman I, Beijnen JH, Schellens JHM. An update on *in vitro* test methods in human hepatic drug biotransformation research: pros and cons. *Toxicol. Appl. Pharmacol*., 2003, 189, 233-246. DOI: 10.1016/s0041-008x(03)00128-5.

Burkard A, Dähn C, Heinz S, Zutavern A, Sonntag-Buck V, Maltman D, Przyborski S, Hewitt NJ, Braspenning J. Generation of proliferating human hepatocytes using Upcyte® technology: characterisation and applications in induction and cytotoxicity assays. *Xenobiotica*, 2012, 42, 939-956. DOI: 10.3109/00498254.2012.675093.

Bykov I, Ylipaasto P, Eerola L, Lindros KO. Functional differences between periportal and perivenous kupffer cells isolated by digitonin-collagenase perfusion. *Comp. Hepatol.,* 2004, 3, S34.

Campbell SB, Wu Q, Yazbeck J, Liu C, Okhovatian S, Radisic M. Beyond polydimethylsiloxane: Alternative materials for fabrication of organ-on-a-chip devices and icrophysiological systems. *ACS Biomater. Sci. Eng.,* 2020, 7, 2880-2899. DOI: 10.1021/acsbiomaterials.0c00640.

Chang CW, Cheng YJ, Tu M, Chen YH, Peng CC, Liao WH, Tung YC. A polydimethylsiloxane-polycarbonate hybrid microfluidic device capable of generating perpendicular chemical and oxygen gradients for cell culture studies. *Lab Chip*, 2014, 14, 37623772. DOI: 10.1039/c4lc00732h.

Chatterjee S, Richert L, Augustijns P, Annaert P. Hepatocyte-based *in vitro* model for assessment of drug-induced cholestasis. *Toxicol. Appl. Pharmacol.,* 2014, 274, 124-136. DOI: 10.1016/j.taap.2013.10.032.

Chen JP, Yu SC, Hsu BRS, Fu SH, Liu HS. Loofa sponge as a scaffold for the culture of human hepatocyte cell line. *Biotechnol. Prog.,* 2003, 19, 522-527. DOI: 10.1021/bp025720j.

Cheng F, Li W, Zhou Y, Shen J, Wu Z, Liu G, Lee PW, Tang Y. admetSAR: a comprehensive source and free tool for assessment of chemical ADMET properties. *J. Chem. Inf. Model.,* 2012, 52, 3099-3105. DOI: 10.1021/ci300367a.

Choucha-Snouber L, Aninat C, Grsicom L, Madalinski G, Brochot C, Poleni PE, Razan F, Guillouzo CG, Legallais C, Corlu A, Leclerc E. Investigation of ifosfamide nephrotoxicity induced in a liver-kidney co-culture biochip. Biotechnol. Bioeng., 2013, 110, 597-608. DOI: 10.1002/bit.24707.

Choucha-Snouber L, Bunescu A, Naudot M, Legallais C, Brochot C, Dumas ME, Elena-Herrmann B, Leclerc E. Metabolomics-on-a-chip of hepatotoxicity induced by anticancer drug flutamide and Its active metabolite hydroxyflutamide using HepG2/C3a microfluidic biochips. *Toxicol. Sci.,* 2013, 132, 8-20. DOI: 10.1093/toxsci/kfs230.

Coll M, Perea L, Boon R, Leite SB, Vallverdú J, Mannaerts I, Smout A, el Taghdouini A, Blaya D, Rodrigo-Torres D, Graupera I, Aguilar-Bravo B, Chesne C, Najimi M, Sokal E, Lozano JJ, van Grunsven LA, Verfaillie CM, Sancho-Bru P. Generation of hepatic stellate cells from human pluripotent stem cells enables *in vitro* modeling of liver fibrosis. *Cell Stem Cell*, 2018, 23, 101-113.e7. DOI: 10.1016/j.stem.2018.05.027.

Cui X, Hartanto Y, Zhang H. Advances in multicellular spheroids formation. J. R. Soc., Interface, 2017, 14, 20160877. DOI: 10.1098/rsif.2016.0877.

Danoy M, Jellali R, Tauran Y, Bruce Y, Leduc M, Gilard F, Gakière B, Scheidecker B, Kido T, Miyajima A, Soncin F, Sakai Y, Leclerc E. Characterization of the proteome and metabolome of human liver sinusoidal endothelial-like cells derived from induced pluripotent stem cells. *Differentiation*, 2021, 120, 28-35. DOI: 10.1016/j.diff.2021.06.001.

de Angelis I, Ricceri L, Vitale A. The 3R principle: 60 years taken well. Preface. *Ann. Ist. Super. Sanita,* 2019, 55, 398-399. DOI: 10.4415/ANN_19_04_15.

de Assuncao TM, Sun Y, Jalan-Sakrikar N, Drinane MC, Huang BQ, Li Y, Davila JI, Wang R, O'Hara SP, Lomberk GA, Urrutia RA, Ikeda Y, Huebert RC. Development and characterization of human-induced pluripotent stem cell-derived cholangiocytes. *Lab. Invest.*, 2015, 95, 684-696. DOI: 10.1038/labinvest.2015.51.

de Bruyn T, Chatterjee S, Fattah S, Keemink J, Nicolaï J, Augustijns P, Annaert P. Sandwich-cultured hepatocytes: utility for *in vitro* exploration of hepatobiliary drug disposition and drug-induced hepatotoxicity. *Expert Opin. Drug Metab. Toxicol.,* 2013, 9, 589-616. DOI: 10.1517/17425255.2013.773973.

Deng J, Cong Y, Han X, Wei W, Lu Y, Liu T, Zhao W, Lin B, Luo Y, Zhang X. A liver-on-a-chip for hepatoprotective activity assessment. *Biomicrofluidics*, 2020, 14, 64107. DOI: 10.1063/5.0024767.

Deng J, Wei W, Chen Z, Lin B, Zhao W, Luo Y, Zhang X. Engineered liver-on-a-chip platform to mimic liver functions and its biomedical applications: A review. *Micromachines*, 2019, 10, 676.

Diamanti-Kandarakis E, Bourguignon JP, Giudice LC, Hauser R, Prins GS, Soto AM, Zoeller RT, Gore AC. Endocrine-disrupting chemicals: an Endocrine Society scientific statement. *Endocr. Rev.,* 2009, 30, 293-342. DOI: 10.1210/er.2009-0002.

Díaz L, Zambrano E, Flores ME, Contreras M, Crispín JC, Alemán G, Bravo C, Armenta A, Valdés VJ, Tovar A, Gamba G, Barrios-Payán J, Bobadilla NA. Ethical considerations in animal research: The principle of 3R's. Rev. *Invest. Clin.,* 2020, 73, s113961211409.

Ding C, Chen X, Kang Q, Yan X. Biomedical application of functional materials in organ-on-a-Chip. *Front. Bioeng. Biotechnol.,* 2020, 8, 823. DOI: 10.3389/fbioe.2020.00823.

Donato MT, Jover R, Gómez-Lechón M. Hepatic cell lines for drug hepatotoxicity testing: limitations and strategies to upgrade their metabolic competence by gene engineering. *Curr. Drug Metab.,* 2013, 14, 946-968. DOI: 10.2174/1389200211314090002.

Donato MT, Tolosa L. Stem-cell derived hepatocyte-like cells for the assessment of drug-induced liver injury. *Differentiation,* 2019, 106, 15-22. DOI: 10.1016/j.diff.2019.02.004.

Dosch AR, Imagawa DK, Jutric Z. Bile metabolism and lithogenesis: An update. *Surg. Clin. North Am.,* 2019, 99, 215-229.

Dunn JCY, Yarmush ML, Koebe HG, Tompkins RG. Hepatocyte function and extracellular matrix geometry: long-term culture in a sandwich configuration. *FASEB J.,* 1989, 3, 174-177. DOI: 10.1096/fasebj.3.2.2914628.

Duval K, Grover H, Han LH, Mou Y, Pegoraro AF, Fredberg J, Chen Z. Modeling physiological events in 2D vs. 3D cell culture. *Physiology,* 2017, 32, 266-277. DOI: 10.1152/physiol.00036.2016.

Du Y, Li N, Yang H, Luo C, Gong Y, Tong C, Gao Y, Lü S, Long M. Mimicking liver sinusoidal structures and functions using a 3D-configured microfluidic chip. *Lab Chip,* 2017, 17, 782-794. DOI: 10.1039/c6lc01374k.

Elaut G, Papeleu P, Vinken M, Henkens T, Snykers S, Vanhaecke T, Rogiers V. Hepatocytes in suspension. *Methods Mol. Biol.,* 2006, 320, 255-263. DOI: 10.1385/1-59259-998-2:255.

Esch MB, King TL, Shuler ML. The role of body-on-a-chip devices in drug and toxicity studies. *Annu. Rev. Biomed. Eng.,* 2011, 13, 55-72. DOI: 10.1146/annurev-bioeng-071910-124629.

Esch MB, Mahler GJ, Stokol T, Shuler ML. Body-on-a-chip simulation with gastrointestinal tract and liver tissues suggests that ingested nanoparticles have the potential to cause liver injury. *Lab Chip*, 2014, 14, 3081–3092. DOI: 10.1039/c4lc00371c.

Essaouiba A, Okitsu T, Jellali R, Shinohara M, Danoy M, Tauran Y, Legallais C, Sakai Y, Leclerc E. Microwell-based pancreas-on-chip model enhances genes expression and functionality of rat islets of Langerhans. *Mol. Cell. Endocrinol*., 2020, 514, 110892. DOI: 10.1016/j.mce.2020.110892.

Fang Y, Eglen RM. Three-dimensional cell cultures in drug discovery and development. *SLAS Discovery*, 2017, 22, 456-472. DOI: 10.1177/1087057117696795.

Fernandez-Checa JC, Bagnaninchi P, Ye H, Sancho-Bru P, Falcon-Perez JM, Royo F, Garcia-Ruiz C, Konu O, Miranda J, Lunov O, Dejneka A, Elfick A, McDonald A, Sullivan GJ, Aithal GP, Lucena MI, Andrade RJ, Fromenty B, Kranendonk M, Cubero FJ, Nelson LJ. Advanced preclinical models for evaluation of drug-induced liver injury - consensus statement by the European Drug-Induced Liver Injury Network [PRO-EURO-DILI-NET]. *J. Hepatol.,* 2021, 75, 935-959. DOI: 10.1016/j.jhep.2021.06.021.

Foster JR, Lund G, Sapelnikova S, Tyrrell DL, Kneteman NM. Chimeric rodents with humanized liver: bridging the preclinical/clinical trial gap in ADME/toxicity studies. *Xenobiotica,* 2014, 44, 109-122.

Fromenty B, Pessayre D. Inhibition of mitochondrial beta-oxidation as a mechanism of hepatotoxicity. *Pharmacol. Ther.,* 1995, 67, 101-154. DOI: 10.1016/0163-7258(95)00012-6.

Funamoto K, Zervantonakis IK, Liu Y, Ochs CJ, Kim C, Kamm RD. A novel microfluidic platform for high-resolution imaging of a three-dimensional cell culture under a controlled hypoxic environment. *Lab Chip*, 2012, 12, 4855-4863. DOI: 10.1039/c2lc40306d.

Gage B K, Liu J C, Innes B T, MacParland S A, McGilvray I D, Bader G D, Keller G M. Generation of Functional Liver Sinusoidal Endothelial Cells from Human Pluripotent Stem-Cell-Derived Venous Angioblasts. *Cell Stem Cell*, 2020, *27*(2), 254-269.e9. DOI: 10.1016/J.STEM.2020.06.007

Gebhardt R. Metabolic zonation of the liver: regulation and implications for liver function. *Pharmacol. Ther.,* 1992, 53, 275-354.

Gencturk E, Mutlu S, Ulgen KO. Advances in microfluidic devices made from thermoplastics used in cell biology and analyses. *Biomicrofluidics*, 2017, 11, 051502. DOI: 10.1063/1.4998604.

Godoy P, Hewitt NJ, Albrecht U, Andersen M. E., Ansari, N., Bhattacharya, S., Bode, J. G., Bolleyn, J., Borner, C., Böttger, J., Braeuning, A., Budinsky, R. A., Burkhardt, B., Cameron, N. R., Camussi, G., Cho, C. S., Choi, Y. J., Craig Rowlands, J., Dahmen, U., Damm, G., … Hengstler JG. Recent advances in 2D and 3D *in vitro* systems using primary hepatocytes, alternative hepatocyte sources and non-parenchymal liver cells and their use in investigating mechanisms of hepatotoxicity, cell signaling and ADME. *Arch. Toxicol.,* 2013, 87, 1315-1530. DOI: 10.1007/s00204-013-1078-5.

Donato MT, Lahoz A, Castell JV, Gómez-Lechón MJ. Cell lines: a tool for *in vitro* drug metabolism studies. *Curr. Drug Metab*., 2008, 9, 1-11. DOI: 10.2174/138920008783331086.

Gómez-Lechón MJ, Tolosa L, Conde I, Donato MT. Competency of different cell models to predict human hepatotoxic drugs. *Expert Opin. Drug Metab. Toxicol*., 2014, 10, 1553-1568. DOI: 10.1517/17425255.2014.967680.

Gough A, Soto-Gutierrez A, Vernetti L, Ebrahimkhani MR, Stern AM, Taylor DL. Human biomimetic liver microphysiology systems in drug development and precision medicine. *Nat. Rev. Gastroenterol. Hepatol*., 2020, 18, 252-268. DOI: 10.1038/s41575-020-00386-1.

Griffin MJ, Sul HS. Insulin regulation of fatty acid synthase gene transcription: roles of USF and SREBP-1c. *IUBMB Life*, 2004, 56, 595-600. DOI: 10.1080/15216540400022474.

Guillouzo A. Liver cell models in *in vitro* toxicology. *Environ. Health Perspect.,* 1998, 106, 511-532. DOI: 10.1289/ehp.98106511.

Gu X, Manautou JE. Molecular mechanisms underlying chemical liver injury. *Expert Rev. Mol. Med*., 2012, 14, e4.

Guo XL, Yang KS, Hyun JY, Kim WS, Lee DH, Min KE, Park LS, Seo KH, Kim YI, Cho CS, Kang IK. Morphology and metabolism of Ba-alginate-encapsulated hepatocytes with

galactosylated chitosan and poly(vinyl alcohol) as extracellular matrices. *J. Biomater. Sci., Polym. Ed.,* 2003, 14, 551-565. DOI: 10.1163/15685620360674245.

Hammel S C, Hoffman K, Phillips A L, Levasseur J L, Lorenzo A M, Webster T F, Stapleton H M. Comparing the Use of Silicone Wristbands, Hand Wipes, and Dust to Evaluate Children's Exposure to Flame Retardants and Plasticizers. *Environmental Science and Technology*, 2020, *54*(7), 4484–4494. DOI: 10.1021/acs.est.9b07909

Han W, Wu Q, Zhang X, Duan Z. Innovation for hepatotoxicity *in vitro* research models: A review. *J. Appl. Toxicol.,* 2019, 39, 146-162. DOI: 10.1002/jat.3711.

Hegde M, Jindal R, Bhushan A, Bale SS, McCarty WJ, Golberg I, Usta OB, Yarmush ML. Dynamic interplay of flow and collagen stabilizes primary hepatocytes culture in a microfluidic platform*. Lab Chip*, 2014, 14, 2033-2039. DOI: 10.1039/c4lc00071d.

Hendriks DFG, Puigvert LF, Messner S, Mortiz W, Ingelman-Sundberg M. Hepatic 3D spheroid models for the detection and study of compounds with cholestatic liability. *Sci. Rep.,* 2016, 6, 35434. DOI: 10.1038/srep35434.

Ho CM, Ng SH, Li KH, Yoon YJ. 3D printed microfluidics for biological applications. *Lab Chip,* 2015, 15, 3627-3637. DOI: 10.1039/c5lc00685f.

Hughes JP, Rees S, Kalindjian SB, Philpott KL. Principles of early drug discovery. *Br. J. Pharmacol*., 2011, 162, 1239-1249. DOI: 10.1111/j.1476-5381.2010.01127.x

Hosseini V, Maroufi NF, Saghati S, Asadi N, Darabi M, Ahmad SNS, Hosseinkhani H, Rahbarghazi R. Current progress in hepatic tissue regeneration by tissue engineering. *J. Transl. Med.,* 2019, 17, 383. DOI: 10.1186/s12967-019-02137-6.

Ingber DE. Is it time for reviewer 3 to request human organ chip experiments instead of animal validation studies? *Adv. Sci.,* 2020, 7, 2002030. DOI: 10.1002/advs.202002030.

Jang KJ, Otieno MA, Ronxhi J, Lim HK, Ewart L, Kodella KR, Petropolis DB, Kulkarni G, Rubins JE, Conegliano D, Nawroth J, Simic D, Lam W, Singer M, Barale E, Singh B, Sonee M, Streeter AJ, Manthey C, Jones B, Srivastava A, Andersson LC, Williams D, Park H, Barrile R, Sliz J, Herland A, Haney S, Karalis K, Ingber DE, Hamilton GA. Reproducing human and cross-species drug toxicities using a Liver-Chip. *Sci. Transl. Med.,* 2019, 11, eaax5516. DOI: 10.1126/scitranslmed.aax5516.

Jaroch K, Jaroch A, Bojko B. Cell cultures in drug discovery and development: The need of reliable *in vitro-in vivo* extrapolation for pharmacodynamics and pharmacokinetics assessment. *J. Pharm. Biomed. Anal.,* 2018, 147, 297-312. DOI: 10.1016/j.jpba.2017.07.023.

Jellali R, Bricks T, Jacques S, Fleury MJ, Paullier P, Merlier F, Leclerc E. Long-term human primary hepatocyte cultures in a microfluidic liver biochip show maintenance of mRNA levels and higher drug metabolism compared with Petri cultures. *Biopharm. Drug Dispos.,* 2016, 37, 264-275. DOI: 10.1002/bdd.2010.

Jellali R, Gilard F, Pandolfi V, Legendre A, Fleury MJ, Paullier P, Legallais C, Leclerc E. Metabolomics-on-a-chip approach to study hepatotoxicity of DDT, permethrin and their mixtures. *J. Appl. Toxicol.,* 2018a, 38, 1121-1134. DOI: 10.1002/jat.3624.

Jellali R, Jacques S, Essaouiba A, Gilard F, Letourneur F, Gakière B, Legallais C, Leclerc E. Investigation of steatosis profiles induced by pesticides using liver organ-on-chip model and omics analysis. *Food Chem. Toxicol.,* 2021, 152, 112155. DOI: 10.1016/j.fct.2021.112155.

Jellali R, Paullier P, Fleury MJ, Leclerc E. Liver and kidney cells cultures in a new perfluoropolyether biochip. *Sens. Actuators, B,* 2016, 229, 396-407. DOI: 10.1016/j.snb.2016.01.141.

Jellali R, Zeller P, Gilard F, Legendre A, Fleury MJ, Jacques S, Tcherkez G, Leclerc E. Effects of DDT and permethrin on rat hepatocytes cultivated in microfluidic biochips: Metabolomics and gene expression study. *Environ. Toxicol. Pharmacol.,* 2018b, 59, 1-12. DOI: 10.1016/j.etap.2018.02.004.

Jiang T, Guo H, Xia YN, Liu Y, Chen D, Pang G, Feng Y, Yu H, Wu Y, Zhang S, Wang Y, Wang Y, Wen H, Zhang LW. Hepatotoxicity of copper sulfide nanoparticles towards hepatocyte spheroids using a novel multi-concave agarose chip method. *Nanomedicine,* 2021, 16, 1487-1504. DOI: 10.2217/nnm-2021-0011.

Jouin D, Blanchard N, Alexandre E, Delobel F, David-Pierson P, Lavé T, Jaeck D, Richert L, Coassolo P. Cryopreserved human hepatocytes in suspension are a convenient high throughput tool for the prediction of metabolic clearance. *Eur. J. Pharm. Biopharm.,* 2006, 63, 347-355. DOI: 10.1016/j.ejpb.2006.01.014.

Karagiannis P, Takahashi K, Saito M, Yoshida Y, Okita K, Watanabe A, Inoue H, Yamashita JK, Todani M, Nakagawa M, Osawa M, Yashiro Y, Yamanaka S, Osafune K. Induced pluripotent stem cells and their use in human models of disease and development. *Physiol. Rev.,* 2019, 99, 79-114. DOI: 10.1152/physrev.00039.2017.

Kartasheva-Ebertz D, Gaston J, Lair-Mehiri L, Massault PP, Scatton O, Vaillant JC, Morozov VA, Pol S, Lagaye S. Adult human liver slice cultures: Modelling of liver fibrosis and evaluation of new anti-fibrotic drugs. *World J. Hepatol.,* 2021, 13, 187–217. DOI: 10.4254/wjh.v13.i2.187.

Katila N, Bhurtel S, Park PH, Choi DY. Metformin attenuates rotenone-induced oxidative stress and mitochondrial damage via the AKT/Nrf2 pathway. *Neurochem. Int.,* 2021, 148, 105120. DOI: 10.1016/j.neuint.2021.105120.

Kazemnejad S. Hepatic tissue engineering using scaffolds: state of the art. *Avicenna J. Med. Biotechnol.,* 2009, 1, 135-145.

Keemink J, Oorts M, Annaert P. Primary hepatocytes in sandwich culture. *Methods Mol. Biol.,* 2015, 1250, 175-188. DOI: 10.1007/978-1-4939-2074-7_12.

Khazali AS, Clark AM, Wells A. A pathway to personalizing therapy for metastases using liver-on-a-chip platforms. *Stem Cell Rev. Rep.,* 2017, 13, 364-380. DOI: 10.1007/s12015-017-9735-3.

Khetani SR, Berger DR, Ballinger KR, Davidson MD, Lin C, Ware BR. Microengineered liver tissues for drug testing. *J. Lab. Autom.,* 2015, 20, 216-250. DOI: 10.1177/2211068214566939.

Kidambi S, Sheng L, Yarmush ML, Toner M, Lee I, Chan C. Patterned co-culture of primary hepatocytes and fibroblasts using polyelectrolyte multilayer templates. *Macromol. Biosci.,* 2007, 7, 344-353. DOI: 10.1002/mabi.200600205.

Kietzmann T. Metabolic zonation of the liver: The oxygen gradient revisited. *Redox Biol*., 2017, 11, 622-630.

Kimoto E, Chupka J, Xiao Y, Bi YA, Duignan DB. Characterization of digoxin uptake in sandwich-cultured human hepatocytes. *Drug Metab. Dispos.,* 2011, 39, 47-53. DOI: 10.1124/dmd.110.034298.

Knowlton S, Tasoglu S. A bioprinted liver-on-a-chip for drug screening applications. *Trends Biotechnol.,* 2016, 34, 681-682. DOI: 10.1016/j.tibtech.2016.05.014.

Koui Y, Kido T, Ito T, Oyama H, Chen SW, Katou Y, Shirahige K, Miyajima A. An *in vitro* human liver model by iPSC-derived parenchymal and non-parenchymal cells. *Stem Cell Rep.,* 2017, 9, 490-498. DOI: 10.1016/j.stemcr.2017.06.010.

Kulsharova G, Kurmangaliyeva A, Darbayeva E, Rojas- Solórzano L, Toxeitova G. Development of a hybrid polymer-based microfluidic platform for culturing hepatocytes towards liver-on-a-chip applications. *Polymer*, 2021, 13, 3215. DOI: 10.3390/polym13193215.

Kuna L, Bozic I, Kizivat T, Bojanic K, Mrso M, Kralj E, Smolic R, Wu GY, Smolic M. Models of drug induced liver injury (DILI) - current issues and future perspectives. *Curr. Drug Metab.,* 2018, 19, 830-838. DOI: 10.2174/1389200219666180523095355.

Kurth F, Györvary E, Heub S, Ledroit D, Paoletti S, Renggli K, Revol V, Verhulsel M, Weder G, Loizeau F. Organs-on-a-chip engineering. In: Hoeng J, Bovard D, Peitsch MC, eds. Organ-on-a-chip: Engineered Microenvironments for Safety and Efficacy Testing, Academic Press, 2020, pp. 47-130.

Kyffin JA, Sharma P, Leedale J, Colley HE, Murdoch C, Mistry P, Webb SD. Impact of cell types and culture methods on the functionality of *in vitro* liver systems - A review of cell systems for hepatotoxicity assessment. *Toxicol. In Vitro,* 2018, 48, 262–275. DOI: 10.1016/j.tiv.2018.01.023.

Lauschke VM, Hendriks DFG, Bell CC, Andersson TB, Ingelman-Sundberg M. Novel 3D culture systems for studies of human liver function and assessments of the hepatotoxicity

of drugs and drug candidates. *Chem. Res. Toxicol.,* 2016, 29, 1936-1955. DOI: 10.1021/acs.chemrestox.6b00150.

LeCluyse EL, Alexandre E, Hamilton GA, Viollon- Abadie C, Coon DJ, Jolley S, Richert L. Isolation and culture of primary human hepatocytes. *Methods Mol. Biol.,* 2005, 290, 207-229. DOI: 10.1385/1-59259-838-2:207.

Lee BH, Koh WJ, Choi MS, Suh GY, Chung MP, Kim H, Kwon OJ. Inactive hepatitis B surface antigen carrier state and hepatotoxicity during antituberculosis chemotherapy. *Chest,* 2005, 127, 1304-1311. DOI: 10.1378/chest.127.4.1304.

Lee H, Cho DW. One-step fabrication of an organ-on-a-chip with spatial heterogeneity using a 3D bioprinting technology. *Lab Chip*, 2016, 16, 2618-2625. DOI: 10.1039/c6lc00450d.

Lee HW, Kook YM, Lee HJ, Park H, Koh WG. A three-dimensional co-culture of HepG2 spheroids and fibroblasts using double-layered fibrous scaffolds incorporated with hydrogel micropatterns. *RSC Adv.,* 2014, 4, 61005-61011. DOI: 10.1039/C4RA12269K.

Lee J, Choi B, No DY, Lee G, Lee SR, Oh H, Lee SH. A 3D alcoholic liver disease model on a chip. *Integr. Biol.,* 2016, 8, 302-308. DOI: 10.1039/c5ib00298b.

Lee JH, Ho KL, Fan SK. Liver microsystems *in vitro* for drug response*. J. Biomed. Sci.,* 2019, 26, 88. DOI: 10.1186/s12929-019-0575-0.

Lee-Montiel FT, George SM, Gough AH, Sharma AD, Wu J, DeBiasio R, Vernetti LA, Taylor DL. Control of oxygen tension recapitulates zone-specific functions in human liver microphysiology systems. *Exp. Biol. Med*., 2017, 242, 1617-1632. DOI: 10.1177/1535370217703978.

Lee SY, Kim D, Lee SH, Sung JH. Microtechnology-based *in vitro* models: Mimicking liver function and pathophysiology. *APL Bioeng.,* 2021, 5, 041505. DOI: 10.1063/5.0061896.

Lefkowitch JH, Scheuer's Liver Biopsy Interpretation, 2016, pp. 383–403. ISBN: 9780702075889

Leist M, Single B, Castoldi AF, Kühnle S, Nicotera P. Intracellular adenosine triphosphate (ATP) concentration: a switch in the decision between apoptosis and necrosis. *J. Exp. Med.,* 1997, 185, 1481-1486. DOI: 10.1084/jem.185.8.1481.

Lewis JH, Kleiner DE. Hepatic injury due to drugs, herbal compounds, chemicals and toxins. In: Burt AD, Portmann BC, Ferrell LD, eds. MacSween's pathology of the liver. 6th ed. Edinburgh: Churchill Livingstone, 2012, pp 645-760.

Li L, Gokduman K, Gokaltun A, Yarmush ML, Usta OB. A microfluidic 3D hepatocyte chip for hepatotoxicity testing of nanoparticles. *Nanomedicine,* 2019, 14, 2209-2226. DOI: 10.2217/nnm-2019-0086.

Liu X, Chism JP, LeCluyse EL, Brouwer KR, Brouwer KL. Correlation of biliary excretion in sandwich-cultured rat hepatocytes and *in vivo* in rats. *Drug Metab. Dispos.,* 1999, 27, 637-644.

Li, Z. *In vitro* micro tissue and organ models for toxicity testing. In comprehensive Biotechnology (second edition), Moo-Young, M., Ed.; Academic press, 2011, pp. 551-563. DOI: 10.1016/B978-0-08-088504-9.00503-1.

Li Z, Li D, Guo Y, Wang Y, Su W. Evaluation of hepatic drug-metabolism for glioblastoma using liver-brain chip. *Biotechnol. Lett.,* 2021, 43, 383-392. DOI: 10.1007/s10529-020-03043-4.

Luo Y S, Chen Z, Hsieh N H, Lin T E. Chemical and biological assessments of environmental mixtures: A review of current trends, advances, and future perspectives. *Journal of Hazardous Materials*, 2022, *432*, 128658. DOI: 10.1016/J.JHAZMAT.2022.128658

Maepa SW, Ndlovu H. Advances in generating liver cells from pluripotent stem cells as a tool for modeling liver diseases. *Stem Cells,* 2020, 38, 606-612. DOI: 10.1002/stem.3154.

Makadia HK, Siegel SJ. Poly Lactic-co-Glycolic Acid (PLGA) as Biodegradable Controlled Drug Delivery Carrier. *Polymer,* 2011, 3, 1377-1397. DOI: 10.3390/polym3031377.

Malarkey DE, Johnson K, Ryan L, Boorman G, Maronpot RR. New insights into functional aspects of liver morphology. *Toxicol. Pathol*., 2005, 33, 27-34.

Maqbool F, Mostafalou S, Bahadar H, Abdollahi M. Review of endocrine disorders associated with environmental toxicants and possible involved mechanisms. *Life Sci.,* 2016, 145, 265-273. DOI: 10.1016/j.lfs.2015.10.022.

Martignoni M, Groothuis GMM, de Kanter R. Species differences between mouse, rat, dog, monkey and human CYP-mediated drug metabolism, inhibition and induction. *Expert Opin. Drug Metab. Toxicol.,* 2006, 2, 875-894. DOI: 10.1517/17425255.2.6.875.

Matai I, Kaur G, Seyedsalehi A, McClinton A, and Laurencin CT. Progress in 3D bioprinting technology for tissue/organ regenerative engineering. *Biomaterials*, 2020, 226, 119536. DOI: 10.1016/j.biomaterials.2019.119536.

Materne EM, Ramme AP, Terrasso AP, Serra M, Alves PM, Brito C, Sakharov DA, Tonevitsky AG, Lauster R, Marx U. A multi-organ chip co-culture of neurospheres and liver equivalents for long-term substance testing. *J. Biotechnol.,* 2015, 205, 36-46. DOI: 10.1016/j.jbiotec.2015.02.002.

Mathijs K, Kienhuis AS, Brauers KJJ, Jennen DGJ, Lahoz A, Kleinjans JCS, van Delft JHM. Assessing the metabolic competence of sandwich-cultured mouse primary hepatocytes. *Drug Metab. Dispos.,* 2009, 37, 1305-1311. DOI: 10.1124/dmd.108.025775.

Ma LD, Wang YT, Wang JR, Wu JL, Meng XS, Hu P, Mu X, Liang QL, Luo GA. Design and fabrication of a liver-on-a-chip platform for convenient, highly efficient, and safe in situ perfusion culture of 3D hepatic spheroids. *Lab Chip*, 2018, 18, 2547-2562. DOI: 10.1039/c8lc00333e.

Malik M, Yang Y, Fathi P, Mahler GJ, Esch MB. Critical considerations for the design of multi-organ microphysiological systems (MPS). *Front. Cell Dev. Biol.,* 2021, 9, 721338. DOI: 10.3389/fcell.2021.721338.

Marin TM, de Carvalho Indolfo N, Rocco SA, Basei FL, de Carvalho M, de Almeida Gonçalves K, Pagani E. Acetaminophen absorption and metabolism in an intestine/liver microphysiological system. *Chem. Biol. Interact*., 2019, 299, 59-76. DOI: 10.1016/j.cbi.2018.11.010.

Massa S, Sakr MA, Seo J, Bandaru P, Arneri A, Bersini S, Zare-Eelanjegh E, Jalilian E, Cha BH, Antona S, Enrico A, Gao Y, Hassan S, Acevedo JP, Dokmeci MR, Zhang YS, Khademhosseini A, Shin SR. Bioprinted 3D vascularized tissue model for drug toxicity analysis. *Biomicrofluidics,* 2017, 11, 044109. DOI: 10.1063/1.4994708.

McCarty WJ, Usta OB, Yarmush ML. A microfabricated platform for generating physiologically-relevant hepatocyte zonation. *Sci. Rep.,* 2016, 6, 26868. DOI: 10.1038/srep26868.

McGill MR, Jaeschke H. Animal models of drug-induced liver injury. *Biochim. Biophys. Acta, Mol. Basis Dis.,* 2019, 1865, 1031-1039.

McGonigle, P., & Ruggeri, B. Animal models of human disease: Challenges in enabling translation. *Biochemical Pharmacology*, 2014, *87*(1), 162–171. DOI: 10.1016/J.BCP.2013.08.006

Mérida-Ortega A, Rothenberg SJ, Torres-Sánchez L, Schnaas L, Hernández-Alcaraz C, Cebrián ME, García-Hernández RM, Ogaz-González R, López-Carrillo L. Polyunsaturated fatty acids and child neurodevelopment among a population exposed to DDT: a cohort study*. Environ. Health*, 2019, 18, 17. DOI: 10.1186/s12940-019-0456-8.

Milner E, Ainsworth M, McDonough M, Stevens B, Buehrer J, Delzell R, Wilson C, Barnhill J. Emerging three-dimensional hepatic models in relation to traditional two-dimensional *in vitro* assays for evaluating drug metabolism and hepatoxicity*. Med. Drug Discovery*, 2020, 8, 100060. DOI: 10.1016/j.medidd.2020.100060.

Mingoia RT, Nabb DL, Yang CH, Han X. Primary culture of rat hepatocytes in 96-well plates: effects of extracellular matrix configuration on cytochrome P450 enzyme activity and inducibility, and its application in *in vitro* cytotoxicity screening. *Toxicol. In Vitro*, 2007, 21, 165-173. DOI: 10.1016/j.tiv.2006.10.012.

Moradi E, Jalili-Firoozinezhad S, Solati-Hashjin M. Microfluidic organ-on-a-chip models of human liver tissue. *Acta Biomater.,* 2020, 116, 67-83. DOI: 10.1016/j.actbio.2020.08.041.

Mostafalou S, Abdollahi M. Pesticides: an update of human exposure and toxicity. *Arch. Toxicol.,* 2017, 91, 549-599. DOI: 10.1007/s00204-016-1849-x.

Nakamura T, Fujiwara K, Saitou M, Tsukiyama T. Non-human primates as a model for human development. *Stem Cell Rep.,* 2021, 16, 1093-1103. DOI: 10.1016/j.stemcr.2021.03.021.

Nakao Y, Kimura H, Sakai Y, Fujii T. Bile canaliculi formation by aligning rat primary hepatocytes in a microfluidic device. *Biomicrofluidics*, 2011, *5*(2), 022212. DOI: 10.1063/1.3580753

Nawroth JC, Petropolis DB, Manatakis DV, Maulana TI, Burchett G, Schlünder K, Witt A, Shukla A, Kodella K, Ronxhi J, Kulkarni G, Hamilton G, Seki E, Lu S, Karalis KC. Modeling alcohol-associated liver disease in a human Liver-Chip. *Cell Rep.,* 2021, 36, 109393. DOI: 10.1016/j.celrep.2021.109393.

Ng S, Han R, Chang S, Ni J, Hunziker W, Goryachev AB, Ong SH, Yu H. Improved hepatocyte excretory function by immediate presentation of polarity cues. *Tissue Eng*., 2006, 12, 2181-2191. DOI: 10.1089/ten.2006.12.2181.

Norikazu M, Yukina F, Haruo I, Ikumi T. Sandwich-Cultured Hepatocytes for Mechanistic Understanding of Hepatic Disposition of Parent Drugs and Metabolites by Transporter-Enzyme Interplay. *Drug Metab. Dispos.,* 2018, 46, 680-691. DOI: 10.1124/dmd.117.079236.

Olson H, Betton G, Robinson D, Thomas K, Monro A, Kolaja G, Lilly P, Sanders J, Sipes G, Bracken W, Dorato M, van Deun K, Smith P, Berger B, Heller A. Concordance of the toxicity of pharmaceuticals in humans and in animals. *Regul. Toxicol. Pharmacol.,* 2000, 32, 56-67. DOI: 10.1006/rtph.2000.1399.

Omiecinski CJ, vanden Heuvel JP, Perdew GH, Peters JM. Xenobiotic metabolism, disposition, and regulation by receptors: from biochemical phenomenon to predictors of major toxicities. *Toxicol. Sci.,* 2011, 120, S49-S75.

Palacio-Castañeda V, Velthuijs N, le Gac S, Verdurmen WPR. Oxygen control: the often overlooked but essential piece to create better *in vitro* systems. *Lab Chip,* 2022, 22, 1068-1092. DOI: 10.1039/d1lc00603g.

Pampaloni F, Reynaud EG, Stelzer EHK. The third dimension bridges the gap between cell culture and live tissue. *Nat. Rev. Mol. Cell Biol.,* 2007, 8, 839-845. DOI: 10.1038/nrm2236.

Pampaloni F, Stelzer E, Masotti A. Three-dimensional tissue models for drug discovery and toxicology. *Recent Pat. Biotechnol.,* 2009, 3, 103-117. DOI: 10.2174/187220809788700201.

Pati F, Cho DW. Bioprinting of 3D tissue models using decellularized extracellular matrix bioink. *Methods Mol. Biol.,* 2017, 1612, 381-390. DOI: 10.1007/978-1-4939-7021-6_27.

Picollet-D'hahan N, Zuchowska A, Lemeunier I, le Gac S. Multiorgan-on-a-chip: A systemic approach to model and decipher inter-organ communication. *Trends Biotechnol.,* 2021, 39, 788-810. DOI: 10.1016/j.tibtech.2020.11.014.

Piergiovanni M, Leite SB, Corvi R, Whelan M. Standardisation needs for organ on chip devices. *Lab Chip,* 2021, 21, 2857-2868. DOI: 10.1039/d1lc00241d.

Poisson J, Lemoinne S, Boulanger C, Durand F, Moreau R, Valla D, Rautou PE. Liver sinusoidal endothelial cells: Physiology and role in liver diseases. *J. Hepatol*., 2017, 66, 212-227.

Pires De Mello CP, Carmona-Moran C, McAleer CW, Perez J, Coln EA, Long CJ, Oleaga C, Riu A, Note R, Teissier S, Langer J, Hickman JJ. Microphysiological heart-liver body-on-a-chip system with a skin mimic for evaluating topical drug delivery. *Lab Chip*, 2020, 20, 749-759. DOI: 10.1039/c9lc00861f.

Polidoro MA, Ferrari E, Marzorati S, Lleo A, Rasponi M. Experimental liver models: From cell culture techniques to microfluidic organs-on-chip. *Liver Int.,* 2021, 41, 1744-1761. DOI: 10.1111/liv.14942.

Prior H, Baldrick P, de Haan L, Downes N, Jones K, Mortimer-Cassen E, Kimber I. Reviewing the utility of two species in general toxicology related to drug development. *Int. J. Toxicol.,* 2018, 37, 121-124. DOI: 10.1177/1091581818760564.

Prodanov L, Jindal R, Bale SS, Hegde M, Mccarty WJ, Golberg I, Bhushan A, Yarmush ML, Usta OB. Long-term maintenance of a microfluidic 3D human liver sinusoid. *Biotechnol. Bioeng.,* 2016, 113, 241-246. DOI: 10.1002/bit.25700.

Prot JM, Briffaut AS, Letourneur F, Chafey P, Merlier F, Grandvalet Y, Legallais C, Leclerc E. Integrated proteomic and transcriptomic investigation of the acetaminophen toxicity in liver microfluidic biochip. *PLoSOne*, 2011, 6, e21268. DOI: 10.1371/journal.pone.0021268.

Puryear JR, Yoon JK, Kim YT. Advanced fabrication techniques of microengineered physiological systems. *Micromachines*, 2020, 11, 730. DOI: 10.3390/mi11080730.

Radad K, Al-Shraim M, Al-Emam A, Wang F, Kranner B, Rausch WD, Moldzio R. Rotenone: from modelling to implication in Parkinson's disease. *Folia Neuropathol.,* 2019, 57, 317-326. DOI: 10.5114/fn.2019.89857.

Ramachandran SD, Vivarès A, Klieber S, Hewitt NJ, Muenst B, Heinz S, Walles H, Braspenning J. Applicability of second-generation upcyte® human hepatocytes for use in CYP inhibition and induction studies. *Pharmacol. Res. Perspect.,* 2015, 3, e00161. DOI: 10.1002/prp2.161.

Redaelli A, Long M. Bioengineering of the liver. *APL Bioeng.*, 2022, 6, 020401. DOI: 10.1063/5.0087886.

Ren K, Zhou J, Wu H. Materials for microfluidic chip fabrication. *Acc. Chem. Res.,* 2013, 46, 2396-2406. DOI: 10.1021/ar300314s.

Rodríguez-Alcalá LM, Sá C, Pimentel LL, Pestana D, Teixeira D, Faria A, Calhau C, Gomes A. Endocrine disruptor DDE associated with a high-fat diet enhances the impairment of

liver fatty acid composition in rats. *J. Agric. Food Chem.,* 2015, 63, 9341-9348. DOI: 10.1021/acs.jafc.5b03274.

Ruoß M, Vosough M, Königsrainer A, Nadalin S, Wagner S, Sajadian S, Huber D, Heydari Z, Ehnert S, Hengstler JG, Nussler AK. Towards improved hepatocyte cultures: Progress and limitations. *Food Chem. Toxicol*., 2020, 138, 111188. DOI: 10.1016/j.fct.2020.111188.

Sampaziotis F, de Brito MC, Madrigal P, Bertero A, Saeb-Parsy K, Soares FAC, Schrumpf E, Melum E, Karlsen TH, Bradley JA, Gelson WTH, Davies S, Baker A, Kaser A, Alexander GJ, Hannan NRF, Vallier L. Cholangiocytes derived from human induced pluripotent stem cells for disease modeling and drug validation. *Nat. Biotechnol.,* 2015, 33, 845-852. DOI: 10.1038/nbt.3275.

Sandson NB. Uridine 5′-diphospho-glucuronoslytransferases (UGTs): conjugating cousins, in A case approach to perioperative drug-drug Interactions. Editor Marcucci C. et al., New York, NY: Springer New York, 2015, pp 57-60.

Schaefer O, Ohtsuki S, Kawakami H, Inoue T, Liehner S, Saito A, Sakamoto A, Ishiguro N, Matsumaru T, Terasaki T, Ebner T. Absolute quantification and differential expression of drug transporters, cytochrome P450 enzymes, and UDP-glucuronosyltransferases in cultured primary human hepatocytes. *Drug Metab. Dispos.,* 2012, 40, 93-103. DOI: 10.1124/dmd.111.042275.

Schepers A, Li C, Chhabra A, Seney BT, Bhatia S. Engineering a perfusable 3D human liver platform from iPS cells. *Lab Chip*, 2016, 16, 2644-2653. DOI: 10.1039/c6lc00598e.

Schimek K, Frentzel S, Luettich K, Bovard D, Rütschle I, Boden L, Rambo F, Erfurth H, Dehne EM, Winter A, Marx U, Hoeng U. Human multi-organ chip co-culture of bronchial lung culture and liver spheroids for substance exposure studies. *Sci. Rep*., 2020, 10, 7865. DOI: 10.1038/s41598-020-64219-6.

Schmitt G, Barrow P, Stephan-Gueldner M. Alternatives to the use of nonhuman primates in regulatory toxicology. In The nonhuman primate in nonclinical drug development and safety assessment, Academic Press: Cambridge, MA, USA, 2015, pp. 337-355. DOI: 10.1016/B978-0-12-417144-2.00017-2.

Schoenenberger CA, Zuk A, Zinkl GM, Kendall D, Matlin KS. Integrin expression and localization in normal MDCK cells and transformed MDCK cells lacking apical polarity. *J. Cell Sci.,* 1994, 107, 527-541. DOI: 10.1242/jcs.107.2.527.

Schultz A, Saville B R, Marsh J A, Snelling T L. An introduction to clinical trial design. *Paediatric Respiratory Reviews*, 2019, *32*, 30–35. DOI: 10.1016/J.PRRV.2019.06.002

Seeff LB, Cuccherini BA, Zimmerman HJ, Adler E, Benjamin SB. Acetaminophen hepatotoxicity in alcoholics. A therapeutic misadventure. *Ann. Intern. Med*., 1986, 104, 399-404. DOI: 10.7326/0003-4819-104-3-399.

Selden C, Spearman CW, Kahn D, Miller M, Figaji A, Erro E, Bundy J, Massie I, Chalmers SA, Arendse H, Gautier A, Sharratt P, Fuller B, Hodgson H. Evaluation of encapsulated liver cell spheroids in a fluidised-bed bioartificial liver for treatment of ischaemic acute liver failure in pigs in a translational setting. *PLoS One,* 2013, 8, 82312. DOI: 10.1371/journal.pone.0082312.

Semba RD. The discovery of the vitamins. *Int. J. Vitam. Nutr. Res.,* 2012, 82, 310-315.

Shaw AJ, Gescher A, Mráz J. Cytotoxicity and metabolism of the hepatotoxin N-methylformamide and related formamides in mouse hepatocytes. *Toxicol. Appl. Pharmacol.,* 1988, 95, 162-170. DOI: 10.1016/s0041-008x(88)80015-2.

Shetty S, Lalor PF, Adams DH. Liver sinusoidal endothelial cells - gatekeepers of hepatic immunity. *Nat. Rev. Gastroenterol. Hepatol.*, 2018, 15, 555–567.

Singh N, Jenkins GJS, Asadi R, Doak SH. Potential toxicity of superparamagnetic iron oxide nanoparticles (SPION). *Nano Rev.,* 2010, 1, 5358. DOI: 10.3402/nano.v1i0.5358.

Si-Tayeb K, Lemaigre FP, Duncan SA. Organogenesis and development of the liver. *Dev. Cell*, 2010, 18, 175-189.

Si-Tayeb K, Noto FK, Nagaoka M, Li J, Battle MA, Duris C, North PE, Dalton S, Duncan SA. Highly efficient generation of human hepatocyte-like cells from induced pluripotent stem cells. *Hepatology,* 2010, 51, 297-305. DOI: 10.1002/hep.23354.

Sivaraman A, Leach J, Townsend S, Iida T, Hogan B, Stolz D, Fry R, Samson L, Tannenbaum S, Griffith L. A microscale *in vitro* physiological model of the liver: predictive screens for drug metabolism and enzyme induction. *Curr. Drug Metab.,* 2005, 6, 569-591. DOI: 10.2174/138920005774832632.

Sleeboom JJF, den Toonder JMJ, Sahlgren CM. MDA-MB-231 Breast Cancer Cells and Their CSC Population Migrate Towards Low Oxygen in a Microfluidic Gradient Device. *Int. J. Mol. Sci.,* 2018, 19, 3047. DOI: 10.3390/ijms19103047.

Skardal A, Smith L, Bharadwaj S, Atala A, Soker S, Zhang Y. Tissue specific synthetic ECM hydrogels for 3-D *in vitro* maintenance of hepatocyte function. *Biomaterials*, 2012, 33, 4565-4575. DOI: 10.1016/j.biomaterials.2012.03.034.

Soldatow VY, Lecluyse EL, Griffith LG, Rusyn I. *In vitro* models for liver toxicity testing. *Toxicol. Res.,* 2013, 2, 23-39.

Soltantabar P, Calubaquib EL, Mostafavi E, Ghazavi A, Stefan MC. Heart/liver-on-a-chip as a model for the evaluation of cardiotoxicity induced by chemotherapies. *Organs-on-a-Chip*, 2021, 3, 100008. DOI: 10.1016/j.ooc.2021.100008.

Snyder JE, Hamid Q, Wang C, Chang R, Emami K, Wu H, Sun W. Bioprinting cell-laden matrigel for radioprotection study of liver by pro-drug conversion in a dual-tissue microfluidic chip. *Biofabrication,* 2011, 3, 034112. DOI: 10.1088/1758-5082/3/3/034112.

Sollier E, Murray C, Maoddi P, di Carlo D. Rapid prototyping polymers for microfluidic devices and high-pressure injections. *Lab Chip,* 2011, 11, 3752-3765. DOI: 10.1039/c1lc20514e.

Son YW, Choi HN, Che JH, Kang BC, Yun JW. Advances in selecting appropriate non-rodent species for regulatory toxicology research: Policy, ethical, and experimental considerations. *Regul. Toxicol. Pharmacol.,* 2020, 116, 104757. DOI: 10.1016/j.yrtph.2020.104757.

Štampar M, Breznik B, Filipič M, Žegura B. Characterization of *in vitro* 3D cell model developed from human hepatocellular carcinoma (HepG2) cell line. *Cell,* 2020, 9, 2557. DOI: 10.3390/cells9122557.

Steinmetz K L, Spack E G. The basics of preclinical drug development for neurodegenerative disease indications. *BMC Neurology*, 2009, *9*(SUPPL. 1), 1–13. DOI: 10.1186/1471-2377-9-S1-S2/FIGURES/3

Suzuki H, Mitsuno K, Shiroguchi K, Tsugane M, Okano T, Dohi T, Tsuji T. One-step micromolding of complex 3D microchambers for single-cell analysis. *Lab Chip,* 2017, 17, 647-652. DOI: 10.1039/c6lc01313a.

Szafranska K, Kruse L D, Holte C F, McCourt P, Zapotoczny B. The wHole Story About Fenestrations in LSEC. *Frontiers in Physiology*, 2021, *12*, 1468. DOI: 10.3389/FPHYS.2021.735573/BIBTEX

Takahashi K, Tanabe K, Ohnuki M, Narita M, Ichisaka T, Tomoda K, Yamanaka S. Induction of pluripotent stem cells from adult human fibroblasts by defined factors. *Cell*, 2007, 131, 861-872. DOI: 10.1016/j.cell.2007.11.019.

Takayama K, Inamura M, Kawabata K, Katayama K, Higuchi M, Tashiro K, Nonaka A, Sakurai F, Hayakawa T, Kusuda Furue M, Mizuguchi H. Efficient generation of functional hepatocytes from human embryonic stem cells and induced pluripotent stem cells by HNF4α transduction. *Mol. Ther.,* 2012, 20, 127-137. DOI: 10.1038/mt.2011.234.

Tan K, Keegan P, Rogers M, Lu M, Gosset JR, Charest J, Bale SS. A high-throughput microfluidic microphysiological system (PREDICT-96) to recapitulate hepatocyte function in dynamic, re-circulating flow conditions. *Lab Chip,* 2019, 19, 1556-1566. DOI: 10.1039/c8lc01262h.

Tasnim F, Xing J, Huang X, Mo S, Wei X, Tan MH, Yu H. Generation of mature kupffer cells from human induced pluripotent stem cells. *Biomaterials,* 2019, 192, 377-391. DOI: 10.1016/j.biomaterials.2018.11.016.

Theobald J, Ghanem A, Wallisch P, Banaeiyan AA, Andrade-Navarro MA, Taškova K, Haltmeier M, Kurtz A, Becker H, Reuter S, Mrowka R, Cheng X, Wölfl S. Liver-kidney-on-chip to study toxicity of drug metabolites. *ACS Biomater. Sci. Eng.,* 2018, 4, 78-89. DOI: 10.1021/acsbiomaterials.7b00417.

Toepke MW, Beebe DJ. PDMS absorption of small molecules and consequences in microfluidic applications. *Lab Chip,* 2006, 6, 1484-1486. DOI: 10.1039/b612140c.

Toh YC, Lim TC, Tai D, Xiao G, van Noort D, Yu H. A microfluidic 3D hepatocyte chip for drug toxicity testing. *Lab Chip,* 2009, 9, 2026-2035. DOI: 10.1039/b900912d.

Tolosa L, Gómez-Lechón MJ, López S, Guzmán C, Castell JV, Donato MT, Jover R. Human upcyte hepatocytes: Characterization of the hepatic phenotype and evaluation for acute and long-term hepatotoxicity routine testing. *Toxicol. Sci.,* 2016, 152, 214-229. DOI: 10.1093/toxsci/kfw078.

Tonin M, Descharmes N, Houdré R. Hybrid PDMS/glass microfluidics for high resolution imaging and application to sub-wavelength particle trapping. *Lab Chip*, 2016, 16, 465-470. DOI: 10.1039/c5lc01536g.

Tricot T, Verfaillie CM, Kumar M. Current status and challenges of human induced pluripotent stem cell-derived liver models in drug discovery. *Cell,* 2022, 11, 442. DOI: 10.3390/cells11030442.

Tsao CW. Polymer Microfluidics: Simple, low-cost fabrication process bridging academic lab research to commercialized production. *Micromachines,* 2016, 7, 225. DOI: 10.3390/mi7120225.

Usta OB, McCarty WJ, Bale S, Hegde M, Jindal R, Bhushan A, Golberg, Yarmush ML. Microengineered cell and tissue systems for drug screening and toxicology applications: Evolution of in-vitro liver technologies. *Technology*, 2015, 3, 1-26.

Valdiviezo A, Kato Y, Baker E S, Chiu W A, Rusyn I. Evaluation of Metabolism of a Defined Pesticide Mixture through Multiple *In Vitro* Liver Models. *Toxics*, 2022, *10*(10), 566. DOI: 10.3390/TOXICS10100566/S1

Vallverdú J, Martínez García de la Torre RA, Mannaerts I, Verhulst S, Smout A, Coll M, Ariño S, Rubio-Tomás T, Aguilar-Bravo B, Martínez-Sánchez C, Blaya D, Verfaillie CM, van Grunsven LA, Sancho-Bru P. Directed differentiation of human induced pluripotent stem cells to hepatic stellate cells, *Nat. Protoc.,* 2021, 16, 2542-2563. DOI: 10.1038/s41596-021-00509-1.

van Berlo D, van de Steeg E, Amirabadi HE, Masereeuw R. The potential of multi-organ-on-chip models for assessment of drug disposition as alternative to animal testing. *Curr. Opin. Toxicol.,* 2021, 27, 8-17. DOI: 10.1016/j.cotox.2021.05.001.

van Delft J, Mathijs K, Polman J, Coonen M, Szalowska E, Verheyen GR, van Goethem F, Driessen M, van de Ven L, Ramaiahgari S, Price LS. Hepatotoxicity screening on *in vitro* models and the role of 'omics. In Toxicogenomics-Based Cellular Models: Alternatives to animal testing for safety assessment, Elsevier Inc. Academic Press, 2014, pp. 193-212. DOI: 10.1016/B978-0-12-397862-2.00010-3.

Vangijzegem T, Stanicki D, Laurent S. Magnetic iron oxide nanoparticles for drug delivery: applications and characteristics. *Expert Opin. Drug Delivery*, 2019, 16, 69-78. DOI: 10.1080/17425247.2019.1554647.

Vickers AEM, Fisher RL. Human liver slices to investigate injury and repair. *Appl. In Vitro Toxicol.,* 2018, 4, 280-287. DOI: 10.1089/aivt.2018.0017.

Viravaidya K, Sin A, Shuler ML. Development of a microscale cell culture analog to probe naphthalene toxicity. *Biotechnol. Prog*., 2004, 20, 316-323. DOI: 10.1021/bp0341996.

Volarevic V, Markovic BS, Gazdic M, Volarevic A, Jovicic N, Arsenijevic N, Armstrong L, Djonov V, Lako M, Stojkovic M. Ethical and Safety Issues of Stem Cell-Based Therapy. *Int. J. Med. Sci.,* 2018, 15, 36-45. DOI: 10.7150/ijms.21666.

Waldbaur A, Rapp H, Länge K, Rapp BE. Let there be chip—towards rapid prototyping of microfluidic devices: one-step manufacturing processes. *Anal. Methods*, 2011, 3, 2681-2716. DOI: 10.1039/C1AY05253E.

Ware BR, Berger DR, Khetani SR. Prediction of drug-induced liver injury in micropatterned co-cultures containing iPSC-derived human hepatocytes. *Toxicol. Sci*. 2015, 145, 252-262. DOI: 10.1093/toxsci/kfv048.

Weisgrab G, Ovsianikov A, Costa PF. Functional 3D printing for microfluidic chips. *Adv. Mater. Technol.*, 2019, 4, 1900275. DOI: 10.1002/admt.201900275.

Weng YS, Chang SF, Shih MC, Tseng SH, Lai CH. Scaffold-free liver-on-a-chip with multiscale organotypic cultures. *Adv. Mater.,* 2017, 29, 1701545. DOI: 10.1002/adma.201701545.

Wouters OJ, McKee M, Luyten J. Estimated Research and Development Investment Needed to Bring a New Medicine to Market, 2009-2018. JAMA. 2020 ;323(9):844-853. DOI: 10.1001/jama.2020.1166.

Xia L, Ng S, Han R, Tuo X, Xiao G, Leo HL, Cheng T, Yu H. Laminar-flow immediate-overlay hepatocyte sandwich perfusion system for drug hepatotoxicity testing. *Biomaterials*, 2009, 30, 5927-5936. DOI: 10.1016/j.biomaterials.2009.07.022.

Xu L, Hui AY, Albanis E, Arthur MJ, O'Byrne SM, Blaner WS, Mukherjee P, Friedman SL, Eng FJ. Human hepatic stellate cell lines, LX-1 and LX-2: new tools for analysis of hepatic fibrosis. *Gut*, 2005, 54, 142-151. DOI: 10.1136/gut.2004.042127.

Yi HG, Lee H, Cho DW. 3D printing of organs-on-chips. *Bioengineering*, 2017, 4, 10. DOI: 10.3390/bioengineering4010010.

Yu F, Choudhury D. Microfluidic bioprinting for organ-on-a-chip models. *Drug Discov. Today*, 2019, 24, 1248-1257. DOI: 10.1016/j.drudis.2019.03.025.

Yu F, Deng R, Hao Tong W, Huan L, Chan Way N, Islambadhan A, Iliescu C, Yu H. A perfusion incubator liver chip for 3D cell culture with application on chronic hepatotoxicity testing. *Sci. Rep.,* 2017, 7, 14528. DOI: 10.1038/s41598-017-13848-5.

Yuwen P, Chen W, Lv H, Feng C, Li Y, Zhang T, Hu P, Guo J, Tian Y, Liu L, Sun J, Zhang Y. Albumin and surgical site infection risk in orthopaedics: a meta-analysis. *BMC Surg.*, 2017, 17, 7.

Zafrani ES, Ishak KG, Rudzki C. Cholestatic and hepatocellular injury associated with erythromycin esters: report of nine cases. *Dig. Dis. Sci.,* 1979, 24, 385-396. DOI: 10.1007/BF01297126.

Zeilinger K, Freyer N, Damm G, Seehofer D, Knöspel F. Cell sources for *in vitro* human liver cell culture models. *Exp. Biol. Med.,* 2016, 241, 1684-1698. DOI: 10.1177/1535370216657448.

Zheng YB, Ma LD, Wu JL, Wang YM, Meng XS, Hu P, Liang QL, Xie YY, Luo GA. Design and fabrication of an integrated 3D dynamic multicellular liver-on-a-chip and its application in hepatotoxicity screening. *Talanta*, 2022, 241, 123262. DOI: 10.1016/j.talanta.2022.123262.

Zhou Y. The recent development and applications of fluidic channels by 3D printing. *J. Biomed. Sci.,* 2017, 24, 80. DOI: 10.1186/s12929-017-0384-2.

Zuchowska A, Kwapiszewska K, Chudy M, Dybko A, Brzozka Z. Studies of anticancer drug cytotoxicity based on long-term HepG2 spheroid culture in a microfluidic system. *Electrophoresis*, 2017, 38, 1206-1216. DOI: 10.1002/elps.201600417.

Chapter 2: Materials and Methods

In this chapter we will present all the materials and methods used in this project. They are more detailed and precise description of the ones published in our papers in addition to the materials and methods used in **chapter 6**.

Messelmani T, Le Goff A, Souguir Z, Maes V, Roudaut M, Vandenhaute E, Maubon N, Legallais C, Leclerc E, Jellali R. Development of an advanced liver organ-on-chip integrating hydroscaffold mimicking cell matrix, Bioengineering, 2022, no. 9: 443

DOI: 10.3390/bioengineering9090443

Messelmani T, Le Goff A, Soncin F, Souguir Z, Merlier F, Maubon N, Legallais C, Leclerc E, Jellali R. Coculture model of a liver sinusoidal endothelial cell barrier and hepatocyte spheroids-on-chip in an advanced fluidic platform, Biotechnology and Bioengineering, Preprint,

DOI: 10.22541/au.167596570.02002054/v1

Messelmani T, Le Goff A, Soncin F, Gilard F, Souguir Z, Maubon N, Gakière B, Legallais C, Leclerc E, Jellali R. Investigation of the metabolomic crosstalks between liver sinusoidal endothelial cells and hepatocytes exposed to paracetamol using organ-on-chip technology, Toxicology, under review

2.1. Biochip fabrication and characterization

2.1.1. Mould design

The hepatic biochip was fabricated using a PDMS moulding technique. First of all, the patterns for both the bottom and top layers were created using a design software and an SU-8 photosensitive resin was used to replicate that design on the mould masters. The top layer consists of a culture reservoir of around 100 µm depth with an inlet and an outlet for flow circulation. The bottom layer, corresponding to the culture area, is patterned with 15 lines of 9 culture chambers connected with 8 microchannels each line. The rectangular chambers (520 by 510 µm) are the privileged area of culture, and the microchannels 1050 µm are used to ensure a uniform flow circulation all along the culture chambers. The bottom layer has a height of 100 µm making the total height of the bonded biochip to 200 µm with a theorical culture surface of 1.95 cm² and a total volume of 45 µL (Figure 2.1). The design was developed and patented by Dr. Eric Leclerc (FR0954288). The master mould was fabricated by Laboratoire d'analyse et d'architecture des systèmes (LAAS, Toulouse). Briefly, a liquid photoresist (SU-8 serial 2100, microchem) was spin coated on a Silicon (Si) plate to obtain the desired height, then the design was printed on a high-precision photomask which will be used to UV-insolate the exposed part and generate the shallow structures. the plate was then heated to evaporate the solvent and harden the structures then rinsed in an acetate solution to eliminate the uncured photoresist. The same process was done to obtain the two layers. At this point, the wafers were ready to be used for the fabrication of PDMS biochips.

2.1.2. Biochip fabrication

The two layers of the biochip were fabricated separately and then bonded to form a sealed system. The polydimethylsiloxane (PDMS) (SYLGRAD 184 kit, Dow Corning) composed of a kit of pre-polymer (liquid form) (SYLGRAD 184, silicone elastomer Base, USA) and a curing agent (SYLGRAD 184, silicon elastomer curing agent, USA) which were mixed in a 10/1 ratio in mass (depending on the ratio, different stiffnesses are obtained) then poured on the moulds: 3 g used for the lower side and 5 g for the upper side (Figure 2.1A). The PDMS was then degassed using a vacuum bell to eliminate the trapped air bubbles for 30 minutes then the PDMS was cured for 2 h at 75°C. The cured PDMS was pealed from the Si wafer, two 2 mm holes were drilled in the reservoir part as an inlet and an outlet for flow circulation. Finally, the two structured surfaces were ionized using reactive air plasma (300 mTorr, 1 min, Harrick Scientific) and aligned together to form an irreversible bonding. Silicon tubes were then introduced in the inlet and the outlet with two polypropylene connectors (female Luer ID

= 0.16 cm, Cole Parmer, France) which will interface with the microfluidic circuit. Finally, the biochips were shaped with a puncher for shape standardization.

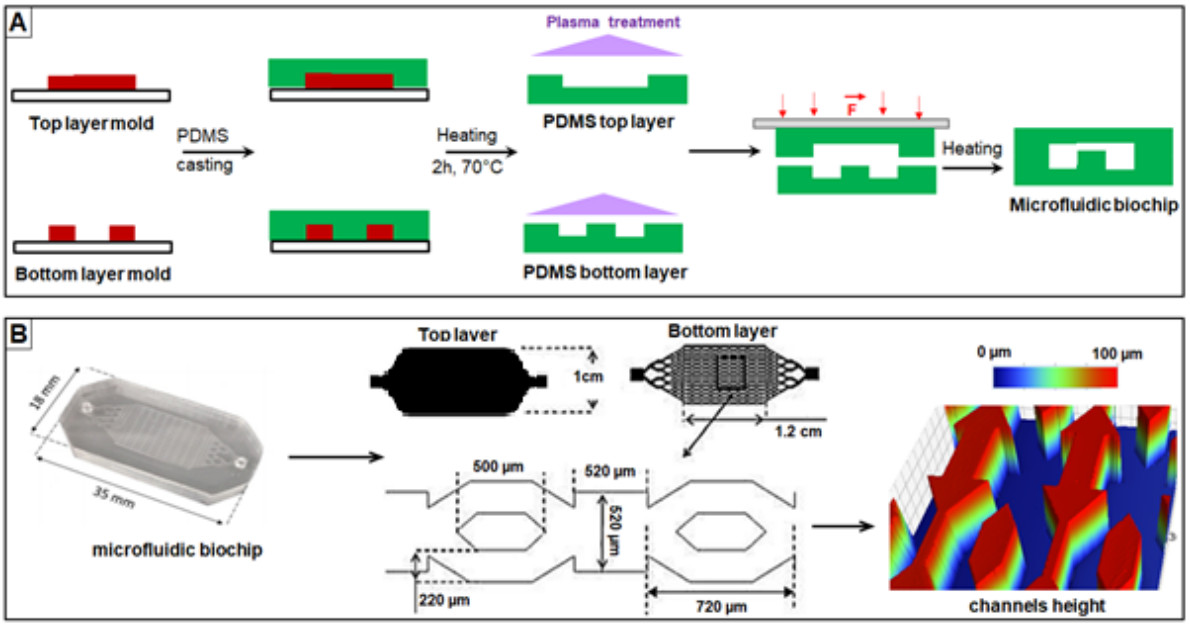

Figure 2.1. *Different steps for the microfabrication of liver biochip (A) Soft lithography process used for biochip fabrication; (B) Biochip design and dimensions.*

2.1.3. Hydroscaffolds integration

In order to organize the cells in 3D we converged on using a hyaluronic-acid (HA) based hydroscaffold. Hyaluronic acid is natural and biologically active polymer produced by the mesenchymal cells and liberated in the ECM space to provide mechanical support. We used BIOMIMESYS® liver (HCS Pharma, France). It is mainly composed of hyaluronic acid to which the tripeptide Arg-Gly-Asp (RGD) was grafted. The RGD motif is usually found within the extracellular matrix protein and it mediates cell-substratum and cell-cell interactions. In addition, the HA is grafted with galactosamine allowing the binding between the cell surface receptors and the other ECM proteins that were added. The hydroscaffold was crosslinked with adipic dihydrazide crosslinker (ADH). Rat tail type I and placenta type IV were integrated to confer strength stretching mechanics. The hydroscaffold is porous with 117±23 µm pores (Figure 2.2C) and a Young modulus of around 0.6 kPa corresponding to the stiffness ranges of healthy liver (Desai et al., 2016).

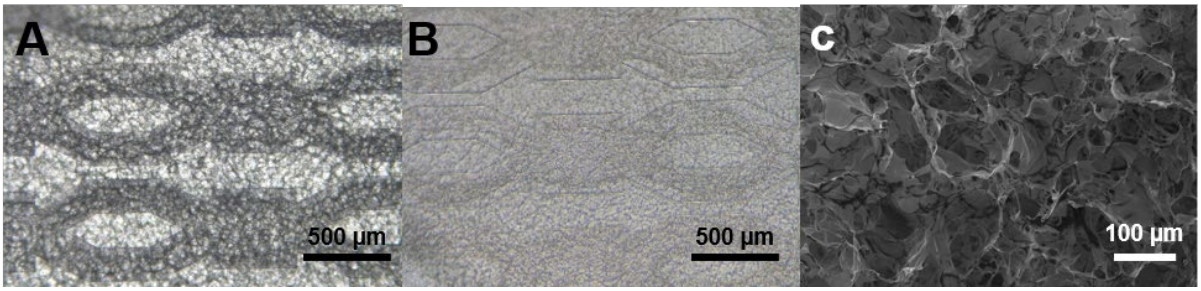

Figure 2.2. *Organization and structure of the hydroscaffold (A) dehydrated hydroscaffold integrated in the liver biochip (B) Hydrated hydroscaffold integrated in the biochip (C) SEM analysis of the hydroscaffold structure.*

Once the biochips were fabricated they are sent to HCS pharma for the hydroscaffold integration. The prepolymer aqueous solution composed of HA-g-RGDs, HA-g-GalN, collagen and ADH were injected in the biochip and the crosslinking was realized *in situ*. The hydroscaffold was then freeze-dried (Figure 2.2A) and the biochip was UV sterilized to allow preservation until use. The same hydroscaffold was injected into 48-well plate. Each well corresponding to the same culture surface as the biochip was used as 3D static culture condition. The hydroscaffold was hydrated using culture prior use (Figure 2.2B).

2.1.4. Hydrodynamic resistance of the biochip

In order to characterize the hydrodynamic resistance of the biochip, at different steps, the biochip was detached from the peristaltic pump perfusion circuit and introduced into a new circuit with pressure-driven flow circulation (Figure 2.3). The circuit was composed of a pressure controller (MFCS-EX, Fluigent, France) pressurizing an inlet and outlet tubes (corning, centristar, USA), the inlet tube was connected to a flow sensor (flow Unit type M, Fluigent, France) which was connected to the biochip and then the outlet tube. The different components were interconnected via PEEK tubes (1/32" x 0.25mm x 30 cm, CLUZEAU, France). The flow rate was then calculated following the equation $\Delta P = R_h \times Q$, where ΔP is the pressure differential between the inlet and the outlet of the perfusion circuit, R_h is the sum of the hydrodynamic resistance of the different components of the circuit and Q is the flow rate.

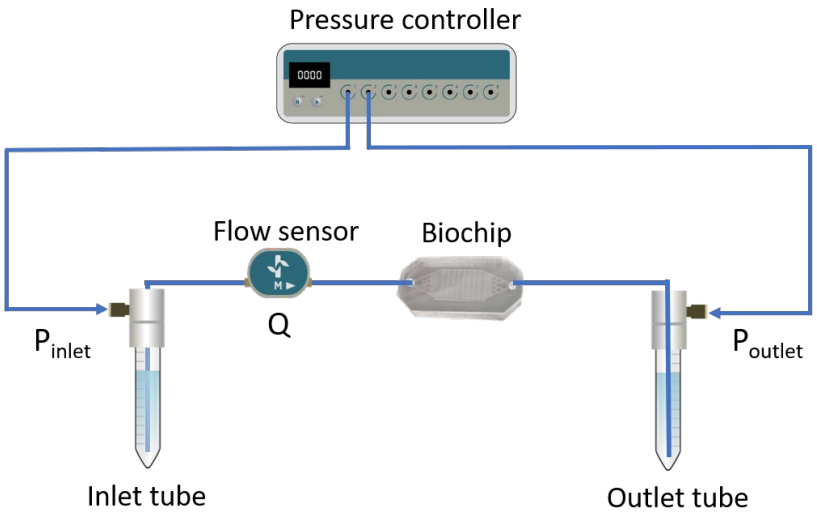

***Figure 2. 3**. Pressure controlled microfluidic circuit used to control the flow circulation in the biochip.*

The hydrodynamic resistance of the different tubes, caused by the friction loss, was measured and subtracted from the total hydrodynamic resistance of the microfluidic circuit to characterize the hydrodynamic resistance of the biochip.

2.2. Cell culture platforms

2.2.1. Integrated Dynamic Cell Culture Microchip

In order to parallelize the perfusion circuit and test multiple conditions. Leclerc et al. patented (patent n° WO2011107519A2) the integrated dynamic cell culture microchip (IDCCM) platform (Figure 2.4A). Inspired from a 24-well plate and fabricated by heat press of polycarbonate to form 24 wells, the IDCCM can host 12 independent biochips. The platform was composed of 2 parts. The bottom layer was composed of the 24 culture medium reservoirs to which the 12 biochips were plugged via two polypropylene connectors at the bottom of each couple of reservoirs (2 mL of culture medium volume per well). The top layer was the interface with the perfusion circuit, to each couple reservoir a perfusion circuit was associated ensuring the culture medium circulation. The perfusion circuit was composed of silicone PharMed BTP tubings (ID = 0.089 cm, Cole Parmer) that are squeezed through the peristaltic pump (ISM949, ISMATEC) actuators forcing the circulation of the culture medium from a reservoir to another through the biochip (Figure 2.4B). The two layers were sealed with a silicone gasket and the whole system was quenched with a clamping system. A Plexiglas® support was designed to hold the IDCCM on peristaltic pump. The IDCCM

ensures the culture of independent biochips (Figure 2.4C), or the culture reservoirs can be connected to study the interactions of serial biochips to understand the organs interactions.

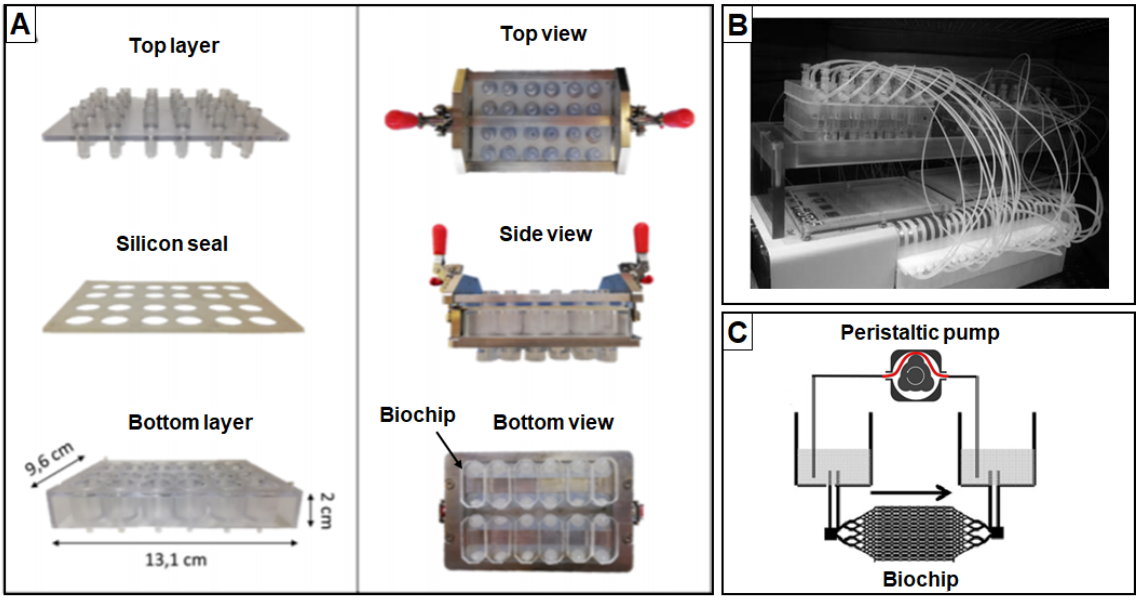

Figure 2.4. *Design of the IDCCM (A) Different compartments of IDCCM device; (B): IDCCM device (with biochip in the bottom) connected to peristaltic pump; (C) principle of the IDCCM device and perfusion cultures.*

2.2.2. Integrated Insert in a Dynamic Microfluidic Platform

We used the previously described coculture system named IIDMP for "Integrated Insert in a Dynamic Microfluidic Platform" (Bricks et al., 2014). The system is a polycarbonate fluidic platform composed of three subunits (Figure 2.5). Each subunit is composed of the association of an insert and a biochip linking two wells. The insert was placed in the first well and defined an apical pole (LSECs barrier) and a basal pole allowing the exchange of culture medium between the LSECs barrier and the hepatocyte compartment (biochip, Figure 2.5). The biochip connected the first and the second well (acting as reservoir). The overall IIDMP device consisted of three subunits and allowed the coculture of three inserts and three biochips simultaneously. The volume of culture medium was 10 mL: 1 mL placed in the apical insert, 5 mL below the insert and 4 ml in the second well. The perfusion was made possible by the circulation of culture medium between the basal compartment of the first well and the second well. The perfusion fluid was provided by a cover connected to a peristaltic pump via PTFE (polytetrafluoroethylene) tubings. This cover allowed to hermetically close the IIDMP device. The other components of the IIDMP platform were silicon gaskets sealing the device and a bottom layer composed of the wells subunits, allowing the connection of biochips (in the bottom, Figure 2.5).

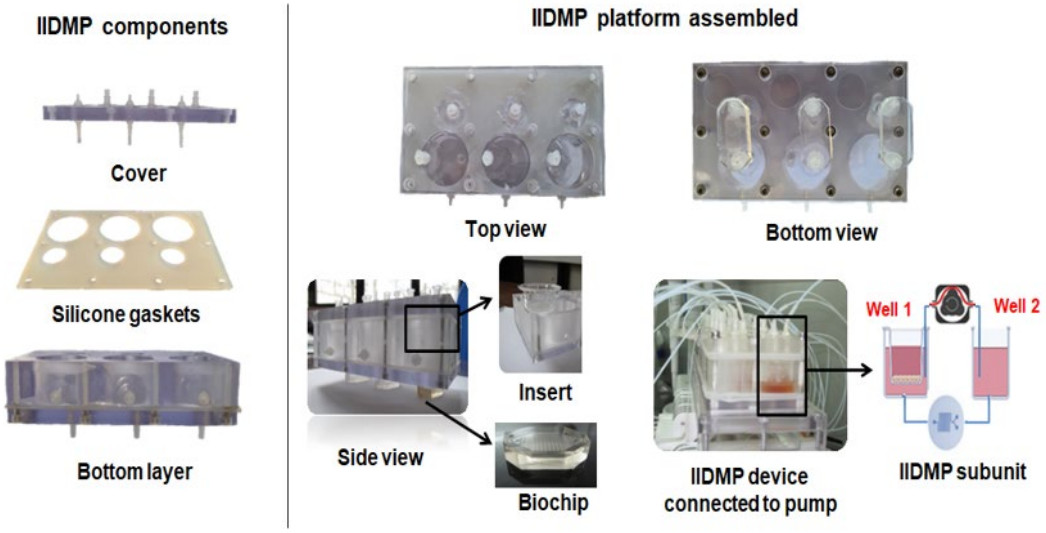

Figure 2. 5. *Specifications and principle of the IIDMP platform.*

2.3. Cell Culture assessments

2.3.1. HepG2/C3a cell line

The HepG2/C3a (ATCC-CRL-10741, France), a clone of the hepG2 line and derived from a human hepatocarcinoma was used as hepatocyte model for the proof of concept for the hepatocytes compartment of the liver-on-chip model. The cells have the ability to produce albumin, alpha fetoprotein (AFP) and the ability to grow in a glucose deficient medium. The HepG2/C3a are adherent cells, they are cultivated in a T75 cm² flask with cell culture treated surface. Cells were cultured in Minimal Essential Medium with phenol red (MEM, Gibco). The culture medium was supplemented with 10% fetal bovine serum, 2 mM L-glutamine, 0.1 mM of nonessential amino acids, 1 mM sodium pyruvate and a mix of 100 U/mL penicillin, 100 µg/mL streptomycin. The supplements were purchased from Pan Biotech, France. The culture medium was renewed every 2 days and at confluence the cells were detached using 0.25% trypsin-EDTA (Gibco) for 5 min at 37°C and the cells were seeded at a density of 13 000 cell/cm² in the T75 flask or at the corresponding densities if used in the biochips.

2.3.2. SK-HEP-1 cell line

The SK-HEP-1 (ATCC-HTB-52, France) is a human cell line derived from an adenocarcinoma of the liver. The cell line expresses endothelial-specific markers with the capacity to form tubular structures. In addition, they possess numerous pores on surface also called fenestrae. The SK-HEP-1 cell line was used as liver sinusoid endothelial cells (LSEC). The LSEC form the barrier between the hepatocytes and the sinusoids and play a crucial role in the exchanges between the two compartments. The SK-HEP-1 are adherent cells, they

were cultivated in a T75 cm² flask with cell culture treated surface. The cells were cultured in a mix of Endothelial cell growth Basal Medium-2 (EBM-2™, Lonza) and Minimal Essential Medium with phenol red (MEM, Gibco) at a 1:3 (v/v) ratio. The MEM was supplemented with 10% foetal bovine serum, 2 mM L-glutamine, 0.1 mM of nonessential amino acids, 1 mM sodium pyruvate and a mix of 100 U/mL penicillin, 100 µg/mL streptomycin. The EBM-2™ is supplemented with its SingleQuots following the supplier recommendations. The Supplement Pack was composed of 2% foetal bovine serum, hydrocortisone, Basic Human Fibroblast Growth Factor (hFGF-B), Vascular endothelial growth factor (VEGF), Insulin-like Growth Factor (R3-IGF), Ascorbic Acid, human epidermal Growth Factor (hEGF), Gentamicin-Amphotericin (GA-1000) and Heparin. The culture medium was renewed every 2 days and at confluence the cells are detached using 0.25% trypsin-EDTA (Gibco) for 5 min at 37°C and the cells were seeded at a density of 3 500 cell/cm² in the T75 flask or in THINCERT® Cell Culture Inserts (0.4 µm, Greiner).

2.3.3. Primary human hepatocytes

Primary human cryoconserved hepatocytes (Cytes® biotechnology, Spain) were used as hepatocytes model in the liver-on-chip. The cells are 3D/spheroids qualified and plateable in collagen I coated plates. The cells were directly thawed following the vendor instructions. The Hepatocytes Thawing Medium (MHT) (Cytes biotechnology, Spain) was used at the thawing step. For the adhesion phase, the Hepatocyte Plating Medium (MHP) (cytes biotechnology, Spain) was used and then replaced, at the culture step, by the Hepatocyte Basal Medium (HBM™ basal medium, Lonza) completed with Hepatocyte Culture Medium supplements (HCM™ Kit SingleQuots™, Lonza) containing Bovine Serum Albumin (BSA) fatty acid free, hydrocortisone, recombinant human Epidermal Growth Factor (rh EGF), transferrin, Ascorbic acid, Insulin, Gentamicin and Amphotericin (GA-1000). The concentrations of the supplements of the primary human cryoconserved hepatocytes culture medium were not disclosed by the supplier.

2.4. Experimental setup for the liver-on-chip cultures

2.4.1. HepG2/C3a culture in the hydroscaffold-integrated biochips

One day before use, the biochips and the Petri dishes were unsealed from the UV-sterilized bags and the hydroscaffold was hydrated by injecting 200 µL of culture medium to each well/biochip. 48-well Petri dishes were used as static control since the culture surface area of each well was equivalent to the culture surface area of the chambers inside the biochip (2 cm²). The biochips and Petri dishes were then incubated overnight at 37°C. Once the hydroscaffold hydrated, the cells were detached from the T75 flask using 0.25% trypsin-

EDTA (Gibco) and an appropriate number is injected (20 000, 125 000, 250 000 cell/cm²). The biochips and the Petri dishes were then placed in a 5% CO_2 and 37°C incubator overnight for cell adhesion. The perfusion circuit and the IDCCM were autoclaved before use.

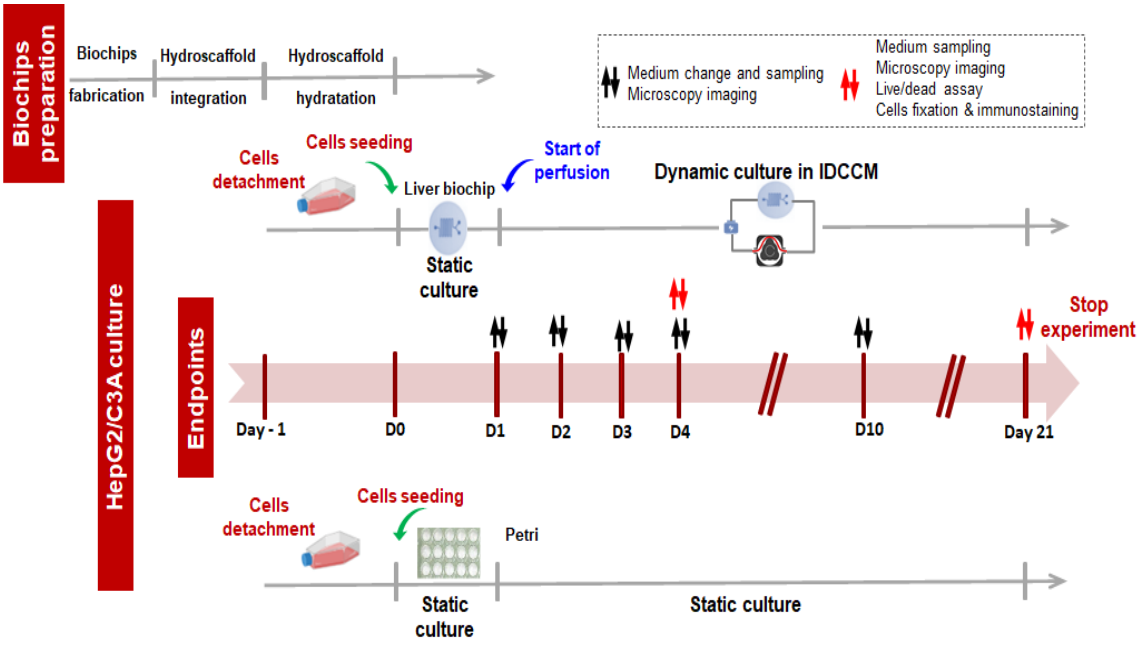

Figure 2. 6. *Experimental procedures used for HepG2/C3a cell culture in the biochip and Petri containing the HA-hydroscaffold.*

Once the cells have adhered, the biochips were plugged into the IDCCM and 2 mL of culture medium were injected in every well. The IDCCM was then connected to the peristaltic pump through the perfusion circuit and the flow rate was set at 10 µL/min. The culture medium for the Petri dishes was renewed and with the IDCCM, they were placed in a humidified incubator at 5% CO_2 and 37°C. The culture medium was renewed daily for the Petri dish and the IDCCM (Figure 2.6). At every culture medium changing, samples were saved for quantification analyses and at different endpoints, biochips and Petri dishes wells were detached and the cells were fixed for staining. At the 21st day of culture, the perfusion was stopped, the biochip detached and the whole system was rinsed in bleach then in Milli-Q® water and left to dry until the next use. The same process was repeated for the tubing.

2.4.2. HepG2/C3a – SK-HEP-1 culture in the IIDMP platform

2.4.2.1. Optimization of common culture medium for HepG2/C3a and SK-HEP-1

Culture medium optimization was performed in static conditions, different MEM/EGM-2 ratios were tested. The SK-HEP-1 cells were seeded in cell culture inserts (6-well format, polyethylene terephthalate membrane, 0.4 µm pore, THINCERT Greiner) at a density of 0.35

10^5 cell/cm^2. The culture medium was renewed every 2 days in the apical (1 mL) and basal (2 mL) compartments, and the culture was maintained until confluence was reached (6-8 days). The HepG2/C3a were seeded in the wells of a 6-well plate at a density of of 10^5 cell/cm^2. The culture was maintained for 4 days and the medium (2 mL) was changed every 2 days. The cultures were continuously maintained at 37°C in a 5% CO_2 supplied incubator and the assays were performed at the end of the experiments.

2.4.2.2. Dynamic monoculture and coculture in the IIDMP device

Each experiment lasted two days (Figure 2.7). The SK-HEP-1 inserts were maintained in culture during 8 days for the formation of a confluent barrier, before performing the dynamic experiments, as mentioned in section 2.4.1. In parallel, 24 h before the dynamic experiments, HepG2/C3a cells were seeded in the biochips containing the hydroscaffold (4 10^5 cell/biochip) and the biochips were incubated overnight at 37°C in a humidified atmosphere with 5% of CO_2.

At day 0 of the experiment, the SK-HEP-1 previously grown for 8 days on inserts were transferred in the first well of the IIDMP device and the HepG2/C3a biochips were connected to the bottom of the device. As shown in Figure 2.7, three conditions were established: SK-HEP-1 monoculture (IIDMP with insert alone), HepG2/C3a monoculture (IIDMP with biochip alone) and coculture (IIDMP containing insert and biochip). Culture medium was added (1 mL in the apical insert side, 5 mL in the basal side and 4 mL in the reservoir well), the IIDMP was closed and connected to the pump. The entire setup was placed in the incubator and perfusion started at 10 µL/min for 48 h in a closed loop. For exposures to drugs, acetaminophen (APAP, Sigma-Aldrich) was loaded in the apical compartment of the insert at 1 mM before perfusion starting (an insert without cells was used for HepG2/C3a monoculture experiments). After dilution into the total medium in the circuit (10 mL), the systemic concentration of APAP was 100 µM.

For each experiment, three IIDMP devices were used simultaneously, in order to achieve 9 replicates/condition and per experiment. At the end of the experiment, the pump was stopped and the cover removed. The culture media were sampled and the SK-HEP-1 inserts and HepG2/C3a biochips were detached from the device to perform the assays.

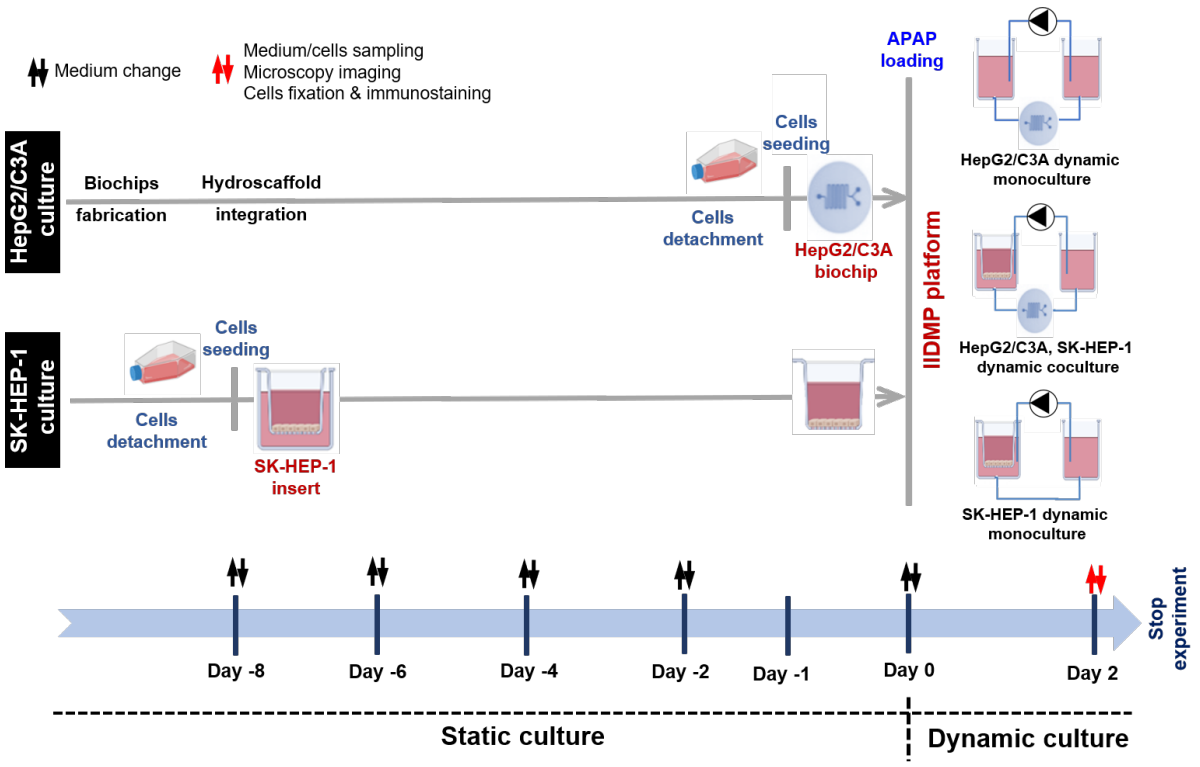

Figure 2. 7. Experimental procedures for SK-HEP-1 and HepG2/C3A monoculture and coculture.

2.4.3. Primary human hepatocytes in the IDCCM

The biochips and the Petri dishes were prepared like described in section 4.1. the primary human cryopreserved hepatocytes were seeded into the hydroscaffold-integrated biochips and Petri dishes at a density of 400 000 cell/cm². The cells were then incubated in a humidified incubator overnight at 37°C with 5% of CO_2 using the Hepatocytes Plating Medium. As shown in figure 2.8, at day 1, the Hepatocytes plating medium in replaced by the supplemented hepatocytes basal medium and the 12 biochips were connected to the bottom of the IDCCM device and mounted on the peristaltic pump for the dynamic culture. The same culture medium exchange is repeated for the Petri dishes. The culture was maintained for 7 days with culture medium renewal and sampling each 2 days for the biochips and each day for the Petri dishes. At day 7, the PHH culture in the Petri dishes is stopped. The culture medium sampled and the biochips detached for further analysis.

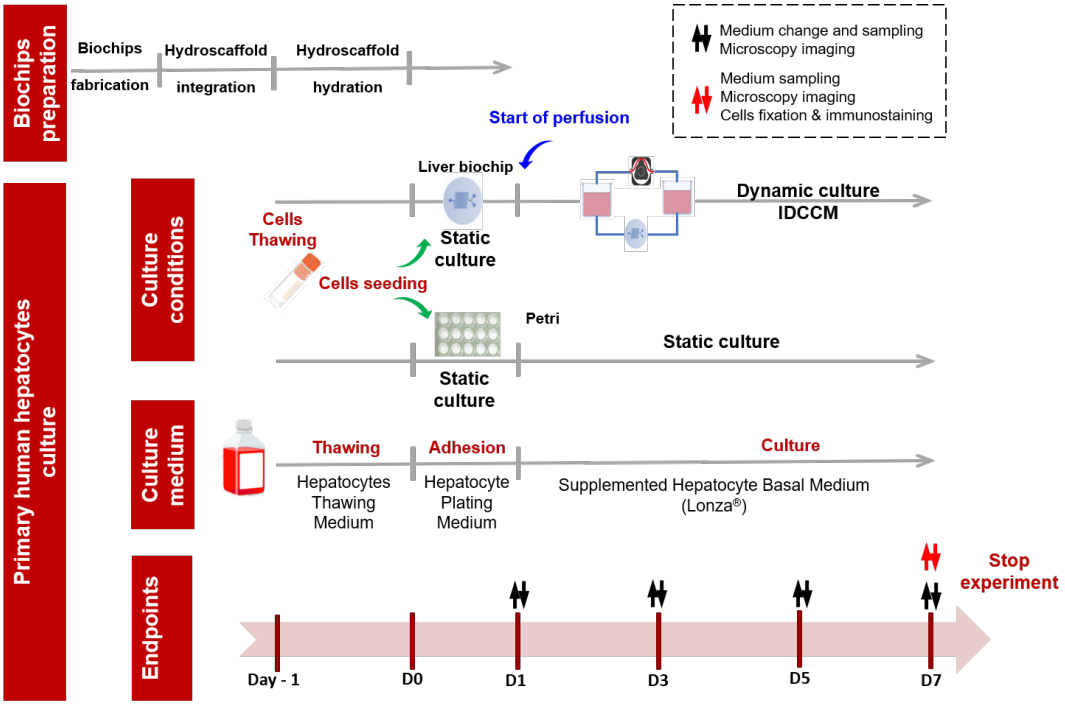

Figure 2. 8. *Experimental procedure for the PHH culture in Petri dishes and the IDCCM*

2.5. Biological and imaging assays

2.5.1. Viability assay

At the end of the experiments, the viability of the spheroids was assessed using the LIVE/DEAD™ kit (Thermo Fisher scientific). The kit is composed of a solution of ethidium homodimer-1 (excitation peak at 528 nm and emission peak at 617 nm) used to stain the dead cells and calcein-AM (excitation peak at 495 nm and emission peak at 520 nm) used to stain the living cells. The ethidium homodimer-1 become fluorescent when bonded with DNA indicating the cells were dead while the calcein-AM is converted by the living cell through non-specific esterase emitting fluorescence indicating the functioning of the cells. The biochips were rinsed 3 times with phosphate-buffered saline (PBS, Gibco) to eliminate the exceeding culture medium and the cells were incubated with a mix of ethidium homodiemer-1 at a concentration of 4 µM and calcein-AM at a concentration of 2 µM in a humidified incubator at 37°C and 5% CO_2 for 20 minutes. The staining solutions are then washed 3 times with PBS and the spheroids are mounted on an epifluorescence microscope (Leica DMI 6000B, Leica Microsystems).

2.5.2. Immunohistochemistry staining and confocal microscopy imaging

Once the biochips or the inserts detached from the culture platform and in order to maintain their structure, the cells were fixed with paraformaldehyde (PFA, MP biomedicals). The PFA

creates covalent cross-links between the molecules making an insoluble meshwork. The culture medium was washed 3 times with PBS then the samples are incubated with paraformaldehyde 30 min at room temperature. The PFA was then washed with PBS and the samples were stored in PBS until staining.

In order to perform the immunohistochemistry staining, the samples were permeabilized with 0.5% Triton X-100 solution for 30 min at room temperature. Then the unspecific binding sites were blocked with 1% bovine serum albumin (BSA, Sigma Aldrich in PBS) for 30 min. The primary antibodies (table 2.1) were diluted in PBS solution with BSA at 1% following the manufacturer recommendations and incubated with the samples overnight at 4°C.

***Table 2.1**. Primary and secondary antibodies used to stain the samples*

Immunostaining / Function	Primary antibody / Dilution	Secondary antibody / Dilution
E-cadherin Mediator for cell-cell adhesion	Mouse anti-E-cadherin, (BDB610181, BD Biosciences) 1/1000	Donkey anti-mouse Alexa Fluor 647 (ab150107, Abcam) 1/1000
MRP2 Polarization of the hepatocytes	Rabbit anti-MRP2, (M8316, Sigma Aldrich) 1/1000	Goat anti-rabbit Alexa Fluor 680, (A21109, Invitrogen) 1/1000
BSEP (ABCB11) The ATP-dependent secretion of bile salts into the canaliculus of hepatocytes	Rabbit anti-ABCB11/BSEP, (ab155421, Abcam) 1/1000	Goat anti-rabbit Alexa Fluor 488, (A11034, Invitrogen) 1/1000
PECAM (CD31) Platelet endothelial cell adhesion molecule	Mouse anti- PECAM/CD31, (ab24590, Abcam) 1/1000	Donkey anti-mouse Alexa Fluor 647 (ab150107, Abcam) 1/1000
Stabilin-2 Scavenger receptor expressed on the sinusoidal endothelial cells of the liver	Rabbit anti-stabilin-2, (ab121893, Abcam) 1/1000	Goat anti-rabbit Alexa Fluor ® 680, (A21109, Invitrogen) 1/1000
Vimentin Maintenance of cellular integrity and resistance against stress	Mouse anti-vimentin, (ab8978, Abcam) 1/1000	Donkey anti-mouse Alexa Fluor ® 647 (ab150107, Abcam) 1/1000
Albumin Specific protein produced by the hepatocytes	Goat anti-human albumin, (A80-129A, Bethyl) 1/1000	Donkey anti-goat Alexa Fluor ® 488 (ab150129, abcam) 1/1000
CYP3A4 Important enzyme produced mainly in the liver Involved in the drug metabolism	Rabbit anti-CYP3A4 (ab3572, abcam) 2/1000	Donkey anti-Rabbit Alexa Fluor ® 568 (A10042, Invitrogen) 1/1000

At the end of the primary antibodies' incubation, the staining solution was washed with PBS three times and the secondary antibody's solution diluted in PBS and BSA at 1% is introduced. The samples were then incubated at 4°C overnight. Apart from the immunostaining, nuclei were stained to identify the position of the cells using DAPI (4′,6-diamidino-2-phenylindole, D1306, Invitrogen) at 10 µg/mL and for the F-actin structure, the phalloidin (Alexa Fluo 488 Phalloidin, Thermo Fisher) was used as a cytoskeleton marker at 25 µM. The DAPI and F-actin were introduced in the secondary antibody's solution.

Prior confocal microscopy observation (Zeiss LSM 710), the staining solution was washed with PBS then the samples are mounted on the observation slide, Mowiol® (81381-50G, Sigma Aldrich) was used as mounting medium.

2.5.3. Scanning electron microscopy (SEM)

The SEM analysis was used to observe the fenestrae for the SK-HEP-1 cell line and the organization of the spheroids in the biochip. At different endpoints, the culture medium was eliminated by three PBS washing and the samples were fixed with a mix of Sodium cacodylate trihydrate (C0250-25G, Sigma Aldrich) at 0.1 M and glutaraldehyde 25 % (1042390250, Sigma Aldrich) at 2.5%. The samples were incubated for 30 min at RT in contact with the fixation solution then washed three times with PBS.

To avoid the alteration of the cellular structures when creating the vaccum with the SEM, and prior observation, the samples were dehydrated through a cascade of dehydration. Alcohol solutions going from 30% to 100% were prepared and the samples were incubated for 1 hour at each step. At the 100% solution step, the samples were left at room temperature to dry. Given the poorly conduction of the biological samples, an ultra-thin coating of platinum was applied in order to increase their electrical-conductivity. The images were taken using an XL30-ESEM FEG (Philips, Eindhoven, The Netherlands).

2.6. Endothelial barrier permeability assays

2.6.1. Lucifer yellow

Lucifer Yellow (LY) is a fluorescent molecule used to test the paracellular transport across the endothelial (SK-HEP-1) barrier. The LY (Lucifer Yellow CH dipotassium salt, Sigma-Aldrich) was diluted in hanks' balanced salt solution (HBSS, with $CaCl_2$ and $MgCl_2$, Gibco) at 50 µM and deposited in the apical compartment of an empty insert and inserts with cells cultured for 4, 8, 12 and 15 days. The basal compartment was only filled with HBSS. The inserts were then incubated at 37°C and 5% of CO_2. After 90 min, the medium was collected from the apical and the basal compartments. The fluorescence intensity (correlated to LY

concentration) was measured with a microplate reader (TECAN Spectafluor Plus) using an excitation wavelength of 485 nm and an emission wavelength of 530 nm. The flow of LY was expressed by the calculation of the apparent permeability (Papp, pm/s) as follows:

$$\mathbf{Papp = (dQ/dt) \times (1/ACa)}$$

Where dQ/dt is the amount of LY transported during a given time (mol/s), Ca is the initial concentration of LY solution (mol/m^3) and A is the surface of the insert (cm^2).

2.6.2. FITC-Dextran

The SK-HEP-1 barrier permeability to molecules of different molecular weights was assessed using fluorescein isothiocyanate-dextrans (FITC-dextran 4, 70 and 150 kDa, Sigma-Aldrich). The assays were performed using confluent SK-HEP-1 barriers (8 days of culture) in static and dynamic (IIDMP device) conditions. The dextrans were diluted in the culture medium at a concentration of 100 µg/mL and deposited in the apical compartment of the culture inserts. Then, culture medium was sampled in the apical and basal compartments at different times. The FITC-dextran fluorescence intensity was measured using a microplate reader (TECAN Spectafluor Plus) at excitation/emission wavelengths of 490/525 nm.

2.7. Quantification assays

2.7.1. Albumin

The albumin, a major protein secreted by the hepatocytes, was quantified through ELISA sandwich assay. The human albumin ELISA Quantitation Set (E80-129, Bethyl Laboratories) was used following the manufacturer instructions. First of all, the surfaces of a flat-bottom 96 well microplates were sensitized with a Carbonate-Bicarbonate 1M buffer and 100 µL of goat anti human albumin antibody (A80-129A-9, Bethyl Laboratories) was incubated at RT for 1 hour. The wells were then washed 5 times with a washing buffer (50mM Tris, 0.14M, 0.05% tween 20, pH 8, Sigma Aldrich). The unspecific bindings were then blocked with Tris 50mM, NaCl 0.14M buffer and 1% BSA solution for 30 min at RT. The exceeding solution was then washed 5 times with the washing buffer. 100 µL of the standards, serially diluted from the Human reference serum at 22 mg/mL (RS10-100-4, Bethyl Laboratories), and the samples were added to each well and incubated 1 h at RT. After the incubation, the exceeding solutions were washed 5 times with the washing buffer and 100µL of the HRP conjugated Human Albumin Detection Antibody (A80-129P, Bethyl Laboratories) diluted (1/50 000) in 50mM Tris, 0.14M NaCl, 1% BSA and 0.05% Tween were incubated in each well 1 hour at RT. After the incubation, the wells were washed 5 times with the washing buffer and the reaction was revealed with o-phenylenediamine dihydrochloride (OPD) (5 mg, Sigma Aldrich) and H_2O_2 (30%, Sigma Aldrich) diluted in citrate buffer (0.05 M, pH 7.4). the plate was

protected from light for 20 min then the reaction was stopped by adding 100 µL of sulfuric acid at 0.18 M in each well. The absorbance was then measured with a microplate reader at 492 nm (Spark 10M, TECAN). The measured albumin concentration was normalized with the initial volume of culture medium. For the HepG2/C3a, the normalization was done by considering the same density of initial seeding in the biochips and the Petri dishes. For the Primary human hepatocytes, the concentration was normalized for 1 million cells since the PHH do not proliferate when cultivated *in vitro*.

2.7.2. Urea

The urea production, a major chemical compound produced in the liver, was measured directly from the culture medium via a colorimetric method using the urea assay kit (QuantiChrom DIUR100, BioAssay Systems). The reaction consists of a first step of condensation of the ortho-phthaldialdedyde with urea followed by the rapid reaction with primaquine diphosphate create a colored product. Prior dosing the two reagent A and B were mixed at a 1:1 (v/v) and equilibrated at room temperature. Then, in a clear bottom 96-well plate 50 µL of the samples, standard and blank were introduced in duplicate in separate wells. To each well was then added 200 µL of the reagent A:B mix and incubated 50 min at RT. The optical density was measured at 430 nm with microplate reader (Spark 10M, TECAN). The measured Urea concentration was normalized with the initial volume of culture medium. For the HepG2/C3a, the normalization was done by considering the same density of initial seeding in the biochips and the Petri dishes. For the Primary human hepatocytes, the concentration was normalized with for 1 million cells since the PHH do not proliferate when cultivated *in vitro*.

2.7.3. Interleukin-6 measurement

ELISA sandwich assays were used to quantify the IL-6 concentration in the culture media collected at the end of the experiments. The assay was performed using human IL-6 ELISA Kit (ab718013, abcam) following the protocols recommended by the manufacturers. The results were acquired using a Spectafluor Plus microplate reader (TECAN) set to a wavelength of 450 nm.

2.7.4. RNA extraction and RTqPCR analysis

At the end of the experiments, the culture media were removed from biochips and inserts, and the cells (HepG2/C3a and SK-HEP-1) were lysed and recovered using 500 µL of TRIzol (Thermofischer Scientific) and stored at -80 °C until use. Total RNA was purified by phenol/chloroform extraction followed by alcohol precipitation, and RNA concentrations

measured using a NanodropOne (Thermofisher Scientific). Reverse transcription reactions were performed using a High-capacity cDNA reverse transcription kit with RNase inhibitor (Applied Biosystems, ThermoFisher Scientific). Quantitative PCRs were performed using a StepOnePlus machine (Applied Biosystems, Thermofisher Scientific) in duplex reactions, mixing the cDNA with the TaqMan FAM-labelled probes of the selected gene (Applied Biosystems, ThermoFisher Scientific) and a β2-microglobulin-VIC-labeled probe as a reference endogenous control (Table 2.2.). The threshold cycle (C_T) values were calculated at the upper linear range of the logarithm^{-2} amplification curve using the StepOne v2.3 software (Thermofisher scientific). The data were then expressed as $2^{-\Delta\Delta C_T}$ with ΔC_T is the difference between C_T of the transcript of interest and C_T of the reference, and $\Delta\Delta C_T$ is the difference between the mean ΔC_T of experimental samples the mean ΔC_T of control samples (Livak & Schmittgen, 2001). The relative quantity (RQ) corresponds to $2^{-\Delta\Delta C_T}$ which transforms the logarithmic^{-2} data into decimal values.

Table 2. 2. *TaqMan probes used for RTqPCR assays*

Gene	Probe ID	Fluorophore
B2M	Human B2M (beta-2-microglobulin) Endogenous Control	VIC/MGB probe, primer limited
STAB1	Hs01109068_m1	FAM/MGB
PECAM1	Hs01065279_m1	FAM/MGB
MRC1	Hs00267207_m1	FAM/MGB
KDR	Hs00911700_m1	FAM/MGB
CD32b	Hs01634996_s1	FAM/MGB
VCAM1	Hs01003372_m1	FAM/MGB
ICAM1	Hs00164932_m1	FAM/MGB
CD45	Hs04189704_m1	FAM/MGB
CLEC4M	Hs03805885_g1	FAM/MGB
UGT2B7	Hs00426592_m 1	FAM/MGB
UGT1A1	Hs02511055_s1	FAM/MGB
SULT1A2	Hs02340929_g1	FAM/MGB
CYP1A2	Hs00167927 _m1	FAM/MGB
CYP1A1	Hs01054796_g1	FAM/MGB
TNFα	Hs01113624_g1	FAM/MGB

IL-1	Hs01555410_m1	FAM/MGB
IL-6	Hs00985639_m1	FAM/MGB
IL-8/ CXCL8	Hs00174103_m1	FAM/MGB

2.7.5. HPLC-HRMS

APAP and APAP metabolites detection and quantitative evaluation were performed by LC-HRMS. The HPLC system (Infinity 1290, Agilent Technologies, France) with DAD, was connected to a Q-TOF micro hybrid quadrupole time of flight mass spectrometer (Agilent 6538, Agilent Technologies, France) with electrospray ionization (ESI). HPLC was carried out on a Thermo Hypersyl Gold C18 (USP L1) column (150 mm × 4.6 mm ID, 5 µm, 175 A), connected to an Agilent Infinity 1290 HPLC at 40°C. The solvent system was A: 0.1% formic acid in H_2O and B: Acetonitrile. The gradient program began with 5% B, held at 5% for 1 min and ramped to 20% B at 5 min and to 95% at 7 min, held at 95% for 3 min, until decreased to initial condition and held at 5 % for 1 min. The flow rate was set at 1 mL/min. All compounds responses were measured in ESI+ and ESI- alternatively and were calibrated externally. The ESI Gas Temp was 350 °C, at electrospray voltage +3800 V or – 3500V. Drying Gaz was set at 10 L/min and Nebuliser was at 30 psi. Fragment voltage was set at 110 V. HRMS spectrum was registered at 5 Hz in the mass range of 50 to 1200 *m*/*z* with internal calibration. Software MassHunter (Version B.07.00, Agilent Technologies, Santa Clara, CA 95051, United States), was used for data processing, quantification and data acquisition. APAP and APAP metabolites were validated by the conjunction of exact mass and retention time from standards.

2.7.6. Metabolomics

The culture medium from the basal compartment was collected for the different conditions and the samples were frozen in liquid nitrogen until analysis.

2.7.6.1. Sample preparation

The samples were thawed and 250 µL was completed with 500 µL of frozen solution (-20°C) of water:acetonitrile:isopropanol (2:3:3) containing 4 mg/L of adonitol, 2.75 mg/L of α-aminobutyric acid solution (αABA), and placed in an Eppendorf thermomixer for 10 min at 4°C with shaking at 1500 rpm. Insoluble material was removed during two centrifugation steps at 14000 rpm for 10 min. Three aliquots of each extract (200 µL) were dried for 4 h at 35 °C in a speed-vac and stored at -80°C until analysis.

For GC-MS injection, samples were taken out of -80°C, warmed for 15 min and dried again for 1.5 h at 35 °C before adding 10 µL of 20 mg/mL methoxyamine in pyridine and the reaction was performed for 90 min at 30 °C with shaking. Then, 90 µL of N-methyl-N-trimethylsilyl-trifluoroacetamide (MSTFA, Regis Technologies) was added and the reaction continued for 30 min at 37 °C. After cooling, 100 µL was transferred to an Agilent vial for injection. Four hours after derivatization, 1 µL of sample was injected in splitless mode on an Agilent 7890B gas chromatograph coupled to an Agilent 5977A mass spectrometer. The column was a Rxi-5SilMS from Restek (30 m with 10 m Integra-Guard column - ref 13623-127). An injection in split mode with a ratio of 1:30 was systematically performed for saturated compound quantification. The oven temperature ramp was 60 °C for 1 min then 10 °C/min to 325 °C for 10 min. Helium constant flow was 1.1 mL/min. Temperatures were the following: injector: 250 °C, transfer line: 290 °C, source: 230 °C and quadrupole 150 °C. The quadrupole mass spectrometer was switched on after a 5.90 min solvent delay time, scanning from 50-600 u. Samples were randomized and a fatty acid methyl ester mix (C8, C9, C10, C12, C14, C16, C18, C20, C22, C24, C26, C28, C30) was injected in the middle of the queue for external RI calibration.

Raw Agilent datafiles were analyzed with AMDIS (http://chemdata.nist.gov/mass-spc/amdis/). The Agilent Fiehn GC/MS Metabolomics RTL Library (version June 2008) was employed for metabolite identifications. Peak areas were determined with the Masshunter Quantitative Analysis (Agilent) in splitless and split 30 modes. Because automated peak integration was occasionally erroneous, integration was verified manually for each compound and peak areas were normalized to ribitol. Metabolite contents are expressed in arbitrary units (semi-quantitative determination).

2.7.6.2. Metabolomic statistical analyses

The metabolomic multivariate data analyses were performed using MetaboAnalyst 5.0 (Pang et al., 2021). Supervised partial least squares-discriminant analysis (PLS-DA, comparison of more than two groups) and orthogonal projections to latent structures discriminant analysis (OPLS-DA, comparison of two groups) were applied to get the maximum separation between control and treated groups, and to explore the variables that contributed to this separation. The quality of PLS-DA and OPLS-DA models was evaluated by the R^2Y (fitting degree) and Q^2 (prediction parameter) values. To determine the best discriminators metabolites, the P value and fold change were used to build the volcano plot -log10P = f (log2FC). Variables with P value < 0.05 and fold change > 1.2 (upregulated) or < 0.8 (down regulated) represent possible discriminating metabolites. The significant metabolites were confirmed using

variable importance in the projection value (VIP > 1). Finally, pathway enrichment analysis was performed with MetaboAnalyst using the selected significant metabolites.

2.8. Bi-compartmentalized biochip

2.8.1. Design of the biochip

In order to mimic the physiological organization of the cells in the liver sinusoid, we proposed to design and develop a bicompartimentalized biochip composed of an apical compartment hosting the LSEC cells and a basal compartment hosting the hepatocytes. The two PDMS compartments were intended to be separated by a porous membrane allowing the exchanges (figure 2.9A). The Polyethylene terephthalate (PET) membrane (ipCELLCULTURE™ Track-Etched Membrane, it4ip) was chosen with characteristics corresponding to the culture insert with pore size of 0.4 µm, a density of 1.60E+06 cm^{-2}, a thickness of 23 µm and 2% of porosity. Once the whole system bonded, each compartment was intended to be connected to an independent perfusion circuit making the porous membrane the only exchange surface between the two circuits (figure 2.9B).

In order to achieve the bonding between the different materials composing the biochip (PDMS-PET-PDMS), two bonding techniques using (3-Aminopropyl)triethoxysilane (APTES) and bis(3- (trimethoxysilyl)propyl)amine inspired from (Sip & Folch, 2014) and (Loskill et al., 2017) protocols were adapted and established.

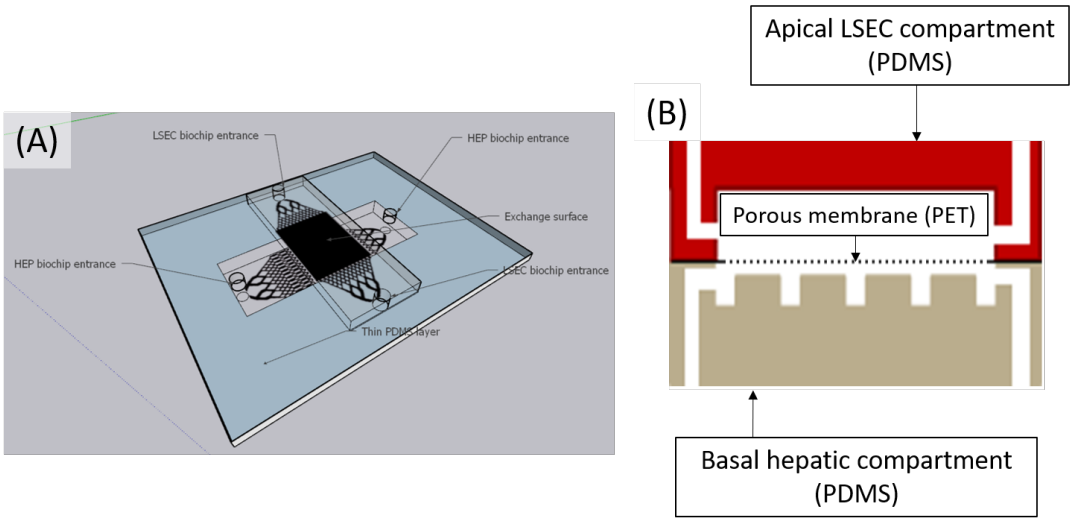

Figure 2. 9. *Design of the bi-compartmentalized biochip (A) 3D design of the biochip (B) schematic presentation of the different compartments.*

2.8.2. Fabrication process

2.8.2.1. APTES bonding protocol

The APTES (A3648, Sigma-Aldrich) was used to pre-treat the membrane adding attachment sites that can be activated using oxygen plasma. Firstly, as shown in figure 2.10, the membrane was cut into a circle with a diameter of 38 mm and cleaned with isopropanol for 10 minutes. Once dried, the membrane surface is activated with oxygen plasma at 300 mTorr for 60 seconds. The membranes were then immersed in a mix of 95% of Milli-Q water and 5% APTES for 20 minutes at 80°C. The membrane was dried and introduced to oxygen plasma with the upper compartment for surface activation for 60 seconds at 300 mTor, the two parts were then assembled. The same process was repeated for the lower chamber.

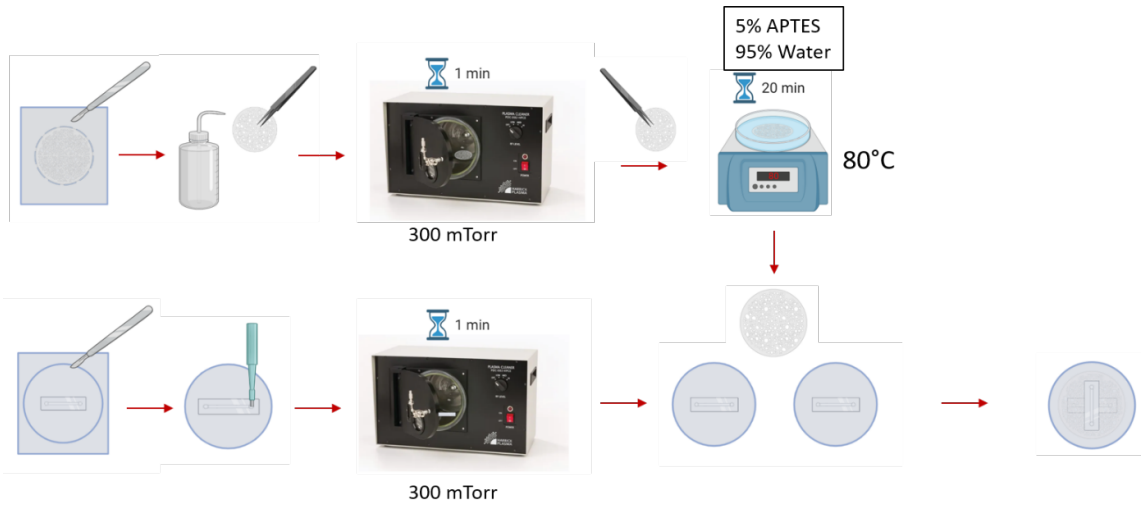

Figure 2. 10. Surface activation and bounding using the APTES primer.

2.8.2.2. Bis(3-(trimethoxysilyl)propyl)amine bonding protocol

The Bis(3-(trimethoxysilyl)propyl)amine (413356, Sigma-Aldrich) like the APTES was used to create covalent bonds. Briefly, as shown in figure 2.11., the membrane was cut into circle with a diameter of 38 mm then rinsed with isopropanol for 10 minutes and dried. The membrane's surface was then activated for 60 seconds at 300 mTorr with oxygen plasma. Once activated, the membrane was immersed in a mix of 97% isopropanol, 2% bis(3-(trimethoxysilyl)propyl)amine and 1% Milli-Q water for 20 minutes at 80°C. The membrane was then rinsed with isopropanol and dried at 70°C for 30 minutes. Once the membrane has dried, it was immersed in 70% ethanol and then air dried. For the bonding with oxygen plasma activation, the same steps described in section 2.8.2.1 are repeated.

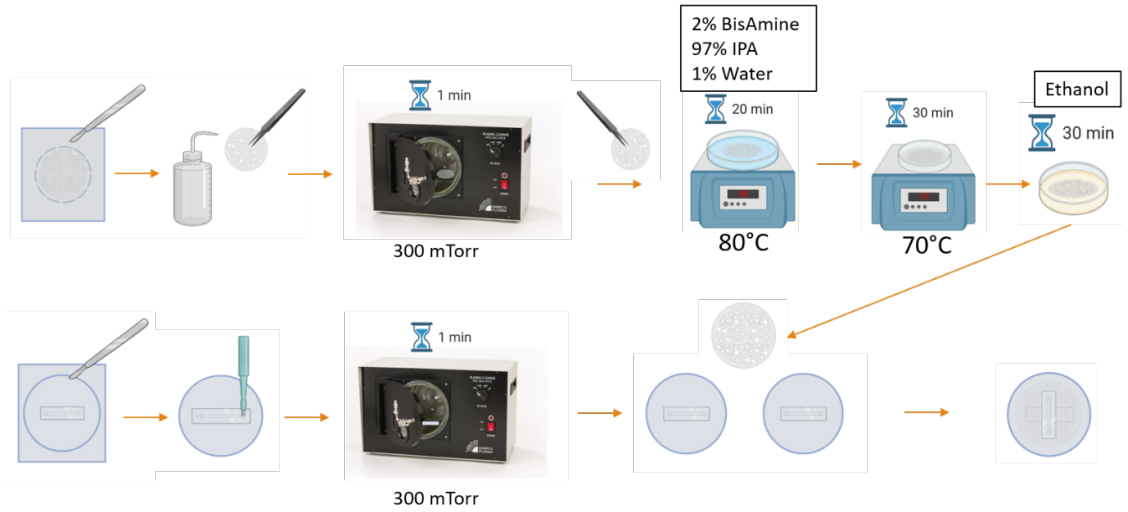

Figure 2. 11. Surface activation and bounding using the Bis(3-aminopropyl)amine(BisAmine) primer.

2.8.3. Characterization of the biochip

2.8.3.1. FITC-dextran permeability assay

The permeability of FITC-dextran (4 kDa, Sigma-Aldrich) was assessed. The tracer passage from the apical to the basal compartment through the APTES and bis(3-(trimethoxysilyl)propyl)amine treated membranes was measured. The FITC-dextran was diluted in Milli-Q and at a concentration of 100 µg/mL and introduced in the apical circuit of the bi-compartmentalized biochip through the bubble trap. The perfusion was started in both circuits independently ensuring that the exchanges only occur through the permeable membrane. The circulating liquid from the bubble trap linked to the basal compartment was sampled at different times. The FITC-dextran fluorescence intensity was measured using a microplate reader (TECAN Spectafluor Plus) at excitation/emission wavelengths of 490/525 nm.

2.8.3.2. Shear stress simulations

The shear stress applied on the cells in the apical compartment was estimated for different designs using COMSOL Multiphysics 5.1. The design of the biochip was recreated considering a height at the inlet/outlet of 100 µm and 80 µm at the culture chambers level. The theoretical shear forces applied on the cells was measured at a flow rate of 10 µL/min in the central part of the biochip, at 5 µm above the membrane. The shear stress for the condition where the upper part consist of a culture reservoir was compared with the condition where the upper part is microstructured.

2.8.4. Cell culture

For cell culture proof of concept, only the APTES bonded biochips and the SK-HEP-1 cell line were used. After the fabrication process and for each experiment, 3 biochips were, firstly, incubated for 1 hour with a UV sterilizer at 253 and 230 nm to inactivate bacteria, viruses and fungi. Then, each compartment of each biochip was linked to a closed perfusion circuit including a bubble trap and a peristaltic pump. The bubble traps were used as culture medium reservoir. The biochips were subsequently perfused with ethanol 70% and Milli-Q water to eliminate the potential residual APTES on the membrane. Then the apical culture chambers were filled with EGM-2/MEM (25%/75%) common culture medium for SK-HEP-1 cells HepG2/C3a. Between the 10^{th} and the 20^{th} passage, the SK-HEP-1 cells were detached from the T75 cm² flasks using trypsin-EDTA and injected in the apical compartment. The biochips were incubated overnight in a humidified incubator at 37°C and 5% CO_2. The perfusion at 10 µL/min was launched once the cells have adhered.

2.9. Statistical analyses

The experiments are repeated at least three times and a minimum of 2 biochips/conditions were used in each experiment (N = 3 experiments and 6 ≤ n (biochip) ≤ 12). The data are presented as the mean ± standard deviations (SD) (for RTqPCR assays, only 3 replicates from 3 different experiments were used). To determine significant statistical differences, a one-way ANOVA test was performed using GraphPad software (Prism 8). Data with P-values < 0.05 were identified as statistically significant and highlighted in the figures.

2.10. References

Bricks T, Paullier P, Legendre A, Fleury MJ, Zeller P, Merlier F, Anton PM, Leclerc E. Development of a new microfluidic platform integrating co-cultures of intestinal and liver cell lines. *Toxicology in Vitro*, 2014, *28*(5), 885–895. DOI: 10.1016/J.TIV.2014.02.005

Desai S S, Tung JC, Zhou VX, Grenert JP, Malato Y, Rezvani M, Español-Suñer R, Willenbring H, Weaver V M, Chang T T. Physiological ranges of matrix rigidity modulate primary mouse hepatocyte function in part through hepatocyte nuclear factor 4 alpha. *Hepatology*, 2016, *64*(1), 261–275. DOI: 10.1002/HEP.28450/SUPPINFO

Livak KJ, Schmittgen TD. Analysis of Relative Gene Expression Data Using Real-Time Quantitative PCR and the 2−ΔΔCT Method. *Methods*, 2001, *25*(4), 402–408. DOI: 10.1006/METH.2001.1262

Loskill P, Sezhian T, Tharp KM, Lee-Montiel FT, Jeeawoody S, Reese WM, Zushin PJH, Stahl A, Healy KE. WAT-on-a-chip: A physiologically relevant microfluidic system incorporating white adipose tissue. *Lab on a Chip*, 2017, *17*(9), 1645. DOI: 10.1039/C6LC01590E

Pang Z, Chong J, Zhou G, de Lima Morais D A, Chang L, Barrette M, Gauthier C, Jacques P E, Li S, Xia J. Metabo-Analyst 5.0: narrowing the gap between raw spectra and functional insights. Nucleic Acids Res. 2021, 49, W388-W396. DOI: 10.1093/nar/gkab382.

Sip CG, Folch A. Stable chemical bonding of porous membranes and poly(dimethylsiloxane) devices for long-term cell culture. *Biomicrofluidics*, 2014, *8*(3). DOI: 10.1063/1.4883075

Chapter 3: Development of Liver-On-Chip Integrating a Hydroscaffold Mimicking the Liver's Extracellular Matrix

In this section, we demonstrated the proof of concept of using our hydroscaffold-integrated biochip for the 3D organization of the cells. We used the HepG2/C3a cell line as hepatocyte model to study their organization into spheroids inside the biochip. The formed spheroids were analysed structurally and functionally and compared to spheroids formed in hydroscaffold-integrated Petri dishes. Finally, we discussed the advantages of using our liver-on-chip model and the potential of using such a model in drug toxicity and metabolism applications. The core of the chapter is literally extracted from our article "Development of Liver-On-Chip Integrating a Hydroscaffold Mimicking the Liver's Extracellular Matrix"[2]. The article abstract is presented as a summary of the chapter 3. The material and methods are not presented in this chapter, an extended version is described in chapter 2. The supplementary files of the article are provided at the end of this chapter.

[2] **Messelmani T,** Le Goff A, Souguir Z, Maes V, Roudaut M, Vandenhaute E, Maubon N, Legallais C, Leclerc E, Jellali R, Development of an advanced liver organ-on-chip integrating hydroscaffold mimicking cell matrix, ***Bioengineering, 2022, 9, 443, Article,*** **DOI:10.3390/bioengineering9090443**

Summary

The 3Rs guidelines recommend replacing animal testing with alternative models. One of the solutions proposed is organ-on-chip technology in which liver-on-chip is one of the most promising alternatives for drug screening and toxicological assays. The main challenge is to achieve the relevant *in vivo*-like functionalities of the liver tissue in an optimized cellular microenvironment. Here, we investigated the development of hepatic cells under dynamic conditions inside a 3D hydroscaffold embedded in a microfluidic device. The hydroscaffold is made of hyaluronic acid and composed of liver extracellular matrix components (galactosamine, collagen I/IV) with RGDS (Arg-Gly-Asp-Ser) sites for cell adhesion. The HepG2/C3a cell line was cultured under a flow rate of 10 µL/min for 21 days. After seeding, the cells formed aggregates and proliferated, forming 3D spheroids. The cell viability, functionality, and spheroid integrity were investigated and com-pared to static cultures. The results showed a 3D aggregate organization of the cells up to large spheroid formations, high viability and albumin production, and an enhancement of HepG2 cell functionalities. Overall, these results highlighted the role of the liver-on-chip model coupled with a hydroscaffold in the enhancement of cell functions and its potential for engineering a relevant liver model for drug screening and disease study.

Keywords: organ-on-chip; liver; extracellular matrix; hydroscaffold; spheroid

3.1. Introduction

Drug discovery and development is a long and complex process involving several steps before commercialization. This process, from identifying the potential molecule to its commercialization, takes up to 10 to 15 years and costs approximately 3 to 5 billion dollars of investment (Hughes et al., 2011; Khetani et al., 2015). Moreover, approximately 90% of drug candidates fail to receive approval by the regulatory authorities, mainly due to their lack of efficacy or toxic effects (Freyer et al., 2016). Among the key steps in drug development, the preclinical trials stage makes it possible to evaluate biological efficacy and potential safety problems prior to initiating the clinical phase. This stage involves the use of *in vitro* models followed by extensive animal testing (Sivaraman et al., 2005). However, it is estimated that approximately 90% of molecules that successfully pass the preclinical steps fail during clinical trials (Khetani et al., 2015). Although useful in preclinical tests, animal models have their limitations and fail to mimic complex human biology because of species differences, resulting in poor extrapolation of the results obtained from animal to human (Mann, 2015; Merlier et al., 2017). In addition, animal experiments pose problems from an ethical and a regulatory viewpoint (Mann, 2015). Thus, there is now an increasing need to develop relevant *in vitro* models that can reliably mimic the human response to drugs (Bell et al., 2017).

The liver is a major organ that plays an essential role in a variety of functions, such as digestion, storage, the production and secretion of plasma, and essentially the de-toxification and purification of blood (Polidoro et al., 2021). As the major site of xenobiotic metabolism, the liver is one of the organs most affected by drug-induced toxicity. Drug-induced liver injury (DILI) is a common cause of liver injury and accounts for approximately 50% of cases of acute liver failure in the United States and Western Europe (Bernal and Wendon, 2013; Donato and Tolosa, 2019; Ghabril et al., 2010). DILI is also the most common cause of a drug's withdrawal from the market and restriction of use (Kuna et al., 2018). The failure to detect DILI during the drug development process is attributable to the poor predictability of the screening methods (*in vitro*, *in vivo*, *ex vivo*, and *in silico*) used in the preclinical phase (Chen et al., 2014; Donato and Tolosa, 2019; Ghabril et al., 2010; Segovia-Zafra et al., 2021).

In current *in vitro* preclinical assays, the hepatotoxicity of drug candidates is most commonly tested using two dimensional (2D) monolayer cultures (Polidoro et al., 2021). These cultures are mainly performed in a static macroscale environment such as Petri dishes or multi-well plates. Although 2D static cultures have provided significant contributions to biomedical research and the pharmaceutical industry, they fail to both reproduce *in vivo* physiology and

metabolism, and accurately predict cellular responses to drugs (Bhatia and Ingber 2014; Chen et al., 2021). These limitations are associated with the lack of specific architecture in the tissues, mechanical and biomechanical cues, and cell-cell and cell-matrix interactions (Fang and Eglen 2017). Several studies have shown that primary human hepatocytes (PHH), which are considered the gold standard for *in vitro* drug screening, dedifferentiate and rapidly lose their key phenotypic and specific detoxification functions, when cultured in 2D static conditions (Chen et al., 2021; Gómez-Lechón et al., 2014). Therefore, there is an increasing need for the development of reliable *in vitro* human liver models. These models must reproduce as closely as possible the *in vivo* characteristics of the liver microenvironment.

In an attempt to improve *in vitro* liver models, different approaches based on tissue engineering, microfabrication, and microfluidics have been proposed during the last decade: 3D cell culture (spheroids, culture in hydroscaffold/hydrogel, and 3D bi-oprinting), organoids derived from stem cells, dynamic organ-on-chip (OoC) culture, coculture models of different liver cells and liver coculture with other organs (Fang and Eglen 2017; Lauschke et al., 2016; Ruoß et al., 2020). Of those models, dynamic organ-on-chip and 3D spheroids seem to be two of the most promising models for hepatic cell cultures (Foster et al., 2019). In particular, OoC technology makes it possible to build a well-controlled microenvironment and create "physiological-like" situations, such as 3D architectures, cell-cell and cell-matrix interactions, continuous nutrient exchange, zonation, physiological shear stress, and chemical gradients (Bhatia and Ingber, 2014; Ingber, 2020). Moreover, microfluidic OoC offers the possibility of reproducing physiological organ-to-organ interactions, when cells from different organs are cultivated in separate biochips and chemical factor exchange is made possible through microfluidic tubing (Essaouiba et al., 2020). The culture in 3D spheroids also exhibits several features making it possible to both mimic *in vivo* cell conditions and maintain liver-specific functions. It promotes adhesion between cells, their interaction with the extracellular matrix (ECM), and the development of gas, nutrients, and metabolite gradients (Cui et al., 2017; Fang and Eglen, 2017; Godoy et al., 2013). Spheroids can be produced by self-aggregation of cells (non-adhesive surface, bioreactor, hanging drop technique) or using a hydrogel/scaffold matrix (Cui et al., 2017; Fu et al., 2020). The use of hydrogel and scaffold offers the possibility of tuning the cell microenvironment by modifying the composition of the matrix and/or the mechanical properties (Cui et al., 2017; Fang and Eglen 2017).

In previous works, our group has developed liver-on-chip models with different hepatic cells (HepG2/C3a, HepaRG, PHH, primary rat hepatocytes and human induced pluripotent stem cells hiPSCs) to investigate liver metabolism (Jellali et al., 2016; Prot et al., 2011), drugs and pesticide toxicity (Choucha-Snouber et al., 2013; Jellali et al., 2018; Leclerc et al., 2015), and liver regeneration and the development process (Danoy et al., 2021). Recently, we integrated

an alginate cryogel into our biochip to promote 3D cell organization. The cells colonize the entire surface of the collagen-coated cryogel, forming a thick (200 µm) tissue-like 3D structure from the bottom to the top of the biochip (Boulais et al., 2021). In the present study, we propose a new liver-on-chip model integrating a hydroscaffold allowing cells to organize into a complex 3D spheroid architecture. To promote a more *in vivo*-like environment for cells, we used a hydroscaffold containing the key liver extracellular matrix (ECM) components (hyaluronic acid (HA), RGDS, galactosamine, collagen I and IV). We studied the behavior and functionalities of HepG2/C3a, a liver cell line often used as an *in vitro* model for human hepatocytes, cultured in dynamic conditions in the biochip integrating the scaffold. Different cell densities and times of culture, ranging from 4 days (short-term culture) to 21 days (long-term culture), were investigated.

3.2. Integration of the hydroscaffold into the biochip

The hydroscaffold crosslinking was performed in situ in the biochip. The purified pseudo-hydrogel was easily injected into the biochip using a syringe and the crosslinking took place for 2h. Figure 3.1 A-E shows the pictures and optical microscope observations of the biochips without and with the hydroscaffold, respectively. The hydroscaffold is easily identifiable both in the picture (Figure 3.1C, white color) and in the microscopic observations (Figures 3.1D and 3.1E, dried and hydrated hydroscaffold, respectively). It is well distributed and homogenously occupies the entire space of the biochip, from the inlet to the outlet. The contrast in color observed in Figure 3.1D is due to the difference in height between the bottom of the biochip and the top of the microstructures. The SEM observations of the scaffold highlighted a homogeneous porous network with a pore size of approximately 120 ± 20 µm (Figure 3.1F).

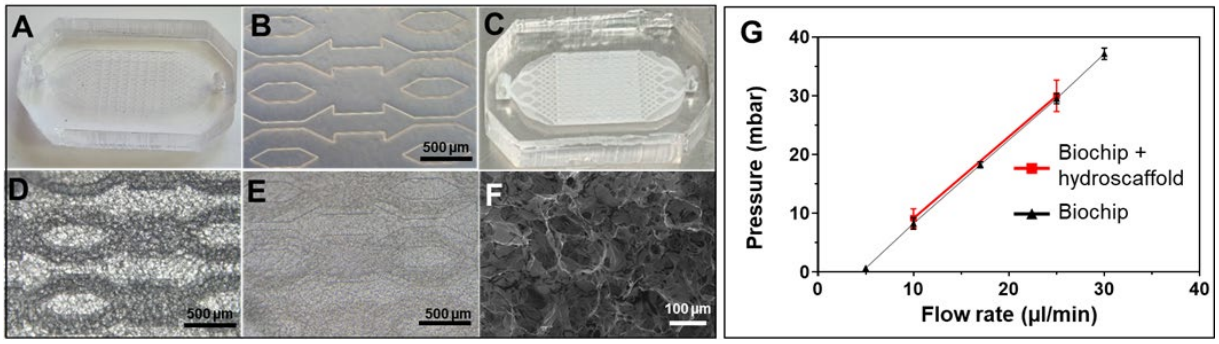

Figure 3.1. *Microfluidic devices and hydroscaffold characterization. (A) microfluidic biochip; (B) microscopic observation of biochip microstructures; (C) biochip containing the hydroscaffold; (D) microscopic observation of dehydrated hydroscaffold inside biochip; (E) microscopic observation of hydrated hydroscaffold inside biochip; (F) SEM observation of the hydroscaffold and (G) characterization of the pressure variation in the biochip with and without hydroscaffold.*

Considering the possible additional resistance to flow generated by the scaffold integration, it was important to confirm that culture medium can circulate and is distributed evenly inside the biochip. To investigate this effect, biochips with and without a hydroscaffold were connected to a pressure-controlled circuit and the pressure drop was monitored for flow rates relevant for cell culture (Baudoin et al., 2011). The pressure variations plotted against the flow rates are presented in Figure 3.1G. We found that the two plots (biochips with and without a hydroscaffold) fit well, with no significant difference. Using the equation for hydraulic resistance (Rh = ΔP/Q, were Rh is the hydraulic resistance, ΔP the pressure variation between the inlet and the outlet of the biochip, and Q the flow rate), we calculated hydraulic resistance of $5.9 \times 10^{12} \pm 0.4 \times 10^{12}$ and $5.9 \times 10^{12} \pm 1.0 \times 10^{12}$ $kg \cdot m^{-4} \cdot s^{-1}$ for the biochips without and with a hydroscaffold, respectively.

3.3. Cell culture in biochip containing the hydroscaffold

3.3.1. Effect of cell seeding density: morphology

To evaluate the effect of starting cell density on the formation, size, and organization of spheroids, we investigated three different seeding densities: 20.000 (low density), 125.000 (intermediate density), and 250.000 cells/cm² (high density). For comparison, the high and intermediate densities were chosen based on our previous works with a scaffold-free biochip and biochip containing alginate cryogel (Baudoin et al., 2011; Boulais et al., 2021). The evolution of cell morphologies throughout the 96 h of culture in biochips containing the hydroscaffold (including 24 h of adhesion and 72 h of dynamic culture) are illustrated in Figure 3.2A.

24 h after seeding, the cells embedded in the hydroscaffold started to aggregate and create spheroids. The number and size of the spheroids were proportional to the starting cell density. Furthermore, spheroids created from high and intermediate densities were less uniform in size and shape, compared to spheroids resulting from low seeding density. In comparison, 24 h after seeding in a scaffold-free biochip, the cells adhered to the bottom of the biochip and formed a monolayer (Figure 3.2B). After the medium flow started, the spheroids remained embedded in the scaffold and grew continuously, especially for high and intermediate starting densities. After 96 h of culture, they created irregular large spheroids or cell aggregates (Figure 3.2A). In the case of low density seeding, we obtained uniform spheroids with an approximate diameter of 100–200 µm (Figure 3.2A). From 8–10 days of culture with high and intermediate seeding densities, the growth of spheroids led to the formation of large clusters of spheroids in the whole biochip. These clusters blocked the flow as indicated by a significant increase in the pressure drop (detailed in Section 3.4), which

played a part in damaging the perfusion circuit (results not shown). Finally, the cultures in a well-plate containing a hydroscaffold showed similar results after 96 h of culture: large spheroids/aggregates with high and intermediate density and uniform spheroids in the case of the low starting density (Figure 3.S1).

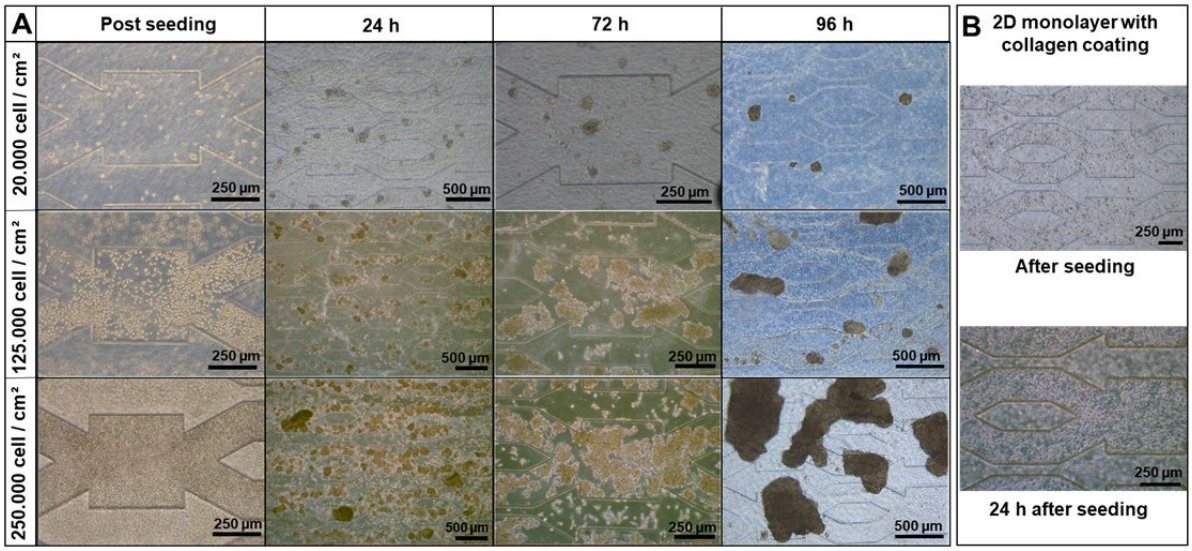

Figure 3.2. *Morphology of HepG2/C3a cells cultivated in (A) biochip containing the hydroscaffold and (B) biochip coated with collagen.*

3.3.2. Cell viability and functionality

After 96 h of culture (24 h in static and 72 h in dynamic conditions), cell viability was evaluated with live/dead staining for the three starting densities (20.000, 125.000 and 250.000 cells/cm^2). As shown in Figure 3.3, all spheroids presented uniform green fluorescent intensity (living cells). The red fluorescent signal was very low, indicating a negligible number of dead cells in the three conditions (in comparison with the number of living cells). However, the red fluorescence intensity in the spheroids obtained from high (250.000 cells/cm^2) and intermediate (125.000 cells/cm^2) starting densities seemed to be higher compared to spheroids created with low (20.000 cells/cm^2) density.

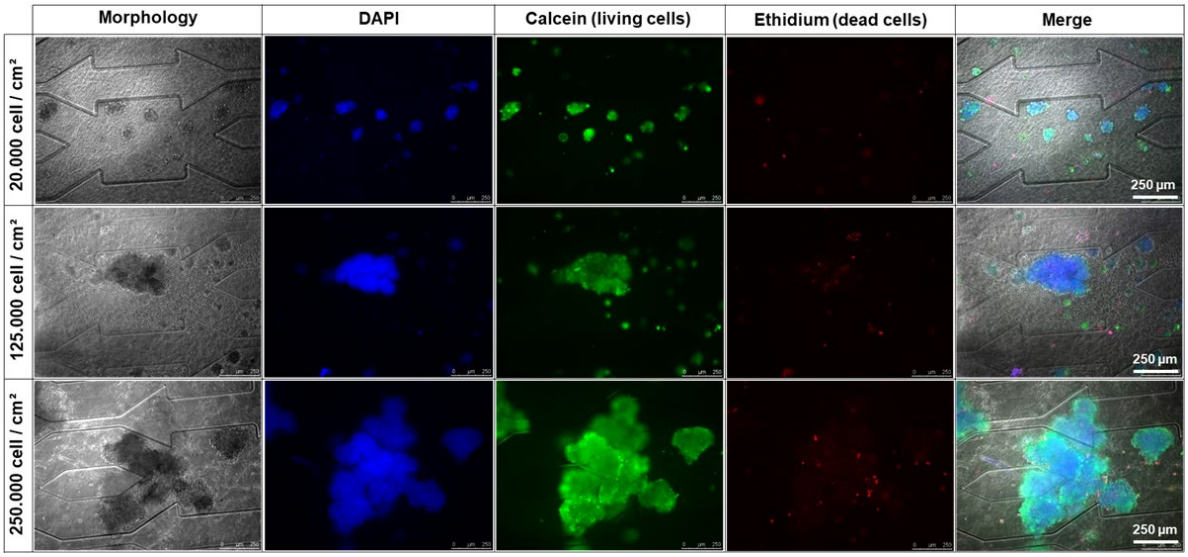

Figure 3.3. *Cell viability for different seeding densities after 96h of culture in the biochip containing the hydroscaffold: DAPI (nuclei, blue), calcein (living cells, green), and ethidium (dead cells, red).*

To evaluate the effect of culture in a biochip containing a scaffold on HepG2/C3a specific functions, albumin production was quantified and compared, with results obtained in static culture in a well-plate with a hydroscaffold. The results are shown in Figure 5. In both culture modes (dynamic and static), albumin production increased from day 2 to day 4 for the three starting densities. However, albumin production in biochips containing the scaffold were approximately 2, 3 and 10-fold higher than the 3D hydroscaffold in Petri for low, intermediate, and high starting densities, respectively. In the biochip, albumin production after 4 days of culture reached 25 ± 8 ng/h for low starting density (Figure 3.4A), 91 ± 18 ng/h for intermediate starting density (Figure 3.4B) and 132 ± 34 ng/h for high starting density (Figure 3.4C).

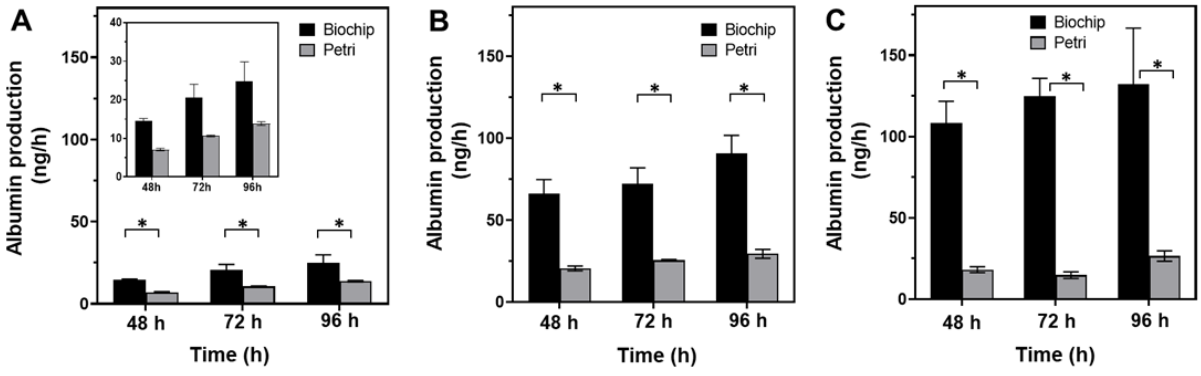

Figure 3.4. *Albumin secretion by HepG2/C3a cultivated in a dynamic biochip and static Petri containing the hydroscaffold. Starting cell density of 20.000 (A), 125.000 (B) and 250.000 cells/cm² (C). The insert in panel (A) is a close-up on the vertical axis (* P <0.005).*

Table 3.1 summarizes albumin production in the biochip containing the hydroscaffold and in two other biochips from our previous works: a biochip containing alginate cryogel and a hydroscaffold/cryogel-free biochip (Baudoin et al., 2011; Boulais et al., 2021). For the starting density of 250.000 cells/cm^2, there was no significant difference between the three types of biochips. At 96 h, albumin production was of 132 ± 34 ng/h in the biochip with the hydroscaffold, 135 ± 60 ng/h in the biochip with alginate, and 190 ± 85 ng/h in the empty biochip. Similar albumin production was also found with a starting density of 125.000 cells/cm^2 in the biochip containing the hydroscaffold and the empty biochip.

Table 3.1. *Albumin production (ng/h) for several seeded cell densities and culture modes.*

	Seeded Cells	48 h	96 h
Biochip + hydroscaffold	1.25 × 10^5 cells/cm^2	66 ± 15	91 ± 18
	2.5 × 10^5 cells/cm^2	108 ± 13	132 ± 34
Petri + hydroscaffold	1.25 × 10^5 cells/cm^2	20.5 ± 2.55	29.5 ± 5
	2.5 × 10^5 cells/cm^2	18 ± 1.8	26.5 ± 3.2
Biochip **	1.25 × 10^5 cells/cm^2	95 ± 5	90 ± 40
	2.5 × 10^5 cells/cm^2	118 ± 25	190 ± 85
Biochip + alginate cryogel *	2.5 × 10^5 cells/cm^2	88 ± 25	135 ± 60

** Boulais et al., 2021; ** Baudoin et al., 2012; hydroscaffold = BIOMIMESYS® Liver.*

3.4. Long-term cell culture in a biochip containing the hydroscaffold

The longevity of *in vitro* liver models is a critical parameter. Hepatotoxicity most often manifests after a long time and several exposures to drugs. To evaluate our model in long-term culture, and considering the results obtained in the previous section, we chose to work with a low starting density (20,000 cells/cm2) to prevent the formation of large clusters of spheroids and create flow blockage.

3.4.1. Cell proliferation and spheroid formation

A total of 20.000 HepG2/C3a cells/cm^2 (40.000 cells/biochip) were seeded into the biochip containing the HA hydroscaffold. After 24 h in static conditions, the pump was started at 10 µL/min. The flow rate was maintained constant throughout the experiment and the pressure was monitored using the setup described in chapter 2 (section 2.8).

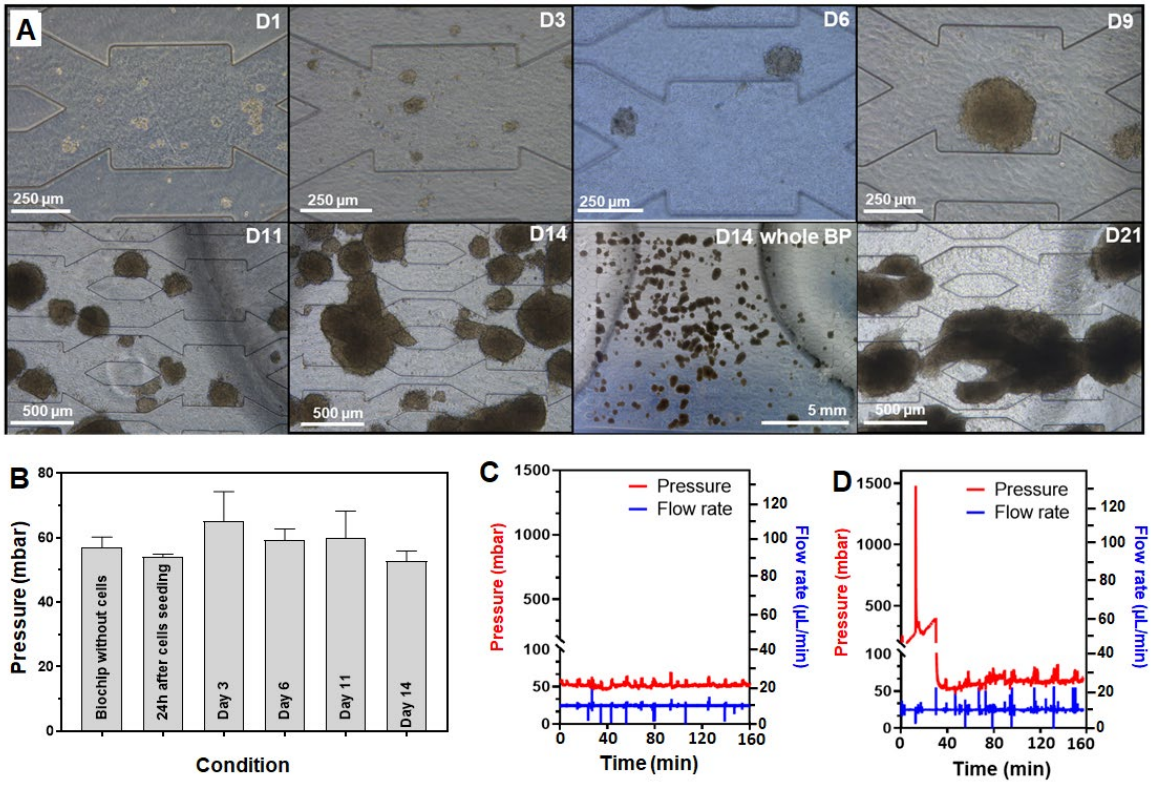

Figure 3.5. *Long-term (21 days) culture of HepG2/C3a cells in a biochip with the hydroscaffold (Starting cell density of 20.000 cells/cm²). (A) evolution of the morphology of HepG2/C3a spheroids throughout the 21 days of culture; (B) pressure evolution during the first 14 days of culture; (C and D) pressure measured inside the biochip on day 14 and 21, respectively.*

The evolution of HepG2/C3a spheroids throughout 21 days of culture is presented in Figure 3.5. From day 1, the cells attached to the hydroscaffold and self-aggregated in small clusters of cells. Then, the cell clusters gradually formed spheroids with well-defined shapes throughout the first 11 days of culture. The size of the spheroids increased over time to reach diameters of between 150 and 450 µm by day 11. The pressure inside the biochips remained stable, close to 60 mbar, during this period (first 11 days of culture, Figure 3.5B). From the 14th day of culture, the cells proliferated strongly, and the spheroids started to overlap and occupy most of the biochip area (Figure 3.5A). Nevertheless, as shown in Figure 3.5C, the pressure inside the biochip did not increase. Finally, on day 21 of culture, large clusters of spheroids were formed in the whole biochip (Figure 3.5A). Consequently, the hydraulic resistance of the biochip increased, affecting the circulation of the culture medium. This was confirmed by a significant pressure jump, reaching 1.5 bar (Figure 3.5D, the initial pressure at 10 µL/min was of 60 mbar). Normal pressure (60 mbar) was restored after detaching a spheroid cluster (nb: the same behavior was observed in Section 3.3.1 with a higher density inoculation but at an earlier time point due to tissue growth).

3.4.2. Spheroid morphology and integrity

Live/dead assays were performed on the spheroids at the end of the experiments, after the 21 days of dynamic culture (Figure 3.6A and Figure 3.S2). Despite the large spheroid size (diameter ≥ 500 µm), the fluorescence images demonstrated high viability (green fluorescent signal) of the cells in the 3D structure. We did not observe any specific necrotic core within the spheroids. Only some dead cells (red fluorescent signal) were observed, distributed over different areas of the spheroids.

The internal structure of the spheroids and cell-cell adhesion and interaction were analyzed using immunofluorescence with phalloidin for F-actin staining and anti-E-cadherin antibody. F-actin plays an important role in the mediation of cell shape and spreading. As shown in Figure 3.6B, the actin cytoskeleton of the cells can be seen clearly (intense green fluorescence signal) in the whole spheroid. The actin filaments appeared well organized, creating a complex network throughout the entirety of the spheroid. In parallel, abundant E-cadherin expression was observed in the 3D spheroids, as shown by the purple fluorescence in Figure 3.6C. The positive staining of E-cadherin confirmed the well-developed adherent junctions, the overall cell adhesion integrity within the spheroids and the epithelial status of the tissue. In comparison, F-actin and E-cadherin networks seemed to be less developed in the spheroids after 21 days of culture in a static well-plate containing the hydroscaffold (Figure 3. S3).

To study the structure and organization of the cells and spheroids inside the biochips containing the hydroscaffold, the samples (fixed after 21 days of culture) were observed under scanning electron microscope (SEM). SEM imaging was performed on the device's cross-sections and the bottom layer of the biochip (top view) after disbanding the top layer (Figure 3.6D and Figure 3.S4). The SEM images in the top view show the formation of large 3D spheroids surrounded by the hydroscaffold. The cross-section images confirmed the cell organization in a tissue-like 3D structure from the bottom to the top of the biochips and the cell-scaffold interactions.

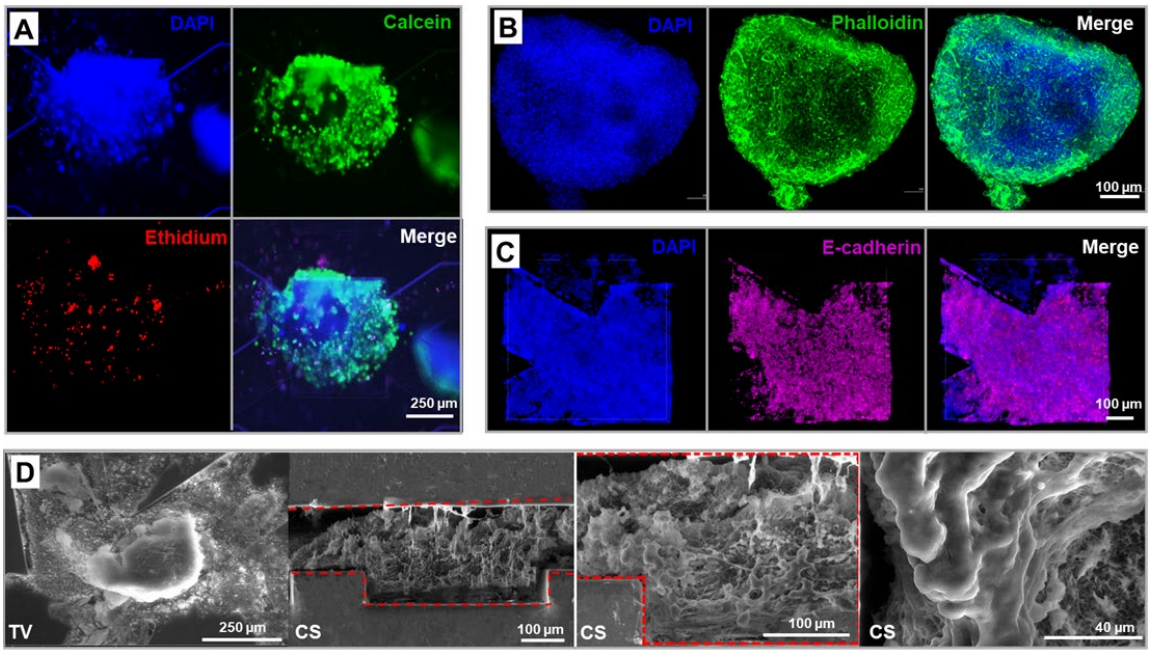

Figure 3.6. *Characterization of HepG2/C3a spheroids after 21 days of dynamic culture in a biochip containing the hydroscaffold. (A) cell viability: DAPI (nuclei, blue), calcein (living cells, green) and ethidium (dead cells, red); (B) F-actin staining: DAPI (nucle i, blue) and phalloidin (F-actin, green); (C) E-cadherin staining: DAPI (nuclei, blue) and E-cadherin (purple); (D) SEM observation (TV: top view and CS: cross section). The immunostaining images (B and C) correspond to z-stack projections.*

3.4.3. Spheroid functionality

Cell polarization is one of the key characteristics of hepatocytes. To investigate the polarity of the cells within the spheroids and confirm the formation of bile canalicular-like structures, MPR2 (coupled to actin) and BSEP stainings, performed on spheroids after 21 days of culture, were used as markers. BSEP and MRP2 are two proteins localized at the canalicular membrane of the hepatocytes and they normally transport bile acids and drugs from hepatocytes to the bile network. Both stainings confirmed the presence of a biliary-like network within the spheroids. As shown in Figure 3.7A, the immunofluorescence images highlighted the co-localization of the canalicular MRP2 transporter signal (red) with the actin fluorescent signal (green) resulting in the yellow overlay signal (merge panel in Figure 3.7A). The expression of the BSEP transporter was demonstrated by the intense yellow fluorescence in Figure 3.7B.

Albumin production is one of the main functions of the liver and is often used as a specific marker to evaluate hepatocyte functionality. The albumin production from spheroids cultured in dynamic biochips containing the hydroscaffold was quantified over the 21 days of culture and compared to albumin produced in static cultures in a well-plate with the hydroscaffold (Figure 3.7C). In the biochips, the albumin production gradually increased throughout the 21 days of the experiment. The productions were of 14.49 ± 1.15, 24.79 ± 8.7, 231.25 ± 30, and

1066.25 ± 83 ng/h at days 2, 4 10, and 21, respectively. Concerning the static Petri cultures, the production of albumin also increased over the 21 days of culture. However, albumin levels were significantly lower than the values obtained in the biochip cultures: 2- and 10-times lower at the beginning (days 2 and 4) and the end (days 10 and 21) of cultures, respectively (Figure 3.7C).

Finally, urea production was analyzed at different time points during the 21 days of culture (in biochips and Petri cultures, Figure 3.7D). In biochips, urea synthesis remained at a steady approximate level over the 21 days (between 0.55 ± 0.1 and 1.08 ± 0.36 µg/h). On the other hand, in the static Petri cultures, urea production gradually decreased over time. Productions were of 0.96 ± 0.02, 0.74 ± 0.04, 0.30 ± 0.03, and 0.20 ± 0.01 µg/h at days 3, 7, 14, and 21, respectively.

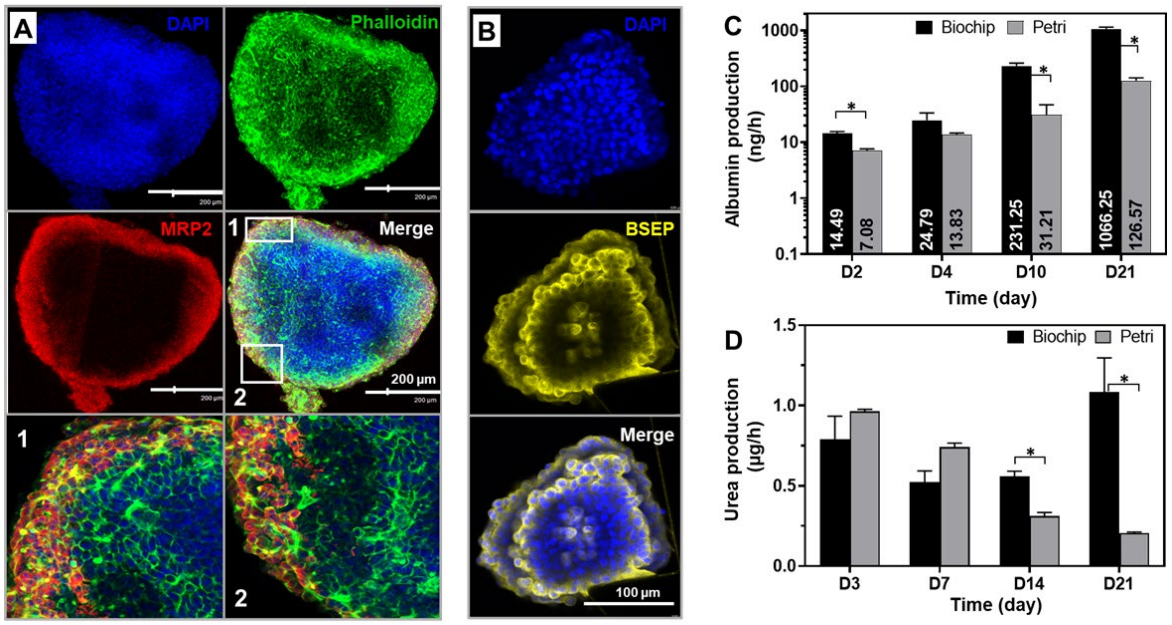

Figure 3.7. *Characterization of HepG2/C3a spheroids after 21 days of dynamic culture in a biochip containing the hydroscaffold. (A) F-actin and MRP2 staining showing the formation of bile canalicular-like structures: DAPI (nuclei, blue), phalloidin (F-actin, green); MRP2 (red) and biliary-like network (co-localization MRP2 and F-actin signals, yellow overlay signal, the two pictures in the bottom correspond to an enlargement from the merge picture); (B) BSEP staining: DAPI (nuclei, blue) and BSEP (yellow); (C and D) albumin and urea production in the dynamic biochip and static Petri conditions throughout 21 days of culture (both biochip and Petri contained the hydroscaffold, * P < 0.05). The immunostaining images (A and B) correspond to z-stack projections.*

3.5. Discussion

The literature reports improved liver functions, cellular morphology reorganization, and higher metabolic capability in *in vitro* models thanks to the integration of advanced bioengineering and biomaterial techniques. Among them, the liver cultures in 3D configurations (spheroids/organoids), coupled or not with the extracellular matrix microenvironment reproduction (due to functionalized gels and hydroscaffolds), have played a part in enhancing

hepatic functions (Gaskell et al., 2016; Moscato et al., 2015; Ramaiahgari et al., 2014; Wrzesinski et al., 2013). In addition, it has been widely reported that liver cell cultures under flow reproduce zonation-like patterns and reduce the accumulation of waste and toxic compounds (Allen et al., 2004; Baudoin et al., 2007; Danoy et al., 2020; Lee et al., 2007; Matsumoto et al., 2019). Furthermore, coupling both flow and 3D cultures appeared to promote higher physiological relevance, when compared to 3D static cultures (Yu et al., 2017). The present work combines the advantages of (i) the 3D configuration cultures using a hydroscaffold mimicking the liver's extracellular matrix, (ii) dynamic cultures and (iii) PDMS organ on chip (transparent material, gas permeable).

The HepG2/C3a cells attached to the scaffold and proliferated, creating spheroids. Over the culture time, the spheroids became increasingly larger. Spheroids in the perfusion cultures reached a larger size than spheroids in static controls. One specific benefit of the present hydroscaffold relied on its composition, that is, a finely-tuned hyaluronic acid scaffold including RGDS peptide (Arg-Gly-Asp-Ser), galactosamine, collagen type I, and collagen type IV. The choice of extracellular matrix has its importance in epithelial polarization including hepatocytes and liver tissues (Gissen and Arias, 2015). The ECM is reported as a key regulator for improving hepatic functionality (Bual and Ijima, 2019) and liver regeneration (Andez and Amenta 1995), but also regulating the development of liver disorders (Arriazu et al., 2014). Furthermore, a complex ECM in hydrogel such as that obtained from the decellularized liver confirmed the importance of this environment in an *in vitro* model and in *in vivo* transplantation applications (Ijima et al., 2019). The BIOMIMESYS® Liver HA-hydroscaffolds' ECM proteins were selected according to the liver matrix microenvironment (Gressner et al., 1994). More particularly, previous works have shown that the BIOMIMESYS® Liver in static Petri made it possible to develop a protocol for differentiating human induced pluripotent stem cells (iPSCs) into human liver organoids (including not only hepatocytes but also biliary, stellate, and endothelial cell types) suitable for molecular screening (patent pending). Furthermore, the manufacturer's own data reported a higher expression of albumin secretion in their 3D Petri culture, when compared to 2D Petri culture of HepG2 cells (Figure 3.S5).

The present study demonstrated that the hydroscaffold allowed higher levels of albumin production in dynamic culture, when compared to static 3D Petri. However, we did not detect any specific difference in albumin secretion with our other biochip technologies (PDMS biochip without gel (Baudoin et al., 2011; 2012) and 3D alginate cryogel biochip (Boulais et al., 2021)). We also confirmed that F-actin and E-Cadherin were significantly organized at the cell-cell contact throughout the spheroids within the biochip containing the HA-hydroscaffold. These observations indicated intercellular adhesive interactions in our tissues

that was consistent with the literature (Liu et al., 2011). Furthermore, we detected successful polarization of the tissue within the hydroscaffold, which is a typical expectation for HepG2 cell cultures in a 3D configuration and under perfusion in a biochip environment (Deng et al., 2019; Gaskell et al., 2016).

The hydroscaffold integrated into the microfluidic biochip contributed to creating large spheroids, when compared to BIOMIMESYS® Liver 3D Petri. The HepG2/C3a, a liver cell line with a high capacity for proliferation, led to a specific range of uses in the present configuration. The spheroids' over-growth contributed to clogging the biochips and to blocking fluid flow, which in turn led to the devices' failure. This was characterized by the fluid leakage that resulted from a significant increase in pressure in the perfusion circuit. This behavior was time-dependent, based on cell inoculation density; lower was the inoculation density, later was the device failure. This phenomenon was also previously observed with our alginate cryogel biochip with HepG2/C3a (Boulais, 2020). Conversely, we never observed this situation in the biochips without gel in which cultures of up to 4 weeks were successful with HepG2/C3a (Figure 3.S6, Baudoin et al., 2009). In fact, without gel, the cells grow layer-by-layer and their over-growth is limited by the height of the microstructure inside the biochips. Nevertheless, the hydroscaffold biochips made it possible to increase the cell culture density within the biochips, creating a full-scale 3D tissue, concomitantly with a healthy culture given low necrotic cores were observed. This was attributed to better nutrient and oxygen distributions to the spheroids due to their random location within the biochips. Our observations suggested the necessity for a fine balance between the choice of applications (chronic vs. acute biological processes), time of culture, cell density, cell viability, and the type of 3D biochips. Furthermore, it also demonstrated the importance of biochip design and flow perfusion conditions. Additional endothelial cultures may provide an alternative solution via the formation of tubular-like tissues within the hydrogel and spheroids, thus facilitating the circulation of fluid (Melchiorri et al., 2016; Pauty et al., 2018; Pettinato et al., 2019). Finally, cells with a limited proliferation rate, such as primary hepatocytes, will only mildly modify flow resistance and thus be fully compatible with those technologies, as already demonstrated in our previous works (in Boulais et al., 2020 for alginate cryogel, and by Jellali et al., 2016 for a 3D biochip without gel).

Reconstructing an *in vitro* liver model that mimics *in vivo* conditions is very challenging and aims to maintain the morphological characteristics and cellular functions of hepatocytes over long periods of culture. In past decades, different liver models based on one or more advanced technologies, such as OoC, 3D spheroids and cells embedded in hydroscaffolds, have been developed (Fang and Eglen, 2017; Messelmani et al., 2022; Ruoß et al., 2020). However, to our knowledge, only a few studies have focused on integrating a

hydrogel/hydroscaffold into the biochip and there is no system describing a dynamic liver-on-chip model making hepatocyte cultures possible in spheroids, embedded into a hydroscaffold that closely mimics the liver's ECM. In this proof of concept, we used HepG2/C3a cells, which are a good compromise between the ease of use and the expression of certain funtions of liver cells (Štampar et al., 2020). Although PHHs are considered the gold standard for liver models, their use is not suitable for this first stage of development (high costs, complexity of culturing). Overall, our liver-on-chip model made possible the culture of HepG2/C3a cells in 3D spheroids embedded into liver-like ECM under dynamic flow for a long period (21 days). The cells showed high viability and stable hepatic functions throughout the 21 days of culture. However, the use of other cell models, such as PHHs and hiPSCs-derived hepatocytes, is required to confirm the potential of the device.

In OoC technology, the small amount of cells and culture medium volume represent a major limitation for biological characterization (Freyer et al., 2018). In our device, a significant number of cells (up to 2–3 million) can be hosted, and each device is perfused with 4 mL of culture medium. Thus, various analyses could be performed with the available biological material. Furthermore, a significant number of cells leads to high secretion of metabolites, chemicals, and proteins, resulting in easy detection using standard analytic tools. Finally, our biochip integrating hydroscaffold was adapted to our OoC fluidic platform allowing middle throughput analysis (IDCCM, Baudoin et al., 2012).

3.6. Conclusions

In this study, we propose to create a relevant microenvironment for culturing liver cells. The technology relied on the combination of a hydroscaffold embedded inside a microfluidic device. This combination made it possible to perform the liver HepG2/C3a cell culture in a complex 3D dynamic configuration. The HepG2/C3a formed spheroids and then large clusters of spheroids in the whole biochip. The live/dead staining revealed a high viability, with weak necrotic tissue at the center of the spheroids. Furthermore, tissue polarity was demonstrated by the MRP2 and BSEP networks, illustrating ongoing bile-like canicular network formation. The functional analysis demonstrated higher levels of albumin and urea secretions in the 3D cultures within the dynamic hydroscaffold-biochip conditions, when compared to the 3D hydroscaffold Petri controls. These results show the potential of combining organ-on-chip technology and hydroscaffold mimicking ECM to build relevant 3D liver models *in vitro*. We believe that the hydroscaffold-based liver-on-chip combined with primary hepatocytes or hiPSCs could play a role in producing a promising device for drug screening and risk assessment.

3.7. Supplementary figures

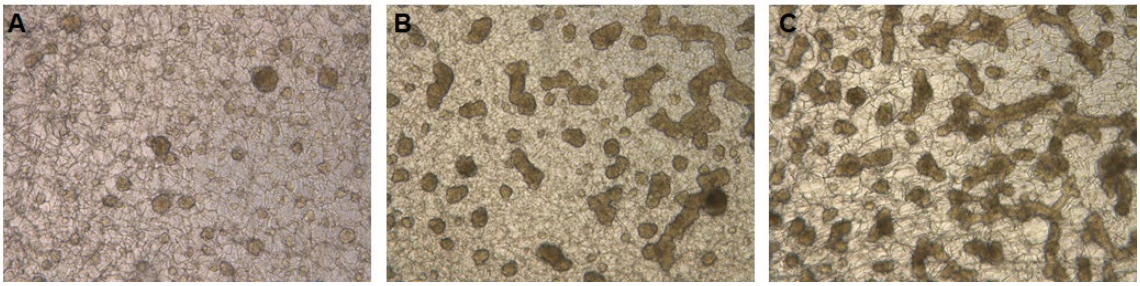

Figure 3.S1. *Morphology of spheroids in well-plates containing hydroscaffold after 96 h of culture: (A) low, (B) intermediate and (C) high starting densities.*

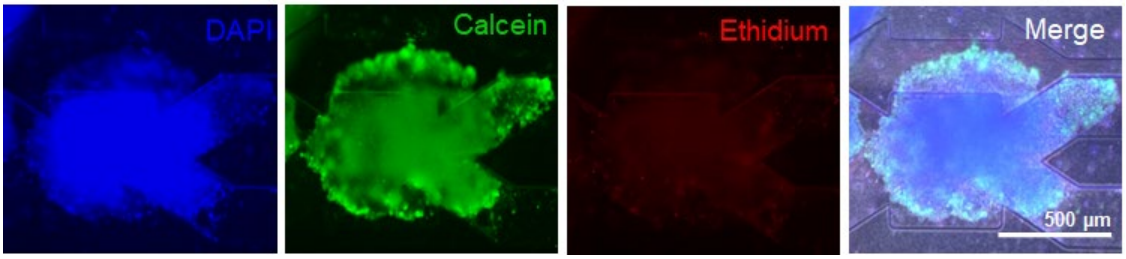

Figure 3.S 2. *DAPI (nuclei), calcein (living cells) and ethidium (dead cells) staining of spheroids after 21 days of culture in a biochip containing a hydroscaffold.*

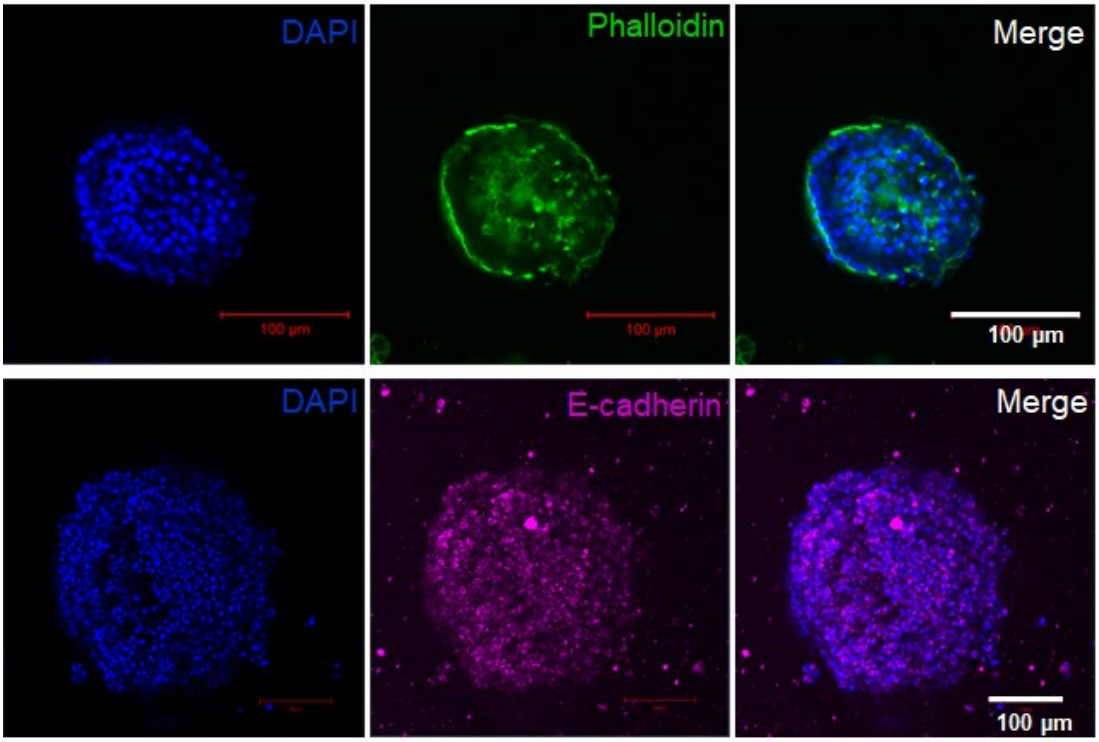

Figure 3.S3. *DAPI (nuclei), phalloidin (F-actin) and E-cadherin staining of spheroids after 21 days of culture in a static well-plate containing a hydroscaffold.*

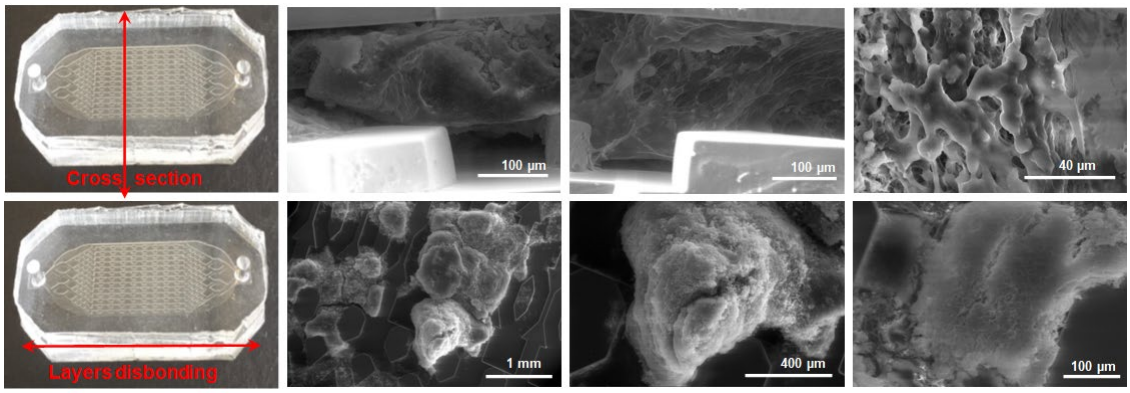

Figure 3.S4. *SEM images of cell spheroids cultured 21 days in a biochip containing a hydroscaffold.*

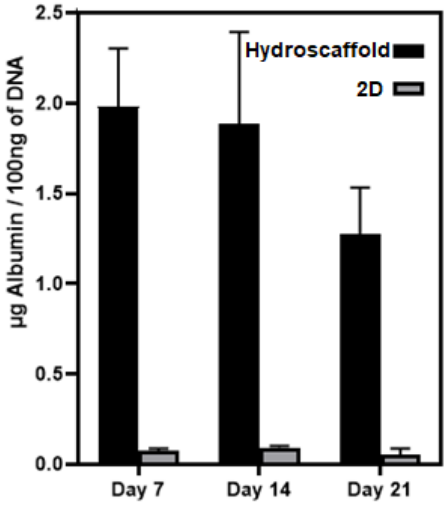

Figure 3.S5. *Albumin secreted by HepG2/C3a cells in 2D and 3D (hydroscaffold) static cultures.*

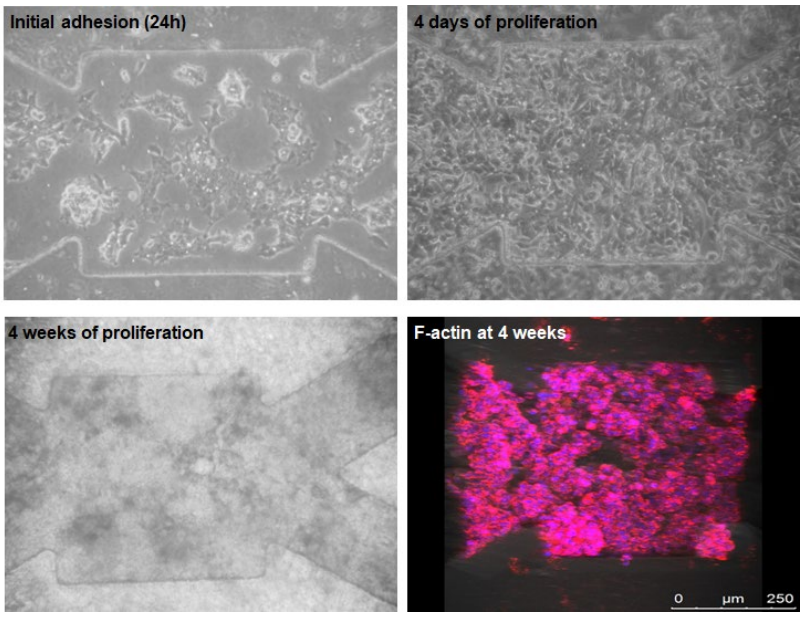

Figure 3.S6. *Morphologies and F-actin staining of HepG2/C3a inside a PDMS biochip (without hydrogel/hydroscaffold, Baudoin et al 2009 reprinted with permission).*

3.8. References

Allen JW, Khetani SR, Bhatia SN. *In vitro* zonation and toxicity in a hepatocyte bioreactor. *Toxicol. Sci.,* 2004, 84, 110-119. DOI: 10.1093/toxsci/kfi052

Andez AMH, Amenta PS. The extracellular matrix in hepatic regeneration. *FASEB J.,* 1995, 9, 1401-1410. DOI: 10.1096/fasebj.9.14.7589981

Arriazu E, de Galarreta MR, Cubero FJ, Varela-Rey M, de Obanos MPP, Leung TM, Lopategi A, Benedicto A, Abraham-Enachescu I, Nieto N. Extracellular matrix and liver disease. Antioxid. *Redox Signal*., 2014, 21, 1078-1097. DOI: 10.1089/ars.2013.5697

Baudoin R, Alberto G, Paullier P, Legallais C, Leclerc E. Parallelized microfluidic biochips in multi well plate applied to liver tissue engineering. *Sens. Actuators B Chem*., 2012, 173, 919-926. DOI: 10.1016/j.snb.2012.06.050

Baudoin R, Corlu A, Griscom L, Legallais C, Leclerc E. Trends in the development of microfluidic cell biochips for *in vitro* hepatotoxicity. *Toxicol. In Vitro*, 2007, 21, 535-544. DOI: 10.1016/j.tiv.2006.11.004

Baudoin R, Griscom L, Prot JM, Legallais C, Leclerc E. Behaviour of HepG2/C3a cell culture in a microfluidic bioreactor. *Biochem. Eng. J.*, 2011, 53, 172-181. DOI: 10.1016/j.bej.2010.10.007

Baudoin R, Prot JM, Legallais C, Leclerc E. Microfluidic biochip for *in vitro* toxicity analysis. *ESAO*: Compiegne, France, 2009. DOI: 10.1177/039139880903200707.

Bell CC, Lauschke VM, Vorrink SU, Palmgren H, Duffin R, Andersson TB, Ingelman-Sundberg M. Transcriptional, functional, and mechanistic comparisons of stem cell-derived hepatocytes, HepaRG cells, and three-dimensional human hepatocyte spheroids as predictive *in vitro* systems for drug-induced liver injury. *Drug Metab. Dispos*., 2017, 45, 419-429. DOI: 10.1124/dmd.116.074369

Bernal W, Wendon J. Acute liver failure. *N. Engl. J. Med*., 2013, 369, 2525-2534. DOI: 10.1056/NEJMra1208937

Bhatia SN, Ingber DE. Microfluidic organs-on-chips. *Nat. Biotechnol*., 2014, 32, 760-772. DOI: 10.1038/nbt.2989

Boulais L. Cryogel-integrated hepatic cell culture microchips for liver tissue engineering. *Ph.D. Thesis*, Université de Technologie de Compiègne, Compiègne, France, 2020. NNT: 2020COMP2561

Boulais L, Jellali R, Pereira U, Leclerc E, Bencherif SA, Legallais C. Cryogel-integrated biochip for liver tissue engi-neering. *ACS Appl. Bio Mater*., 2021, 4, 5617-5626. DOI: 10.1021/acsabm.1c00425

Bual RP, Ijima H. Intact extracellular matrix component promotes maintenance of liver-specific functions and larger ag-gregates formation of primary rat hepatocytes. *Regen. Ther.,* 2019, 11, 258-268. DOI: 10.1016/j.reth.2019.08.006

Chen M, Bisgin H, Tong L, Hong H, Fang H, Borlak J, Tong W. Toward predictive models for drug-induced liver injury in humans: Are we there yet? *Biomark. Med.,* 2014, 8, 201-213. DOI: 10.2217/bmm.13.146

Chen X, Zhang YS, Zhang X, Liu C. Organ-on-a-chip platforms for accelerating the evaluation of nanomedicine. *Bioact. Mater.,* 2021, 6, 1012-1027. DOI: 10.1016/j.bioactmat.2020.09.022

Choucha-Snouber L, Aninat C, Grsicom L, Madalinski G, Brochot C, Poleni PE, Razan F, Guillouzo CG, Legallais C, Corlu A, Leclerc E. Investigation of ifosfamide nephrotoxicity induced in a liver–kidney co-culture biochip. *Biotechnol. Bioeng.,* 2013, 110, 597-608. DOI: 10.1002/bit.24707

Cui, X.; Hartanto, Y.; Zhang, H. Advances in multicellular spheroids formation. J. R. Soc. Interface 2017, 14, 20160877. DOI: 10.1098/rsif.2016.0877

Danoy M, Poulain S, Lereau-Bernier M, Kato S, Scheidecker B, Kido T, Miyajima A, Sakai Y, Plessy C, Leclerc E. Characterisation of the liver zonation like transcriptomic patterns in HLCs derived from hiPCs in a microfluidic biochip environment. *Biotechnol. Prog*., 2020, 36, e3013. DOI: 10.1002/btpr.3013

Danoy M, Tauran Y, Poulain S, Jellali R, Bruce J, Leduc M, Le Gall M, Gilard F, Kido T, Arakawa H, Araya K, Mori D, Kato Y, Kusuhara H, Plessy C, Miyajima A, Sakai Y, Leclerc E. Multi-omics analysis of hiPSCs-derived HLCs matured on-chip revealed patterns typical of liver regeneration. *Biotechnol. Bioeng*., 2021, 118, 3716-3732. DOI: 10.1002/bit.27667

Deng J, Zhang X, Chen Z, Luo Y, Lu Y, Liu T, Wu Z, Jin Y, Zhao W, Lin B. A cell lines derived microfluidic liver model for investigation of hepatotoxicity induced by drug-drug interaction. *Biomicrofluidics*, 2019, 13, 024101. DOI: 10.1063/1.5070088

Donato MT, Tolosa L. Stem-cell derived hepatocyte-like cells for the assessment of drug-induced liver injury. *Differentiation*, 2019, 106, 15-22. DOI: 10.1016/j.diff.2019.02.004

Essaouiba A, Okitsu T, Jellali R, Shinohara M, Danoy M, Tauran Y, Legallais C, Sakai Y, Leclerc E. Microwell-based pancreas-on-chip model enhances genes expression and functionality of rat islets of Langerhans. *Mol. Cell. Endocrinol*., 2020, 514, 110892. DOI: 10.1016/j.mce.2020.110892

Fang Y, Eglen RM. Three-dimensional cell cultures in drug discovery and development. *SLAS Discov.,* 2017, 22, 456-472. DOI: 10.1177/1087057117696795

Foster AJ, Chouhan B, Regan SL, Rollison H, Amberntsson S, Andersson LC, Srivastava A, Darnell M, Cairns J, Lazic SE, Jang KJ, Petropolis DB, Kodella K, Rubins JE, Williams D, Hamilton GA, Ewart L, Morgan P. Integrated *in vitro* models for hepatic safety and

metabolism: Evaluation of a human liver-chip and liver spheroid. *Arch. Toxicol.*, 2019, 93, 1021-1037. DOI: 10.1007/s00204-019-02427-4

Freyer N, Greuel S, Knöspel F, Gerstmann F, Storch L, Damm G, Seehofer D, Harris J.F, Iyer R, Schubert F, Zeilinger K. Microscale 3D liver bioreactor for *in vitro* hepatotoxicity testing under perfusion conditions. *Bioengineering*, 2018, 5, 24. DOI: 10.3390/bioengineering5010024

Freyer N, Knöspel F, Strahl N, Amini L, Schrade P, Bachmann S, Damm G, Seehofer D, Jacobs F, Monshouwer M, Zeilinger K. Hepatic differentiation of human induced pluripotent stem cells in a perfused three-dimensional multicompartment bioreactor. *Biores. Open Access,* 2016, 5, 235-248. DOI: 10.1089/biores.2016.0027

Fu JJ, Lv XH, Wang LX, He X, Li Y, Yu L, Li CM. Cutting and bonding parafilm® to fast prototyping flexible hanging drop chips for 3D spheroid cultures. *Cell. Mol. Bioeng.,* 2020, 14, 187–199. DOI: 10.1007/s12195-020-00660-x

Gaskell H, Sharma P, Colley HE, Murdoch C, Williams DP, Webb SD. Characterization of a functional C3A liver spheroid model. *Toxicol. Res.,* 2016, 5, 1053-1065. DOI: 10.1039/c6tx00101g

Ghabril M, Chalasani N, Björnsson E. Drug-induced liver injury: A clinical update. *Curr. Opin. Gastroenterol.*, 2010, 26, 222-226. DOI: 10.1097/MOG.0b013e3283383c7c

Gissen P, Arias IM. Structural and functional hepatocyte polarity and liver disease. *J. Hepatol.,* 2015, 63, 1023-1037. DOI: 10.1016/j.jhep.2015.06.015

Godoy P, Hewitt NJ, Albrecht U, Andersen ME, Ansari N, Bhattacharya S, Bode JG, Bolleyn J, Borner C, Böttger J, Hengstler JG. Recent advances in 2D and 3D *in vitro* systems using primary hepatocytes, alternative hepatocyte sources and non-parenchymal liver cells and their use in investigating mechanisms of hepatotoxicity, cell signaling and ADME. *Arch. Toxicol.*, 2013, 87, 1315-1530. DOI: 10.1007/s00204-013-1078-5

Gómez-Lechón MJ, Tolosa L, Conde I, Donato MT. Competency of different cell models to predict human hepatotoxic drugs. *Expert Opin. Drug Metab. Toxicol.,* 2014, 10, 1553-1568. DOI: 10.1517/17425255.2014.967680

Gressner AM, Krull N, Bachem MG. Regulation of proteoglycan expression in fibrotic liver and cultured fat-storing cells. *Pathol. Res. Pract.,* 1994, 190, 864-882. DOI: 10.1016/S0344-0338(11)80990-8

Hughes JP, Rees S, Kalindjian SB, Philpott KL. Principles of early drug discovery. *Br. J. Pharmacol*., 2011, 162, 1239-1249. DOI: 10.1111/j.1476-5381.2010.01127.x

Ijima H, Nakamura S, Bual RP, Yoshida K. Liver-specific extracellular matrix hydrogel promotes liver-specific functions of hepatocytes *in vitro* and survival of transplanted hepatocytes *in vivo*. *J. Biosci. Bioeng*., 2019, 128, 365-372. DOI: 10.1016/j.jbiosc.2019.02.014

Ingber DE. Is it time for reviewer 3 to request human organ chip experiments instead of animal validation studies? *Adv. Sci.*, 2020, 7, 2002030. DOI: 10.1002/advs.202002030

Jellali R, Bricks T, Jacques S, Fleury MJ, Paullier P, Merlier F, Leclerc E. Long-term human primary hepatocyte cultures in a microfluidic liver biochip show maintenance of mRNA levels and higher drug metabolism compared with Petri cultures. *Biopharm. Drug Dispos*., 2016, 37, 264-275. DOI: 10.1002/bdd.2010

Jellali R, Gilard F, Pandolfi V, Legendre A, Fleury MJ, Paullier P, Legallais C, Leclerc E. Metabolomics-on-a-chip approach to study hepatotoxicity of DDT, permethrin and their mixtures. *J. Appl. Toxicol*., 2018, 38, 1121-1134. DOI: 10.1002/jat.3624

Khetani SR, Berger DR, Ballinger KR, Davidson MD, Lin C, Ware BR. Microengineered liver tissues for drug testing. *J. Lab. Autom*., 2015, 20, 216-250. DOI: 10.1177/2211068214566939

Kuna L, Bozic I, Kizivat T, Bojanic K, Mrso M, Kralj E, Smolic R, Wu GY, Smolic M. Models of drug induced liver injury (DILI)—Current issues and future perspectives. *Curr. Drug Metab.,* 2018, 19, 830-838. DOI: 10.2174/1389200219666180523095355

Lauschke VM, Hendriks DF, Bell CC, Andersson TB, Ingelman-Sundberg M. Novel 3D culture systems for studies of human liver function and assessments of the hepatotoxicity of drugs and drug candidates. *Chem. Res. Toxicol*., 2016, 29, 1936-1955. DOI: 10.1021/acs.chemrestox.6b00150

Leclerc E, Hamon J, Claude I, Jellali R, Naudot M, Bois F. Investigation of acetaminophen toxicity in HepG2/C3a microscale cultures using a system biology model of glutathione depletion. *Cell Biol. Toxicol.,* 2015, 31, 173-185. DOI: 10.1007/s10565-015-9302-0

Lee PJ, Hung PJ, Lee LP. An artificial liver sinusoid with a microfluidic endothelial-like barrier for primary hepatocyte culture. *Biotechnol. Bioeng*., 2007, 97, 1340-1346. DOI: 10.1002/bit.21360

Liu J, Abate W, Xu J, Corry D, Kaul B, Jackson SK. Three-dimensional spheroid cultures of A549 and HepG2 cells exhibit different lipopolysaccharide (LPS) receptor expression and LPS-induced cytokine response compared with monolayer cultures. *Innate Immun.,* 2011, 17, 245-255. DOI: 10.1177/1753425910365733

Mann DA. Human induced pluripotent stem cell-derived hepatocytes for toxicology testing. *Expert Opin. Drug Metab. Toxicol.,* 2015, 11, 1-5. DOI: 10.1517/17425255.2015.981523

Matsumoto S, Rizki Safitir A, Danoy M, Maekawa T, Kinoshita H, Shinohara M, Sakai Y, Fujii T, Leclerc E. Investigation of the hepatic respiration and liver zonation on rat hepatocytes using an integrated oxygen biosensor in a microscale device. *Biotechnol. Prog.*, 2019, 35, e2854. DOI: 10.1002/btpr.2854

Melchiorri AJ, Bracaglia, LG, Kimerer LK, Hibino N, Fisher JP. *In vitro* endothelialization of biodegradable vascular grafts via endothelial progenitor cell seeding and maturation in a

tubular perfusion system bioreactor. *Tissue Eng. Part C Methods*, 2016, 22, 663-670. DOI: 10.1089/ten.TEC.2015.0562

Merlier F, Jellali R, Leclerc E. Online hepatic rat metabolism by coupling liver biochip and mass spectrometry. *Analyst*, 2017, 142, 3747-3757. DOI: 10.1039/C7AN00973A

Messelmani T, Morisseau L, Sakai Y, Legallais C, Le Goff A, Leclerc E, Jellali R. Liver organ-on-chip models for toxicity studies and risk assessment. *Lab Chip*, 2022, 22, 2423-2450. DOI: 10.1039/D2LC00307D

Moscato S, Ronca F, Campani D, Danti S. Poly(vinyl alcohol)/gelatin hydrogels cultured with HepG2 cells as a 3D model of hepatocellular carcinoma: A morphological study. *J. Funct. Biomater.,* 2015, 6, 16-32. DOI: 10.3390/jfb6010016

Pauty J, Usuba R, Cheng IG, Hespel L, Takahashi H, Kato K, Kobayashi M, Nakajima H, Lee E, Yger F, Soncin F, Matsunaga YT. A vascular endothelial growth factor-dependent sprouting angiogenesis assay based on an *in vitro* human blood vessel model for the study of anti-angiogenic drugs. *EBioMedicine*, 2018, 27, 225-236. DOI: 10.1016/j.ebiom.2017.12.014

Pettinato G, Lehoux S, Ramanathan R, Salem MM, He LX, Muse O, Flaumenhaft R, Thompson MT, Rouse EA, Cummings RD, Wen X, Fisher RA. Generation of fully functional hepatocyte-like organoids from human induced pluripotent stem cells mixed with Endothelial Cells. *Sci. Rep.,* 2019, 9, 8920. DOI: 10.1038/s41598-019-45514-3

Polidoro MA, Ferrari E, Marzorati S, Lleo A, Rasponi M. Experimental liver models: From cell culture techniques to microfluidic organs-on-chip. *Liver Int.,* 2021, 41, 1744-1761. DOI: 10.1111/liv.14942

Prot JM, Videau O, Brochot C, Legallais C, Bénech H, Leclerc E. A cocktail of metabolic probes demonstrates the relevance of primary human hepatocyte cultures in a microfluidic biochip for pharmaceutical drug screening. *Int. J. Pharm.*, 2011, 408, 67-75. DOI: 10.1016/j.ijpharm.2011.01.054

Ramaiahgari SC, den Braver MW, Herpers B, Terpstra V, Commandeur JNM, van de Water B, Price LS. A 3D *in vitro* model of differentiated HepG2 cell spheroids with improved liver-like properties for repeated dose high-throughput toxicity studies. *Arch. Toxicol.,* 2014, 88, 1083-1095. DOI: 10.1007/s00204-014-1215-9

Ruoß M, Vosough M, Königsrainer A, Nadalin S, Wagner S, Sajadian S, Huber D, Heydari Z, Ehnert S, Hengstler JG, Nussler AK. Towards improved hepatocyte cultures: Progress and limitations. *Food Chem. Toxicol*., 2020, 138, 111188. DOI: 10.1016/j.fct.2020.111188

Segovia-Zafra A, Di Zeo-Sánchez D, López-Gómez C, Pérez-Valdés Z, García-Fuentes E, Andrade R, Lucena I, Villanueva-Paz M. Preclinical models of idiosyncratic drug-induced liver injury (iDILI): Moving towards prediction. *Acta Pharm. Sin. B*, 2021, 11, 3685-3726. DOI: 10.1016/j.apsb.2021.11.013

Sivaraman A, Leach JK, Townsend S, Iida T, Hogan BJ, Stolz DB, Fry R, Samson LD, Tannenbaum SR, Griffith LG. A microscale *in vitro* physiological model of the liver: Predictive screens for drug metabolism and enzyme induction. *Curr. Drug. Metab*., 2005, 6, 569-591. DOI: 10.2174/138920005774832632

Štampar M, Breznik B, Filipič M, Žegura B. Characterization of *in vitro* 3D cell model developed from human hepatocellular carcinoma (HepG2) cell line. *Cells*, 2020, 9, 2557. DOI: 10.3390/cells9122557

Wrzesinski K, Magnone MC, Hansen LV, Kruse ME, Bergauer T, Bobadilla M, Gubler M, Mizrahi J, Zhang K, Andreasen CM, Olesen JB, Schaffalitzky de Muckadellg OB, Fey SJ. HepG2/C3a 3D spheroids exhibit stable physiological functionality for at least 24 days after recovering from trypsinisation. *Toxicol. Res.,* 2013, 2, 163-172. DOI: 10.1039/C3TX20086H

Yu F, Deng R, Tong WH, Huan L, Way NC, IslamBadhan A, Iliescu C, Yu H. A perfusion incubator liver chip for 3D cell culture with application on chronic hepatotoxicity testing. *Sci. Rep.,* 2017, 7, 14528. DOI: 10.1038/s41598-017-13848-5

Chapter 4: Coculture model of a liver sinusoidal endothelial cell barrier and hepatocyte spheroids-on-chip in an advanced fluidic platform

In this section, we used the IIDMP parallelization platform to coculture the HepG2/C3a and SK-HEP-1 cell lines as a biomimetic liver model. Firstly, we characterized the permeability/ transport properties of the SK-HEP-1 cell line. Then, we analysed the effect of the coculture and a drug exposure on the expression level of specific genes, the LSEC permeability, and the drug metabolism. Finally, we discussed the potential of our model to mimic the hepatic first pass. The core of the chapter is literally extracted from our article “Coculture model of a liver sinusoidal endothelial cell barrier and hepatocyte spheroids-on-chip in an advanced fluidic platform”[3]. The article abstract is presented as a summary of the chapter 3. The material and methods are not presented in this chapter, an extended version is described in chapter 2. The supplementary files of the article are provided at the end of this chapter.

[3] **Messelmani T,** Le Goff A, Soncin F, Merlier F, Maubon N, Legallais C, Leclerc E, Jellali R. Coculture model of a liver sinusoidal endothelial cell barrier and hepatocyte spheroids-on-chip in an advanced fluidic platform, ***Biotechnology & Bioengineering, 2023, Preprint, DOI: 10.22541/au.167596570.02002054/v1***

Summary

The liver is one of the main organs involved in the metabolism of xenobiotics and a key organ in toxicity studies. Prior to accessing the hepatocytes, xenobiotics pass through the hepatic sinusoid formed by liver sinusoidal endothelial cells (LSECs). The LSECs barrier regulates the kinetics (absorption, distribution, metabolism, and excretion) and concentrations of the xenobiotics before their metabolic processing by the hepatocytes. To mimic this physiological situation, we developed an *in vitro* model reproducing an LSECs barrier in coculture with a hepatocyte biochip, using a fluidic platform. This technology made dynamic coculture and tissue crosstalk possible. SK-HEP-1 and HepG2/C3a cells were used as LSECs and as hepatocyte models, respectively. We confirmed the LSECs phenotype by measuring PECAM-1 and stabilin-2 expression levels and the barrier's permeability/transport properties with various molecules. The tightness of the SK-HEP-1 barrier was enhanced in the dynamic coculture. The morphology, albumin secretion, and gene expression levels of markers of HepG2/C3a were not modified by coculture with the LSECs barrier. Using paracetamol, a well-known hepatotoxic drug, to study tissue crosstalk, there was a reduction in the expression levels of the LSECs markers stabilin-2 and PECAM-1, and a modification of those of CLEC4M and KDR. No HepG2/C3a toxicity was observed. The metabolisation of paracetamol by HepG2/C3a monocultures and cocultures was confirmed. Although primary cells are required to propose a fully relevant model, the present approach highlights the potential of our system for investigating xenobiotic metabolism and toxicity.

Keywords: Organ-on-chip, Liver, LSECs barrier, HepG2/C3a, coculture, microfluidic

4.1. Introduction

Humans are continuously and increasingly exposed to a variety of xenobiotics such as drugs, chemicals, pesticides, and environmental pollutants. Before commercialisation, drugs undergo a thorough testing process to evaluate their effects and toxicity (Khetani et al., 2015). Since 2007, enforcement of the REACH (Registration, Evaluation, Authorisation and Restriction of CHemical substances) legislation imposes the evaluation of risks of all chemical substances (Zeller et al., 2016). The need for toxicological evaluation is thus increasing. Animal models are widely used as reference tools for predictive studies in drug development and risk assessment (Messelmani et al., 2022). However, due to differences between animal and human metabolism and physiology, animal models fail to accurately reproduce the human condition, and this issue challenges the extrapolation of data to humans (Son et al., 2020). For example, the predictivity of animal models for chemical-induced hepatotoxicity is only 50% (Ruoss et al., 2020). Moreover, animal experiments are costly, time-consuming, and, most importantly, raise ethical and regulatory issues (Ruoss et al., 2020; Soldatow et al., 2013). To decrease the use of laboratory animals, the REACH legislation and the 3R rules, recommended to reduce as much as possible the use of animal models, have pressed industrial companies and scientists to develop alternative approaches to animal testing (Son et al., 2020). Consequently, developing reliable methods not based on using animals and *in vivo* experimentation has become necessary.

The liver is the main site involved in the metabolism of xenobiotics and is therefore the most commonly used organ in toxicological and pharmacological tests. It is a multifunctional and complex organ performing a variety of vital functions focused on biotransformation, storage, and synthesis (Polidaro et al., 2021; Bale, S. S., & Borenstein, 2018). The liver is composed of several cell types, the main ones being hepatocytes (parenchymal cells) and non-parenchymal cells (NPCs): sinusoidal endothelial cells (LSECs), Kupffer cells (KCs), hepatic stellate cells (HSCs), and biliary epithelial cells (LeCluyse et al., 2012, Moradi et al., 2020). Hepatocytes represent approximately 60% of the total liver cells, and are the main cell type, ensuring most metabolic activities (Beckwitt et al., 2018). The NPCs are involved in several key functions, such as the production of growth factors and mediators of cellular functions, maintenance of tissue architecture, and regulation of liver response to xenobiotics (LeCluyse et al., 2012, Moradi et al., 2020).

Given that hepatocytes ensure the major functions of the liver, especially xenobiotic metabolism, most of the current *in vitro* liver models are focused on hepatocytes and do not include NPCs (Bale et al., 2016). Moreover, the models used for drug screening and risk assessment are mainly based on cell culture in static two-dimension (2D) monolayers using

conventional Petri dishes (Messelmani et al., 2022). These 2D cultures present some advantages, such as allowing high-throughput analyses, ease of manipulation, and a lower cost (Milner et al., 2020; Moradi et al., 2020). However, 2D monocultures of hepatocytes or of hepatic cell lines suffer from several disadvantages associated with the loss of tissue-specific architecture, mechanical and biomechanical cues, and cell-cell and cell-matrix interactions. Consequently, these models fail to recapitulate the complexity of the *in vivo* physiological environment, show limited prediction capacity for xenobiotics, and cells are prone to dedifferentiation within 48-72 h (Messelmani et al., 2022. Milner et al., 2020; Panwar et al., 2021).

Recently, several approaches have been proposed to overcome the drawbacks associated with 2D monolayer cultures of hepatocytes. Microfluidic devices, or organ-on-chip (OoC) technology, are a promising tool for building more relevant *in vitro* liver models aimed at mimicking the *in vivo* environment (Merlier et al., 2017). The microfluidic perfusion improves the exchanges and transport of nutrients, oxygen, metabolites, and other chemicals, and creates a controlled microenvironment and physiological-like features, including the liver zonation, cell-cell interactions, shear stress, and chemical concentration gradients (Moradi et al., 2020; Messelmani et al., 2022; Lee et al., 2021; Lee et al., 2019). Several studies have reported that perfused microfluidic cultures enhance the long-term viability and functionality of hepatocytes (Jellali et al., 2016; Schepers et al., 2016; Yu et al., 2017). The three-dimensional (3D) cell culture (spheroids/organoids), with and without polymer matrix, also makes it possible to maintain tissue architecture similar to the *in vivo* situation and maintains liver-specific functions. This organisation enhances cell-cell and cell-matrix interactions and the creation of chemical gradients (Polidaro et al., 2021; Fang et al., 2017; Yun et al., 2023). Among other approaches used to maintain hepatocyte functions, cocultures with NPCs are commonly used strategies (Ruoss et al., 2020). Among NPCs, LSECs participate in liver metabolic functions and maintain hepatocyte phenotype and functions through paracrine communication (Ortega-Ribera et al., 2018). The benefits of coculturing LSECs and hepatocytes have been reported in several works (Ortega-Ribera et al., 2018; Bale et al., 2015; Xiao et al., 2015).

Previously, we developed a liver-on-chip model integrating a hydroscaffold containing key liver extracellular matrix (ECM) components (Messelmani et al., 2022). This device made possible the dynamic culture of HepG2/C3a organised into 3D spheroids for the long-term, while maintaining their functionalities. Here, to better reproduce the physiology of the liver, our liver-on-chip model was cocultured with liver sinusoidal endothelial cells. The coculture was performed using a fluidic platform making it possible to connect the liver biochip previously developed by our laboratory (Bricks et al., 2014) to a new LSEC barrier insert. The

behaviour and functionalities of the LSECs barrier (SK-HEP-1 cell line) and hepatocyte biochip (HepG2/C3a cells) in monoculture and coculture were studied and compared. Then, the coculture model was exposed to paracetamol (APAP), and the crosstalk between both compartments was studied and compared to monocultures exposed to APAP.

4.2. Selecting a culture medium for SK-HEP-1 and HepG2/C3a coculture

The culture of cells of different origin in the same system requires an adapted coculture medium capable of maintaining both cell types in good conditions, without impairing their characteristics and functionalities. The routine culture medium used in our conditions for SK-HEP-1 is EGM-2/MEM (75%/25%) and the cells formed a well-structured cell monolayer at confluence, as needed for the barrier function (Figure 4.1A, Figure 4.S1). On the other hand, when SK-HEP-1 cells were cultured in HepG2/C3a medium, which is based on MEM only, the endothelial cell morphology was greatly altered, and the cells failed to form a confluent monolayer (Figure 4.S1). In an attempt to, first, create the endothelial barrier, and then to switch to a hepatocyte culture medium, SK-HEP-1 cells were cultured in their normal medium for 6 days, followed by culture in MEM for 3 days (as the coculture period). In these conditions again, the endothelial cells failed to maintain a confluent monolayer (Figure 4.S1). Finally, when cells were maintained in EGM-2/MEM (25%/75%) medium for 7 days, the SK-HEP-1 cells formed a confluent monolayer (Figure 4.1A and Figure 4S.1) and exhibited the characteristic morphology of SK-HEP-1, as when cultured in their original medium. The gene expression levels of several LSECs markers were investigated. No major differences were observed for most of the genes when cells were cultured in EGM-2/MEM (25%/75%) when compared to their original medium. A downregulation of CLEC4M and VCAM1 was observed when cells were maintained in EGM-2/MEM (25%/75%) in comparison with native medium, with fold changes (FC) of 0.25 and 0.48, respectively (Figure 4.1B).

The EGM-2/MEM (25%/75%) medium was also tested on HepG2/C3a cells and compared to culturing in MEM. After 4 days of static culture, the HepG2/C3a presented a typical morphology and formed a monolayer in both conditions (Figure 4.1C). Additionally, secretion of albumin was measured to assess whether HepG2/C3a cells retained their hepatic properties. Similar albumin secretion levels were observed in both conditions. The levels were approximately 125 ± 11 and 114 ± 17 ng/h for cells cultured in MEM and EGM-2/MEM 1/3 mixture, respectively (Figure 4.1D).

Based on the results obtained with SK-HEP-1 and HepG2/C3a cells, the mixture of EGM-2/MEM (25%/75%) was chosen for the dynamic coculture experiments. To facilitate the comparisons between monoculture and coculture, this medium was also used for SK-HEP-1 and HepG2/C3a maintenance in monocultures.

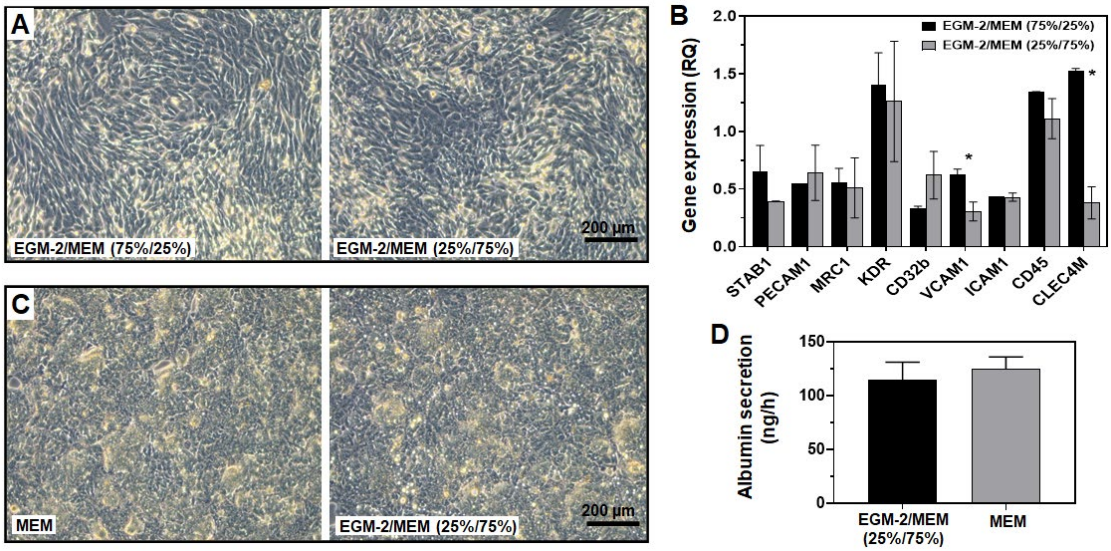

Figure 4.1. *Effect of culture medium composition on SK-HEP-1 and HepG2/C3a cells. (A) morphology of SK-HEP-1 after 7 days of culture in different culture media mixtures; (B) gene expression of several LSECs markers in SK-HEP-1 cultured in different mixtures of MEM and EGM-2; (C) HepG2/C3a cells morphology after 4 days of culture in MEM and MEM/EGM-2 mixture media; (D) albumin secretion by HepG2/C3a cultured in MEM and EGM-2/MEM (25%/75%) media, * $P < 0.05$.*

4.3. Characterisation of the SK-HEP-1 endothelial barrier

LSECs act as a physical barrier to molecules and play a significant role in transportation from circulating blood to the hepatocytes. Therefore, before using SK-HEP-1 to form a liver endothelial barrier in our coculture model, it was essential to characterise the formation, integrity, and permeability of the barrier. The SK-HEP-1 cells were seeded in static inserts using the selected coculture medium and followed over time. The cells proliferated continuously to reach full confluence and form homogenous and continuous monolayers from Days 7-8 and thereafter (Figure 4.S2). Then, overgrowth could be observed, resulting in the formation of a second layer of cells on top of the first one (Day 10, Figure 4.S2). Nevertheless, the formation of continuous layers of confluent cells was confirmed by nuclei, vimentin, and actin stainings. As shown in Figure 4.2A, the tissue was dense with contiguous cells and a well-developed actin network. The LSEC phenotype of the SK-HEP-1 barrier was confirmed by the positive staining for LSEC markers PECAM-1 and stabilin-2 (Figure 4.2B).

The formation of a confluent barrier was associated with major modifications in paracellular permeability. The flow through the barrier was directly correlated to the integrity and homogeneity of the barrier. To confirm the formation of the barrier, permeability to Lucifer Yellow was checked using SK-HEP-1 inserts at different times of culture. PET inserts without cells exhibited a permeability value of 177 10^{-15} ± 9 10^{-15} m/s (Figure 4.2C). When SK-HEP-1 cells were added, a significant decrease in Lucifer Yellow paracellular flow from the apical to the basal compartment was observed, with apparent permeability values of 98 10^{-15} ± 10 10^{-15} and 35 10^{-15} ± 10^{-15} m/s at Days 4 and 8, respectively. This latter value remained stable, at

approximately 40 10^{-15} ± 8 10^{-15} m/s until Day 15. These results suggested that the SK-HEP-1 cells were capable of forming a barrier which reached relative stability at Day 8, and could be used for coculture with HepG2/C3a and permeability experiments.

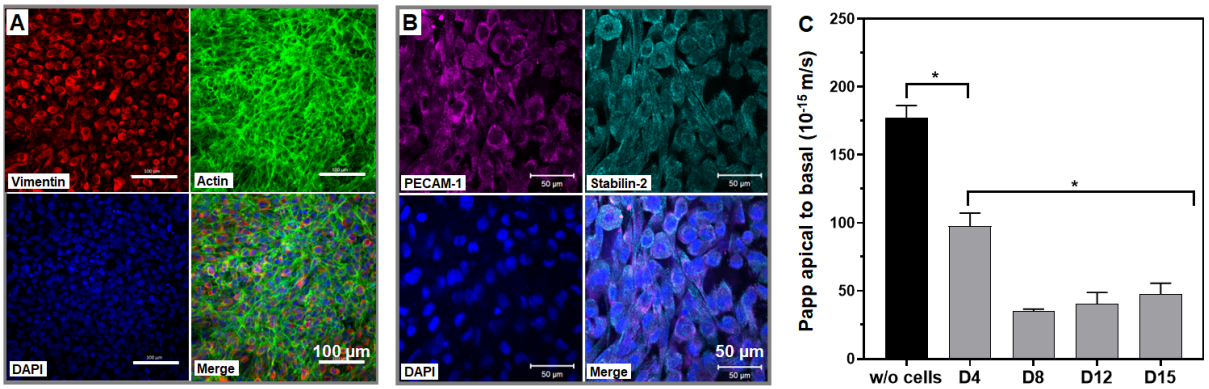

Figure 4.2. *Characterisation of the SK-HEP-1 endothelial barrier. (A) vimentin, actin, and nuclei staining of the SK-HEP-1 cells after 8 days of culture on inserts; (B) PECAM-1, stabilin-2, and nuclei staining at Day 8; (C) apparent permeability measured using Luc Lucifer Yellow, * P < 0.05.*

The permeability of the SK-HEP-1 barrier to molecules with different molecular weights was also assessed, using FITC-dextran of 4, 70 and 150 kDa. The experiments were performed using confluent SK-HEP-1 cultures at Day 8 in static inserts. For comparison, the same experiments were performed using inserts without cells. When using each of the different molecular weight dextrans, we found that the tracer concentrations decreased from the apical compartment and increased in the basal one over time (Figure 4.3). Thus, the tracer molecules were able to pass through the insert membranes whether the cells were present or not. However, the FITC dextrans diffused at faster rates into the basal compartment when the inserts were not seeded with endothelial cells, whereas the presence of a SK-HEP-1 cell layer slowed the diffusion process for the three molecular weight markers, confirming that the SK-HEP-1 made an efficient diffusion barrier. As expected, the diffusion rates were dependent on the FITC-dextran molecular weight and were slower when using FITC-dextran of 150 kDa when compared to 4 kDa- dextran.

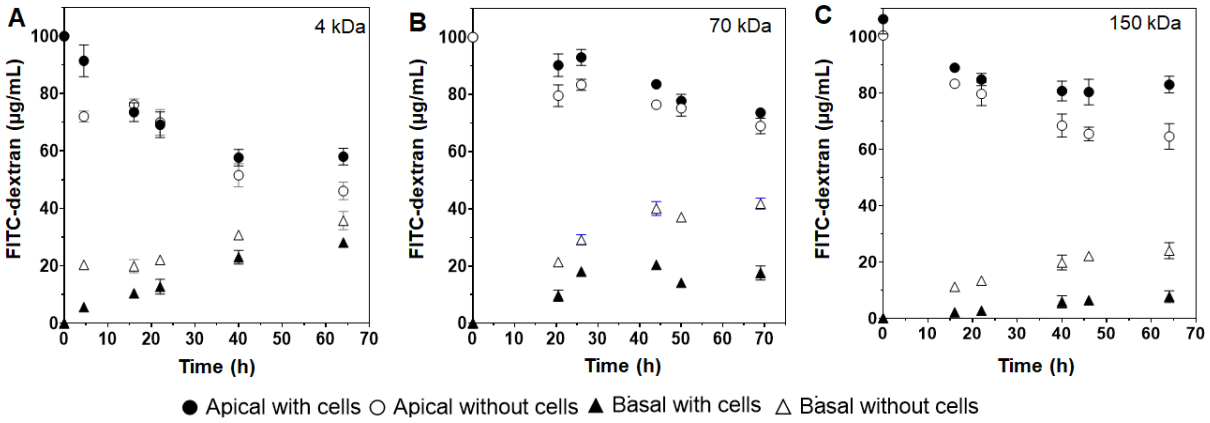

Figure 4.3. *Diffusion of FITC-dextran through the SK-HEP-1 barrier and insert without cells: (A) FITC-dextran 4 kDa; (B) FITC-dextran 70 kDa; (C) FITC-dextran 150 kDa.*

4.4. Dynamic coculture of the SK-HEP-1 barrier and HepG2/C3a biochip

Following the previous characterisations and optimisations, the coculture of SK-HEP-1 barrier (LSEC compartment) with HepG2/C3a cells cultured in 3D in the biochip (the hepatocyte compartment as previously characterised, Messelmani et al., 2022) was assessed. The coculture was performed for 48 h in the IIDMP platform and the communication between both compartments was ensured by culture medium circulation. In parallel, for comparison, SK-HEP-1 and HepG2/C3a monocultures were also used in the IIDMP platform.

4.4.1. Effect of the dynamic coculture on the SK-HEP-1 barrier

After 8 days of barrier maturation in static conditions followed by 48 h of dynamic coculture or monoculture, the SK-HEP-1 inserts were collected and characterised. Although cells were barely distinguishable because of the density at confluence, the morphology of the SK-HEP-1 tissues appeared similar in coculture and monoculture. In both culture modes, the cells formed homogenous and continuous barriers and grew beyond confluence (Figure 4.S3). Confocal microscopy imaging of actin, vimentin and nuclei staining confirmed the formation of a continuous endothelial barrier, with different cell layers and a developed actin/vimentin network (Figure 4.4A). Furthermore, no obvious differences were observed between the staining of cocultured and monocultured endothelial barriers. SK-HEP-1 barriers in monoculture and coculture expressed typical LSEC markers without any apparent difference between the two modes of culture, as illustrated by the detection of PECAM-1 and stabilin-2 positive SK-HEP-1 cells (Figure 4.4B).

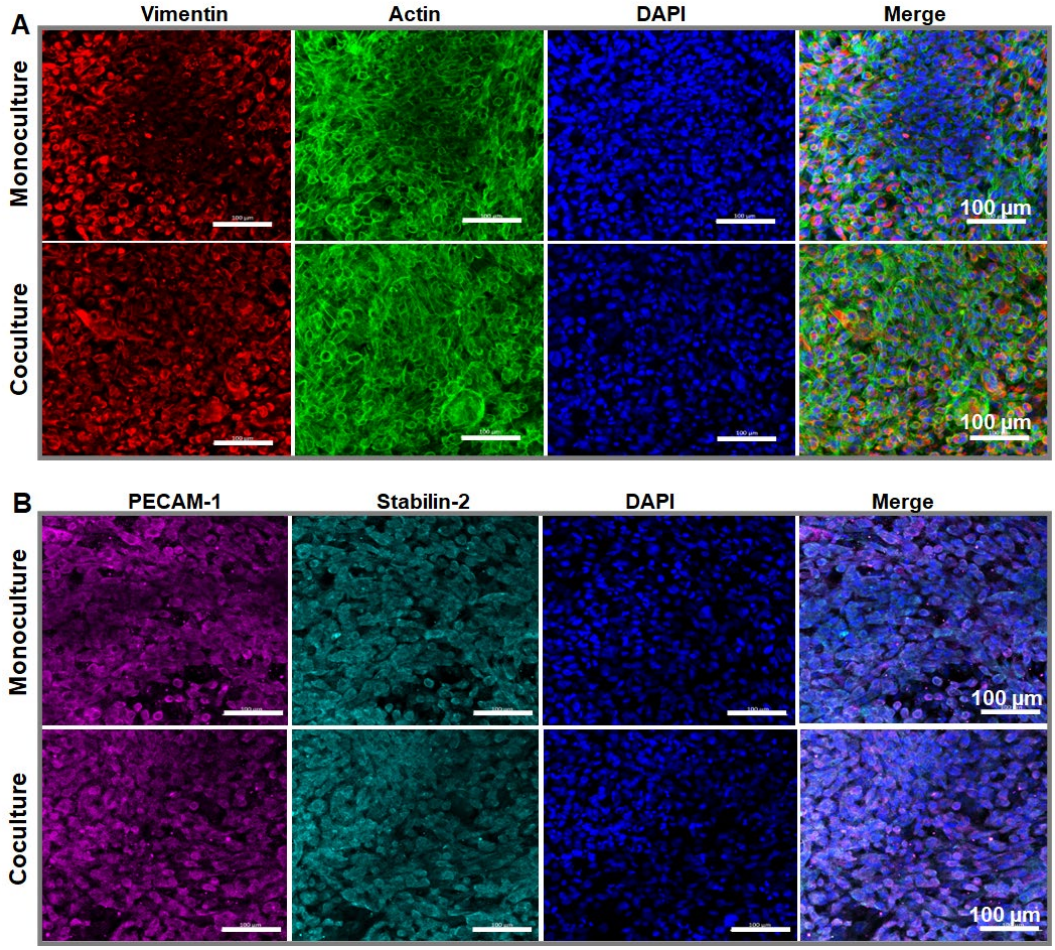

Figure 4.4. *Characterisation of the SK-HEP-1 endothelial barrier in dynamic monoculture and coculture (8 days of maturation followed by 2 days in the IIDMP platform). (A) vimentin, actin and nuclei staining; (B) PECAM-1, stabilin-2 and nuclei staining.*

Gene expression level analyses of several LSEC markers revealed the significant upregulation of CLEC4M (FC: 2.05) whereas KDR was downregulated (FC: 0.49) in SK-HEP-1 cocultures (Figure 4.5A). The expression levels of PECAM-1, MRC1 and CD32b were similar in SK-HEP-1 monocultures and cocultures. Finally, the diffusion rates of FITC-dextran 4 kDa through the SK-HEP-1 barrier, in dynamic monoculture and coculture with HepG2/C3a, were compared. The changes in FITC-dextran concentrations in the apical (decrease) and basal (increase) compartments confirmed the permeability of the barrier and the communication between the apical side of the barrier and the HepG2/C3a biochip (Figure 4.5B). The variations in FITC-dextran concentrations in the apical compartment revealed a lower diffusion rate through the barrier in coculture when compared to that in monoculture, notably after 24 h.

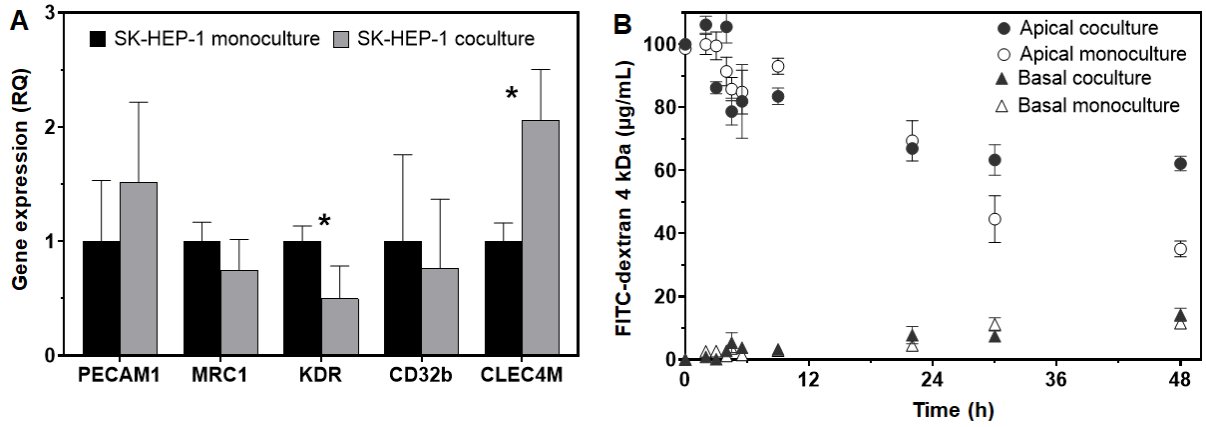

Figure 4.5. *Comparison of the SK-HEP-1 barrier in dynamic monoculture and coculture. (A) gene expression of LSEC markers in SK-HEP-1 monoculture and coculture; (B) FITC-dextran 4 kDa diffusion through SK-HEP-1 barriers in dynamic monoculture and coculture.*

4.4.2. Behaviour and functionality of HepG2/C3a in coculture with SK-HEP-1 barrier

The day before starting the dynamic monocultures or cocultures in the IIDMP devices, HepG2/C3a cells were seeded into the biochips containing the hydroscaffold and incubated for 24 h in static conditions (adhesion phase). Twenty-four hours after seeding, the cells were embedded in/adhered to the hydroscaffold and started to create spheroid-like aggregates (Figure 4.6A). Then, the biochips were connected to the IIDMP device, with and without an SK-HEP-1 barrier, and perfusion was started. The hepatocytes maintained in coculture with an endothelial barrier had a similar morphology to cells maintained in monoculture. In both conditions, the HepG2/C3a formed a dense tissue, organised in 3D spheroids ranging between 200 and 500 µm in diameter, similar in both monoculture and coculture (Figure 4.6A).

To evaluate the effects of coculture on the specific functions of HepG2/C3a, albumin secretion rates were quantified and found to be similar to those in monoculture (Figure 4.6B). After 48 h of culture, the albumin secretion levels were 127 ± 24 and 134 ± 28 ng/h in monoculture and coculture, respectively. The expression levels of several specific marker genes of HepG2/C3a cells (UGT2B7, UGT1A1, SULT1A2, CYP1A2 and CYP1A1) were also evaluated to determine whether the SK-HEP-1 barrier influenced the HepG2/C3a cultures. As shown in Figure 4.6C, there were no differences in expression levels in the selected genes between HepG2/C3a maintained as a monoculture and HepG2/C3a in coculture with SK-HEP-1.

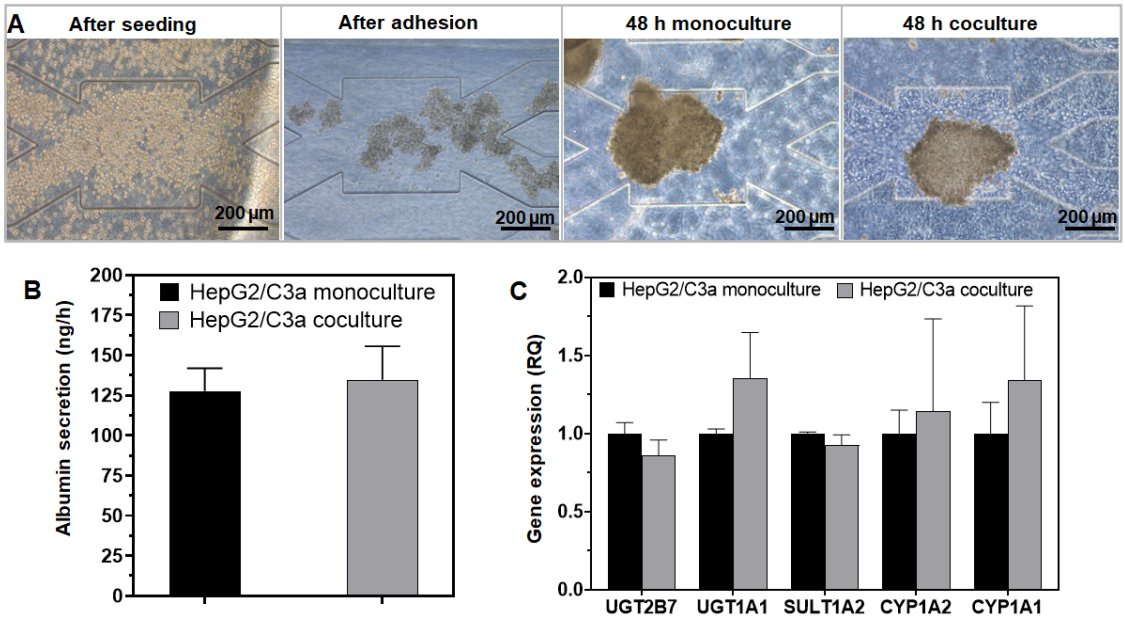

Figure 4. 6. *Characterisation of HepG2/C3a cells cultured in the biochip, in monoculture, and coculture with the SK-HEP-1 endothelial barrier. (A) Cell morphology after seeding, 24 h of adhesion in static conditions, 48 h of dynamic monoculture, and 48 h of dynamic coculture in the presence of SK-HEP-1; (B) albumin secretion by HepG2/C3a after 48 h of monoculture and coculture with SK-HEP-1; (C) gene expression levels of markers in HepG2/C3a monocultures and cocultures.*

4.5. Exposure of the coculture and monoculture models to acetaminophen (APAP)

To test the coculture model and demonstrate the crosstalk between the HepG2/C3a biochips and SK-HEP-1 barrier in the configuration of a drug study, we exposed the SK-HEP-1 barrier to APAP with and without coculture with the HepG2/C3a biochip. APAP was chosen because it is i) metabolised by HepG2/C3a cells, ii) widely studied with liver *in vitro* models and iii) not adsorbed onto the PDMS biochip (Bricks et al., 2015). APAP was introduced into the apical side of the SK-HEP-1 barrier at 1 mM, leading to a systemic theorical concentration of 100 µM after diffusion in the total circuit. For comparative purposes, a HepG2/C3a monoculture in the IIDMP was also performed and the APAP was deposited into the insert without SK-HEP-1.

SK-HEP-1 cells exposed to APAP for 48 h in coculture or in monoculture exhibited a confluent and continuous barrier composed of several cell layers, forming a dense tissue. The cell morphologies between the treated SK-HEP-1 barrier in coculture and in monoculture showed no significant differences (Figure 4.S4). Moreover, the SK-HEP-1 cells exposed to APAP were similar to those without APAP (monoculture and coculture, Figure 4.S3). As shown in Figure 4.7A, APAP treatment appeared to affect the actin cytoskeleton of the barrier. Compared to barrier monoculture and coculture without APAP (Figure 4.4A), the actin network was disordered and composed of more elongated filaments. The immunostaining of specific LSEC markers showed weaker expression levels of PECAM-1

and stabilin-2 in SK-HEP-1 exposed to APAP (Figure 4.7B), when compared to monoculture and coculture without APAP (Figure 4.4B). This effect was more striking in the coculture. Gene expression levels analyses of cultures treated or not with APAP showed an upregulation of KDR (FC: 1:8) after APAP exposure in coculture (Figure 4.8A). Conversely, both this gene and CLEC4M were downregulated in the monoculture exposed to APAP (FC: 0.54 and 0.49 for CLEC4M and KDR, respectively). APAP treatment of the monoculture also led to the upregulation of MRC1 (FC 1.4).

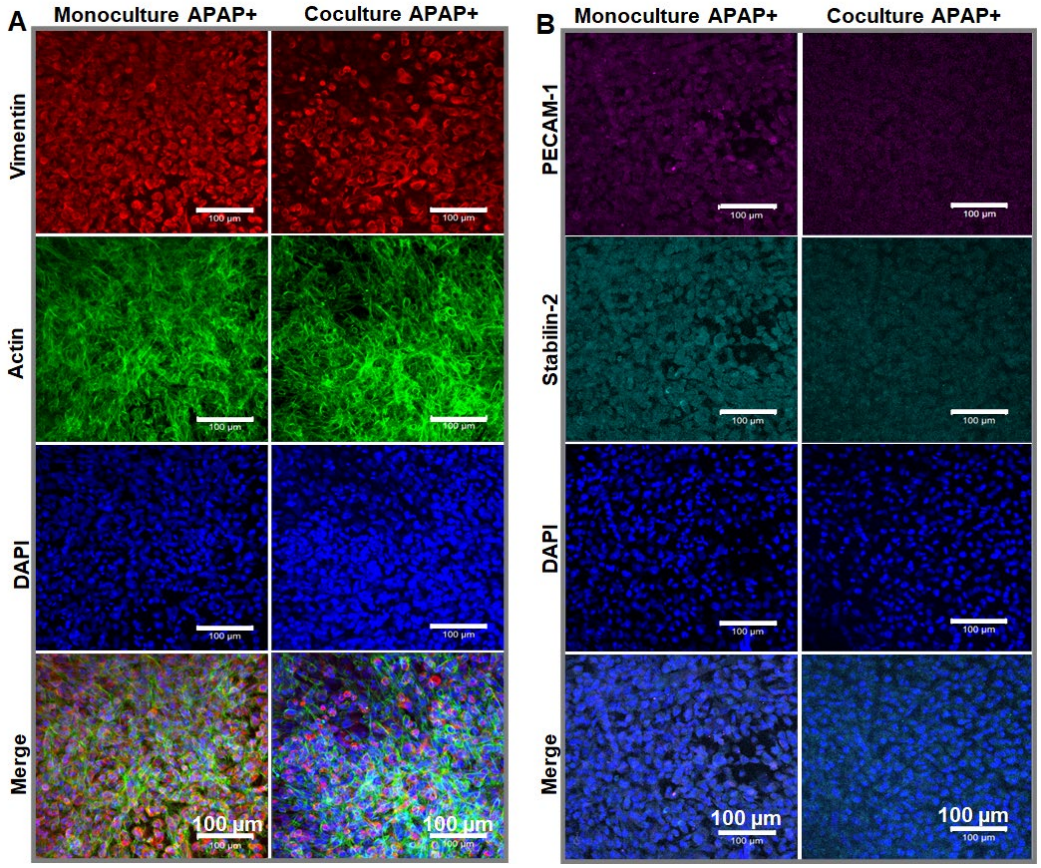

Figure 4. 7. *Characterisation of the SK-HEP-1 endothelial barrier exposed to APAP in dynamic monoculture and coculture (8 days of maturation followed by 2 days in the IIDMP platform with APAP exposure). (A) vimentin, actin, and nuclei staining; (B) PECAM-1, stabilin-2 and nuclei staining.*

Regarding the HepG2/C3a compartment, the cells exposed to APAP (coculture and monoculture) maintained their organisation in 3D spheroids up until the end of the culture (Figure 4.S4). The cells formed dense tissues, without any apparent difference compared to non-treated cultures. Analysis of gene expression levels showed no differences between the biochip monocultures treated or not with APAP (Figure 4.8B). In HepG2/C3a cocultured with the SK-HEP-1 barrier, UGT2B7 expression levels were downregulated (FC: 0.7). In addition, the ratios of albumin secretion (culture with APAP versus without APAP) were 0.92 ± 0.25 and 0.95 ± 0.09 for monoculture and coculture, respectively (Figure 4.8C).

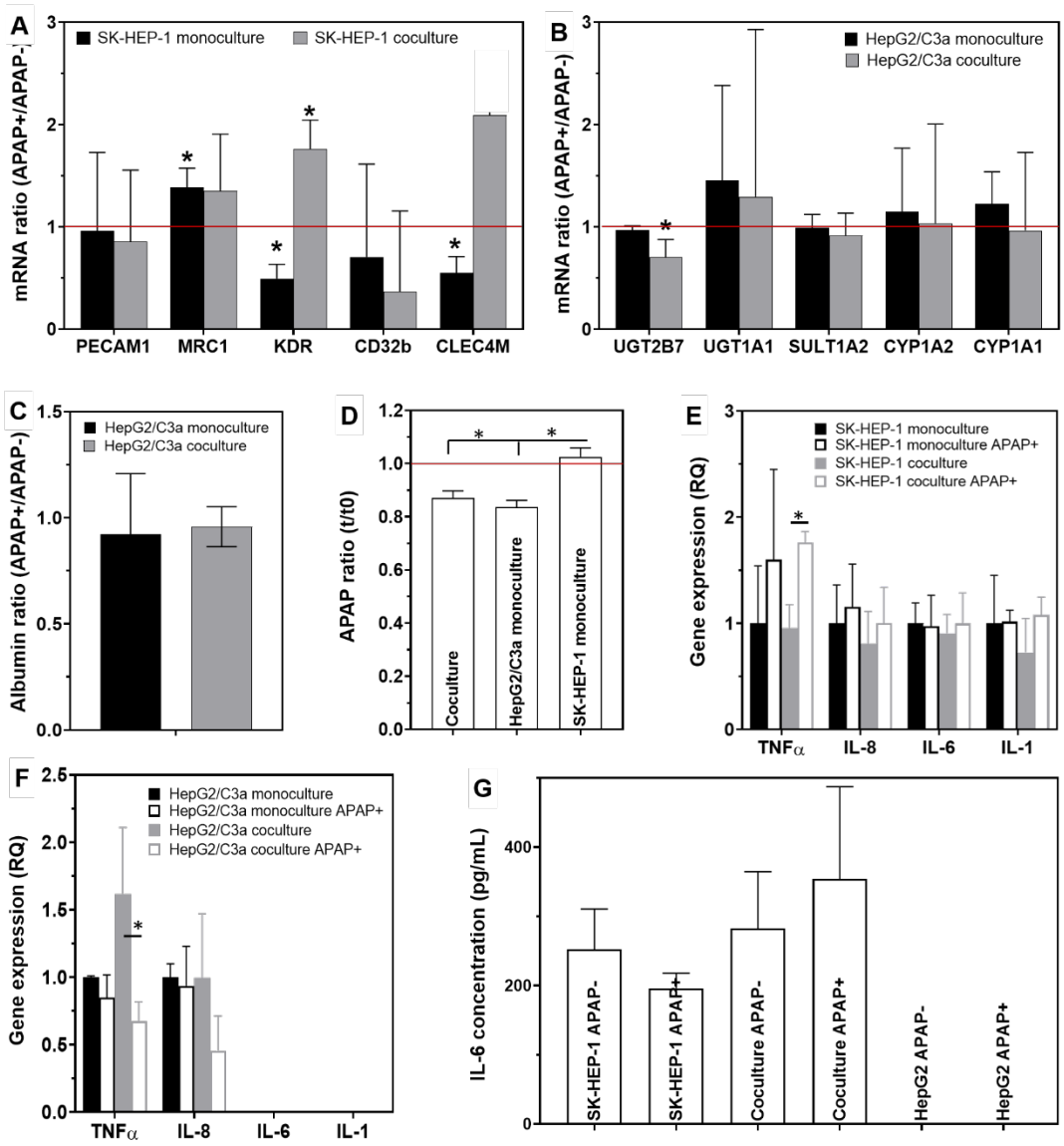

Figure 4. 8. *Characterization of monocultures and cocultures with and without APAP treatment. (A) mRNA ratio (APAP+/APAP-) of selected markers in SK-HEP-1 monoculture and coculture (* P < 0.05, comparison APAP+ versus APAP-); (B) mRNA ratio (APAP+/APAP-) of selected markers in HepG2/C3a monoculture and coculture (* P < 0.05, comparison APAP+ versus APAP-); (C) ratio (APAP+/APAP-) of albumin secreted by HepG2/C3a monoculture and coculture; (D) ratio of APAP recovered at the end of the experiments for HepG2/C3a monoculture, SK-HEP-1 monoculture and coculture; (E) expression of inflammatory genes in SK-HEP-1 monoculture and coculture, with and without APAP; (F) expression of inflammatory genes in HepG2/C3a monoculture and coculture, with and without APAP; (G) IL-6 secreted in different culture conditions.*

The metabolism of APAP was then investigated in SK-HEP-1 and HepG2/C3a cocultures, or monocultures using HPLC coupled to MS. We used the culture medium collected in the basal compartment to confirm the passage of APAP through the SK-HEP-1 barrier. The ratios of APAP (compared to the initial systemic concentration of 100 µM) recovered at the end of the experiment are provided in Figure 4.8D. For the SK-HEP-1 monoculture, the APAP ratio at the end of the experiment was 1.02 ± 0.07, indicating that SK-HEP-1 did not metabolise APAP. The recovered ratio, corresponding to a concentration of 100 µM, confirmed the

passage of APAP through the barrier, allowing the equilibrium of APAP concentration between the apical and basal sides. In the HepG2/C3a monoculture and SK-HEP-1/HepG2/C3a coculture, the APAP ratios were 0.83 ± 0.05 and 0.87 ± 0.08, respectively, illustrating the metabolism (Figure 4.8D). However, for both conditions, the paracetamol sulfate and paracetamol glucuronide concentrations were below detection limits.

4.6. Expression of inflammatory cytokines

The expression of inflammatory cytokines was evaluated in all culture conditions (with and without APAP) by analysing mRNA levels for TNFα, IL-1, IL-6 and IL-8 genes, and by quantifying IL-6 secretion in the culture medium. SK-HEP-1 cells expressed the four genes in all culture conditions (monoculture/coculture and APAP+/APAP-). Gene expression levels of IL8, IL6 and IL1 were similar, regardless of the culture conditions. There was a noticeable significant upregulation of TNFα in SK-HEP-1 cocultured with APAP (Figure 4.8E). Regarding HepG2C3a cells, there were no significant differences in expression levels of IL-8 in the conditions tested. On the other hand, there was a slight but significant overexpression of TNFα in HepG2/C3a cocultured without APAP when compared to monocultures (Figure 4.8F). IL-6 protein quantification in culture medium showed that it was only expressed by SK-HEP-1 cells and that HepG2/C3a monocultures with and without APAP did not produce detectable amounts of IL-6 (Figure 4.8G).

4.7. Discussion

Classic 2D *in vitro* coculture models consist of cells randomly mixed and heterogeneously distributed at the bottom of well-plates and dishes. However, *in vivo,* LSECs and hepatocytes are separated by the space of Disse which, in 3D models, is generally mimicked by a gel or collagen matrix which physically separates LSECs and hepatocytes (Bale et al., 2015). Furthermore, the controlling of the homotypic and heterotypic cell-to-cell interactions appears to be a key feature for maintaining and enhancing the hepatocyte phenotype (Bhatia et al., 1999; Bhatia 1997). In the present work, we have established a coculture model of liver sinusoidal endothelial cells with liver hepatocytes. Thanks to our platform which integrates a liver-on-chip solution and a barrier insert, we were able to propose technology that physically separated both cell types. In this model, cell-to-cell paracrine-like communication was made possible by exchanges through the insert membrane, as this model did not allow direct contact between LSECs and hepatocytes. Although this type of technology has already been presented for organ-to-organ models such as the intestine barrier–liver (Bricks et al., 2014), to our knowledge, only two other such dynamic LSEC barrier-hepatocyte coculture models have previously been described (van Grunsven 2017; Lauschke et al., 2019).

We demonstrated the functionality of the coculture model using two human cell lines, SK-HEP-1 and HepG2/C3a. For this purpose, we optimised the culture medium, confirmed the innocuity of the fluid flow and coculture on the LSECs barriers, and characterised the cytokine crosstalk between cells. Establishing a coculture medium that is healthy for two or more types of cells is a critical step in *in vitro* physiological models (Vis et al., 2020), including liver cells (Lauschke et al., 2019). Similarly, it was reported that LSECs are sensitive to serum components (Elvevold, et al., 2008). Our data demonstrated that the HepG2/C3a MEM-based medium which contained serum contributed to damaging the LSEC layer, whereas the conventional LSEC medium (also containing serum) did not. Interestingly a mixture of the HepG2/C3a and SK-HEP-1 media led to both healthy LSECs and HepG2/C3a. Although we did not identify the specific factors leading to this result, we postulate that the presence of pro-angiogenic factors in EGM-2 medium played a part in stabilising the LSEC cultures. Interestingly, the present dynamic conditions did not affect the cell junctions or the expression levels of LSEC markers.

Endothelial cells are normally exposed to flow, and dynamic *in vitro* models have largely been reported as regulating their functions and physiology (Akbari et al., 2018, van Duinen et al, 2017). However, a decrease in endothelial barrier permeability was only reported in dynamic cultures coupled to high shear stress (0.7-1 Pa, van Duinen et al, 2017). In the present work, we did not observe significant variations in barrier permeability functions between static and dynamic SK-HEP-1 monocultures (Figure 4.3A and 6.6B). Conversely, the permeability was reduced in dynamic LSEC cocultures (Figure 4.6B), illustrating stronger cell junctions in the presence of HepG2/C3a, and suggesting that there is a synergistic effect of coculturing cells in our conditions. Furthermore, we found that the LSECs produced basal levels of the pro inflammatory cytokines IL6 and TNF without any significant morphology damage. The dynamic coculture also did not play a part in significantly increasing cytokine levels in LSECs. As high levels of production of pro inflammatory cytokines in the liver by LSECs leads to fibrosis (DeLeve et al., 2015), our result illustrated the fact that the basal dynamic cocultures of LSECs were not pro-inflammatory.

Previous works reported an improved hepatocyte phenotype when cocultured with endothelial cells (Gugen Guillouzo et al., 2010; Xiao et al., 2015; Bale et al., 2015; Ortega-Ribera et al., 2018). In the present model, we did not detect any striking benefit of the presence of LSECs on the HepG2/C3a phenotype (no albumin increase, no mRNA gene metabolism upregulation, no clear cytokine over secretion). In fact, the enhanced maturation of hepatocytes was mainly reported on primary hepatocytes that tend to rapidly dedifferentiate (Gugen Guillouzo et al., 2010). It is clear that the hepatocarcinoma HepG2/C3a cell line is probably not an ideal model for liver-on-chip approaches. Although it

has been widely used in works related to cancer and liver disease (Donato et al., 2015), and shown that interactions between the liver endothelium (include SK-HEP-1) and this liver carcinoma were reported in studies investigating liver disorders (Thomann et al., 2020; Lee et al., 2022), it has a weak maturation profile. It is certainly a robust model for proof-of-principle studies, but the present on-chip approach would clearly benefit from being extended and refined using normal human primary hepatocytes.

Regarding liver toxicology, the liver's *in vivo* features, suggest that xenobiotics must first pass the endothelial barrier before accessing the hepatocytes. Analysing kinetics and toxicity of APAP *via* the LSEC barrier and its subsequent metabolism inside the liver compartment was presented as a proof of concept of our technology. APAP toxicity directly on LSEC has already been reported in the literature (Badmann et al., 2012; Holt et al., 2010). The presence of APAP contributed to modifying the expression of LSEC markers in this work. This was illustrated by degradation of the actin and vimentin network, and the reduction of the PECAM-1 and STAB2 expression levels as shown in the immunostaining images. We also confirmed APAP metabolism in the presence of the HepG2/C3a cells. The barrier led to modulation of the concentration of APAP reaching the liver cells and we did not detect any particular sign of HepG2/C3a toxicity in our experiments. Consistently with the literature, the 100 µM concentration of APAP on HepG2 is not a toxic concentration, as most studies reported effects between 1 to 2 mM (Gonzales et al., 2017; Prot et al., 2012; Odeyemi et al., 2019).

The development of *in vitro* liver models that mimic the key elements of the in vivo liver environment is very challenging due to the complexity of liver architecture and physiology. With progress made in tissue engineering, bioprinting and microfluidics, several microfluidic-based *in vitro* liver models that reproduce a physiologically relevant microenvironment have been developed in recent years (Lee et al., 2021; Moradi et al., 2021). Although most of these models are based on hepatocyte monoculture, a growing number of groups are interested in developing microfluidic cocultures of different liver cells, especially hepatocytes and LSECs, to reproduce liver sinusoid and cell-cell interactions (Kang et al., 2015; Prodanov et al., 2016; Ortega-Ribera et al., 2018; Du et al., 2017; Lee et al., 2021; Moradi et al., 2021). In these models, the different cell types are randomly mixed or organized in layers separated by a porous membrane, collagen layer or microstructures (Bale et al., 2015; Lee et al., 2021). The present model combines the advantages of the LSEC barrier and hepatocytes cultured in 3D spheroids thanks to the hyaluronic acid hydroscaffold functionalised with ECM components. A critical issue in microfluidic culture development is the balance between model relevance, complexity and practicality. For liver cell cocultures, all cell types are usually seeded in the same irreversibly sealed microfluidic device/membrane, which makes it

extremely difficult to analyse the different cell types separately (Ma et al., 2018). Our model consists of two separate compartments easily assembled in IIDMP devices: hepatocytes in PDMS biochips and the LSEC barrier in commercially standard inserts. Each cell type can be cultured and characterised separately before being connected to an IIDMP device for coculture. At the end of the experiments, the inserts and biochips can also be easily removed for separate external analyses.

4.8. Conclusion

In conclusion, we present here a new *in vitro* coculture model for LSEC and hepatocytes using two human cell lines. The coculture was performed inside a platform integrating a cell culture insert to build the endothelial barrier, and liver organ-on-chip technology. The platform made dynamic perfusion possible and reproduced cell-to-cell communications. The biological characterisation confirmed that the integrity and functionality of the LSECs were not altered by either the perfusion or the coculture conditions. Furthermore, the model showed lower LSEC permeability that increased the barrier functions. However, we did not detect any particular effects of the LSECs on the HepG2/C3a phenotypes. Finally, we successfully demonstrated APAP modulation on the LSEC phenotype, its transit to the liver compartment and its metabolism, as an example of a liver first pass metabolism. We believe that our model could be used as a relevant model for investigating drug kinetics and subsequent physio pathological hepatotoxicity.

4.9. Supplementary figures

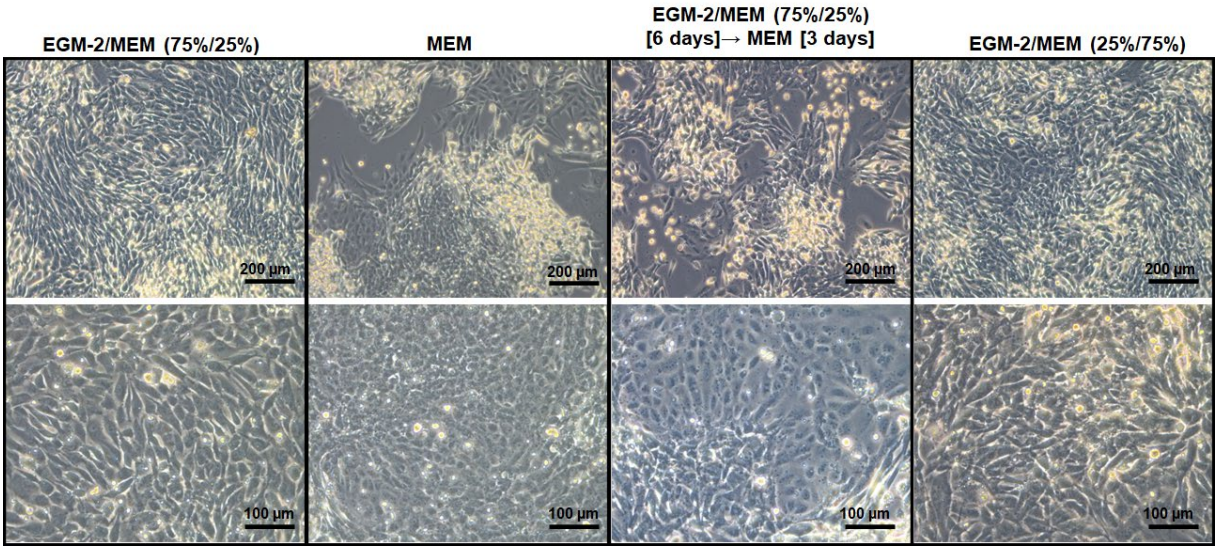

Figure 4.S1. *Morphologies of SK-HEP-1 cells cultured in different culture media mixtures.*

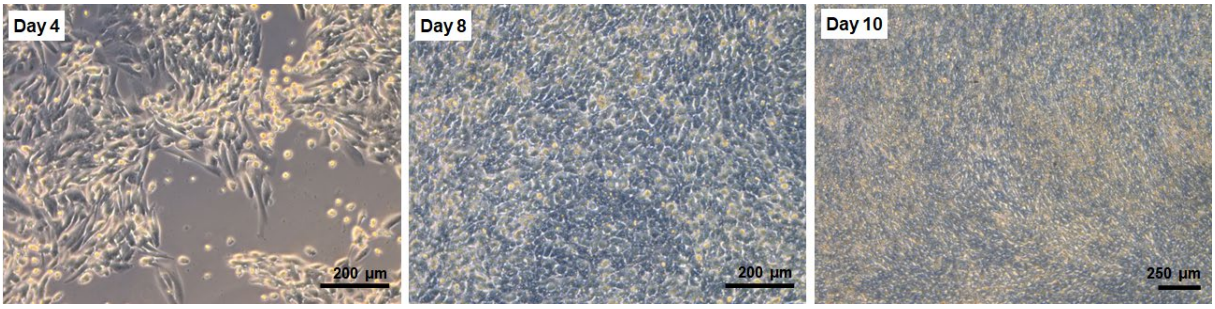

Figure 4.S 2. *Morphologies of SK-HEP-1 cells cultured on static inserts at days 4, 8 and 10.*

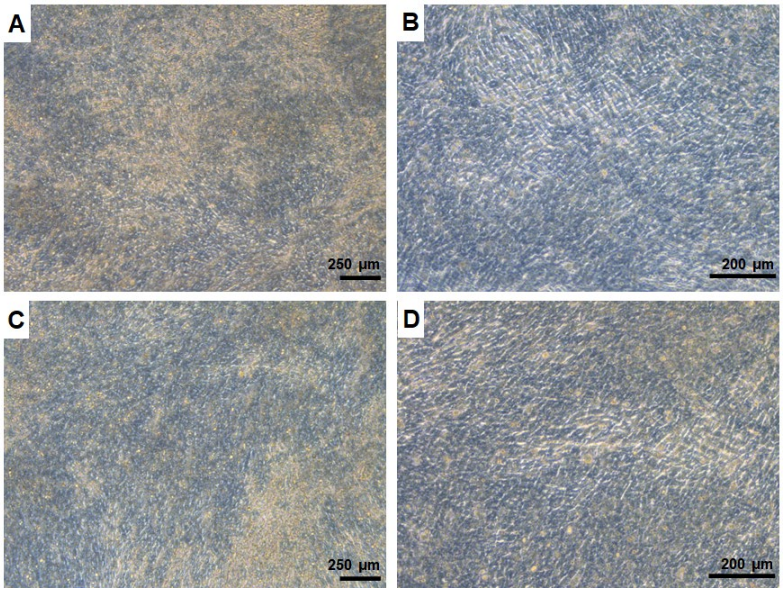

Figure 4.S 3. *Morphologies of SK-HEP-1 cells monoculture and coculture after 10 days of culture (8 days of maturation in static inserts and 2 days of dynamic culture in IIDMP platform).*

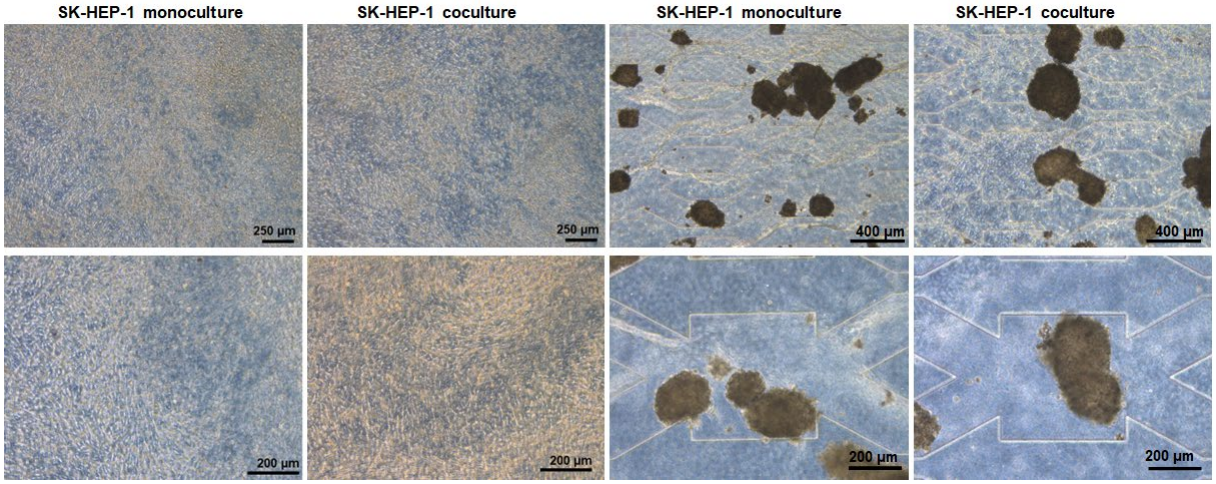

Figure 4.S 4. *Morphologies of SK-HEP-1 and HepG2/C3a cells monoculture and coculture after exposure to APAP for 2 days.*

4.10. References

Akbari E, Spychalski GB, Rangharajan KK, Prakash S, Song JW. Flow dynamics control endothelial permeability in a microfluidic vessel bifurcation model. Lab Chip. 2018, 18, 1084-1093. DOI: 10.1039/c8lc00130h.

Badmann A, Langsch S, Keogh A. TRAIL enhances paracetamol-induced liver sinusoidal endothelial cell death in a Bim- and Bid-dependent manner. Cell Death Dis. 2012, 3, e447. DOI: 10.1038/cddis.2012.185.

Bale SS, Golberg I, Jindal R, McCarty W J, Luitje M, Hegde M, Bhushan A, Usta OB, Yarmush ML. Long-term coculture strategies for primary hepatocytes and liver sinusoidal endothelial cells. Tissue engineering. Part C, Methods 2015, 21, 413-422. DOI: 10.1089/ten.TEC.2014.0152.

Bale SS, Borenstein, JT. Microfluidic Cell Culture Platforms to Capture Hepatic Physiology and Complex Cellular Interactions. Drug Metab. Dispos. 2018, 46, 1638-1646. DOI: 10.1124/dmd.118.083055.

Bale SS, Geerts S, Jindal R, Yarmush ML. Isolation and co-culture of rat parenchymal and non-parenchymal liver cells to evaluate cellular interactions and response. Sci. Rep. 2016, 6, 25329. DOI: 10.1038/srep25329.

Beckwitt CH, Clark AM, Wheeler S, Taylor DL, Stolz DB, Griffith L, Wells A. Liver 'organ on a chip'. Exp. Cell. Res. 2018, 363, 15-25. DOI: 10.1016/j.yexcr.2017.12.023.

Bhatia SN, Balis UJ, Yarmush ML, Toner M. Effect of cell-cell interactions in preservation of cellular phenotype: cocultivation of hepatocytes and nonparenchymal cells. FASEB J. 1999, 13, 1883-900. DOI: 10.1096/fasebj.13.14.1883.

Bhatia SN, Yarmush ML, Toner M. Controlling cell interactions by micropatterning in co-cultures: hepatocytes and 3T3 fibroblasts. J. Biomed. Mater. Res.1997, 34, 189-199. DOI: 10.1002/(SICI)1097-4636(199702)34:2<189::AID-JBM8>3.0.CO;2-M.

Bricks T, Paullier P, Legendre A, Fleury M J, Zeller P, Merlier F, Anton P M, Leclerc E. Development of a new microfluidic platform integrating co-cultures of intestinal and liver cell lines. Toxicol. *in vitro* 2014, 28, 885-895. DOI: 10.1016/j.tiv.2014.02.005.

Bricks T, Hamon J, Fleury MJ, Jellali R, Merlier F, Herpe YE, Seyer A, Regimbeau JM, Bois F, Leclerc E. Investigation of omeprazole and phenacetin first-pass metabolism in humans using a microscale bioreactor and pharmacokinetic models. Biopharm. Drug Dispos. 2015, 36, 275-293. DOI: 10.1002/bdd.1940.

DeLeve LD. Liver sinusoidal endothelial cells in hepatic fibrosis. Hepatology 2015, 61, 1740-1746. DOI: 10.1002/hep.27376.

Donato MT, Tolosa L, Gómez-Lechón MJ. Culture and Functional Characterization of Human Hepatoma HepG2 Cells. Methods Mol. Biol. 2015, 1250, 77-93. DOI: 10.1007/978-1-4939-2074-7_5.

Du Y, Li N, Yang H, Luo C, Gong Y, Tong C, Gao Y, Lü S, Long M. Mimicking liver sinusoidal structures and functions using a 3D-configured microfluidic chip. Lab Chip, 2017, 17, 782-794. DOI: 10.1039/c6lc01374k.

Elvevold K, Smedsrød B, and Martinez I, The liver sinusoidal endothelial cell: a cell type of controversial and confusing identity. Am. J. Physiol. Gastrointest. Liver Physiol. 2008, 294, G391-G400. DOI: 10.1152/ajpgi.00167.2007.

Fang Y, Eglen RM. Three-dimensional cell cultures in drug discovery and development. SLAS Discov. 2017, 22, 456-472. DOI: 10.1177/1087057117696795.

González LT, Minsky NW, Espinosa LEM. *In vitro* assessment of hepatoprotective agents against damage induced by acetaminophen and CCl4. BMC Complement. Altern. Med. 2017, 17, 39. DOI: 10.1186/s12906-016-1506-1.

Guguen-Guillouzo C, Guillouzo A. General review on *in vitro* hepatocyte models and their applications. In: Maurel, P. (eds) Hepatocytes. Methods in Molecular Biology, 2010, vol 640. Humana Press. DOI: 10.1007/978-1-60761-688-7_1.

Jellali R, Bricks T, Jacques S, Fleury MJ, Paullier P, Merlier F, Leclerc E. Long-term human primary hepatocyte cultures in a microfluidic liver biochip show maintenance of mRNA levels and higher drug metabolism compared with Petri cultures. Biopharm. drug dispos. 2016, 37, 264-275. DOI: 10.1002/bdd.2010.

Holt MP, Yin H, Ju C. Exacerbation of acetaminophen-induced disturbances of liver sinusoidal endothelial cells in the absence of Kupffer cells in mice. Toxicol. Lett. 2010, 194, 34-41. DOI: 10.1016/j.toxlet.2010.01.020.

Jellali R, Paullier P, Fleury MJ, Leclerc E. Liver and kidney cells cultures in a new perfluoropolyether biochip. Sens. Actuators B Chem. 2016, 229, 396-407. DOI: 10.1016/j.snb.2016.01.141.

Kang YB, Sodunke TR, Lamontagne J, Cirillo J, Rajiv C, Bouchard, M.J., Noh, M. Liver sinusoid on a chip: Long-term layered co-culture of primary rat hepatocytes and endothelial cells in microfluidic platforms. Biotechnol. Bioeng. 2015, 112, 2571-2582. DOI: 10.1002/bit.25659.

Khetani SR, Berger DR, Ballinger KR, Davidson MD, Lin C, Ware BR. Microengineered liver tissues for drug testing. J. Lab. Autom. 2015, 20, 216-250. DOI: 10.1177/2211068214566939.

Lauschke VM, Shafagh RZ, Hendriks DFG, Ingelman-Sundberg M. 3D primary hepatocyte culture systems for analyses of liver diseases, drug metabolism, and toxicity: Emerging

culture paradigms and applications. Biotechnol. J., 2019, 14: 1800347. DOI: 10.1002/biot.201800347.

LeCluyse L, Witek R P, Andersen ME, Powers MJ. Organotypic liver culture models: meeting current challenges in toxicity testing. Crit Rev Toxicol. 2012, 42, 501-548. DOI: 10.3109/10408444.2012.682115.

Lee SY, Kim D, Lee SH, Sung JH. Microtechnology-based *in vitro* models: Mimicking liver function and pathophysiology. APL bioengineering, 2021, 5, 041505. DOI: 10.1063/5.0061896.

Lee JH, Ho KL, Fan SK. Liver microsystems *in vitro* for drug response. J. Biomed. Sci. 2019, 26, 88. DOI: 10.1186/s12929-019-0575-0.

Lee D, Park JS, Kim D, Hong HS. Substance P hinders bile acid-induced hepatocellular injury by modulating oxidative stress and inflammation. Antioxidants 2022, 11, 920. DOI: 10.3390/antiox11050920.

Livak, KJ, Schmittgen TD. Analysis of relative gene expression data using real-time quantitative PCR and the the 2(-Delta Delta C(T)) method. Methods 2001, 25, 402-408. DOI: 10.1006/meth.2001.1262.

Ma LD, Wang YT, Wang JR, Wu JL, Meng XS, Hu P, Mu X, Liang QL, Luo GA. Design and fabrication of a liver-on-a-chip platform for convenient, highly efficient, and safe in situ perfusion culture of 3D hepatic spheroids. Lab Chip, 2018, 18, 2547-2562. DOI: 10.1039/C8LC00333E.

Merlier F, Jellali R, Leclerc E. Online hepatic rat metabolism by coupling liver biochip and mass spectrometry. Analyst 2017, 142, 3747-3757. DOI : 10.1039/C7AN00973A

Messelmani T, Le Goff A, Souguir Z, Maes V, Roudaut M, Vandenhaute E, Maubon N, Legallais C, Leclerc E, Jellali R. Development of liver-on-chip integrating a hydroscaffold mimicking the liver's extracellular matrix. Bioengineering 2022, 9, 443. DOI: 10.3390/bioengineering9090443.

Messelmani T, Morisseau L, Sakai Y, Legallais C, Le Goff A, Leclerc E, Jellali R. Liver organ-on-chip models for toxicity studies and risk assessment. Lab Chip 2022, 22, 2423-2450. DOI: 10.1039/D2LC00307D

Milner E, Ainsworth M, McDonough M, Stevens B, Buehrer J, Delzell R, Wilson C, Barnhill J. Emerging three-dimensional hepatic models in relation to traditional two-dimensional *in vitro* assays for evaluating drug metabolism and hepatoxicity. Med. Drug Discov. 2020, 8, 100060. DOI: 10.1016/j.medidd.2020.100060

Moradi E, Jalili-Firoozinezhad S, Solati-Hashjin M. Microfluidic organ-on-a-chip models of human liver tissue. Acta biomater. 2020. 116, 67–83. DOI: 10.1016/j.actbio.2020.08.041.

Odeyemi S, Dewar J. Repression of acetaminophen-induced Hhepatotoxicity in HepG2 cells by polyphenolic compounds from Lauridia tetragona (L.f.) R.H. Archer. Molecules. 2019, 24, 2118. DOI: 10.3390/molecules24112118.

Ortega-Ribera M, Fernández-Iglesias A, Illa X, Moya A, Molina V, Maeso-Díaz R, Fondevila C, Peralta C, Bosch J, Villa R, Gracia-Sancho J. Resemblance of the human liver sinusoid in a fluidic device with biomedical and pharmaceutical applications. Biotechnol. Bioeng. 2018, 115, 25852594. DOI: 10.1002/bit.26776.

Panwar A, Das P, Tan LP. 3D hepatic organoid-based advancements in liver tissue engineering. Bioengineering 2021, 8, 185. DOI: 10.3390/bioengineering8110185.

Polidoro M A, Ferrari E, Marzorati S, Lleo A, Rasponi M. Experimental liver models: From cell culture techniques to microfluidic organs-on-chip. Liver Int. 2021, 41, 1744-1761.

Prodanov L, Jindal R, Bale SS, Hegde M, McCarty WJ, Golberg I, Bhushan A, Yarmush ML, Usta OB. Long-term maintenance of a microfluidic 3D human liver sinusoid. Biotechnol. Bioeng. 2016, 113, 241-246. DOI: 10.1002/bit.25700.

Prot JM, Bunescu A, Elena-Hermann B, Aninat C, Choucha Snouber L, Griscom L, Razan F, Bois F, Legallais C, Brochot C, Corlu A, Dumas M-E, Leclerc E, Predictive toxicology using systemic biology and liver microfluidic “on chip” approaches: application to acetaminophen injury. Toxicol. Appl. Pharmacol. 259, 270-280, 2012. DOI: 10.1093/toxsci/kfs230.

Ruoß M, Vosough M, Königsrainer A, Nadalin S; Wagner S, Sajadian S, Huber D, Heydari Z, Ehnert S, Hengstler J G, Nussler A K. Towards improved hepatocyte cultures: Progress and limitations. Food Chem. Toxicol. 2020, 138, 111188. DOI: 10.1016/j.fct.2020.111188.

Schepers A, Li C, Chhabra A, Seney BT, Bhatia S. Engineering a perfusable 3D human liver platform from iPS cells. Lab Chip, 2016, 16, 2644-2653. DOI: 10.1039/c6lc00598e.

Soldatow VY, Lecluyse EL, Griffith LG, Rusyn I. *In vitro* models for liver toxicity testing. Toxicol. Res. 2013, 2, 23-39. DOI: 10.1039/C2TX20051A.

Son YW, Choi HN, Che JH, Kang BC, Yun JW. Advances in selecting appropriate non-rodent species for regulatory toxicology research: Policy, ethical, and experimental considerations. Regul. Toxicol. Pharmacol. 2020, 116, 104757. DOI: 10.1016/j.yrtph.2020.104757.

Souguir Z, Vidal G, Demange E, Louis F. WO Pat., 2016166479A1 2016.

Thomann S, Weiler SME, Marquard S, Rose F, Ball CR, Tóth M, Wei T, Sticht C, Fritzsche S, Roessler S, De La Torre C, Ryschich E, Ermakova O, Mogler C, Kazdal D, Gretz N, Glimm H, Rempel E, Schirmacher P, Breuhahn K. YAP Orchestrates Heterotypic Endothelial Cell Communication via HGF/c-MET Signaling in Liver Tumorigenesis. Cancer Res. 2020, 80, 5502-5514. DOI: 10.1158/0008-5472.CAN-20-0242.

van Duinen V, van den Heuvel A, Trietsch SJ, Lanz HL, van Gils JM, van Zonneveld AJ, Vulto P, Hankemeier T. 96 perfusable blood vessels to study vascular permeability *in vitro*. Sci. Rep. 2017, 7, 18071. DOI: 10.1038/s41598-017-14716-y.

Van Grunsven LA, 3D *in vitro* models of liver fibrosis. Adv. Drug Deliv. Rev. 2017, 121, 133-146. DOI: 10.1016/j.addr.2017.07.004.

Vis MAM, Ito K, Hofmann S, Impact of culture medium on cellular interactions in *in vitro* co-culture systems. Front. Bioeng. Biotechnol. 2020, 8, 911. DOI: 10.3389/fbioe.2020.00911.

Xiao W, Perry G, Komori K, Sakai, Y. New physiologically-relevant liver tissue model based on hierarchically cocultured primary rat hepatocytes with liver endothelial cells. Integr. Biol. 2015, 7, 1412-1422. DOI: 10.1039/c5ib00170f.

Yu F, Deng R, Hao Tong W, Huan L, Chan Way N, IslamBadhan A, Iliescu C, Yu, HA perfusion incubator liver chip for 3D cell culture with application on chronic hepatotoxicity testing. Sci. Rep. 2017, 7, 14528. DOI: 10.1038/s41598-017-13848-5.

Yun C, Kim SH, Jung YS. Current research trends in the application of *in vitro* three-dimensional models of liver cells. Pharmaceutics 2023, 15, 54. DOI : 10.3390/pharmaceutics15010054

Zeller P, Legendre A, Jacques S, Fleury MJ, Gilard F, Tcherkez G, Leclerc, E. Hepatocytes cocultured with Sertoli cells in bioreactor favors Sertoli barrier tightness in rat. J. Appl. Toxicol. 2017, 37, 287-295. DOI: 10.1002/jat.3360

Chapitre 5: Investigation of the metabolomic crosstalk between liver sinusoidal endothelial cells and hepatocytes exposed to paracetamol using organ-on-chip technology

In this section, we used a metabolomic-on-chip approach to study the effect of the different cell culture conditions on the metabolomic profiles. Firstly, we identified the metabolomic signatures of each cell individually. Then we studied the coculture and APAP synergy effect on the metabolic signatures. Finally, we discussed the correlation between the specific metabolomic partterns and the culture conditions. The core of the chapter is literally extracted from our article “Investigation of the metabolomic crosstalks between liver sinusoidal endothelial cells and hepatocytes exposed to paracetamol using organ-on-chip technology”[4]. The article abstract is presented as a summary of the chapter 5. The material and methods are not presented in this chapter, an extended version is described in chapter 2. The supplementary files of the article are provided at the end of this chapter.

[4] **Messelmani T,** Le Goff A, Soncin F, Gilard F, Souguir Z, Maubon N, Garière B, Legallais C, Leclerc E, Jellali R. Investigation of the metabolomic crosstalks between liver sinusoidal endothelial cells and hepatocytes exposed to paracetamol using organ-on-chip technology***, 2023, Submitted to Toxicology***

Abstract

Organ-on-chip technology represents is a *in vitro* approach summarizing human physiology for the study of responses to drug exposure. Organs-on-chip cell cultures have paved new grounds for testing and understand metabolic dose-responses when evaluating pharmaceutical and environmental toxicity. Here, we present a metabolomic investigation of a coculture of liver sinusoidal endothelial cells (LSECs, SK-HEP-1) with hepatocytes (HepG2/C3a) using advanced organ-on-chip technology. To reproduce the physiology of the sinusoidal barrier, LSECs were separated from hepatocytes by a membrane (culture insert integrated organ-on-chip platform). The tissues were exposed to the analgesic drug acetaminophen (APAP) used as a model compound. The differences between the SK-HEP-1, HepG2/C3a monocultures and SK-HEP-1/HepG2/C3a cocultures, treated or not with APAP, were identified from metabolomic profiles using supervised multivariate analysis. The pathway enrichment coupled with metabolite analysis of the corresponding metabolic fingerprints contributed to extracting the specificity of each type of culture and condition. In addition, we analysed the response to APAP's treatmentby mapping the signatures with significant modulation of the biological processes of the SK-HEP-1 APAP, HepG2/C3a APAP and SK-HEP-1/HepG2/C3a APAP conditions. Furthermore, our model shows how the presence of LSEC barrier and APAP first pass can modify the metabolism of the HepG2/C3a. Altogether, this study demonstrates the potential of a "metabolomics-on-a-chip" strategy for pharmaco-metabolomic applications predicting individual response to drugs.

Keywords: organ-on-chip, LSECs, Hepatocytes, coculture, metabolomic, acetaminophen

5.1. Introduction

Toxicological evaluation of a substance is usually achieved through the combined use of several types of experimental models, including *in vitro* cell culture models, *in vivo* animal models, and *in silico* computer simulations which make it possible to predict biochemical interactions between the organism and a chemical substance (Guillouzo, 1998; Bhushan et al., 2016; Caloni et al., 2022). However, animal models display different responses compared to humans and raise ethical issues, while conventional *in vitro* culture are poorly representative of human *in vivo* physiology, metabolism and toxicity (Ruoß et al., 2020).Therefore,the development of novel *in vitro* methodologies, including fast and effective screening tools to predict individual toxicity of chemical compounds, is of prime interest in the context of international regulations, such as the European registration, evaluation, authorization and restriction of chemical substances (REACH) which requires any substance to be evaluated for possible risks to humans, animals, or the environment (Caloni et al., 2022; Rim, 2020; Tsaioun et al., 2016).

Among the advanced *in vitro* methods, organs-on-chip is a technology that has emerged from the combination of microelectronics, tissue engineering and biomaterial sciences (Messelmani et al., 2022a). An organ-on-chip consists in a miniaturized tissue culture system that makes it possible to create and maintain 3D organs on a small scale, as well as engineering dynamic conditions, and which reproduces some of the key *in vivo* features within a well-controlled environment (see example for liver in Messelmani et al., 2022a; Moradi et al 2020; Dalsbecker et al., 2022). In this context, our team has built an organ-on-chip platform for the coculture in 3D of liver tissues with barrier models to investigate organ-to-organ interactions (intestine-liver, Bricks et al., 2014; liver- testis, Zeller et al., 2017), and first pass metabolism of drugs (Bricks et al., 2015). The platform was recently used to investigate the coculture of a liver sinusoidal endothelial cell barrier with hepatocyte biochip. Then, the technology was applied to the acetaminophen passage through the sinusoidal-like barrier and the subsequent metabolism by the hepatic cells (Messelmani et al., 2023).

In parallel to these technological developments, our group propose a “metabolomics-on-a-chip” approach combining organ-on-chip technologies with metabolomic analyses. Metabolomic analyses relate to the untargeted identification of low-molecular weight compounds (metabolites < 1500 Da) present in a biological system and variations in concentrations in response to a pathophysiological perturbation or genetic modifications (Canzler et al., 2020; Dufour-Rainfray et al., 2020; Jellali et al., 2021). Metabolic phenotyping studies can be used as a tool understanding the metabolic modifications after exposure to a substance (Song et al., 2016). Analytical spectroscopic methods, such as NMR spectroscopy

and mass spectrometry (MS), make it possible to detect and quantify metabolites in various samples from biofluids such as serum or urine, as well as cells and tissues (Duarte and Gil 2012; Agin et al., 2016). We previously characterized organ-to-organ communications (such as liver and testis, Zeller et al., 2017, liver-kidney, Shintu et al., 2012) and the effects of several molecules (including drugs, solvents, pesticides) in liver organ-on-chip models populated with HepG2/C3A cells (Shintu et al., 2012), with rat primary hepatocytes (Jelalli et al., 2018) and islets of Langerhans (Essaouiba et al., 2022).

To improve knowledge on the interactions between liver sinusoids and hepatocytes, we suggested characterizing their crosstalk using the metabolomics-on-a-chip approach in our coculture platform using LSECs-HepG2/C3A. Then, we extended the analysis to the tissue crosstalk during an acetaminophen treatment. Acetaminophen was selected as the primary model compound because it is a widely used antipyretic and analgesic treatment which has also been studied extensively. Furthermore, APAP overdose is a well-recognized cause of hepatotoxicity (Shen at al., 2006) and cytotoxicity (Milam and Byard 1985). APAP is essentially metabolized in the liver, and major phase 2 detoxification pathways are sulphate and glucuronic acid conjugations. Acetaminophen is mainly excreted in urine as glucuronide (APAP-G) and sulphate (APAP-S) metabolites in humans and rats. However, a minor phase 1 metabolic pathway leads to the formation of a toxic intermediary, *N*-acetyl-*p*-benzoquinone-imine (NAPQI, Dahlin et al., 1984). This intermediary can cause delayed and irreversible liver lesions (Reid et al., 2005). NAPQI can be retro-converted to the APAP glutathione conjugate (APAP-GSH) through glutathione-S-transferase activity, which can later produce cysteine and *N*-acetylcysteine conjugates (APAP-CYS and APAP-NAC, respectively). APAP metabolism in HepG2/C3A liver on chip, and the APAP overdose metabolomic profile in our liver-on-chip have been characterized previously (Prot et al., 2012).

In the present study we extended this analysis using SK-HEP-1 cells as a LSEC barrier to reproduce a more physiological situation mimicking liver APAP penetration from the sinusoids to the hepatocytes. For this purpose, we firstly investigated the crosstalk between the HepG2/C3a and SK-HEP-1 tissues. Then, we exposed the SK-HEP-1 to APAP to investigate the changes in the metabolome illustrating HepG2/C3A and SK-HEP-1 tissue interactions.

5.2. Morphology and functional characterization of the tissues

The SK-HEP-1 cells were cultured in static inserts until the formation of a confluent and homogenous LSECs barrier (8 days). Then, they were cultured in dynamic conditions for two days, with or without APAP exposure. The SK-HEP-1 morphology at the end of the experiments, in monoculture and coculture (control and exposed to APAP), is presented in

Figure 5.1A. SK-HEP-1 cells were able to form and maintain a confluent and continuous barrier constituted of several cell layers. No obvious differences in morphology were observed between monoculture and coculture samples. Furthermore, APAP did not seem to impact morphology at the tissue level. Actin staining confirmed the development of the microfilament cytoskeleton in all cells across the whole insert surface, and the formation of different cell layers (Figure 5.1B and 5.1C, examples of z-stack performed using confocal microscopy in Figure 5.S1). Finally, SK-HEP-1 monocultures with and without APAP and in coculture without APAP were positive to the LSEC specific marker PECAM-1 (Figure 2B and 2C). Conversely, PECAM-1 signal intensity was strongly reduced in SK-HEP-1 cocultures exposed to APAP (Figure 5.1C).

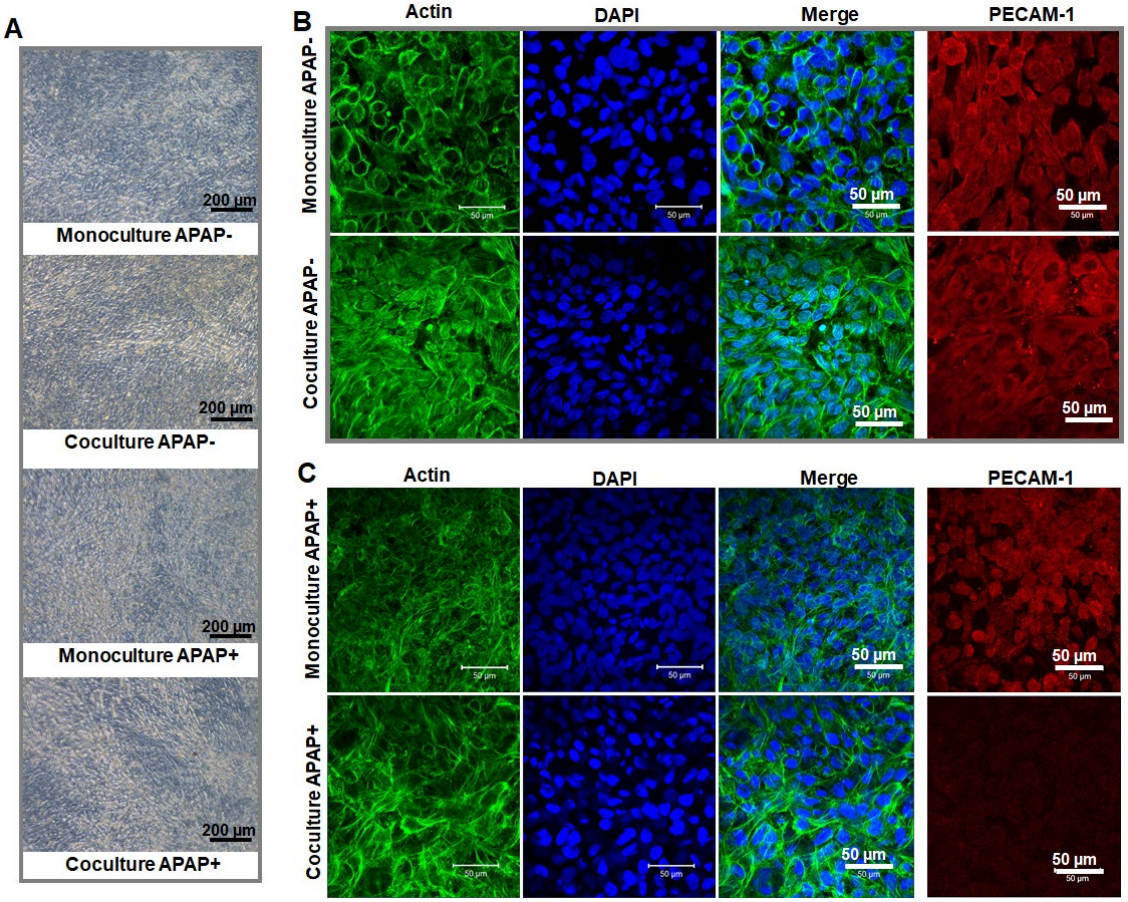

Figure 5.1. *Characterisation of the SK-HEP-1 endothelial barrier in dynamic monoculture and coculture (with and without APAP, 8 days of maturation followed by 2 days in the IIDMP platform). (A) cell morphologies; (B) actin, nuclei (DAPI) and PECAM-1 staining.*

In the biochips, the HepG2/C3a cells attached to the hydroscaffold and aggregated in small clusters of cells after 24 h in static conditions (Figure 5.2A). Then, the biochips were connected to the fluidic platform and monocultured or cocultured with SK-HEP-1 barrier for 48h. As for SK-HEP-1 cells, we did not detect any difference in the HepG2/C3a morphologies at the end of the experiments, when compared to the HepG2/C3a

monocultures, the SK-HEP-1/HepG2/C3A cocultures without or with APAP. After 48 h in dynamic cultures, the cells proliferated and formed large aggregates/spheroids in all culture conditions (Figure 5.2B). Actin formed a complex filament network across all the spheroids, without any significant difference between monocultures and cocultures (with and without APAP, Figure 5.2C). The hepatic functionality of the HepG2/C3a was confirmed by measuring the secretion of albumin. As shown in Table 5.1, the HepG2/C3a monocultures and cocultures treated or not with APAP secreted similar quantities of albumin (secretions ranging between 114 ± 16 and 129 ± 27 ng/h).

Finally, the diffusion of APAP through the SK-HEP-1 barrier and its metabolism by HepG2/C3a metabolism were demonstrated by measuring APAP concentrations in the basolateral circulating culture medium at the end of the experiments (48 h of exposure). The concentrations of APAP measured were 103 ± 7 µM in SK-HEP-1 monocultures, 84 ± 5 µM in the HepG2/C3a monocultures and 87 ± 8 µM in the coculture conditions (Table 1). The difference between the APAP metabolized (compared to an initial APAP concentration of 100 µM) by HepG2/C3a monocultures and SK-HEP-1/HepG2/C3a cocultures was non-significant. The APAP concentration of 103 ± 7 µM, measured in the basal compartment of the SK-HEP-1 monoculture confirmed the full passage of APAP from the apical to basal side through the barrier and that SK-HEP-1 cells did not metabolize APAP.

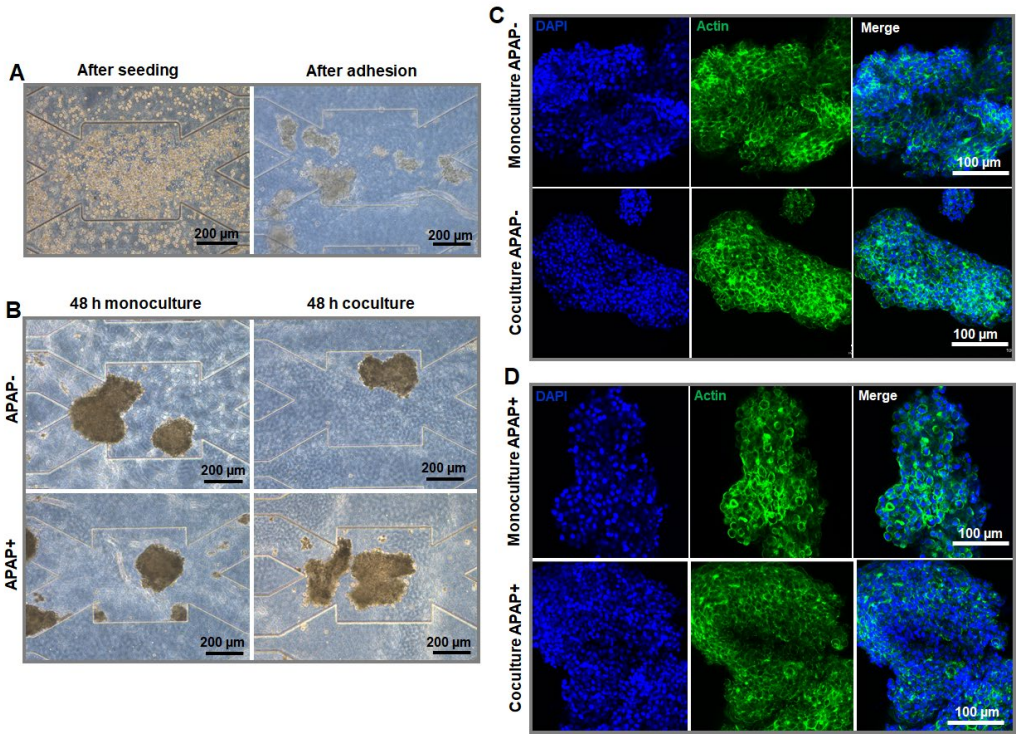

Figure 5.2. *Characterisation of HepG2/C3a cells cultured in the biochip, in monoculture, and coculture (with and without APAP). (A) cell morphology after seeding, 24 h of adhesion in static conditions; (B) cell morphology after 48 h of dynamic culture; (C) and (D)* actin and nuclei (DAPI) staining after 48 h of dynamic coculture.

Table 5.1. *Albumin secretion in the IIDMP and paracetamol concentration in the basal compartment of the IIDMP.*

	Albumin secretion (ng/h)	Basal APAP concentration (µM)
LSEC monoculture without APAP	---	---
HepG2/C3A monoculture without APAP	114.2 ± 16.6	---
LSEC_HepG2/C3A coculture without APAP	129.7 ± 27.6	---
LSEC monoculture with APAP	---	107 ± 4
HepG2/C3A monoculture with APAP	113.4 ± 5.9	84 ± 5
LSEC_HepG2/C3A coculture with APAP	127.6 ± 21.7	88 ± 12

5.3. Identification of the HepG2/C3a, SK-HEP-1 and SK-HEP-1/HepG2/C3a specific metabolomic signatures

At the end of the experiments, the supernatants from the different culture conditions were collected and analysed with gas chromatography coupled to mass spectrometry (GC-MS). The analysis led to the identification of 94 metabolites (Table 5.S1, supplementary file 1). To identify the metabolomic signature of each culture mode without APAP exposure, we performed a multivariate analysis using the metabolomes of SK-HEP-1 monoculture, HepG2/C3a monoculture, SK-HEP-1/HepG2/C3a coculture and basal culture medium. The PLS-DA score plots showed a clear separation between the three culture modes and basal medium, indicating distinct metabolic profiles (Figure 5.3A). The distance between HepG2/C3a monoculture and coculture groups was weak due to the closer metabolic profiles of these modes compared to the others. The PLS-DA analysis (VIP > 1.0) coupled to the ANOVA test (*P* value < 0.05) identified 58 metabolites. The heatmap of the top 40 significant metabolites is given in Figure 5.3B. The detailed heatmap with the 58 metabolites is presented in Figure 5.S2 and the full list of the 58 metabolites with the corresponding P value in Table 5.S2 (supplementary file 1).

The specific signature of the HepG2/C3A monoculture was characterized by the high production of urea, ornithine, glycine, iminodiacetic acid and glycerol-1-phosphate, and the high consumption of glycerol and pantothenic acid. The HepG2/C3A cells displayed moderate lipid synthesis including caprylic, capric, hexanoic, oleic and palmitoleic acids, when compared to SK-HEP-1 and the cocultures. There was also a weak production of the pentose phosphate metabolites (ribose, arabinose) and a moderate consumption of glucose, fructose, allose and pyruvic acid, coupled to moderate lactate production, when compared to other conditions.

The SK-HEP-1 monoculture produced the highest levels of palmitoleic acid, oleic acid, ribose, arabinose, galactitol, hypoxanthine and 2,3 butanediol. Overall, the SK-HEP-1 cells were characterized by high lipid synthesis (oleic, palmitoleic, capric, caprylic, and hexanoic acids), an active pentose phosphate pathway (high ribose and arabinose secretion) and intense polyol metabolism highlighted by the high consumption of mannitol, xylitol, sorbitol, and threitol, when compared to HepG2/C3a monocultures. The LSECs cultures metabolome revealed high consumption of glucose, tagatose, and fructose, associated with lactic acid production, suggesting an intense glycolysis activity compared to HepG2/C3a monoculture. Finally, there was production of TCA cycle intermediates: succinic, alpha ketoglutaric, malic, and citric acids, in comparison with the basal medium.

The SK-HEP-1/HepG2/C3a coculture presented a signature in synergy with the HepG2/C3a and SK-HEP-1 monocultures. The HepG2/C3A monocultures and the cocultures presented a common signature, including high levels of alanine, 2-ketoisocaproic acid, benzoic acid, glycerol 1 phosphate, and glutamic acid, and low levels of pantothenic acid, succinic acid, and glycerol. The common metabolites highlighted by SK-HEP-1 monocultures and SK-HEP-1/HepG2/C3a cocultures included high levels (production) of oleic acid, palmitoleic acid, lactic acid, ribose, arabinose, and asparagine, and low levels (consumption) of myo-inositol, citraconic acid, carbohydrates (mannitol, allose, fructose, glucose, sorbitol, threitol, and xylitol), threonine, serine, ethanolamine and beta-alanine.

Finally, all three culture conditions (SK-HEP-1 monocultures, HepG2/C3a monocultures and cocultures) presented several common signatures, such as the production of capric acid, hexanoic acid, caprylic acid, lactic acid, alpha ketoglutaric acid, malic acid, ornithine, and 3-methyl-2-oxobutaric acid. In parallel, high consumption of amino acids (isoleucine, methionine, threonine, glutamine, citrulline and phenylalanine), pyridoxine, glucose-6 phosphate, and 4-hydroxyproline was observed.

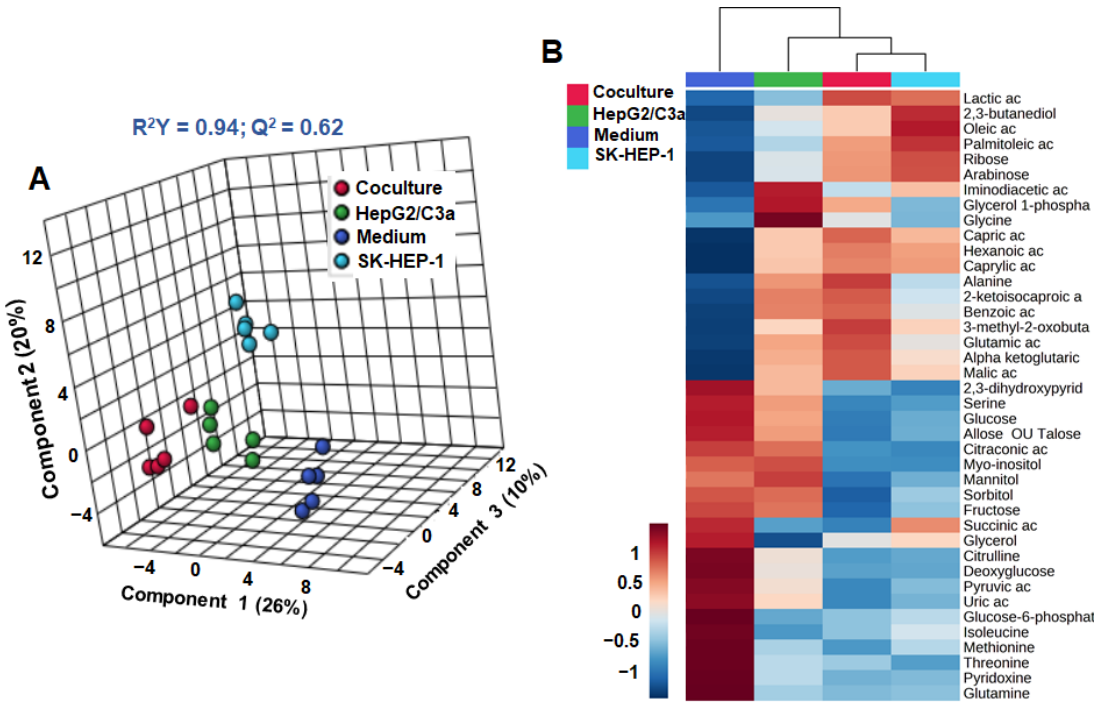

Figure 5.3. *Global multivariate statistical analysis of SK-HEP-1 monoculture, HepG2/C3a monoculture, SK-HEP-1/HepG2/C3a coculture and basal medium metabolomic profiles. (A) PLS-DA scores plot discriminating different culture modes; (B) heatmap of the top 40 metabolites significantly modulated.*

5.4. Effect of APAP on the HepG2/C3a monoculture

To identify potential biomarkers and the effects of APAP exposure on HepG2/C3a monocultures, a supervised OPLS-DA analysis was applied to the metabolomes of HepG2/C3a control and APAP-treated HepG2/C3a. As shown in the OPLS-DA score plot (Figure 5.4A), the analysis played a part in clearly identifying cultures treated or not with APAP, indicating significant differences between the two metabolomes. To extract the biomarkers, a volcano plot was drawn using the P value (-log10P) and fold change (log2FC). The volcano plot revealed 13 metabolites modulated by APAP exposure ($P < 0.05$): 2 downregulated ($FC < 0.8$) and 11 upregulated ($FC > 1.2$; Figure 5.4B and 5.4C). When considering the P value < 0.1, 26 metabolites were significantly modulated (heatmap in Figure 5.S3).

The effect of APAP on HepG2/C3a cultures was characterized by the specific over production of glycolic acid, myristic acid, heptadecanoic acid, ribose, arabinose, hypoxanthine, tyrosine, leucine, cystine, pyroglutamic acid, proline and glycerol-1-phosphate, when compared to the HepG2/C3a control. APAP increased the consumption of mannitol and beta-alanine, and reduced the production of sucrose, galactitol and glycine. Finally,stearic acid, palmitic acid, valine levels, and pyruvic acid were higher in cultures exposed to APAP when compared to the control, indicating a lower consumption or a change

in the production/consumption balance. The pathway enrichment analysis with the metabolites discriminating HepG2/C3a control and HepG2/C3a exposed to APAP highlighted the ammonia recycling, glycerolipid metabolism, galactose metabolism, glutathione metabolism, and glycolysis (Figure 5.4D).

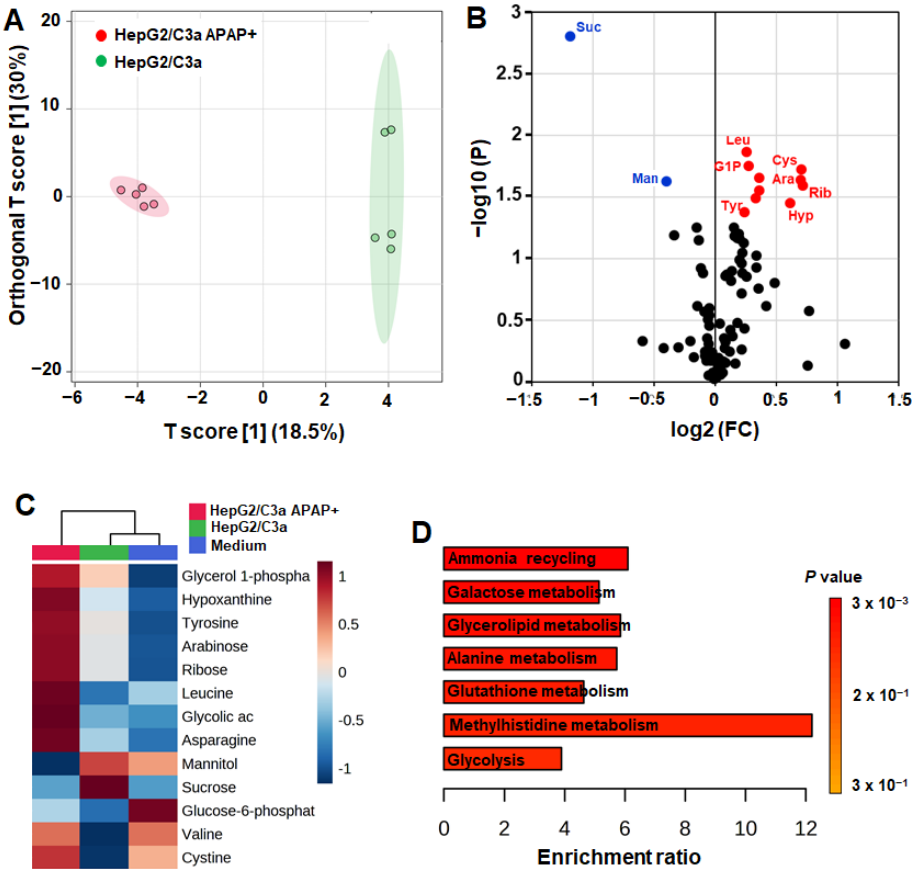

Figure 5.4. Comparison of metabolomic profiles of HepG2/C3a cultured in biochip, with and without APAP treatment. (A) OPLS-DA score plot of biochip control culture compared to biochip treated with APAP (B) volcano plot (log2 fold change (treated biochip/control biochip) plotted against −log10 P-value) highlighting metabolites differentially expressed between HepG2/C3a control and HepG2/C3a treated with APAP (metabolites upregulated and downregulated in the treated cultures are labelled in red and blue, respectively); (C) heatmap of the 13 metabolites significantly modulated (P < 0.05); (D) pathway impact enrichment based on metabolites discriminating HepG2/C3a control and HepG2/C3a treated with APAP.

5.5. Effect of APAP on the SK-HEP-1 monoculture

The OPLS-DA analysis performed with the SK-HEP-1 control and APAP exposed SK-HEP-1 samples successfully separated both groups with a high quality of fit and predictability (R^2 = 0.84, Q^2 = 0.74; Figure 5.5A). The volcano plot construction made it possible to extract 26 metabolites (P value < 0.05 and VIP > 1) significantly modulated in SK-HEP-1 exposed to APAP: 4 downregulated FC < 0.8 and 22 upregulated FC > 1.2 (Figure 5.5B, 5.5C). The heatmap of 38 metabolites with P value < 0.1 and the full statistical analysis (including P value, FC and VIP scores) are presented in Figure 5.S4.

The VIP plot in Figure 5.5C and the heatmap in Figure 5.S3 show that the APAP treatment reduced the consumption of citrulline, fructose, xylitol, tagatose, and pyruvic acid, and the production of hexanoic acid and galactitol. In parallel, compared to SK-HEP-1 control cultures, APAP treatment increased the production of asparagine, leucine, creatinine, ornithine, proline, valine, cysteine, glycolic acid, lipids, and fatty acids (benzoic acid, glycerol, glycerol-1-phosphate, myristic acid, palmitic acid, and lauric acid), TCA cycle substrate (fumaric acid), xanthine, hypoxanthine and uric acid (purine metabolism). Finally, the pentose carbohydrate (arabinose and ribose), hippuric acid, pyroglutamic acid, and glutamic acid secretions also increased in SK-HEP-1 exposed to APAP when compared to the SK-HEP-1 control. The pathway enrichment analysis using the metabolites differentially expressed between SK-HEP-1 cultures with and without APAP revealed that urea cycle, aspartate metabolism, glycine, and serine metabolism, ammonia recycling and amino sugar metabolism were the top 5 enriched pathways. Of the top 10 pathways, we also found fatty acid biosynthesis, glutathione metabolism, and glycerolipid metabolism (Figure 5.5D).

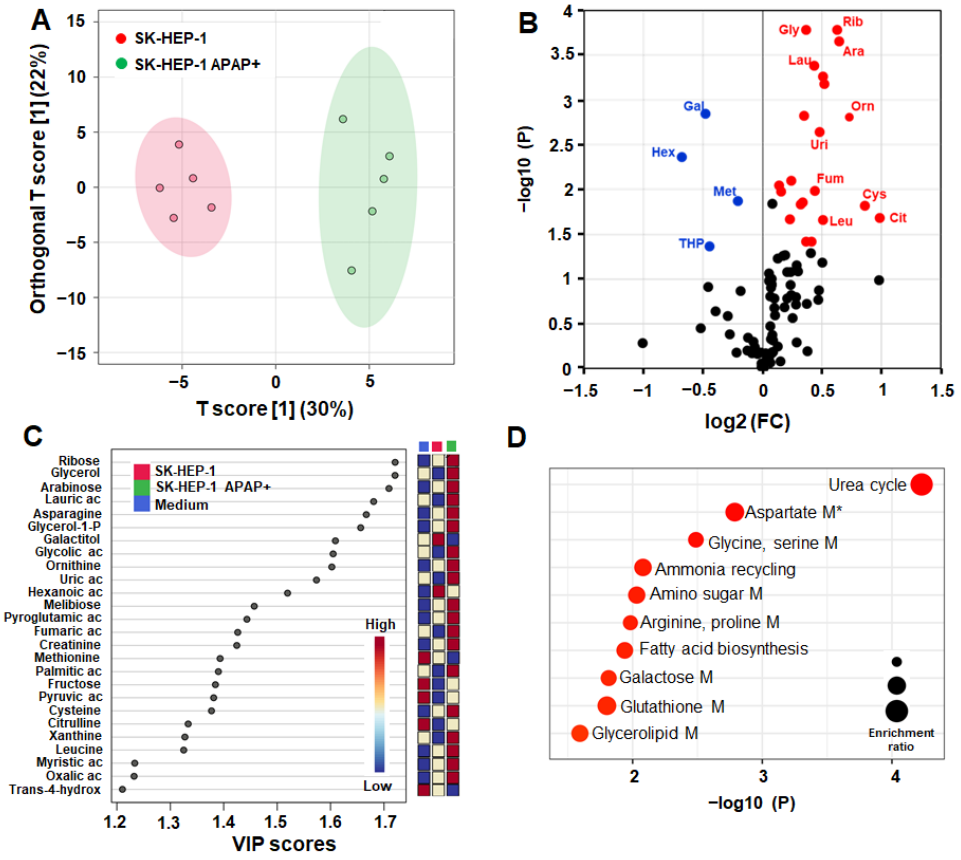

Figure 5.5.*Comparison of metabolomic profiles of SK-HEP-1 barrier culture, with and without APAP treatment. (A) OPLS-DA score plot of SK-HEP-1 control culture compared to SK-HEP-1 treated with APAP (B) volcano plot (log2 fold change (treated culture/control culture) plotted against −log10 P-value) highlighting metabolites significantly modulated between SK-HEP-1 control and SK-HEP-1 treated with APAP (metabolites upregulated and downregulated in the treated cultures are labelled in red and blue, respectively); (C) 26 metabolites discriminating both cultures based on VIP scores (variable importance in projection) from OPLS-DA and corresponding detection intensity; (D) Pathway impact enrichment extracted from comparison of SK-HEP-1 culture with and without APAP (* metabolism).*

5.6. Effect of APAP on the SK-HEP-1/HepG2/C3a cocultures

Metabolomic profiling was also performed on the SK-HEP-1 barrier cocultured with the HepG2/C3a biochip and exposed to APAP. Figures 5.6A shows the OPLS-DA score plot from multivariate analysis performed with the metabolome of control and APAP treated coculture. Clearly, the OPLS-DA score plot shows significant separation of the two groups in distinct clusters (R^2 = 0.82, Q^2 = 0.7). In total, 27 metabolites were modulated by APAP treatment (P < 0.05), with 6 and 21 metabolites downregulated (FC < 0.8) and upregulated (FC > 1.2), respectively (volcano plot and heatmap in Figure 5.6B and 5.6C). The extension of the analysis to P value < 0.1 highlighted 38 metabolites differentially expressed between coculture control and exposed to APAP. The correspondent heatmap and the full statistical analysis are provided in Figure 5.S5.

The coculture exposed to APAP exhibited notable high production levels of oxalic acid, proline, ornithine, glutamic acid, TCA cycle intermediates (fumaric acid, citric acid and malic acid), alpha ketoglutaric acid, asparagine, threonic acid, urea, cysteine, leucine, and glycerol-1 phosphate. Compared to the control coculture, APAP exposure increased the consumption of phenylalanine, methionine, and cystine. Conversely, the consumption of valine, citrulline, and mannitol was reduced by APAP treatment. Finally, APAP contributed to the reduction of hexanoic acid. The pathway enrichment analysis highlighted the urea cycle, arginine and proline metabolism, Warburg effect, citric acid cycle, and gluconeogenesis among the top enriched pathways (P value < 0.05, Figure 5.6D).

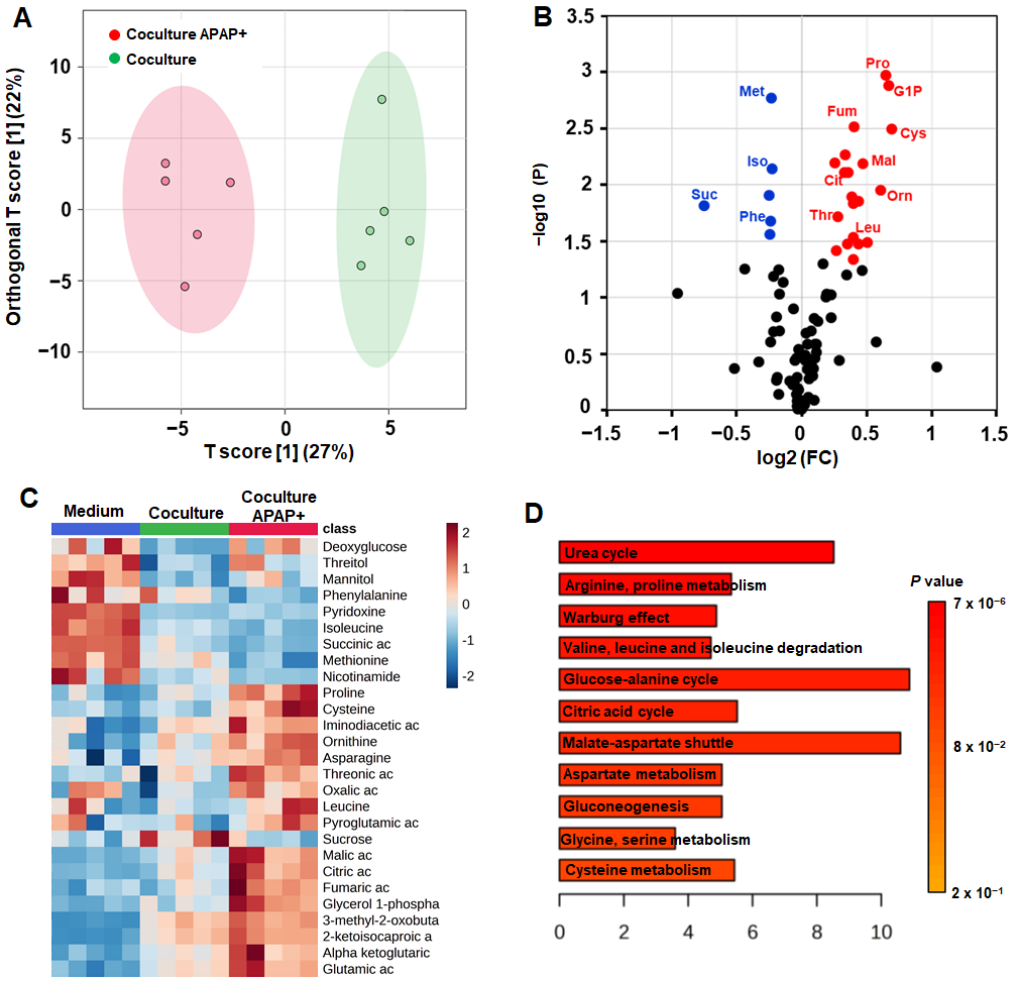

Figure 5.6. *Comparison of metabolomes of HepG2/C3a/SK-HEP-1 coculture, with and without APAP treatment. (A) OPLS-DA score plot discriminating both culture conditions; (B) volcano plot (log2 fold change (APAP/control) plotted against −log10 P-value) discriminating metabolites differentially expressed between coculture control and coculture exposed to APAP (metabolites upregulated and downregulated in the treated cocultures are labelled in red and blue, respectively); (C) heatmap of the 27 metabolites significantly modulated (P < 0.05); (D) pathway impact enrichment based on 27 metabolites modulated between coculture with and without APAP.*

5.7. Common and specific biomarkers of three cultures exposed to APAP

To elucidate the common and specific signatures of each culture condition after APAP treatment, a Venn diagram was designed using the biomarkers of three cultures conditions: SK-HEP-1 monoculture, HepG2/C3a monoculture and SK-HEP-1/HepG2/C3a coculture. As shown in Figure 5.7 and Table 5.S3, eight, three biomarkers were common to SK-HEP-1 and HepG2/C3a monocultures, ten to the coculture and HepG2/C3a monocultures, coculture and SK-HEP-1 monocultures, and the seven to the three conditions. After exposure to APAP, the three culture conditions presented a common signature including high production of pyroglutamic acid, asparagine, glycerol 1-phosphate, leucine, and valine. Among the metabolites common to the SK-HEP-1 monoculture and coculture exposed to APAP, we found increased secretion of fumaric acid, glutamic acid, ornithine, and cysteine, and consumption of methionine, whereas hexanoic acid production and pantothenic acid

consumption decreased. Finally, the common metabolites highlighted by the SK-HEP-1 and HepG2/C3a monocultures treated with APAP included higher production of glycolic acid, myristic acid, arabinose, ribose when compared to monoculture without APAP. In parallel, a change in the production/consumption balance of palmitic acid and glycerol was observed.

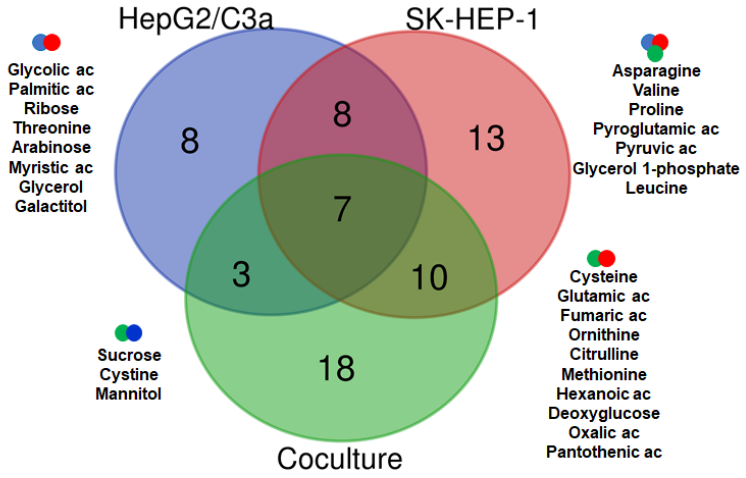

Figure 5.7. *Venn diagram showing the specific and common signature between the different culture conditions.*

5.8. Discussion

In this study, metabolomic profiling was used to investigate the effect of APAP on LSEC-hepatocyte coculture, and the crosstalk between the two cell types. Organ-on-chip technology coupled to the use of a hydroscaffold mimicking the liver ECM made it possible to culture hepatocytes (HepG2/C3a) in a complex 3D dynamic configuration. To mimic the physiology of the liver sinusoid, the HepG2/C3a biochip was cocultured with a LSEC barrier (the SK-HEP-1 cell line cultured on a membrane insert). The LSEC-hepatocyte paracrine-like communication was made possible by exchanges through the insert membrane and the dynamic culture in a microfluidic platform. Characterizing the coculture confirmed that both cell types maintained their typical morphologies and functionalities. We also demonstrated APAP transit through the LSEC barrier to the liver compartment and its metabolization by HepG2/C3a cells. The metabolomic analyses contributed to extracting a common signature and specific patterns in culture conditions tested.

5.8.1. Identification of the specific metabolic signatures from mono to cocultures

The metabolomic analyses revealed a synergy in metabolic profiles between the cell types when they are cultured together. First, comparing the culture medium of the SK-HEP-1 monocultures, HepG2/C3a monocultures, SK-HEP-1/HepG2/C3a cocultures and basal culture medium illustrated clear differences between the culture conditions. The SK-HEP-1 monocultures were characterized by cellular activity in the polyol pathway, in the pentose phosphate pathway, intense glycolysis and TCA activation, and an intense lipids synthesis.

In comparison, in the HepG2/C3a monoculture, we found no specific activation of polyol pathway, moderate activation of the pentose phosphate pathway (PPP), and glycolysis, and consistently of the TCA. We also found moderate lipid synthesis. HepG2/C3a were characterized by a high glycerol metabolism. Interestingly, the coculture included a synergy of both SK-HEP-1 and HepG2/C3a metabolism. As such, in cocultures, we found activation of the polyol pathway, pentose phosphate pathway, and intense glycolysis activation coupled with TCA activation, similar to the SK-HEP-1 monocultures. We also detected significant lipid synthesis.

Then, consistently with HepG2/C3a monocultures, the coculture signature included intense glycerol metabolism, and alanine, benzoic acid, 2-ketoisocaproic acid and glutamic acid productions when compared to SK-HEP-1. Interestingly, 2-ketoisocaproic acid (a degradation of leucine) is associated with production of diacyglycerol in hepatocytes (Yagasaki et al., 2002), which appeared consistent with the glycerol metabolism in our data. In parallel, benzoic acid metabolism is reported to reflect the mitochondrial functions in rat hepatocytes (Krahenbul et al., 1997), which may reflect oxidative phosphorylation in the HepG2/C3a cells.

5.8.2. Identification of APAP metabolic perturbation in HepG2/C3a

In our previous work using a HepG2/C3a liver-on-chip, we identified a toxic metabolomic signature of APAP after exposure at 1 mM for 96 h which was associated with cell death. Among the metabolites, this toxic signature was characterized by the production of pyroglutamic acid, 2-hydroxybutyric acid, 3-hydroxybutyric acid, serine, proline, alanine, and lactate (Prot et al., 2012). The kinetics analysis of the exposure of 1 mM of APAP for 24h to 144 h in a HepG2/C3a liver-on-chip was associated with the induction of reactive oxygen species (ROS) at 72h of exposure (Leclerc et al., 2015). This ROS expression was correlated with extensive GSH depletion after 48h of culture, reduction of cell proliferation after 72h of exposure, and with cell toxicity after 96h of exposure, especially above 0.5 mM (Leclerc et al., 2015).

The present exposures were performed at 1 mM in the LSEC insert, resulting a systemic APAP concentration of 100 µM (HepG2/C3a exposure for 48h). The condition used here did not lead to specific cell death, nor to HepG2/C3a inflammation, consistently with our previous work (no IL-6 nor TNFα secretion, Messelmani et al., 2023). Furthermore, in the present metabolomic signature, we did not detect the element of the metabolites associated with HepG2/C3a cell death in biochips (Choucha Snouber et al., 2013; Prot et al. 2012), nor typical APAP toxicity biomarkers such as 5-oxoproline/pyroglutamic acid, a typical drug-induced liver injury biomarker (Lu 1999; Yang et al., 2012; Lord and Bralley, 2008), hippurate (Schnackenberg et al., 2017) and ROS biomarkers (Gall et al. 2010). Nevertheless, the present APAP-treated HepG2/C3a signature was characterized by high levels of glycolic acid. This compound is a natural antioxidant molecule that reduces reactive oxygen species-induced cell death (Diez et al., 2021). Detecting this compound may reflect an early response to the APAP stress.

In the present experiments, we detected changes in carbohydrate homeostasis and a glycolytic switch, as we detected activation of the pentose phosphate pathway (accumulation of ribose and arabinose, low production of sucrose, and consumption of mannitol). As APAP disrupts mitochondrial functions and oxidative phosphorylation (Jaeschke et al., 2019), APAP poisoning leads to disrupted aerobic respiration (Shah et al, 2011). In parallel, we also detected a weak lipid accumulation with the overproduction of myristic, stearic, and palmitic acid (Supplementary file 2). Consistently with our observation, APAP was reported to reduce fatty acid β-oxidation due to the suppression of the PPAR activation (Chen et al., 2009). APAP was also reported to perturbate mitochondrial fatty acid β-oxidation leading to steatosis (Fromently, 2019). Overall, we observed the onset of the effects of APAP illustrated by the hallmarks of early but weak hepatotoxicity (respiration switch, lipid perturbation), however the signature did not present either cell death markers or strong inflammation propagation. Furthermore, one natural molecule involved in the cell defense mechanism was detected.

5.8.3. Identification of APAP metabolic perturbation in SK-HEP-1 monocultures

APAP was reported to induce LSEC death *via* the TRAIL (TNFα) pathway (Badmann et al., 2012). It was also reported that TRAIL apoptosis alters lipid mitochondrial homeostasis, including the phosphocholine and diacylglycerol (DAG) balance, leading to caspase 8 activation (Ferry et al., 2005). In our study, APAP did not lead to significant TNFα release in LSEC monocultures (Messelmani et al., 2023), but it contributed to increasing the glycerol and glycerol-1-phosphate that are metabolites involved in DAG production. We also detected

high lipid production, illustrated by the high levels of palmitic, lauric, myristic, and hexanoic acids. Interestingly, it was reported that lipids promoted LSEC survival, proliferation, and the maintenance of the differentiation in rat *in vitro* cell cultures (Hang et al., 2012). However, high levels of palmitic acid supplementation played a part in damaging LSEC fenestration and modifying molecule clearance (Cogger et al. 2016). Furthermore, the excess of palmitic acid is widely reported in the literature as a source of cell death, including in LSECs (Geng et al., 2020). Although we detected the production of pyroglutamic acid (a ROS production biomarker), we did not detect such cell death in our experiments and additional assays are required to address this point.

SK-HEP-1 treatment with APAP increased the accumulation of ornithine, creatinine, citrulline, glutamine and glutamic acid in the medium. Arginine is synthetized using glutamic acid as a substrate (Li et al., 2022). Then, arginase is a key enzyme degrading arginine to ornithine and urea (Li et al., 2022). However, under nitric oxide synthetase (NOS), arginine can also be degraded into citrulline and nitric oxide (NO). Urea is excreted as the final product, whereas ornithine is recycled for polyamine synthesis (Li et al., 2022). Therefore, we observed potential arginine metabolism modulation in our LSEC cultures when treated with APAP. Although NO is very important in LSEC function (Xie et al., 2012; Wang and Peng 2021), an over production of NO (due to NOS) leads to LSEC toxicity and even liver disorders (Iwakiri and Kim 2015; Wang and Peng 2021). Interestingly, the increases in fatty acid and TNF activation are reported to increase NO activity and then cell stress in liver (Stanimirovic et al., 2015).

Finally, the APAP signature modified carbohydrate metabolism and the TCA cycle in SK-HEP-1 monocultures. We observed repression of the glycolysis pathway *via* weaker pyruvate and fructose consumptions, and an accumulation of arabinose and melibiose. Furthermore, the pentose phosphate pathway (PPP) appeared active, as shown by the production of ribose and arabinose, illustrating a glycolysis switch. The switch was concomitant with the accumulation of the TCA substrate, fumaric acid. Although excess arabinose is reported to open tight-junctions in endothelial brain cells (Dorovini-Zis et al., 1984), it has also been reported as repairing tight-junction proteins in the brain and providing protection against inflammatory cytokine-induced endothelial permeability by down regulating NF-κB signals (Li et al., 2021). Furthermore, low levels of glycolysis in LSECs were associated with the inflammation process (IL-6 stimulated inflammation, Dudek et al., 2022). PPP activation with a glycolysis switch was reported in neutrophils as a defence mechanism to suppress oxidative burst (Britt et al., 2022). In parallel, as in the HepG2/C3a monoculture, SK-HEP-1 produced glycolic acid, an antioxidant reducing ROS-induced cell death (Diez et al., 2021). Interestingly, we detected the secretion of pyroglutamic acid, hippuric acid (P value = 0.08

and FC = 1.2) and 2-hydroxybutyric acid (P value = 0.13 and FC = 1.4), that could reinforce the biomarker signatures related to ROS responses. Such markers are the hallmarks of an oxidative stress, consistent with glutathione pathway enrichment. Overall, the signature illustrated disturbance by APAP of the lipids and arginine cell metabolism coupled with only a weak oxidative stress response, triggering a concomitant anti-inflammatory response by the LSECs to APAP (ie: glycolysis switch and natural anti-oxidant secretion).

5.8.4. Identification of the APAP metabolic perturbation in synergy with SK-HEP-1 and HepG2/C3a cocultures

The metabolomic profile of cocultures treated with APAP presented a signature similar to the SK-HEP-1 APAP+. One of the common signatures was the perturbation innitrogen metabolism, illustrated by the increase in ornithine and glutamic acid secretions. We also observed oxalic acid production, similar to the LSECs APAP+ condition. The GSH and inflammation marker pyroglutamic acid was particularly over expressed in the APAP coculture and similar to SK-HEP-1 monocultures. In fact, APAP was “physiologically” loaded into the SK-HEP1 compartment in the coculture and then transferred to the hepatic compartment through the endothelial barrier, it was expected that we find similarities in the signatures of the LSEC APAP+ and coculture APAP+ conditions. The specific metabolomic signature of the coculture consisted of the production of intermediate TCA (citric, malic, alpha ketoglutaric and fumaric acids). This could reflect either an APAP detoxification process by the liver cells, or an early stage of mitochondrial perturbation either by the NAPQI in HepG2/C3a (Moreno Torres et al., 2022; Chen et al., 2021; Cuykx et al., 2018) or by a stronger toxicity in the LSECs in response to the accumulation of pro-inflammatory cytokines (due to liver cell activity in the presence of APAP) in the medium. The toxicity synergy on LSECs is illustrated by the deterioration in PECAM-1 expression. Further investigations are required to follow up this observation, such as cytokine assays and transcriptomic profiling.

5.9. Conclusions

In summary, we used organ-on-chip technology to investigate liver tissue crosstalk. Our *in vitro* model was based on an apical SK-HEP-1 insert culture coupled with basal 3D biochips in HepG2/C3a cultures, simulating the sinusoid by separating LSECs and hepatocytes. We investigated the modifications in the metabolome of SK-HEP-1, and HepG2/C3a monocultures, and SK-HEP-1/HepG2/C3a cocultures, in a control and in APAP-treated conditions. At the selected concentration, APAP did not present significant hepatoxicity with regard to HepG2/C3a cells. In SK-HEP-1, we detected metabolic switches concomitantly with the apparition of an anti-oxidant marker, but mild levels of ROS biomarkers. The main

characteristics of the LSEC APAP+ signature presented significant similarities with those of the SK-HEP-1/HepG2/C3a APAP+ cocultures. These results make it possible to confirm the specificity of each type of cells in the overall APAP coculture signature. They also play a part in showing the benefits of such an approach for refining knowledge of liver tissues and cultures when exposed to drugs. We believe that the combination of a microfluidic coculture, 3D organization and metabolomic profiling could be a promising tool for chemical risk assessment.

5.10. Supplementary figures

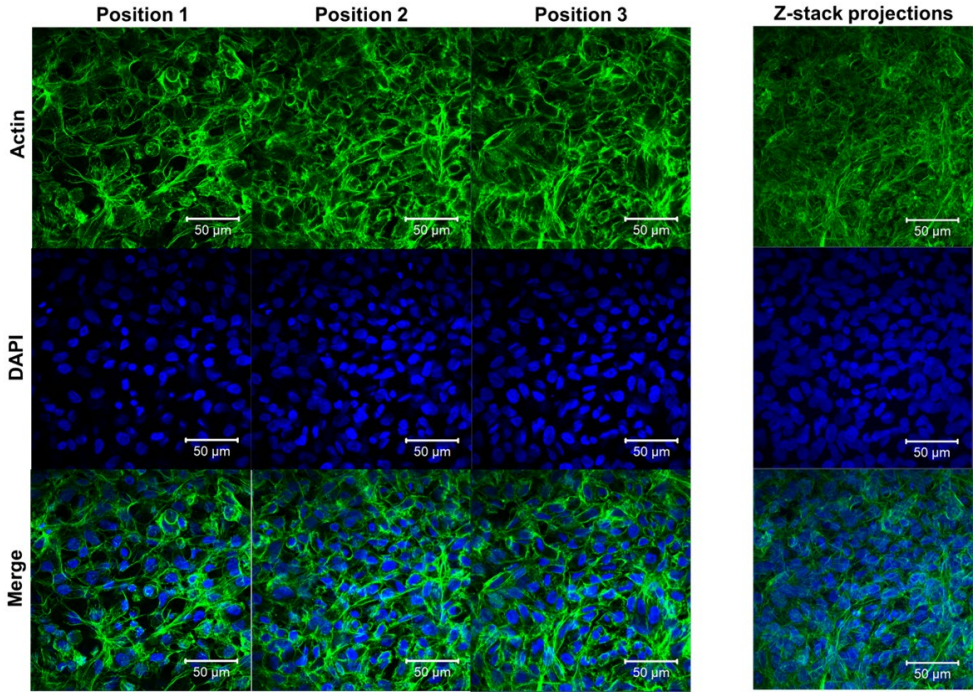

Figure 5.S1. *F-actin (green) and nuclei (blue) stainings of SK-HEP-1 monocultures after 10 days of culture (8 days of maturation in static inserts and 2 days of dynamic culture in IIDMP platform). The images correspond to different Z positions and the z-stack projections.*

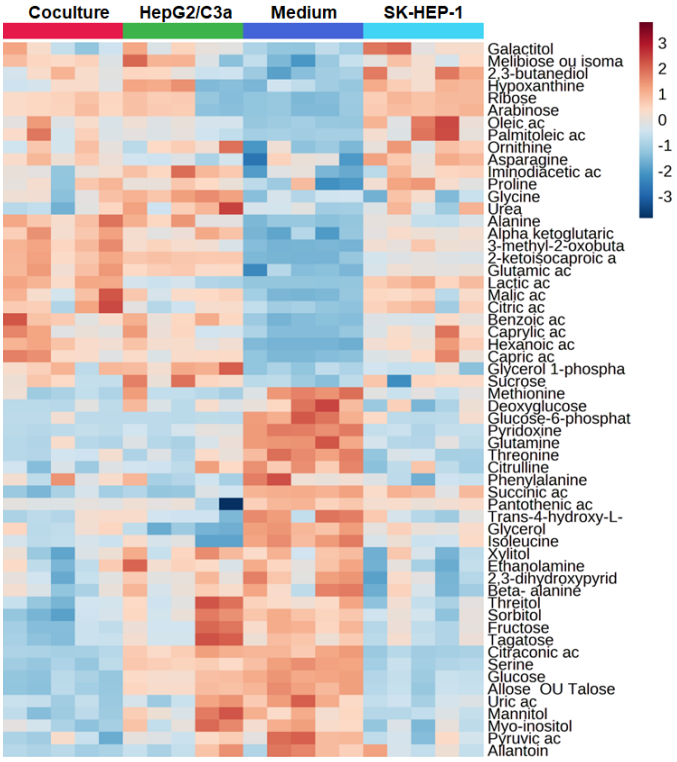

Figure 5.S2. *Heatmap of the 58 metabolites differentially expressed between SK-HEP-1 monoculture, HepG2/C3a monoculture, SK-HEP-1/HepG2/C3a coculture and basal culture medium.*

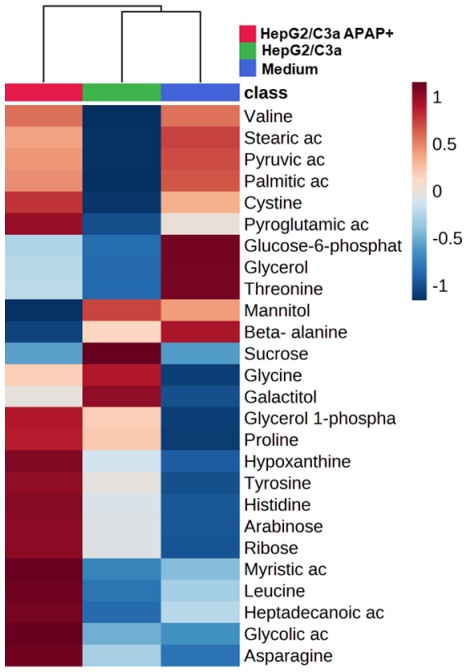

Figure 5.S3. *Heatmap of the 26 metabolites (P value < 0.1) significantly modulated by APAP treatments in HepG2/C3a monocultures.*

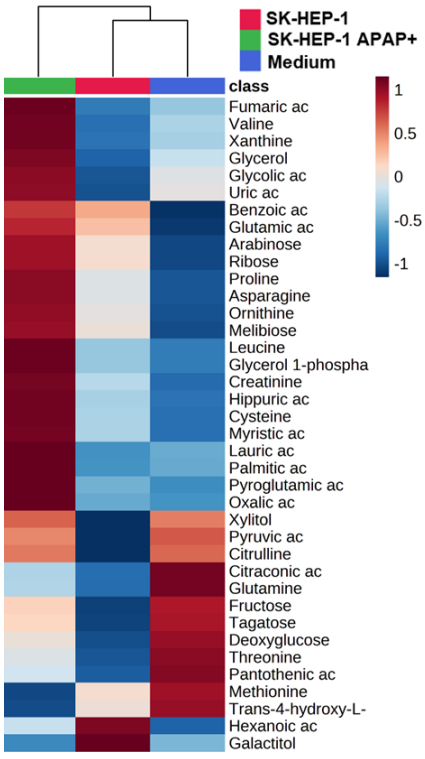

Figure 5.S4. *Heatmap of the 38 metabolites (P value < 0.1) significantly modulated by APAP treatments in SK-HEP-1 monocultures.*

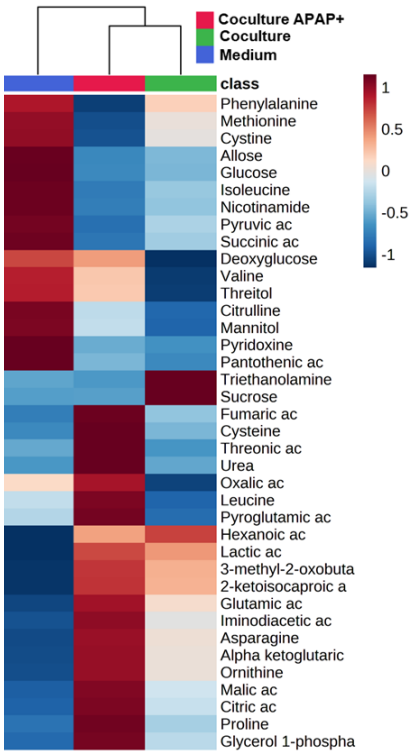

Figure 5.S5. *Heatmap of the 38 metabolites (P value < 0.1) significantly modulated by APAP treatments in SK-HEP-1/HepG2/C3a cocultures.*

Table 5.S1. *Metabolites identified in the culture media by GC-MS.*

Metabolite	PubChem ID	Metabolite	PubChem ID
2,3-butanediol	262	Arabinose	66308
Pyruvic acid	1060	Asparagine	236
Hexanoic acid	8892	Ribose	993
Glycolic acid	757	Xylitol	6912
Alanine	5950	Citrulline	9750
Norvaline	65098	Glycerol 1-phosphate	754
2-hydroxybutyric acid	11266	Deoxyglucose	439268
3-methyl-2-oxobutanoic acid	49	Azelaic acid	2266
Isoleucine	791	Hypoxanthine	790
2-ketoisocaproic acid	70	Citric acid	311
Beta-hydroxyisovalerate	69362	Hippuric acid	464
Valine	6287	Myristic acid	11005
Benzoic acid	243	Methionine sulfoxide	158980
Serine	5951	Fructose	5984

Caprylic acid	379	Tagatose	2724552
Ethanolamine	700	Phenaceturic acid	68144
Glycerol	753	Allantoin	204
Leucine	6106	Pyridoxine	1054
Phosphoric acid	1004	Allose	448388
Threonine	6288	Lysine	5962
Proline	145742	Histidine	6274
Glycine	750	Mannitol	6251
2,3-dihydroxypyridine	28115	Tyrosine	6057
Succinic acid	1110	Sorbitol	5780
Picolonic acid	1018	Galactitol	11850
Glyceric acid	439194	Pantothenic acid	6613
Citraconic acid	638129	Xanthine	1188
Fumaric acid	444972	Palmitoleic acid	445638
Methionine	6137	Palmitic acid	985
Aspartic acid	5960	Uric acid	1175
Beta- alanine	239	Myo-inositol	892
Capric acid	2969	Heptadecanoic acid	10465
Trans-4-hydroxy-L-proline	5810	Tryptophan	6305
Nicotinamide	457	Oleic acid	445639
Malic acid	92824	Stearic acid	5281
Threitol	169019	Cystine	67678
Pyroglutamic acid	7405	Glucose-6-phosphate	439958
Iminodiacetic acid	8897	Arachidic acid	10467
Phenylalanine	994	n-acetylneuraminic acid	445063
Cysteine	594	Sucrose	5988
Creatinine	588	Melibiose	440658
Threonic acid	5460407	Cholesterol	304
Alpha ketoglutaric acid	51	Lactic acid	107689
Ornithine	6262	Oxalic acid	971
Glutamic acid	33032	Urea	1176
Triethanolamine	7618	Glutamine	738
Lauric acid	3893	Glucose	24749

Table 5.S2. *Metabolites differentially expressed between the metabolomes of SK-HEP-1 monoculture, HepG2/C3a monoculture, coculture and basal culture medium (P < 0.05).*

Metabolite	P value	Metabolite	P value
Pyridoxine	9.42×10^{-13}	Pyruvic ac	0.0021824
Serine	1.12×10^{-11}	Methionine	0.0021941
2-ketoisocaproic ac	1.80×10^{-11}	Iminodiacetic ac	0.0022303
Glucose	8.08×10^{-11}	Uric ac	0.0022773
Citraconic ac	2.06×10^{-10}	Fructose	0.0023906
Lactic ac	2.35×10^{-10}	Caprylic ac	0.0025456
Allose ou Talose	5.69×10^{-10}	Glycine	0.0027968
3-methyl-2-oxobutanoic ac	1.93×10^{-9}	Myo-inositol	0.0037971
Hexanoic ac	1.28×10^{-7}	2,3-dihydroxypyridine	0.0041371
Glutamic ac	2.11×10^{-7}	Palmitoleic ac	0.0053894
Succinic ac	5.21×10^{-7}	Deoxyglucose	0.0063703
Glutamine	7.12×10^{-7}	Ethanolamine	0.0077109
Glycerol	8.07×10^{-7}	Threitol	0.0088146
Glucose-6-phosphate	1.02×10^{-6}	Citric ac	0.0089642
Alpha ketoglutaric ac	1.87×10^{-6}	Ornithine	0.0090054
Threonine	2.68×10^{-6}	Galactitol	0.0092401
Alanine	6.83×10^{-6}	Tagatose	0.0093014
Benzoic ac	2.42×10^{-6}	Trans-4-hydroxy-L-proline	0.009467
Ribose	9.62×10^{-5}	Melibiose ou isomaltose	0.010826
2,3-butanediol	9.94×10^{-5}	Asparagine	0.014874
Glycerol 1-phosphate	0.00010663	Beta- alanine	0.020132
Isoleucine	0.00011265	Hypoxanthine	0.025501
Capric ac	0.00011508	Sucrose	0.025737
Arabinose	0.00012185	Xylitol	0.026976
Malic ac	0.00019163	Urea	0.031863
Mannitol	0.00026276	Phenylalanine	0.034987
Oleic ac	0.00064287	Proline	0.041313
Sorbitol	0.00070114	Pantothenic ac	0.046041
Citrulline	0.0019525	Allantoin	0.047924

Table 5.S3. *Common and specific metabolites of different cultures exposed to APAP (extracted from Venn's diagram analysis).*

Groups	Metabolites
Coculture; HepG2/C3a; SK-HEP-1	Asparagine, valine, proline, pyroglutamic ac, pyruvic ac, glycerol 1-phosphate, leucine
HepG2/C3a; SK-HEP-1	Glycolic ac, palmitic ac, ribose, threonine, arabinose, myristic ac, glycerol, galactitol
Coculture; HepG2/C3a	Sucrose, cystine, mannitol
Coculture; SK-HEP-1	Cysteine, glutamic ac, fumaric ac, ornithine, citrulline, methionine, hexanoic ac, deoxyglucose, oxalic ac, pantothenic ac
HepG2/C3a	Glycine, heptadecanoic ac, tyrosine, histidine, stearic ac, hypoxanthine, glucose-6-phosphate, beta- alanine
SK-HEP-1	Xanthine, creatinine, xylitol, uric ac, benzoic ac, lauric ac, melibiose, tagatose, glutamine, trans-4-hydroxy-L-proline, hippuric ac, citraconic ac, fructose
Coculture	Allose, threitol, triethanolamine, nicotinamide, lactic ac, glucose, alpha ketoglutaric ac, 2-ketoisocaproic ac, pyridoxine, iminodiacetic ac, citric ac, threonic ac, succinic ac, 3-methyl-2-oxobutanoic ac, malic ac, urea, isoleucine, phenylalanine

5.11. References

Agin A, Heintz D, Ruhland E, Chao de la Barca JM, Zumsteg J, Moal V, Gauchez AS, Namer IJ. Metabolomics – an overview. From basic principles to potential biomarkers (part 1), Med. Nucl., 2016, 20, 4-10. DOI: 10.1016/j.mednuc.2015.12.006.

Badmann A, Langsch S, Keogh A, Brunner T, Kaufmann T, Corazza N. TRAIL enhances paracetamol-induced liver sinusoidal endothelial cell death in a Bim- and Bid-dependent manner. Cell Death Dis., 2012, 3, e447. DOI: 10.1038/cddis.2012.185.

Bhushan A, Martucci NJ, Usta OB, Yarmush ML. New technologies in drug metabolism and toxicity screening: organ-to-organ interaction. Expert Opin. Drug Metab. Toxicol., 2016, 12, 475-477. DOI: 10.1517/17425255.2016.1162292.

Bricks T, Hamon J, Fleury MJ, Jellali R, Merlier F, Herpe YE, Seyer A, Regimbeau JM, Bois FY, Leclerc E. Investigation of omeprazole and phenacetin first-pass metabolism in humans using a microscale bioreactor and pharmacokinetic models. Biopharm. Drugs Dispo., 2015, 36, 275-293. DOI: 10.1002/bdd.1940.

Bricks T, Paullier P, Legendre A, Fleury MJ, Zeller P, Merlier F, Anton PM, Leclerc E. Development of a new microfluidic platform integrating co-cultures of intestinal and liver cell lines. Toxicol. *in Vitro*, 2014, 28, 885-895. DOI: 10.1016/j.tiv.2014.02.005.

Britt EC, Lika J, Giese MA, Schoen TJ, Seim GL, Huang Z, Lee PY, Huttenlocher A, Fan J. Switching to the cyclic pentose phosphate pathway powers the oxidative burst in activated neutrophils. Nat. Metab., 2022, 4, 389-403. DOI: 10.1038/s42255-022-00550-8.

Caloni F, De Angelis I, Hartung T. Replacement of animal testing by integrated approaches to testing and assessment (IATA): a call for in vivitrosi. Arch. Toxicol., 2022, 96, 1935-1950. DOI: 10.1007/s00204-022-03299-x.

Canzler S, Schor J, Busch W, Schubert K, Rolle-Kampczyk UE, Seitz H, Kamp H, von Bergen M, Buesen R, Hackermüller J. Prospects and challenges of multi-omics data integration in toxicology. Arch. Toxicol., 2020, 94, 371-388. DOI: 10.1007/s00204-020-02656-y.

Chen C, Krausz KW, Shah YM, Idle JR, Gonzalez FJ. Serum metabolomics reveals irreversible inhibition of fatty acid beta-oxidation through the suppression of PPARalpha activation as a contributing mechanism of acetaminophen-induced hepatotoxicity. Chem. Res. Toxicol., 2009, 22, 699-707. DOI: 10.1021/tx800464q.

Chen SS, Huang Y, Guo YM, Li SS, Shi Z, Niu M, Zou ZS, Xiao XH, Wang JB. Serum metabolomic analysis of chronic drug-induced liver injury with or without cirrhosis. Front. Med., 2021, 8, 640799. DOI: 10.3389/fmed.2021.640799.

Choucha Snouber L, Bunescu A, Legallais C, Brochot C, Dumas ME, Elena-Herrmann B, Leclerc E, Metabolomics-on-a-chip of hepatotoxicity induced by anticancer drug flutamide

and its active metabolite hydroxyflutamide using HepG2/C3a microfluidic biochips. Toxicol Sci, 2013, 132, 8-20. DOI: 10.1093/toxsci/kfs230.

Cogger VC, Mohamad M, Solon-Biet SM, Senior AM, Warren A, O'Reilly JN, Tung BT, Svistounov D, McMahon AC, Fraser R, Raubenheimer D, Holmes AJ, Simpson SJ, Le Couteur DG. Dietary macronutrients and the aging lver sinusoidal endothelial cell. Am. J. Physiol. Heart Circ. Physiol., 2016, 310, H1064-H1070. DOI: 10.1152/ajpheart.00949.2015.

Cuykx M, Rodrigues RM, Laukens K, Vanhaecke T, Covaci A. *In vitro* assessment of hepatotoxicity by metabolomics: a review. Arch. Toxicol., 2018, 92, 3007-3029. DOI: 10.1007/s00204-018-2286-9.

Dahlin DC, Miwa GT, Lu AY, Nelson SD. N-acetyl-p-benzoquinone imine: a cytochrome P-450-mediated oxidation product of acetaminophen. Proc. Natl. Acad. Sci. USA,1984, 81, 1327-1331. DOI: 10.1073/pnas.81.5.1327.

Dalsbecker P, Beck Adiels C, Goksör M. Liver-on-a-chip devices: the pros and cons of complexity. Am. J. Physiol. Gastrointest. Liver Physiol, 2022, 323, G188-G204. DOI: 10.1152/ajpgi.00346.2021.

Diez V, Traikov S, Schmeisser K, Adhikari AKD, Kurzchalia TV. Glycolate combats massive oxidative stress by restoring redox potential in Caenorhabditis elegans. Commun. Biol., 2021, 4, 151. DOI: 10.1038/s42003-021-01669-2.

Dorovini-Zis K, Bowman PD, Betz AL, Goldstein GW. Hyperosmotic arabinose solutions open the tight junctions between brain capillary endothelial cells in tissue culture. Brain Res., 1984, 302, 383-386. DOI: 10.1016/0006-8993(84)90254-3.

Duarte IF, Gil AM. Metabolic signatures of cancer unveiled by NMR spectroscopy of human biofluids. Prog. Nucl. Magn. Reson. Spectrosc., 2012, 62, 51-74. DOI: 10.1016/j.pnmrs.2011.11.002.

Dudek M, Lohr K, Donakonda S, Baumann T, Lüdemann M, Hegenbarth S, Dübbel L, Eberhagen C, Michailidou S, Yassin A, Prinz M, Popper B, Rose-John S, Zischka H, Knolle PA. IL-6-induced FOXO1 activity determines the dynamics of metabolism in CD8 T cells cross-primed by liver sinusoidal endothelial cells. Cell Rep., 2022, 38, 110389. DOI: 10.1016/j.celrep.2022.110389.

Dufour-Rainfray D, Lambérioux M, Boulard P, Guidotti M, Delaye JB, Ribeiro MJ, Gauchez A S, Balageas AC, Emond P, Agin A. Metabolomics – an overview. from basic principles to potential biomarkers (part 2). Med. Nucl., 2020, 44,158-163. DOI: 10.1016/j.mednuc.2020.02.004.

Essaouiba A, Jellali R, Gilard F, Gakière B, Okitsu T, Legallais C, Sakai Y, Leclerc E. Investigation of the exometabolomic profiles of rat islets of Langerhans cultured in microfluidic biochip. Metabolites, 2022, 12, 1270. DOI: 10.3390/metabo12121270.

Ferry S, Degli Esposti M, Ndebele K, Gona P, Knight D, Rosenquist M, Khosravi-Far R. Tumor necrosis factor-related apoptosis-inducing ligand alters mitochondrial membrane lipids. Cancer Res., 2005, 65, 8286-8297. DOI: 10.1158/0008-5472.CAN-04-1913.

Fromenty B. Inhibition of mitochondrial fatty acid oxidation in drug-induced hepatic steatosis. Liver Res., 2019, 3, 157-169. DOI: 10.1016/j.livres.2019.06.001.

Gall WE, Beebe K, Lawton KA, Adam KP, Mitchell MW, Nakhle PJ, Ryals JA, Milburn MV, Nannipieri M, Camastra S, Natali A, Ferrannini E, RISC Study Group. alpha-hydroxybutyrate is an early biomarker of insulin resistance and glucose intolerance in a nondiabetic population. PLoS One, 2010, 5, e10883. DOI: 10.1371/journal.pone.0010883.

Geng Y. Lipotoxicity in non-alcoholic fatty liver disease: mechanisms and prevention in experimental models. University of Groningen. 2020, DOI: 10.33612/diss.130260314.

Guillouzo A. Liver cell models in *in vitro* toxicology. Environ. Health Respect, 1998, 106, 511-532. DOI: 10.1289/ehp.98106511.

Hang TC, Lauffenburger DA, Griffith LG, Stolz DB. Lipids promote survival, proliferation, and maintenance of differentiation of rat liver sinusoidal endothelial cells *in vitro*. Am. J. Physiol. Gastrointest. Liver Physiol, 2012, 302, G375-G388. DOI: 10.1152/ajpgi.00288.2011.

Iwakiri Y, Kim MY. Nitric oxide in liver diseases. Trends Pharmacol Sci, 2015, 36, 524-536. DOI : 10.1016/j.tips.2015.05.001.

Jaeschke H, Duan L, Nguyen N, Ramachandran A. Mitochondrial damage and biogenesis in acetaminophen-induced liver injury. Liver Res., 2019, 3, 150-156. DOI: 10.1016/j.livres.2019.10.002.

Jellali R, Gilard F, Pandolfi V, Legendre A, Fleury MJ, Paullier P, Legallais C, Leclerc E. Metabolomics-on-a-chip approach to study hepatotoxicity of DDT, permethrin and their mixtures. J. Appl. Toxicol., 2018, 38, 1121-1134. DOI: 10.1002/jat.3624.

Jellali R, Jacques S, Essaouiba A, Gilard F, Letourneur F, Gakière B, Legallais C, Leclerc E. Investigation of steatosis profiles induced by pesticides using liver organ-on-chip model and omics analysis. Food Chem Toxicol, 2021, 152, 112155. DOI: 10.1016/j.fct.2021.112155.

Jellali R, Lereau Bernier M, Tauran Y, Gilard G, Danoy M, Kido T, Miyajima A, Sakai Y, Leclerc E. Metabolomic profiling during the differentiation of human induced pluripotent stem cells into hepatocyte-like cells. Differentiation, 2020, 112,17-26. DOI: 10.1016/j.diff.2019.10.006.

Jellali R, Paullier P, Fleury MJ, Leclerc E. Liver and kidney cells cultures in a new perfluoropolyether biochip. Sens. Actuators B Chem., 2016, 229, 396-407. DOI: 10.1016/j.snb.2016.01.141.

Krähenbühl L, Reichen J, Talos C, Krähenbühl S. Benzoic acid metabolism reflects hepatic mitochondrial function in rats with long-term extrahepatic cholestasis. Hepatology, 1997, 25, 278-283. DOI: 10.1053/jhep.1997.v25.pm0009021934.

Leclerc E, Hamon J, Claude I, Jellali R, Naudot M, Bois F. Investigation of acetaminophen toxicity in HepG2/C3a microscale cultures using a system biology model of glutathione depletion. Cell Biol. Toxicol., 2015, 31, 173-185. DOI: 10.1007/s10565-015-9302-0.

Li H, Ding R, Shan Y, Ye F, Lin Y, Men X, Chen C, Tan S, Wang Q, Hu B. L-arabinose alleviates diabetes-aggravated cerebral ischemic injury by repairing the blood-brain barrier via downregulating NF-κB signals. J. Funct. Foods, 2021, 87, 104839. DOI: 10.1016/j.jff.2021.104839.

Li M, Wu Y, Ye L. The Role of amino acids in endothelial biology and function. Cells, 2022, 11, 1372. DOI: 10.3390/cells11081372.

Lord RS, Bralley JA. Clinical applications of urinary organic acids. Part 1: Detoxification markers. Altern. Med. Rev., 2008, 13, 205-215. PMID: 18950247

Lu SC. Regulation of hepatic glutathione synthesis: current concepts and controversies. FASEB J., 1999, 13, 1169-1183. DOI: 10.1096/fasebj.13.10.1169

Messelmani T, Le Goff A, Soncin F, Souguir Z, Merlier F, Maubon N, Legallais C, Leclerc E, Jellali R. Coculture model of a liver sinusoidal endothelial cell barrier and hepatocyte spheroids-on-chip in an advanced fluidic platform. Authorea, 2023. DOI: 10.22541/au.167596570.02002054/v1.

Messelmani T, Morisseau L, Sakai Y, Legallais C, Le Goff A, Leclerc E, Jellali R. Liver organ-on-chip models for toxicity studies and risk assessment. Lab chip, 2022a, 2423-2450. DOI: 10.1039/d2lc00307d.

Messelmani T, Le Goff A, Souguir Z, Maes V, Roudaut M, Vandenhaute E, Maubon N, Legallais C, Leclerc E, Jellali R. Development of liver-on-chip integrating a hydroscaffold mimicking the liver's extracellular matrix. Bioengineering 9, 2022b, 443. DOI: 10.3390/bioengineering9090443.

Milam KM, Byard JL. Acetaminophen metabolism, cytotoxicity, and genotoxicity in rat primary hepatocyte cultures. Toxicol Appl Pharmacol, 1985, 79, 342-347. DOI: 10.1016/0041-008x(85)90356-4.

Moradi E, Jalili-Firoozinezhad S, Solati-Hashjin M. Microfluidic organ-on-a-chip models of human liver tissue. Acta Biomater., 2020, 116, 67-83. DOI: 10.1016/j.actbio.2020.08.041.

Moreno-Torres M, Quintás G, Castell JV. The potential role of metabolomics in drug-induced liver injury (DILI) assessment. Metabolites, 2022, 12, 564. DOI: 10.3390/metabo12060564.

Pang Z, Chong J, Zhou G, de Lima Morais DA, Chang L, Barrette M, Gauthier C, Jacques P E, Li S, Xia J. Metabo-Analyst 5.0: narrowing the gap between raw spectra and functional insights. Nucleic Acids Res., 2021, 49, W388-W396. DOI: 10.1093/nar/gkab382.

Prot JM, Bunescu A, Elena-Herrmann B, Aninat C, Snouber LC, Griscom L, Razan F, Bois F Y, Legallais C, Brochot C, Corlu A, Dumas ME, Leclerc E. Predictive toxicology using systemic biology and liver microfluidic "on chip" approaches: application to acetaminophen injury. Toxicol. Appl. Pharmacol., 2012, 259, 270-280. DOI: 10.1016/j.taap.2011.12.017.

Reid AB, Kurten RC, McCullough SS, Brock RW, Hinson JA. Mechanisms of acetaminophen-induced hepatotoxicity: role of oxidative stress and mitochondrial permeability transition in freshly isolated mouse hepatocytes. J Pharmacol Exp Ther ,2005, 312:509–516. DOI: 10.1124/jpet.104.075945.

Rim KT. *In silico* prediction of toxicity and its applications for chemicals at work. Toxicol. Environ. Health Sci., 2020, 12, 191-202. DOI: 10.1007/s13530-020-00056-4.

Ruoß M, Vosough M, Königsrainer A, Nadalin S, Wagner S, Sajadian S, Huber D, Heydari Z, Ehnert S, Hengstler J G, Nussler AK. Towards improved hepatocyte cultures: Progress and limitations. Food Chem. Toxicol., 2020, 138, 111188. DOI: 10.1016/j.fct.2020.111188.

Schnackenberg LK, Sun J, Bhattacharyya S, Gill P, James L P, Beger RD. Metabolomics analysis of urine samples from children after acetaminophen overdose. Metabolites, 2017, 7, 46. DOI: 10.3390/metabo7030046.

Shah AD, Wood DM, Dargan PI. Understanding lactic acidosis in paracetamol (acetaminophen) poisoning. Br. J. Clin. Pharmacol. 71, 2011, 20-28. DOI: 10.1111/j.1365-2125.2010.03765.x.

Shen C, Zhang G, Qiu H, Meng Q. Acetaminophen-induced hepatotoxicity of gel entrapped rat hepatocytes in hollow fibers. Chem. Bio.l Interact., 2006, 162, 53-61. DOI: 10.1016/j.cbi.2006.05.005.

Shintu L, Baudoin R, Navratil V, Prot JM, Pontoizeau C, Defernez M, Blaise B, Domange C, Péry A, Toulhoat P, Legallais C, Brochot C, Leclerc E, Dumas M E. Metabolomics-on-a-chip and predictive systems toxicology in microfluidic bioartificial organs. Anal. Chem., 2012, 84, 1840-1848. DOI: 10.1021/ac2011075.

Song Q, Chen H, Li Y, Zhou H, Han Q, Diao X. Toxicological effects of benzo(a)pyrene, DDT and their mixture on the green mussel Perna viridis revealed by proteomic and metabolomic approaches. Chemosphere, 2016, 144, 214-224. DOI: 10.1016/j.chemosphere.2015.08.029.

Stanimirovic J, Obradovic M, Zafirovic S, Resanovic I, Bogdanovic N, Gluvic Z, Mousa SA, Isenovic E R. Effects of altered hepatic lipid metabolism on regulation of hepatic iNOS. Clin. Lipidol., 2015, 10, 167-175. DOI: 10.2217/clp.15.8.

Tsaioun K, Blaauboer BJ, Hartung T. Evidence-based absorption, distribution, metabolism, excretion (ADME) and its interplay with alternative toxicity methods. ALTEX, 2016, 33, 343-358. DOI: 10.14573/altex.1610101.

Wang XK, Peng ZG. Targeting liver sinusoidal endothelial cells: An attractive therapeutic strategy to control inflammation in nonalcoholic fatty liver disease. Front. Pharmacol., 2021, 12, 655557. DOI: 10.3389/fphar.2021.655557.

Xie G, Wang X, Wang L, Wang L, Atkinson RD, Kanel GC, Gaarde WA, Deleve LD. Role of differentiation of liver sinusoidal endothelial cells in progression and regression of hepatic fibrosis in rats. Gastroenterology, 2012, 142, 918-927.e6. DOI: 10.1053/j.gastro.2011.12.017.

Yagasaki K, Morisaki-Tsuji N, Miura A, Funabiki R. Possible involvement of phospholipase C and protein kinase C in stimulatory actions of L-leucine and its keto acid, alpha-ketoisocaproic acid, on protein synthesis in RLC-16 hepatocytes. Cytotechnology, 2002, 40, 151-154. DOI: 10.1023/A:1023988405518.

Yang X, Salminen W, Schackenberg L. Current and emerging biomarkers of hepatotoxicity. Curr. Biomark. Find., 2012, 2, 43-55. DOI: 10.2147/CBF.S27901.

Zeller P, Legendre A, Jacques S, Fleury MJ, Gilard F, Tcherkez G, Leclerc E. Hepatocyte-Sertoli cells coculture in bioreactor improves the Sertoli barrier permeability. J. Appl. Toxicol., 2017, 37, 287-295. DOI: 10.1002/jat.3360.

Chapter 6: Perspectives for the liver-on-chip model complexification: preliminary results of the primary human hepatocyte culture and the bi-compartmentalized biochip

In the third chapter, we demonstrated the capability of the HepG2/C3a to form spheroids when cultured in the HA-based hydroscaffold under dynamic conditions. In the current chapter, we seek to further validate and improve this model.

First, we explored the potential of using primary human cryopreserved hepatocytes in our hydroscaffold-integrated liver-on-chip model. Primary human cryopreserved hepatocytes (PHH) are commonly used as gold standard in drug discovery programs by pharmaceutical companies. The PHH organization inside the biochip was studied and their metabolic functions were measured.

In the second part, we discuss the potential of a newly developed bi-compartmentalized biochip. The biochip is composed of 2 independent culture chambers separated by a thin permeable membrane. Each culture chamber is designed to host a specific cell type and placed in an independent perfusion circuit. Exchanges between the two compartments take place through the permeable membrane. Different parameters in the design were explored to ensure the dynamic coculture of HepG2/C3a and SK-Hep1 cells.

6.1. Primary human cryopreserved hepatocytes in the hydroscaffold-integrated biochip

6.1.1 Introduction

Hepatic cell lines such as HepG2, HepaRG and Huh-7 are commonly used for the setup of newly developed models. Despite their tumoral origins, these cells present numerous advantages thanks to their capacity of self-renewal and the conservation of some hepatic functions such as albumin production (Nikolic et al., 2018). They remain of limited use in drug discovery process due to their metabolic capacity which is 10 to 1000-fold lower than that of primary hepatocytes. The standard gold used by pharmaceutical groups in this case is freshly isolated or cryopreserved primary hepatocytes. Their metabolic enzyme activities are very similar to that of *in vivo* hepatocytes, making them the best candidate for following the toxicity and metabolism of newly discovered drugs (Fraczek et al., 2013). Primary hepatocytes retain some of the structural functional characteristics of the liver but they lose their cuboidal morphology and their specific functions once cultivated in the conventional Petri dishes. The loss of hepatocyte functions was correlated with the lack of cell-cell interactions and cell-matrix interactions when the cells are cultivated on a non-physiological substratum (Iredale & Arthur, 1994). To overcome these limitations, we propose to culture primary human cryopreserved hepatocytes inside a HA-based hydroscaffold mimicking the liver extracellular matrix in our liver chip.

6.1.2 Preliminary results on spheroid formation

6.1.2.1. Spheroid formation in Petri dishes and biochips

Human cryopreserved primary hepatocytes (PHH) were cultivated in the HA-based hydroscaffold. Cells were seeded in the biochips and their behaviour was compared with cells seeded in 24-well Petri dishes with the same hydroscaffold (the surface culture being equivalent in both cases). Cells were seeded at a density of 400 000 cell/cm² (800 000 cell/biochip) and the biochips were incubated in static condition for the adhesion phase. 24h post seeding, the cells start to assemble forming small clusters in the culture channels of the biochip and in the Petri wells (figure 6.1).

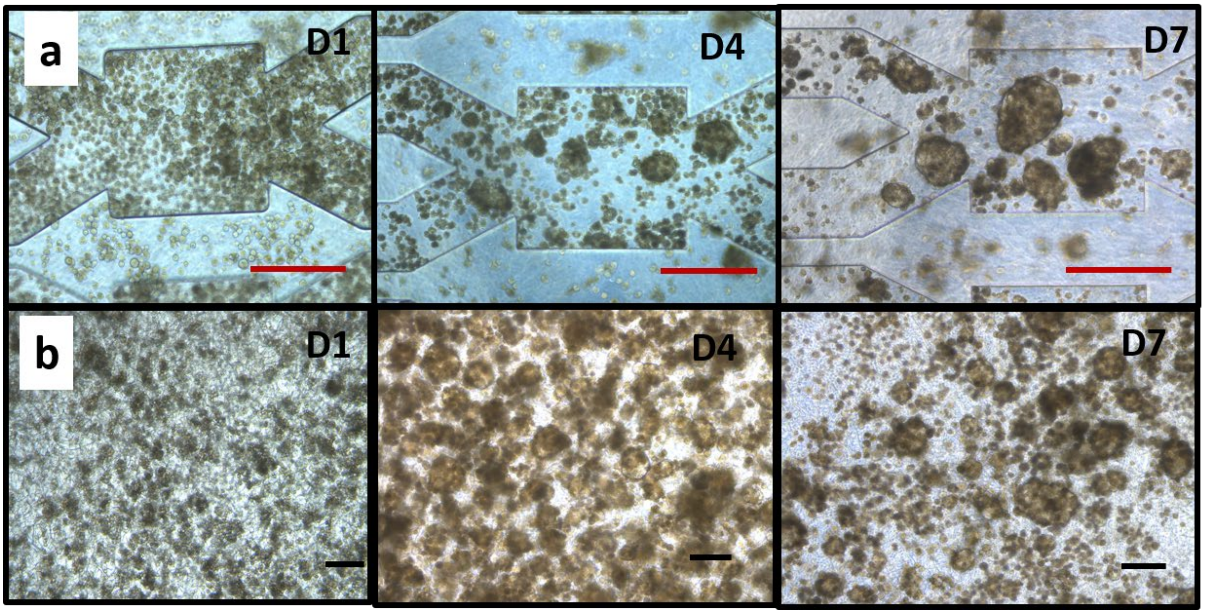

Figure 6. 1. *PHH starting to form small clusters in (A) biochip culture chambers (B) Petri dish well. Scale bar = 300 µm*

Once the cells have adhere, the biochips are connected to the IDCCM and the whole system is mounted on a peristaltic pump to ensure the dynamic culture. The culture medium of the static Petri is renewed daily. At day 4, PHH aggregates observed after the adhesion phase start to organize in 3D conformation in both the culture chambers (figure 6.1 a) and the Petri dishes (figure 6.1 b) to form spheroids with a mean size of 76 ± 19 µm and 94 ± 28 µm respectively. The spheroids seem randomly distributed in the biochip. At day 7, the spheroids keep growing reaching a diameter of 124 µm ± 28 µm and 116 ± 29 µm for the biochip and Petri dish conditions, respectively.

Table 6.1. *Evolution of spheroid diameter formed in dynamic biochips and static Petri dishes*

	D4	**D7**
Biochip	75 ± 19 µm	124 ± 28 µm
Petri dish	93 ± 27 µm	115 ± 29 µm

6.1.2.2. Albumin and urea production

In order to assess the functionalities of PHH spheroids, the albumin and urea production, which are generic markers of liver functions, were measured and compared between the different conditions and at different times of culture. Albumin production increased over time when cells were cultivated in dynamic biochips while it remained relatively constant, around 18 ± 8 ng/h/10^6 cell, in static Petri dishes (figure 6.2A). Moreover, albumin production in the

biochips was 5 to 10-fold higher than in the Petri dishes reaching an average 123 ± 28 ng/h/10^6 cell at day 7.

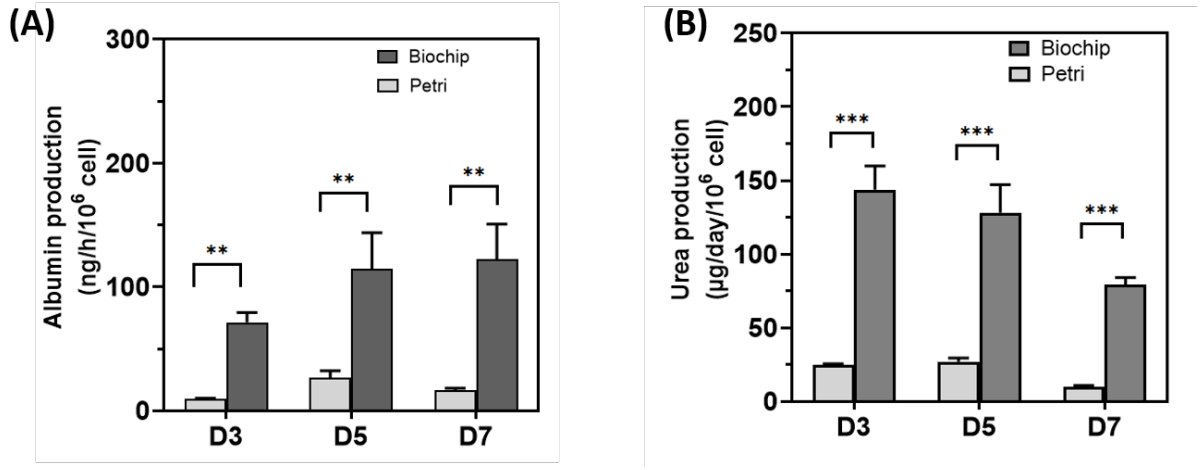

Figure 6.2. *Metabolic activity of PHH spheroids analysed in the culture medium supernatant (A) albumin production in the biochip and the Petri dish (B) urea production in the biochip and the Petri dish (** P < 0.0022; *** P < 0.0001).*

Urea production was measured at different time points and compared between the dynamic biochip and the static Petri dish (figure 6.2B). In the Petri dishes, the urea production remained in low levels over the 7 days of culture (between 10 ± A and 27 ± 2 µg/day/10^6 cell). For the dynamic biochips the urea production decreased over time from 144 ± 16 to 79 ± 49 µg/day/10^6 cell.

6.1.2.3. Spheroid structural characterisation in the biochips

The spheroid organization and structure were assessed after 7 days of dynamic culture by immunostaining. The same characterization could not be achieved for the spheroids formed in the Petri dishes due to the difficulty to adapt the culture well plates installation in our confocal microscope.

The spheroids in the biochips were positive to albumin and CYP3A4, two major markers for hepatocyte functionalities (figure 6.3A). CYP3A4 is usually not expressed with HepG2/C3a cell line due to its low metabolic activity but is expressed in PHH. Structurally, the actin filaments seemed to form a complex network indicating the compaction of the PHH spheroids (figure 6.3B). When coupled with MRP2 stain, a transporter located on the apical membrane of polarised hepatocytes and involved in the detoxification of a wide range of compounds, the colocalization of both stains demonstrated the polarization of the PHH spheroids. In addition, spheroids were stained for BSEP which is known to transport the bile salt from the intracellular compartment of the hepatocytes into bile flow. The spheroids were positive to BSEP which indicates the formation of a bile canalicular-like network corresponding to the maturation of these spheroids (figure 6.C).

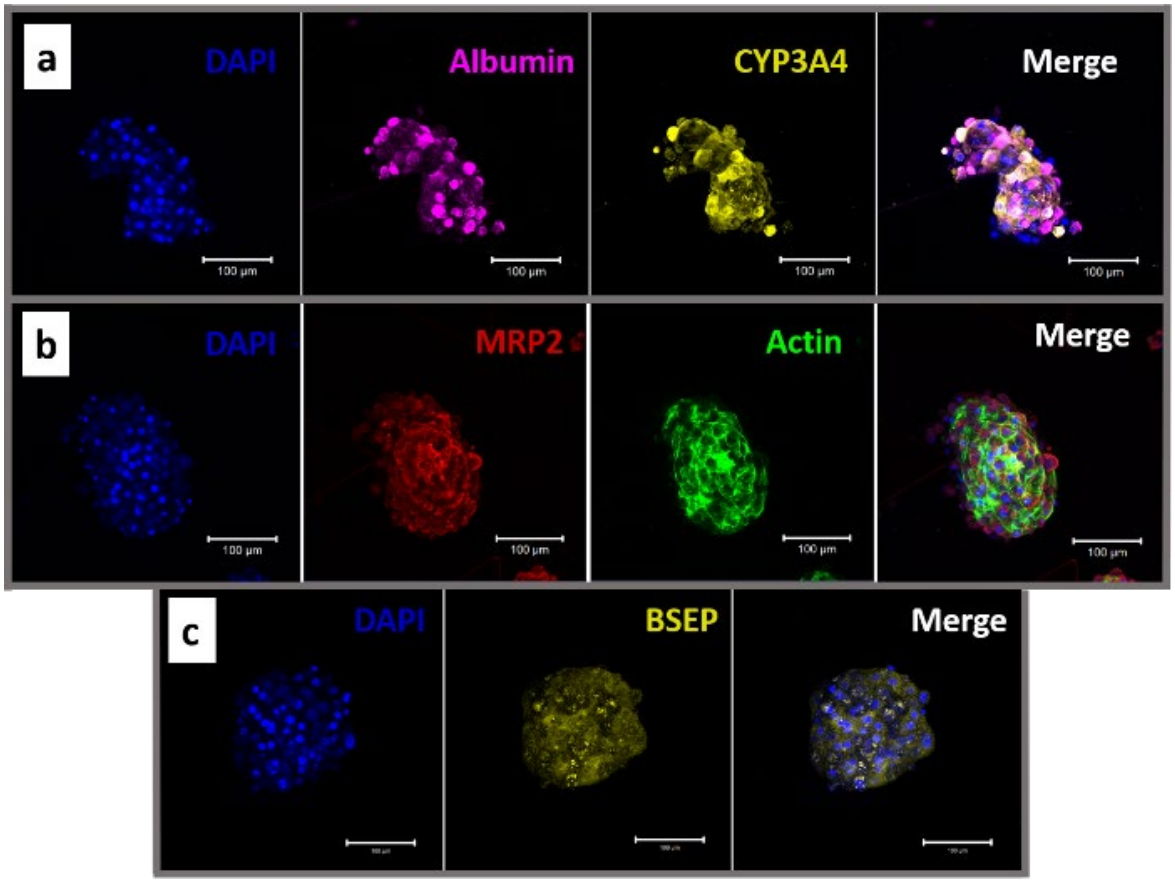

***Figure 6.3**. Characterization of the spheroids after 7 days of culture in the biochip (A) staining of specific functional markers of the hepatocytes : albumin (magenta) , CYP3A4 (yellow) and DAPI (nuclei, blue) for cells positions ; (B) formation of bile canalicular-like structures : MRP2 (red), phalloidin (F-actin, green), DAPI (nuclei, blue), the overlay of the markers (yellow signal) correspond to the polarization of the spheroids; (C) formation of a biliary-like network BSEP (yellow) and DAPI (nuclei, blue) (scale bar 100 µm).*

6.1.3. Discussion and conclusions

The *in vitro* culture of PHH highly depends on the donor liver condition, the viability of the cryopreserved cells and the culture conditions. Indeed, when cultivated *in vitro*, PHH tend to rapidly dedifferentiate, lose their functions and their polarisation. In this work, we used high quality PHH which were qualified to be able to form spheroids. The viability post-thawing has been calculated to be more than 94% which is in the ranges of the recommendations to avoid the induction of apoptosis (Hewitt & Li, 2015). We successfully maintained the culture of PHH for up to 7 days in our HA-hydroscaffold integrated biochip while maintaining structural and functional activities. We observed a significant increase of the spheroid's diameter during the cultivation period. This can be explained by the merge of different smaller spheroids to form bigger aggregates or the ability of the 3D organized PHH to proliferate. Further analysis could be done to study this situation. It is possible to use an enzyme, the hyaluronidase, which catalyses the degradation of hyaluronic acid. Spheroids could be then extracted and the cells detached and counted. Alternatively, a DNA extraction

can be performed and the number of cells can be correlated with the quantity of extracted DNA.

Structurally, using the F-actin staining, we observed an organization of the spheroids which was reported to enhance the cell-to-cell interactions compared to 2D cultured PHH (Bell et al., 2016). In addition, hepatocytes in the spheroids expressed specific functional markers even after 7 days of culture. We observed a maturation of the PHH spheroid structure. This was demonstrated by the BSEP expression indicating the development of a canalicular-like bile salt network and the polarization of the spheroids confirmed by the co-staining of actin and MRP2. These functions are quickly lost when PHH are cultivated in 2D plates (Bell et al., 2018).

PHH cultured in the hydroscaffold containing biochip demonstrated a higher albumin and urea production than in static 3D Petri, highlighting the advantages of the applied shear stress and the culture medium renewal in the enhancement of hepatocytes functionalities (Duivenvoorde et al. 2021). In addition, albumin production matches with our previously published results (Messelmani et al. 2022) when working with the HepG2/C3a cell line for the same initial density of seeding. Despite this, a normalization with the number of cells for both cell types should be considered in order to highlight the relevance of this comparison. When comparing our results with other works from our laboratory, after 2 days of culture, we did not detect a significant variation in the albumin production in our model compared with PHH cultivated in 2D in the same biochip by Jellali et al., 2016. However, our model produced higher albumin compared with (Boulais et al., 2021) who used alginate cryogel integrated biochip. This can be explained by the use of non-adherent PHH by Boulais et al. 2021 and the variability between the donors and the culture condition.

When we used the HepG2/C3a cell line in our advanced liver-on-chip model, seeding with the lowest density, led to the clogging of the biochips after 21 days of culture. This was caused by the continuous growth of the spheroids affecting the culture medium circulation. However, when using PHH this phenomenon is not expected to occur due to the low proliferating potential of these cells. The PHH were reported to be maintained in HA-based hydroscaffold Petri dishes until 21 days (HCS pharma internal data). In our advanced liver-on-chip, we successfully maintained the culture for up to 10 days with no clogging observed. These promising preliminary results opens up the possibility to extend the culture period to reach 30 days, in order to achieve chronic drug exposure. It is also important to note the limited metabolic activity of the HepG2/C3a. Indeed, when we used the APAP as candidate molecule, we observed a poor metabolization of the APAP into APAP-sulf and APAP-glu. Hence, the use of PHH is a pertinent choice. Indeed, PHHs are the cell model that recreates

the closest physiological responses. In addition, they are commonly used for drug toxicity assessment which give a basis for comparisons contrary to HepG2/C3a cell line.

In this work, we developed an advanced liver *in vitro* model using the combination of HA-based hydroscaffold mimicking the liver extracellular matrix, microfluidic device and primary human hepatocytes. We successfully organized the cells in 3D structures and highlighted the potential of our model compared to conventional static Petri dishes. A preliminary characterization was achieved and we observed a conservation of functions and promising results compared to our HepG2/C3a model and conventional models.

6.2. Design and evaluation of a bi-compartmentalized biochip

6.2.1. Introduction

In Chapter 4 we successfully developed a coculture model of the hepatic cell line HepG2/C3a and the liver sinusoidal endothelial cell line Sk-Hep-1. Despite its potential for the recreation of the transport of drugs through the liver endothelial barrier and their metabolism by the hepatocytes, this model relies on the IIDMP coculture device where hepatocytes are exposed to shear forces while LSEC remain in static conditions, which does not reflect the actual physiology of the liver. In the IIDMP, the insert corresponding to the LSEC compartment remain in static condition during the system perfusion. In addition, the space of Disse is represented by the distance between the culture insert and the biochip. By using the IIDMP, we certainly use a biomimetic approach to propose a liver model but we reflect an unusual anatomical configuration of the space of Disse. *in vivo*, LSEC line up to form the wall of blood vessels through which the blood circulates. Blood-borne exogenous molecules have to cross the endothelial layer to reach the hepatocytes and be metabolized. The LSEC and the hepatocytes are separated by a narrow tissue called space of Disse or perisinusoidal space. In addition to the separation between the sinusoidal lumen and the hepatocytes, the space of Disse is the home of hepatic stellate cells or vitamin A storing cells. During hepatic injury, the stellate cells are activated, start secreting extracellular matrix proteins which modify the mechanical properties of the space of Disse leading to a loss of LSEC phenotype (Sanz-García et al., 2021). Several works focused on the establishment of liver-on-chip models integrating an endothelial-like barrier (Hegde et al., 2014; Lu et al., 2018). This was achieved by integrating a thin permeable membrane separating the hepatic compartment from the sinusoidal-like compartment. Hence, the integration of LSEC remain challenging due to the rapid loss of their phenotype.

In order to obtain a more physiological model, in this chapter, we propose to design and evaluate a bi-compartmentalized biochip. The biochip is composed of two chambers separated by a thin permeable membrane allowing the exchanges of molecules through 4 µm pores. In the upper chamber, the LSEC can be cultivated on top of the permeable

membrane to form a confluent monolayer corresponding to the endothelial barrier while the hepatocytes can be cultivated in the micro structured lower chamber. Each chamber can be perfused through an independent perfusion circuit. The results obtained with the bi-compartmentalized biochip is intended to be compared with the ones obtained with the IIDMP. This work has been performed during the internship of a master of engineering student “Orégane Bajeux” from the institut supérieur de l’electronique et du numérique and funded by the MimLiveronChip ANR project.

6.2.2. Characterization of the bi-compartmentalized biochip

6.2.2.1 Design proposition

The PET membrane separating the two compartments was chosen with characteristics similar to the membrane of the cell culture insert used in the IIDMP. Polyester (PET) have naturally a non-polar structure making its activation with oxygen plasma and the assembling of the different parts of the biochip (PDMS-PET-PDMS) impossible. In order to achieve the bonding, the surface needs to be pretreated with primers. These primers create attachment sites on the surfaces which can be activated later by oxygen plasma. In our case, we chose to use two different type of primers: bis(3- (trimethoxysilyl)propyl)amine and APTES.

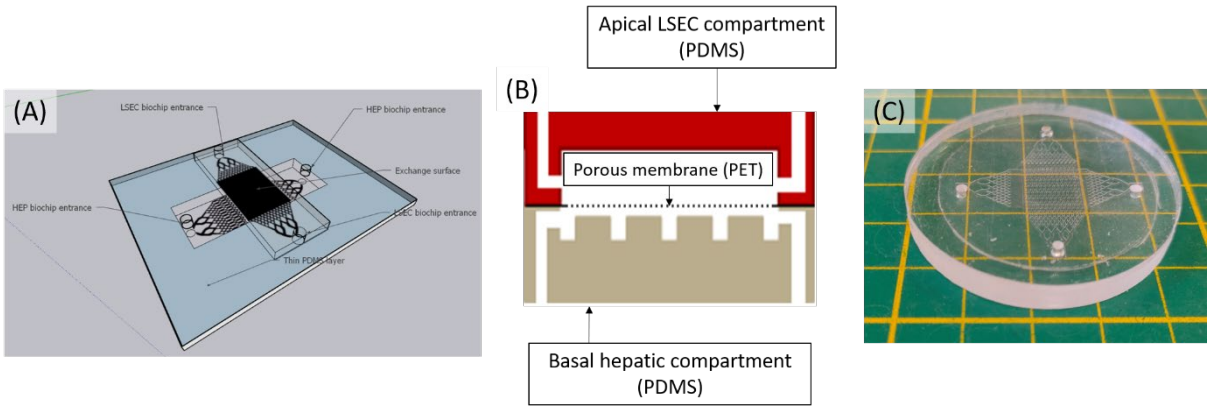

Figure 6.4. *Design of the bi-compartmentalized biochip (A) 3D design of the biochip (B) schematic presentation of the biochip (C) prototype of the biochip.*

6.2.2.2 Characterization of the treated membranes

We compared the surfaces of the untreated membrane (figure 6.6A), with the APTES and bis(3-(trimethoxysilyl)propyl)amine treated ones. The APTES treatment did not seem to affect the density or the diameter of the pores (figure 6.6B). However, an APTES deposit was observed on the surface of the membrane which can be rinsed using 70% ethanol and water. On the other hand, the bis(3-(trimethoxysilyl)propyl)amine treatment seemed to decrease the density and the diameter of the pores while clogging the remaining pores (figure 6.6C & D).

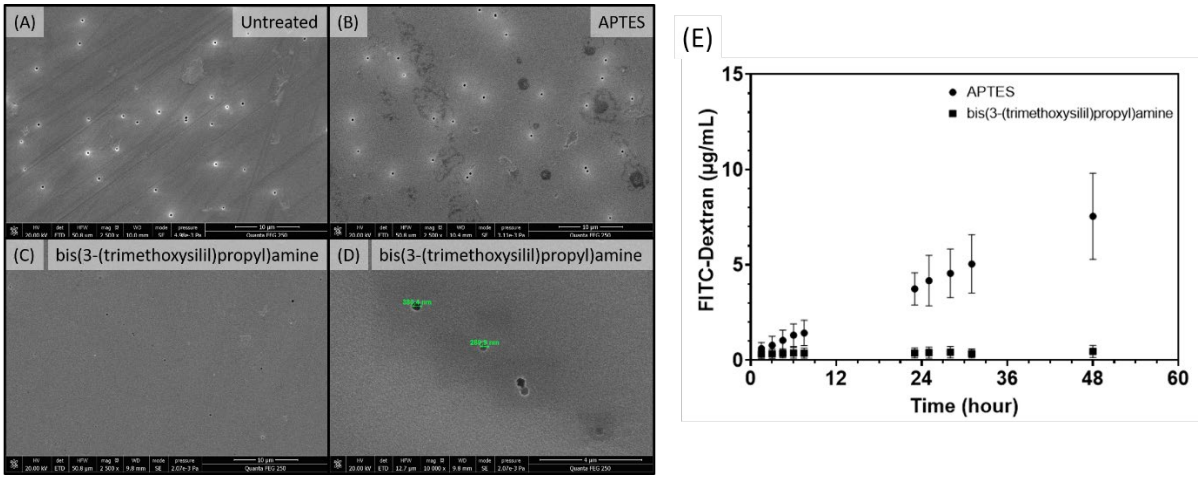

Figure 6.5. *Characterization of the membrane after different treatments (A) SEM analysis of the untreated membranes (B) SEM analysis of the APTES treated membrane (C) SEM analysis of the bis(3-(trimethoxysilyl)propyl)amine treated membrane (D) close-up look at the pore sizes of the bis(3-(trimethoxysilyl)propyl)amine treated membranes (E) FITC-dextran 4 KDa passage through the APTES and bis(3- (trimethoxysilyl)propyl)amine treated membranes measured in the basal compartment.*

When analysing the passage kinetics of the 4 KDa FITC-dextran through the membrane we observe that in both conditions, the tracer was detected in the basal compartment implying its passage through the membrane (figure 6.6E). However, when comparing the two conditions, the tracer passes at faster rates with the APTES treated membranes compared to the bis(3- (trimethoxysilyl)propyl)amine treated ones (figure 6.6E). This validates the exchanges happening between the two compartments and confirms the previously obtained SEM results implying the clogging of the pores for the bis(3- (trimethoxysilyl)propyl)amine treated membranes. The pore size decrease may be explained by the fabrication process. Indeed, compared with the APTES binding technique, an extra drying at 70°C for 30 minutes step is added which may cause the shrinking of the pores.

6.2.3. SK-HEP-1 culture in the bi-compartmentalized biochip

We chose to use only the biochips bonded using the APTES activation for cell culture. A total of 100 000 cells/cm² (200 000 cells/biochips) were seeded in the apical compartment of the biochip. The basal compartment was filled with culture medium and the connectors were sealed. After 24h in static condition, the pump was started at 10 µL/min. The perfusion was maintained constant for 24h then the adhesion and the morphology of the cells were analysed.

6.2.3.1. Proof of concept of the usage of the bi-compartmentalized biochip

After the static adhesion phase, the cells seemed to adhere to the surface forming typical LSEC morphology (figure 6.7A). Once the perfusion started, the cells detached and were evacuated by the flow (figure 6.7B). The remaining cells presented rounded shape corresponding to non-adherent cells (figure 6.7B). Different tracks were considered to explain the reasons of the cell's detachment after launching the perfusion.

The shear stress applied on the cells was estimated 5 µm above the membrane (Gregg et al., 2010), assuming the membrane's position remained horizontal. Only the shear stress in the central chamber is presented in figure 6.8 but the inlet and the outlet of the biochip were taken in consideration. The shear stress was simulated at a stable flow rate at 10 µL/min which does not take in consideration the flow rate fluctuation caused by the peristaltic pump. The shear stress was on average of the order of 21 x 10^{-3} Pa. The primary human LSEC have been previously cultivated under dynamic perfusion with a shear stress of 0.4 x 10^{-3} Pa (Li et al., 2018). Even though, the sensibility of the cells may differ between primary human LSEC and cell lines, we assume that the geometry or the flow rate should be adapted to decrease the shear stress.

It is also possible that the pulsatile flow produced by the peristaltic pump caused the membrane to oscillate between the upper and lower space of the culture chamber, provoking larger-scale flows and disturbing cell adhesion.

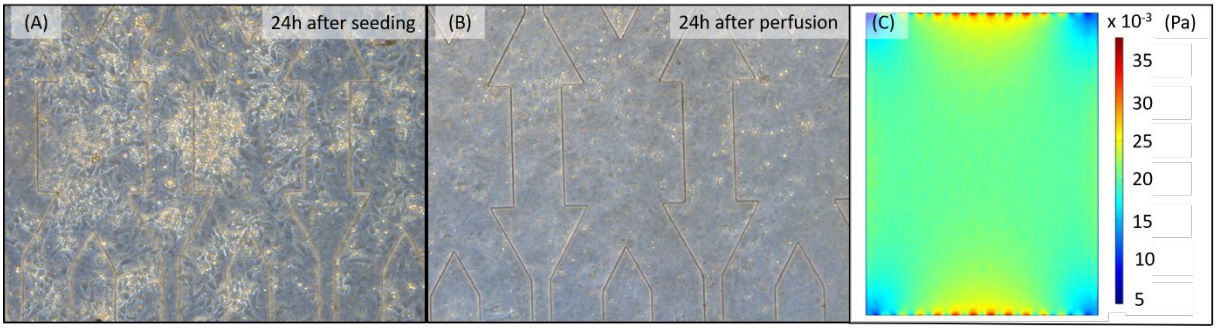

Figure 6.6. *SK-HEP-1 adhesion on the membrane (A) Cells adhesion after 24h of static adhesion phase (B) Cells detachment after 24h of perfusion (C) Simulation of the shear stress applied on the cells on the membrane.*

6.2.3.2. Improvement of the design of the bi-compartmentalized biochip

In order to investigate the reasons behind the SK-HEP-1 detachment from the membrane once cultivated under perfusion, we proposed to change the design of the apical culture chamber to add microstructures. These microstructures will act like micropillars binding the membrane to the chamber, fixing its movement and limiting its oscillation (figure 6.9).

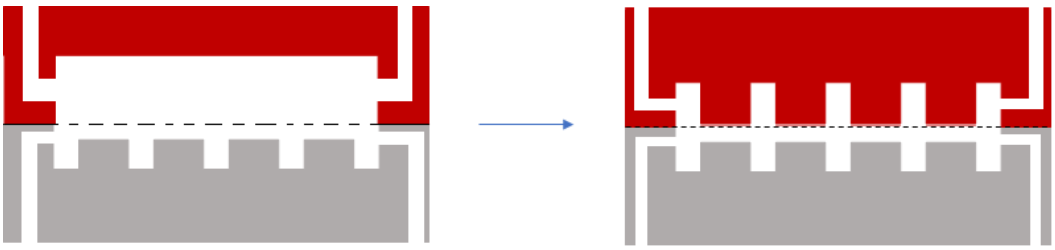

Figure 6.7. *Modification of the biochip design in order to avoid the membrane oscillation.*

The cells were seeded at the same density (100 000 cells/cm²) as the first design, and the basal compartment was filled with culture medium then the connectors were sealed. After

24h in static condition, the perfusion was launched at 10 µL/min. We successfully maintained the culture of the SK-HEP-1 cells under perfusion for 48h.

24h after seeding, the cells adhered to the membrane forming the typical LSEC morphology (figure 6.10A). After 48h of dynamic culture, the SK-HEP-1 cells seemed to adhere in certain regions especially in the culture chambers while were washed out and evacuated from other regions such as the microchannels linking the culture chamber (figure 6.10B). This detachment may be caused by the shear stress forces which are not equal in all the membrane regions (figure 6.10C). Indeed, for a constant flow rate, the different microstructures cause variations of the shear stress. It is also interesting to note that some cells adhered between the membrane and the microstructures which imply that the binding was not permanent. This was confirmed by the simulation of the shear stress forces applied on the cells, the highest values reaching 160. 10^{-3} Pa were noted in the microchannels while they decrease in the culture chambers reaching 100. 10^{-3} Pa.

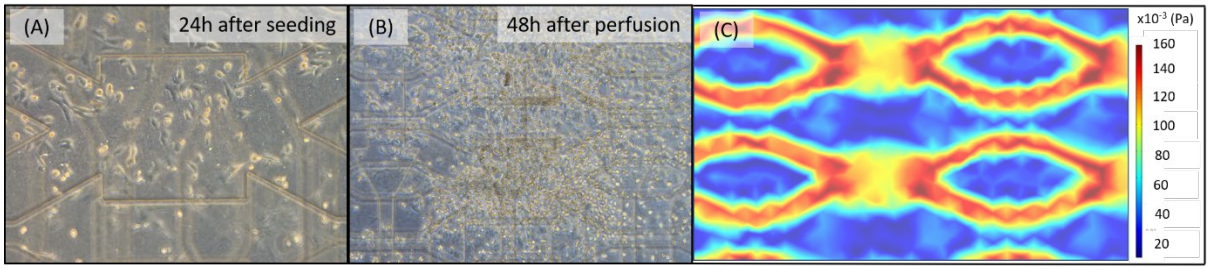

Figure 6.8. *Analysis of SK-HEP-1 adhesion on the membrane with the new biochip design (A) Cells adhesion after 24h of static adhesion phase (B) Cells detachment after 48h of perfusion (C) Simulation of the shear stress applied on the cells on the membrane*

6.2.4. Discussion and conclusion

In the present work, we successfully designed and developed a bi-compartmentalized biochip intended for the coculture of LSEC and hepatocytes. The first challenge regarding the integration of the permeable membrane was addressed using two different surface activation techniques. Following the literature recommendation, we adapted the process to increase the success rates of bonding and optimize the different steps. Even though the bis(3- (trimethoxysilyl)propyl)amine primer is described as the most stable among the different bonding chemical (Sip & Folch, 2014) ensuring the stable bonding for up to 2 weeks for static cell culture application, when used, this treatment affected the size and the density of the pores making the membrane useless in our intended application. Optimization for the binding process may be considered to avoid the material modification. On the other hand, the binding technique using APTES primers was successfully implemented and used to obtain the desired design while conserving the membrane characteristics. Furthermore, the detection of the FITC-dextran in the basal compartment confirms the exchanges happening

between the two chambers through the membrane, which validates the intended application of the biochip.

The second challenge was to set up the culture conditions for the endothelial cells in the apical compartment. We observed that cell adhesion depends on the structures of the biochip. Different hypotheses were made to explain cell detachment and different solutions were proposed. Given the sensibility of the endothelial cells to flow rate, pressure variation and mechanical stretch and substrate stiffness (Shu et al. 2021), we proposed at first to modify the culture chambers structure in order to limit the membrane oscillations and modulate the shear stress applied on the cells. We successfully maintained the endothelial cells in dynamic culture up to 48h with variations at different regions of the biochips. These variations were correlated with shear stress heterogeneity around the culture regions. Based on the shear stress simulations and the approach proposed to limit the membrane oscillation, a compromise should be considered between the used from rate and the design proposed. Indeed, the design should allow the primary application intended for the biochip which is the creation of an endothelial barrier, and, the flow rate should be adapted to the ranges supported by LSEC while maintaining a sufficient oxygenation, nutrients renewal and mechanical stimuli to maintain the LSEC phenotype.

In this work, we developed an advanced bi-compartmentalized biochip allowing the coculture of two or more cell types while ensuring the exchanges through a permeable membrane. The protocol for the microfabrication was set up and the different biochips obtained with the different techniques were characterized. The exchange happening between the two compartments was demonstrated using tracer molecules. We optimized the culture condition for the endothelial cells under perfusion in a vision to better mimic the physiological situation. Further optimizations are proposed to expand the lifespan of LSECs then a coculture with hepatocytes is considered in the basal compartment. The efficiency of using a perfused liver sinusoid could be studied later. The effect of the perfusion on the conservation of the LSEC phenotype, their actin orientation, and their permeability could be assessed and compared with the IIDMP. In addition, the metabolic activity in the hepatic compartment could be studied in a more *in vivo*-like physiology and compared with the biomimetic design developed with the IIDMP.

6.2.5. References

Bell CC, Dankers ACA, Lauschke VM, Sison-Young R, Jenkins R, Rowe C, Goldring CE, Park K, Regan SL, Walker T, Schofield C, Baze A, Foster AJ, Williams DP, van de Ven A W M, Jacobs F, van Houdt J, Lähteenmäki T, Snoeys J, Ingelman-Sundberg M. Comparison of Hepatic 2D Sandwich Cultures and 3D Spheroids for Long-term Toxicity Applications: A Multicenter Study. *Tox. Sci.*, 2018, *162*(2), 655. DOI: 10.1093/TOXSCI/KFX289

Bell CC, Hendriks DFG, Moro SML, Ellis E, Walsh J, Renblom A, Fredriksson Puigvert L, Dankers ACA, Jacobs F, Snoeys J, Sison-Young R L, Jenkins R E, Nordling Å, Mkrtchian S, Park BK, Kitteringham NR, Goldring CEP, Lauschke VM, Ingelman-Sundberg M. Characterization of primary human hepatocyte spheroids as a model system for drug-induced liver injury, liver function and disease. *Sci. Rep.,* 2016, *6:1*, *6*(1), 1–13. DOI: 10.1038/srep25187

Boulais L, Jellali R, Pereira U, Leclerc E, Bencherif SA, Legallais C. Cryogel-Integrated Biochip for Liver Tissue Engineering. *ACS App. Bio Mat.*, 2021, *4*(7), 5617–5626. DOI: 10.1021/ACSABM.1C00425/SUPPL_FILE/MT1C00425_SI_001.PDF

Fraczek J, Bolleyn J, Vanhaecke T, Rogiers V, Vinken M. Primary hepatocyte cultures for pharmaco-toxicological studies: at the busy crossroad of various anti-dedifferentiation strategies. *Arch. of Tox.*, 2013, *87*(4), 577–610. DOI: 10.1007/S00204-012-0983-3

Gregg JL, McGuire KM, Focht DC, Model MA. Measurement of the thickness and volume of adherent cells using transmission-through-dye microscopy. *Pflugers Archiv European J. of Phy.*, 2010, *460*(6), 1097–1104. DOI: 10.1007/S00424-010-0869-2/FIGURES/6

Hegde M, Jindal R, Bhushan A, Bale SS, McCarty WJ, Golberg I, Usta OB, Yarmush ML. Dynamic interplay of flow and collagen stabilizes primary hepatocytes culture in a microfluidic platform. *Lab on a Chip*, 2014, *14*(12), 2033–2039. DOI: 10.1039/C4LC00071D

Hewitt NJ, Li AP. Cryopreservation of hepatocytes. *Methods in Molecular Biology*, 2015, *1250*, 13–26. DOI: 10.1007/978-1-4939-2074-7_2

Iredale JP, Arthur MJP. Hepatocyte-matrix interactions. *Gut*, 1994, *35*(6), 729. DOI: 10.1136/GUT.35.6.729

Jellali R, Bricks T, Jacques S, Fleury MJ, Paullier P, Merlier F, Leclerc E. Long-term human primary hepatocyte cultures in a microfluidic liver biochip show maintenance of mRNA levels and higher drug metabolism compared with Petri cultures. *Bioph. & Drug Disp.*, 2016, *37*(5), 264–275. DOI: 10.1002/BDD.2010

Li X, George SM, Vernetti L, Gough AH, Taylor DL. A glass-based, continuously zonated and vascularized human liver acinus microphysiological system (vLAMPS) designed for

experimental modeling of diseases and ADME/TOX. *Lab on a Chip*, 2018, *18*(17), 2614–2631. DOI: 10.1039/C8LC00418H

Lu S, Cuzzucoli F, Jiang J, Liang L G, Wang Y, Kong M, Zhao X, Cui W, Li J, Wang S Q. Development of a biomimetic liver tumor-on-a-chip model based on decellularized liver matrix for toxicity testing. *Lab on a Chip*, 2018, *18*(22), 3379–3392. DOI: 10.1039/C8LC00852C

Nikolic M, Sustersic T, Filipovic N. *In vitro* models and on-chip systems: Biomaterial interaction studies with tissues generated using lung epithelial and liver metabolic cell lines. *Frontiers in Bioeng. and Biotech.*, 2018, *6*(SEP), 120. DOI: 10.3389/FBIOE.2018.00120/BIBTEX

Sanz-García C, Fernández-Iglesias A, Gracia-Sancho J, Arráez-Aybar L A, Nevzorova Y A, Cubero F J. The Space of Disse: The Liver Hub in Health and Disease. *Livers 2021,* 2021, *Vol. 1, Pages 3-26*, *1*(1), 3–26. DOI : 10.3390/LIVERS1010002

Shu X, Li N, Wu Y. Mechanotransduction of liver sinusoidal endothelial cells under varied mechanical stimuli. *Acta Mech, 2021, Sin.* **37**, 201–217. DOI: 10.1007/s10409-021-01057-3

Sip CG, Folch A. Stable chemical bonding of porous membranes and poly(dimethylsiloxane) devices for long-term cell culture. *Biomicrofluidics*, 2014, *8*(3), 036504. DOI : 10.1063/1.4883075

Duivenvoorde LM, Louisse J, Pinckaers NET. Comparison of gene expression and biotransformation activity of HepaRG cells under static and dynamic culture conditions. *Sci. Rep.* **11**, 10327, 2021. DOI: 10.1038/s41598-021-89710-6

General conclusions and future perspectives

The development of liver-on-chip models as an alternative substitute for animal testing remains a challenging goal. Despite the different models proposed in the literature, none, in our knowledge, is being effectively used by pharmaceutical companies in drug discovery processes. Most of the proposed models are not designed to reproduce *in vivo* biological phenomena nor take in account the complex *in vivo* microenvironment or physiology. The advances in microfluidic devices have been shown to be a powerful tool maintaining cell functionalities and expanding of the lifespan of several cellular populations compared to conventional models. In addition, it was demonstrated that cells are sensitive to the *in vivo* biomechanical stimuli, making the reproduction of such stimuli a mandatory parameter for the recreation of relevant *in vitro* models. Finally, most of the developed liver models limit the cells used to hepatocytes monoculture without considering the rest of the NPC cells. It is in this context that this research project positioned combining organ-on-chip technology, ECM-based hydroscaffold and an organ-barrier biomimetic design to propose an advanced liver-on-chip model. The model is intended to be integrated in a high-throughput drug screening platform.

The research project focuses on the setup of the coculture conditions and the study of the interactions between the two cellular populations. In order to achieve that a full study was realized in three steps:

1. First, we chose the HepG2/C3a cell line as hepatocyte model. The cell line was used because of its robustness, low cost and the existence of a basis for comparison in our laboratory. This step is considered as mandatory before using the PHH which are the gold standard for the pharmaceutical industry. The integration of the hydroscaffold was successfully achieved and the behavior of the cells was assessed structurally and functionally. We successfully maintained the HepG2/C3a culture until up to 21 days in our hydroscaffold integrated biochip in the IDCCM. The formed spheroids were characterized and results were compared with the ones obtained using conventional Petri dishes. We obtained well compact polarized spheroids with a bile salt-like network. By doing so, we demonstrated the potential of our model in the recreation of a more *in vivo* like organization of the hepatocytes in addition to enhancement of their functionalities compared to static Petri dishes.
2. In the second part of this thesis, we focused on the development of a hepatocyte-endothelial coculture model. We characterized the behavior of the SK-HEP-1 cell line when cultivated into a confluent monolayer on a culture insert. The conservation of

LSEC markers was verified by immunostainings and by measuring the expression of specific LSEC genes, then we used different tracers to follow-up the passage of molecules through the barrier and quantify its permeability. In order to achieve the coculture, a coculture medium was set up and different characterizations were realized to ensure the conservation of the cell's phenotype in the coculture medium. Once all the parameters were set-up, the IIDMP was used to integrate the advanced hepatocyte-on-chip and the cell culture insert building the endothelial barrier. The model ensured cell-to-cell communications and this was observed by the diminution of the barrier permeability. For the hepatocyte compartment, no effect was observed on the HepG2/C3a phenotypes. To test our model, we used a candidate molecule (APAP) to mimic the hepatic first pass. The LSEC phenotype was modulated by the APAP before passing to the hepatocytes for its metabolism.

3. In order to deepen our understanding of the metabolic reactions taking place in our advanced liver-on-chip, we investigated the modification of the metabolome in the different culture conditions. First, we identified the specific metabolic signatures for each culture condition, then, we identified the APAP metabolic perturbation pathway. For the HepG2/C3a APAP-treated condition, despite the use of a non-toxic dose, we detected an early but weak hepatotoxicity while for the SK-HEP-1, we observed an oxidative stress response coupled to the perturbation of the lipids and arginine cell metabolism which may trigger an anti-inflammatory response. The same biomarkers were observed in the coculture condition. These results highlight the importance of integrating the LSEC barrier in order to obtain a more *in vivo*-like response for drug exposure.

We established a complete study for the coupling of the HepG2/C3a cells cultivated in an advanced liver on chip, with SK-HEP-1 cells as an endothelial barrier in order to mimic the hepatic first pass. Our model has the potential to be used as a first tool of selection for drug toxicity assessment. And despite the use of a human cell source, the main limitation we encountered is the incapability to obtain a realistic *in vivo*-like metabolic responses. Indeed, the use of the HepG2/C3a cell line present a major limitation for our model due to its limited metabolic activity. We proposed in the last chapter of this thesis to use primary human hepatocytes as hepatocyte model in our advanced liver-on-chip system. As preliminary results, we successfully organized the cells in 3D conformation and obtained promising results about the spheroids compaction, maturation and the maintaining of their functions. These results encourage the exploitation of the PHH into our model by their coupling with the SK-Hep-1 endothelial barrier already characterized. It is even considered to use primary LSEC in order to obtain a more *in vivo* like representation of the liver composition. However,

the rapid loss of their phenotype by primary LSEC represents a main challenge for this approach. Further advances in long-term primary LSEC culture are required prior to the inclusion of primary LSEC in coculture devices.

It is also considered to integrate other non-parenchymal cells to obtain a more *in vivo*-like reaction for drug exposure. Indeed, the integration of Kuppfer and stellate cells has been reported to modulate the hepatoxicity reaction after APAP exposure. So, it is interesting to study their contribution in our model.

Once the model is fully developed, candidate reference molecules should be tested and the obtained results compared with the preexisting models used by pharmaceutical industries in order to justify and validate its usage to reduce animal testing.

Finally, we also presented in a last chapter a technological solution for the integration of the cell culture insert and the liver biochip into a unique advanced bi-compartmentalized biochip. We established and optimized the microfabrication process, demonstrated the exchanges between the two compartments and established recommendations to improve SK-HEP-1 culture in the apical compartment. A coupling between the SK-HEP-1 barrier cultivated in the apical compartment with the hepatocytes is considered and the metabolic potential of the model is supposed to be tested and compared with the results obtained the IIDMP platform.

In this work, we combined different bioengineering technologies to develop a biomimetic liver-on-chip model. We used different approaches for the different application we aimed. The use of cell lines was an appropriate choice for the establishment of the culture conditions of each cell type separately. As a matter of fact, these cells are easy to maintain and despite the loss of some functions they remain an interesting tool for the adjustment of culture conditions. The cells were cultivated separately then served as a proof of concept for the coculture model. Once the proof of concept established, we considered using primary human hepatocytes for the hepatic compartment which can be coupled to primary LSECs for the endothelial compartment. By doing so, we obtain relevant *in vivo*-like responses. In addition, in our approach we integrated a permeable membrane, through the use of culture insert and the integration of the permeable membrane in the bi-compartmentalized biochip, this allowed us to highlight the exchanges happening between the two compartments and study the benefit of integrating such physiological barrier.

Public communications

- **Review**

Messelmani T, Morisseau L, Sakai S, Legallais C, Le Goff A, Leclerc E, Jellali R. Liver organ-on-chip models for toxicity studies and risk assessment, Lab on a Chip, 2022, 22, 2423-2450.

DOI: 10.1039/D2LC00307D

- **Book chapter**

Morisseau L, **Messelmani T**, Essaouiba A, Sakai Y, Legallais C, Leclerc E, Jellali R. Microfluidic and organ-on-chip based technologies for diabetes research, Nanotechnology for diabetes management, Royal Society of Chemistry, 2022, 188-232,

DOI: 10.1039/9781839165498

- **Articles**

Messelmani T, Le Goff A, Souguir Z, Maes V, Roudaut M, Vandenhaute E, Maubon N, Legallais C, Leclerc E, Jellali R. Development of liver-on-chip integrating a hydroscaffold mimicking the liver's extracellular matrix. Bioengineering 9, 2022b, 443.

DOI: 10.3390/bioengineering9090443.

Etxeberria L, **Messelmani T**, Badiola JH, Llobera A, Fernandez L, Vilas-Vilela JL, Leclerc E, Legallais C, Jellali R, Zaldua AM. Validation of HepG2/C3A Cell Cultures in Cyclic Olefin Copolymer Based Microfluidic Bioreactors. Polymers, 2022; 14(21):4478.

DOI: 10.3390/polym14214478

Messelmani T, Le Goff A, Soncin F, Merlier F, Maubon N, Legallais C, Leclerc E, Jellali R. Coculture model of a liver sinusoidal endothelial cell barrier and hepatocyte spheroids-on-chip in an advanced fluidic platform, Submitted to ***Biotechnology & Bioengineering, 2023, Preprint, DOI: 10.22541/au.167596570.02002054/v1***

Messelmani T, Le Goff A, Soncin F, Gilard F, Souguir Z, Maubon N, Garière B, Legallais C, Leclerc E, Jellali R. Investigation of the metabolomic crosstalks between liver sinusoidal endothelial cells and hepatocytes exposed to paracetamol using organ-on-chip technology***, Submitted to Toxicology,* 2023**

- **Intenational conferences**

- ESAO winter school février 2021

Messelmani T, Zied S, Victoria V, Le Goff A, Leclerc E, Vandenhaute E, Legallais C, Maubon N, Jellali R, Association between hydroscaffold and Organ-on-chip technology to study the functionalities of the liver, EUROoCS 2021, online winter school in Jaca, Spain. **Poster**

- EuroOcs juillet 2021

Messelmani T, Zied S, Victoria V, Le Goff A, Leclerc E, Vandenhaute E, Legallais C, Maubon N, Jellali R, Development of an advanced liver organ-on-chip integrating hydrogel mimicking cell matrix, EUROoCS 2021, online conference. **Poster**

- ESAO Septembre 2021

Messelmani T, Zied S, Victoria V, Le Goff A, Leclerc E, Vandenhaute E, Legallais C, Maubon N, Jellali R, Development of an advanced liver organ-on-chip integrating hydroscaffold mimicking cell matrix, ESAO conference 2021 at Brunel University, London 47th ESAO congress 7-11 September 2021. **Oral presentation**

- Termis Novembre 2021

Messelmani T, Zied S, Victoria V, Le Goff A, Leclerc E, Vandenhaute E, Legallais C, Maubon N, Jellali R, Development of an advanced liver organ-on-chip integrating hydroscaffold mimicking cell matrix, TERMIS 6TH World Congress 2021, 15 - 19 November 2021 in Maastricht, the Netherlands. **Oral presentation**

- **National conferences**

- **Microphysio Avril 2022**

Messelmani T, Le Goff A, Soncin F, Souguir Z, Vandenhaute E, Maubon N, Legallais C, Leclerc E, Jellali R, Development of liver-on-chip model integrating LSEC barrier and hepatocytes organoids for toxicity application, The 1st edition of the MicroPhysio conference on "Micro-physiological models: From organoids to organs-on-chip“, cargèse, **Poster**

- **Congrès Français de Mécanique Août 2022**

T. Messelmani, A. Meziane, M. Verhulsel, Z. Souguir, E. Vandenhaute, N. Maubon, C. Legallais, E. Leclerc, R. Jellali, A. LE Goff, Contrôle d’écoulement et suivi de prolifération dans des biopuces hépatiques, 25ème édition du Congrès Français de la Mécanique, Nantes, France. **Oral presentation**